Investigating hepatitis C virus interactions with host lipid pathways that are critical for viral propagation using small molecule inhibitors and chemical biology methods

Rodney Lyn

Supervisor:
Dr. John P. Pezacki

Thesis submitted to the
Faculty of Graduate and Postdoctoral Studies
in partial fulfillment of the requirements
for the PhD degree in Chemistry

Department of Chemistry
Faculty of Science
University of Ottawa

Abstract

Hepatitis C virus (HCV) is remarkably capable of efficiently hijacking host cell pathways including lipid metabolism in the liver in order to create pro-viral environments for pathogenesis. It is becoming increasingly clear that identifying small molecule inhibitors that target host factors exploited by the virus will expand available HCV treatment options. As such, a thorough understanding of host-virus interactions is critical to the development of alternative therapeutic strategies.

Hepatic lipid droplets (LDs) are recruited by HCV to play essential roles in the viral lifecycle. The intracellular location of LDs is modified upon interacting with viral structural core protein. This enables formation of platforms that support viral particle assembly. Because these interactions are non-static, capturing its dynamic processes in order to better understand viral assembly can be achieved with label-free molecular imaging enhanced with live-cell capabilities. Chemical biology approaches that includes CARS microscopy employed in a multi-modal imaging system was used to probe interactions between HCV and host LDs. By successfully tracking LD trajectories, we identified core protein's ability to alter LD speed and control for LD directionality. Using protein expression model systems that allowed for simultaneous tracking of core protein and LDs, our data revealed that mutations in the core protein region that vary in hydrophobicity and LD binding strengths, are factors that control for differential modulation of LD kinetics. Furthermore, we measured bidirectional LD travels runs and velocities, and observed critical properties by which core protein induces LD migration towards regions of viral particle assembly.

Given that many steps in the HCV lifecycle are directly linked to host lipid metabolism, it is not surprising that disrupting lipid biosynthetic pathways would negatively affect viral replication.

From this outlook, we explored small molecule inhibitors that targeted several lipid metabolic pathways to study its antiviral properties. Using fluorescent probes covalently labeled to viral RNA, we captured the visualization of disrupted replication complexes upon antagonizing nuclear hormone receptors that are linked to regulating lipid homeostasis. Correspondingly, biochemistry and molecular imaging techniques were also employed to identify novel antiviral mechanisms of small molecule inhibitors that target additional HCV-dependent lipid metabolic pathways.

Acknowledgements

I sincerely express my utmost gratitude to Dr. John Paul Pezacki for his guidance as a mentor and supervisor. Dr Pezacki's influence has propelled me to excel intellectually and develop as a scientist. While trying to mirror Dr. Pezacki's passion for science, he has inspired me to explore and pursue my own passions to ensure that science always remains at the forefront in my career. I am fortunate to have been taught by his extraordinary coaching and leadership.

The support given by my colleagues in the Pezacki lab at NRC has been remarkable. Particularly, I want to extend my appreciation to Ragunath Singaravelu, Dr. David Kennedy, Dr. Selena Sagan, Dr. David Blais, Yanouchka Rouleau, Sylvie Belanger, Shifawn O'Hara, Dr. Allison Sherratt, and Jenny Cheng, all of whom have assisted in completing my experiments and have contributed to all my projects. I have learned so much from all of you. Beyond this experience, I value the friendships that we had developed throughout my graduate studies.

I would like to extent my gratitude to Dr. Albert Stolow and Dr. Stolow's group members in the CARSLab. It has been a tremendous experience participating in the advancement and transformation of the CARS microscope to a CARSLab user facility. Especially, I would like to thank Dr. Adrian Pegoraro and Dr. Andrew Ridsdale for their help in teaching me the instrumentation of CARS and troubleshooting microscopy issues. I value our collaboration and I credit you both for all the countless hours of research spent in the CARSLab while evolving into an ImageJ master.

I now acknowledge the warm support of my family and friends. In particular, my brother and sister (Roderick and Roberta), and my parents (Harvey and Irene), whom have provided me with encouragement and patience throughout my graduate studies. A special appreciation also belongs to Catriona Gray (lets go Red wings!).

Outside of the lab, the admiration and strength of my teammates in dragon boating, hockey, and rowing, fueled my energy and determination to always push forward inside the lab.

I want to take this opportunity to thank the University of Ottawa and National Research Council of Canada. Lastly, I am thankful for such great faculty members in the department of Chemistry and for all our stimulating intellectual discussions.

Abbreviations

ACAT	acetyl-CoA acyltransferase
ADRP	adipose differentiation related protein
BA	2-chloro-5-nitro-N-(pyridyl) benzamide analogue
BF	bezafibrate
CARS	coherent anti-Stokes Raman scattering
CyPA	cyclophilin A
CyPB	cyclophilin B
DAA	direct-acting antiviral
DGAT-1	diacylglycerol acyltransferase 1
DIC	differential interference contrast
ds-HCV RNA	double-stranded HCV RNA
EC_{50}	effective concentration measured at 50% of its maximal effect on a target
ER	endoplasmic reticulum
FAS	fatty acid synthase
FATP	fatty acid transport protein
FRET	Förster resonance energy transfer
GFP	green fluorescent protein
GPAT	glycerol 3-phosphate acyltransferase
HCV	hepatitis C virus
HepG2	human hepatocyte cell-line
HMG-CoA	3-hydroxy-3-methyl-glutaryl-CoA
hsp	heat shock protein
hsc	heat shock cognate protein
Huh-7	human hepatoma cells

hVAP-33	human vesicle-associated membrane protein-associated protein of 33 kDa
IC_{50}	inhibitor concentration required for 50% inhibition of its target
IRES	internal ribosomal entry site
JFH1	Japanese patient with fulminant hepatitis
LD	lipid droplet
LDLR	low-density lipoprotein receptor
MAPK	mitogen-activated protein kinase
MTOC	microtubule organizing center
MTP	microsomal triglyceride transfer protein
MUFA	monounsaturated fatty acid
NNI	non-nucleoside inhibitor
NI	nucleoside inhibitor
NP-40	nonidet P-40 non ionic detergent
NTP	nucleotide triphosphate
NTPase	nucleotide triphosphatase
OSBP	oxysterol binding protein
peg-IFN	pegylated-interferon
PI4K	phosphatidylinositol 4-kinase
PI4P	phosphatidylinositol 4-phosphate
PKA	protein kinase A
PKD	protein kinase D
PPAR	peroxisome proliferator-activated receptor
PPIase	peptidyl-prolyl cis-trans isomerase
PTEN	phosphatase tensin homolog deleted on chromosome 10
PtdCho	phosphatidylcholine

PtdEtn	phosphatidylethanolamine
PUFA	polyunsaturated fatty acid
qRTPCR	quantitative real-time polymerize chain reaction
RBV	ribavirin
RdRp	RNA-dependent RNA polymerase
RNAi	RNA interference
RPA	RNAse protection assay
RXR	retinoid X-receptor
SCD	stearoyl-CoA desaturase
SFA	saturated fatty acid
SP	signal peptidase
SPP	signal peptide peptidase
siRNAs	small-interfering RNAs
SNARE	N-ethylmaleimide-sensitive factor attachment protein receptor
SR-BI	scavenger receptor class B type I
SRE	sterol regulatory element
SREBP	sterol regulatory element binding protein
SVR	sustained virologic response
TPF	two-photon excited fluorescence
TG	triglyceride
TIP-47	tail-interacting protein 47
UFA	unsaturated fatty acid
UTR	untranslated region
VLDL	very low-density lipoprotein
wt	wild-type

Table of Contents

List of Figures

List of Schematics

List of Tables

1

Introduction

Viruses rely on the host to replicate their genomes [1, 2]. Given this, it is a pretext by which a strategy can be employed to target viral-dependent host mechanisms for antiviral activity, rather than directly targeting the virus, which evidently in some cases, produce high amounts of resistance [1]. With limited drug therapeutic options, this strategy can be applied to target hepatitis C virus (HCV) infections, which is the leading cause of liver transplants worldwide and is responsible for over 20% of new cases of liver cancer that occur each year [3, 4]. The incidence of acute HCV infections is generally masked by the lack of symptoms and therefore is capable of silently manifesting over years and even decades, causing the liver to degenerate over time [4, 5]. Unfortunately, prophylactic treatments are currently unavailable [5]. For this reason, there is an urgency to develop new treatment options and alternate novel antivirals.

The virus' error-prone replication generates a viral population with high heterogeneity that also varies geographically, and as a result, imposes a challenge for developing a therapeutic that targets all genotypes [5-8]. Despite the newly released first set of protease inhibitors that directly target the virus, these inhibitors vary in potency in all six genotypes, exhibit side-effects that are intolerable in some cases, and cause the emergence of resistant strains [9-12]. With the current demand for evaluating alternative therapeutics, an antiviral strategy has shifted in focus towards exploiting specific host pathways that are pertinent for the virus to complete its lifecycle. HCV is capable of altering host metabolic pathways, particularly perturbing cellular lipid metabolism, since lipids

support multiple stages of the HCV lifecycle [2]. Amongst the stages in the viral lifecycle, viral assembly is the least understood. One certainty, however, is that the host lipid droplet (LD) organelle aides in building a critical environment by interacting with multiple viral proteins and providing lipid substrates required for viral particle assembly [13-15]. Using a range of chemical biology techniques, this thesis describes the use of novel multimodal imaging techniques, firstly, to assess viral-induced LD dynamic interactions to gain an improved understanding of an obligate host factor for viral assembly, and secondly, to probe the mechanisms of small molecule inhibitors designed to intercept obligate lipid metabolic pathways.

The instrumental use of molecular multimodal imaging can both provide a better understanding of host-virus interactions, and can also be used as a screening method to evaluate the effect of LDs by using inhibitors of lipid metabolism that correspondingly perturbs HCV replication. Central to the multimodal imaging modality, coherent anti-Stokes Raman scattering (CARS) microscopy employs a multi-photon system to provide live-cell and label-free imaging of cellular LDs [16-18]. It has improved our understanding of LD dynamics in the context of viral-host interactions in the cell, and its capability has drawn attention in the HCV research community. Without CARS microscopy, LDs are normally visualized with chemical perturbation or fixation, which renders the acquired measurements to be static. Biological processes are far from being static in a cell, and therefore, real-time imaging capabilities allowed us to decipher virus-host interactions.

More specifically, in this thesis, we investigate how the viral core protein exerts spatial control of the host cell by recruiting LDs towards specific intracellular locations where it is required in viral assembly. Because HCV is highly dependent upon host lipids and LD organelles, using small molecules that target lipid metabolic pathways as a suitable antiviral strategy was assessed. In one study, we antagonized peroxisome proliferator-activated receptor α (PPARα) and evaluated its mechanism of reducing HCV replication, by directly imaging viral HCV RNA. In another study we used a small molecule inhibitor of stearoyl-CoA desaturase (SCD) to determine whether its antiviral properties were augmenting the structural integrity of viral replication complexes.

Multimodal imaging has allowed us to simultaneously understand dynamic virus-host interactions and directly visualize the effects of small molecule inhibitors targeting lipid metabolism. In the following, we illustrate the complexity by which the host is dynamically modified by HCV. We begin by generally illustrating the biology of the HCV lifecycle that include viral-host protein-protein interactions, and this is followed by discussing a strategy to identify alternative targets, such as the host for the development of novel therapeutics.

HCV infection: A global pandemic

There is an urgent need to identify new antiviral therapeutics to address global health challenges for eliminating HCV infections [19]. Upon acute infection, HCV causes mild flu-like symptoms and in many cases remains asymptomatic, leading to an undiagnosed infection [5]. Consequently, the virus can manifest over decades by attacking the liver and eventually causes cirrhosis or hepatocellular carcinoma [4, 5]. HCV is transmitted primarily through blood transfusions, shared needles, and mishandling of unsterile medical instruments [5]. Because symptoms are rarely observed in acute infections, the epidemiology of HCV infections are likely greater then the number of cases that affect approximately 2.3% of the global population [5]. The cause of death for greater than 350,000 people each year is due to HCV related liver diseases [5, 20]. In Canada, the number of infected amounts to approximately 320,000 Canadians, a volume that is enough to exert an immense burden in the current and future of medical health-care [5, 21]. HCV-induced liver failure is the leading cause for liver transplants world-wide [3]. Even so, liver transplantation is a palliative procedure, with cases demonstrating that post-transplant infections can lead to a more rapid progression for developing fibrosis [22].

Along the research frontier, the advancement in cell culture studies that include full-length and subgenomic replicons expressed in human hepatoma cells (Huh-7) have significantly contributed to the understanding of the biology of host-virus interactions, and with these models comes the ability

to decipher suitable molecular targets for novel inhibitors [23-27]. A breakthrough emerged when the discovery of a Japanese patient with fulminant hepatitis (JFH1), a strain that inherently was capable of producing infectious virus at the cell culture level, enabled studies to better understand the complete viral lifecycle [25-27]. Since then and more recently, adaptive mutations of single amino acid mutations, and intergenotype mutations by exchanging viral genes made up of structural and/or non-structural proteins have enhanced viral titres for adapted cell culture [28-30]. Notably on the nucleotide level, there are six genotypes that differ by greater than 30% [7]. The large genomic heterogeneity arises from HCV's error-prone replication, with an estimate of one error produced for every replicated 10^4 bases. There is also an overwhelming capability for specific viral proteins to suppress innate and adaptive immune responses [31]. Owing to the large heterogenic pool of HCV genomes, this exacerbates the challenge to develop prophylactic treatments (vaccines), which are currently absent from the clinical pipeline of up and coming treatment options [32]. Our challenges are severe and the treatment options, although expanding, are still not optimal. By identifying new host-virus interactions, we can exploit these targets by evaluating novel inhibitors that disrupt these interactions as a valuable therapeutic option. The intent is to identify novel host-directed therapeutics to generate a higher barrier of viral resistance, minimize side-effects, and ultimately work towards options that are free of standard treatments, which include pegylated-interferon (peg-IFN) and ribavirin (RBV).

HCV lifecycle and associated host factors

HCV belongs to the genus, *Hepacivirus,* of the *Flaviviridae* family [7]. It is a positive-strand RNA genome that comprises of approximately 9600 nucleotides [8]. Analogous to the family of Flaviviruses, HCV RNA is translated through a cap-independent internal ribosomal entry site (IRES) mediated process [33]. HCV encodes for a small proteome and relies on multiple host factors for pathogenesis [1, 34]. Host cellular processes are continuously reprogrammed by the virus as a pro-viral ensemble for rapidly replicating the virus [35]. To understand how the virus is capable of subverting

host processes, the current understanding of the viral lifecycle and its associated viral-dependent host factors, herein, are described in depth at the stages of viral entry, polyprotein processing, replication, and assembly (Schematic 1.1). The following examples describe the dynamic interactions between the virus and the host, and importantly illustrate the complexity in identifying suitable host targets.

Viral entry

HCV enters the liver by interacting with multiple cell surface receptors and is orchestrated by a complex and multi-step process [36]. This occurs by two sequential phases that include an early recognition and binding phase for incoming viral particles. This is then followed by an internalization phase completed by clathrin-mediated endocytosis [37, 38]. It is clear that HCV particles are recognized by glycosaminoglycans (GAGs) and low-density lipoprotein receptors (LDLR) at the early binding stages [39]. The latter of these receptors most likely recognize apolipoproteins that are associated with very low-density lipoprotein (VLDL) particles that encase the virion [40-42].

HCV entry steps include viral particle binding, translocation, entry and fusion. Binding is initiated by cell surface proteins such as scavenger receptor class B type I (SR-BI) [43] and CD81 [44]. It has been reported that tight junction proteins, claudin-1 [45] and occludin [46] mediate HCV entry, although it is not entirely clear whether these tight junction proteins, which closely localize between contacting cells are accessible to circulating HCV particles in the bloodstream [39, 47]. However, it is possible that other factors or even CD81 itself, are responsible for viral particle translocation towards these normally inaccessible tight junctions proteins, as HepG2 cells (cells derived from the liver) have demonstrated that claudin-1 may interact with CD81 outside of these tight junctions just prior to receptor-mediated entry [48, 49]. In addition, human CD81 belongs to a tetraspanin superfamily and was observed to bind to a domain of E2 on the virion surface [44, 55]. SR-BI is involved in HCV entry and translocation. SR-BI is a glycoprotein with transmembrane domains that anchor on the plasma

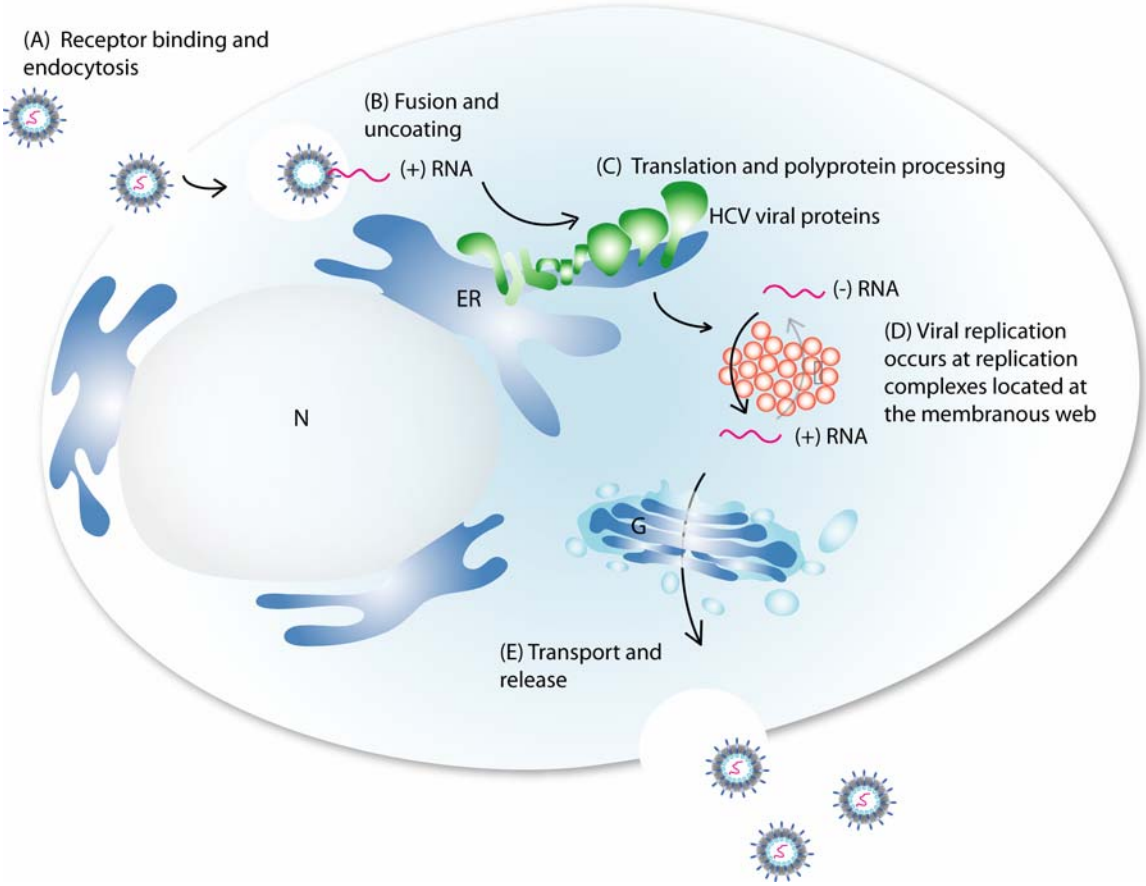

Schematic 1.1: The HCV lifecycle. (A) HCV viral entry is orchestrated by interacting with multiple cell surface protein receptors (glycosaminoglycans, low-density lipoprotein receptors, CD81, SR-BI, claudin-1, occludin and Niemann-Pick C1-like-1) and is then internalized through clathrin-mediated endocytosis. (B) A fusion step releases the viral RNA, which is subsequently translated to generate a large polyprotein that associates with the ER membrane by multiple transmembrane domains. (C) The action of host and viral proteases then cleave structural (core-E2), p7, and non-structural (NS2-NS5B) proteins. (D) Membrane alterations induced by viral protein, NS4B, create replication complexes optimal for HCV viral replication. These sites contain replicase proteins (NS3-NS5B), core protein bound to LDs, and a LD-associated environment that facilitates replication and assembly. Within these replication complexes, multiple copies of positive strand HCV RNA are generated by using the negative strand as a template. The viral RNA is then transported towards regions of viral assembly that are adjacent to core bound LD-associated membranes at the ER. Pre-lipidated VLDL particles interact with the budding viral particle and undergo E) further steps in maturation at the golgi before it is released from the cell. N: Nucleus; ER: Endoplasmic reticulum; G: Golgi apparatus.

membrane [50]. It is highly expressed in the liver and is involved in lipoprotein metabolism [51]. Studies identified that a dose-dependent polyclonal anti-SR-BI serum inhibited entry of HCV pseudoparticles (engineered virions that only comprise of HCV's structural envelope glycoproteins, E1 and E2) [52-54]. A role for SR-BI was further supported by complementary cell culture studies, identifying SR-BI to be a putative receptor involved in entry [54]. Most recently, it was shown that a cholesterol receptor, Niemann-Pick C1-like-1 (NPC1L1), also mediates entry at a post-binding step but prior to fusion, likely by recognizing cholesterol particles on the virion [56]. On the surface of the viral particle, HCV E1 and E2 viral proteins represent the first point of contact with host cell surface receptors required for viral attachment. The highly glycosylated states of these glycoproteins are important for entry [57]. Common amongst enveloped viruses, upon endocytosis, a membrane fusion step that involves a low pH-dependent endosomal compartment facilitates viral uncoating (Schematic 1.1) [58, 59]. Specifically, both glycoproteins appear as good candidates involved in fusion and this was supported by observing a fusion peptide directly in E1 [60], meanwhile, E2 shares structure homology with class II of fusion proteins [61, 62]. Together, E1 and E2 form heterodimers that are stabilized by disulphide bridges, permit entry in a spatiotemporal manner [63].

HCV translation and polyprotein processing

After viral uncoating, HCV is translated by ribosomes recruited to the 5' untranslated region (UTR) of the HCV genome [64]. Multiple highly structured stem loops and hairpins are found at the 5' and 3' UTR ends that flank an open reading frame that encodes the viral polyprotein (Schematic 1.2 A) [64]. Nucleotides 12-40 of the first stem loop at the 5' UTR are important for the proper positioning of cellular ribosomes and IRES dependent translation [65-67]. The HCV genome encodes 10 genes, and upon translation, a single large polypeptide is generated, which is then processed into viral proteins by enzymatic cleavage by viral and host proteases (Schematic 1.2 B) [68]. The viral proteins are categorized, based on specific roles in the virus lifecycle, into 3 structural proteins (core, E1, E2),

which are structural components of the viral particle, a p7 viroporin, and 6 non-structural proteins (NS2, NS3, NS4A, NS4B, NS5A, NS5B) that form important replication components in the host (Schematic 1.2 B) [69].

Structural proteins and p7

The most N-terminal protein of the HCV polypeptide is structural protein, core, which upon oligomerization, forms the viral nucleocapsid that encapsulates the viral RNA [70]. HCV core is a highly basic protein segregated by three domains (DI-DIII), each of which has an independent function for virus-host interactions [70]. The first domain of core (DI) is primarily composed of hydrophilic residues and binds with HCV RNA during nucleocapsid formation of the virion particle [71]. The second domain (DII) was profiled to contain a higher degree of hydrophobic residues that allow core protein to anchor to lipid membranes, such as the endoplasmic reticulum (ER) and surrounding cytoplasmic LDs [70, 72-74]. Viral assembly is highly dependent on the latter interaction with core capable of hijacking the surface of host LDs [75, 76]. For core to bind to LDs it must be successfully cleaved by host proteases located within the ER lumen that releases core as a mature form, which is composed of both DI and DII, while the fate of DIII left in the ER remains unknown (Schematic 1.2 B; core and LD interactions are discussed more in depth in chapters 3 and 4) [70, 76, 77]. The next set of structural proteins at the N-terminus comprise of envelope glycoproteins, E1 and E2 that are important for entry. As previously described, they both form non-covalent heterodimers within their transmembrane regions that are embedded within a lipid bilayer to form the viral envelope [57, 78]. Host signal peptidases that cleave core from E1 also participate in cleaving multiple sites of the polyprotein liberating E1, E2, and p7 (Schematic 1.2 B).

The 3D structure of p7 [79] reveals two-transmembrane helices that are connected by a short cytoplasmic loop [80]. Much was unknown about p7's functional role in the lifecycle until recently, when reports had identified it to play a major role in assembly (Further discussed in the section on

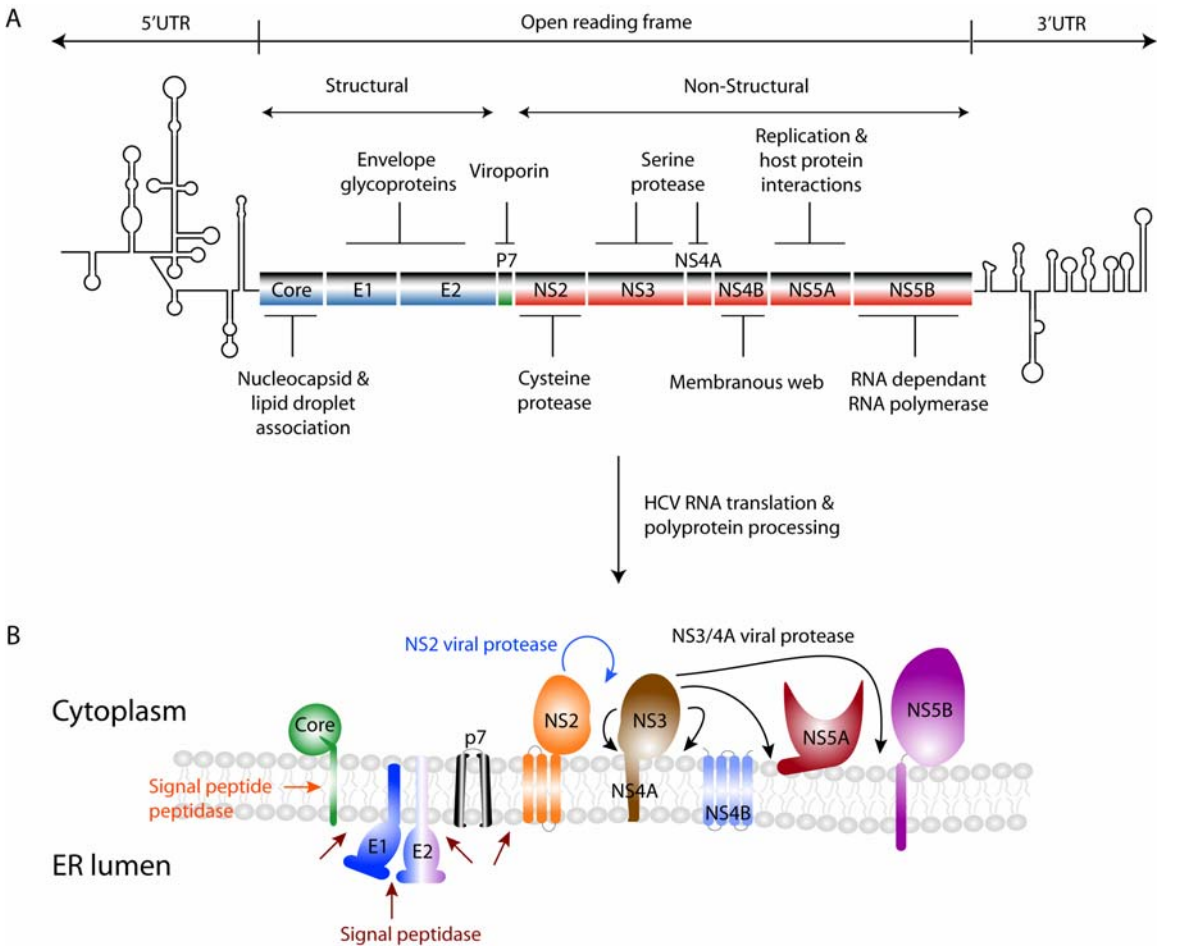

Schematic 1.2: HCV genome. (A) The viral genome encodes for 10 proteins within the open reading frame, which is flanked by a 5' and 3' untranslated region (UTR). Key functions of the structural (core, E1, E2), non-structural (NS2, NS3, NS4A, NS4B, NS5A, NS5B), and p7 proteins are briefly described. (B) Upon translation, the entire polyprotein embeds into the ER membrane and is subsequently cleaved and processed by host proteases (orange and brown arrows) and viral proteases (blue and black arrows) into individual proteins that play critical host and viral protein-protein interactions throughout the HCV lifecycle.

viral assembly) [80, 81]. As such, the function of this protein was elucidated based on structural similarities with viroporin proteins of other viruses [82]. It has been shown that the transmembrane domains of p7 forms cation-selective hydrophilic pores through which ions cross the membrane [81].

Non-structural proteins

While the processing of structural proteins solely rely on host proteases, the non-structural proteins, on the other hand, are dependent on enzymatic cleavages by viral proteases, NS2 and NS3-4A (Schematic 1.2 B). The polytopic NS2 protein is composed of a transmembrane domain and its catalytic activity is dependent on the N-terminal domain of NS3 for autocleavage [83, 84]. Subsequently, a portion of inactive NS2 has been shown to be degraded by the proteasome [85]. More recently, however, NS2 was revealed to participate in viral assembly (Discussed in the viral assembly section) [86, 87]. Following the autocleavage of NS2, further downstream cleavages by NS3-4A protease follow a preferential order when processing the rest of the viral proteins that are involved in the replicase complex.

Importantly, expression from NS3-NS5B is sufficient for stable replication in Huh-7 cells despite the absence of structural proteins [23]. NS3 is a multifunctional protein that contains an N-terminal active site composed of a catalytic serine protease and a C-terminal RNA helicase/nucleotide triphosphatase (NTPase) domain [88]. A crystal structure of NS3 revealed that the C-terminal region encodes for a DexH/D-box, which is required for RNA processing, and that its dimerization facilitates the action of RNA helicase for highly coordinated unwinding of RNA-RNA duplexes in an ATP-dependent manner [89]. Furthermore, its protease activity is enhanced and stabilized by interacting with NS4A, which primarily functions as a co-factor for NS3 activity by acting as a membrane anchor [90-92]. The highly conserved catalytic triad of NS3 contains a shallow active-site pocket at the N-terminus with site specific residues formed by histidine 57, asparagine 81, and serine 139 [93, 94]. The catalytic pocket contains a zinc ion that is required for proper positioning of the NS3 C-terminus [93, 94]. Together the NS3-4A protease sequentially cleaves downstream HCV proteins intermolecularly (trans), at the junctions of NS4A/4B, NS4B/NS5A, and NS5A/NS5B (Schematic 1.2 B) [95-98]. By contrast, NS3/4A, itself, is cleaved intramolecularly (cis) separating NS3 and NS4A into their individual proteins [88, 89].

HCV Replication

Viral proteins responsible for replication

The final three viral proteins NS4B, NS5A, and NS5B represent the replicase of the HCV genome. Specifically, NS4B is an integral membrane protein predominantly composed of highly hydrophobic domains [99]. Its N-terminal region comprises two amphipathic helices, both found in the cytoplasmic region, with the second capable of traversing through the lipid bilayer upon oligomerization [100]. Moreover, the central region entails four transmembrane segments [101]. The C-terminal section also comprises of two α-helices, with two identified palmitoylation sites in the second α-helix, though it is unclear whether these palmitoylated sites are required for replication even though they play a role in aiding oligomerization [102]. The C-terminal domain has also been shown to bind to HCV RNA [103]. Interestingly, expression of NS4B was identified to induce the formation of altered membranes, termed membranous webs, which are located at the perinuclear region where RNA is efficiently replicated (Schematic 1.3; HCV induced altered membranes are discussed in greater detail in chapter 5) [104].

NS5A is a multifunctional protein that dynamically interacts with multiple viral and host proteins at the replication complexes [8]. Importantly, it is one of the many non-structural proteins that are found at cholesterol-rich lipid rafts at these sites for HCV replication [105]. NS5A anchors the ER membrane through an N-terminal amphipathic α-helix by embedding in-plane with phospholipids on the cytosolic leaflet [106]. The inner region of the helix is rich in tryptophan residues while polar charged residues point outside towards the cytosolic milieu [107]. There are three active domains downstream of the N-terminal region. Revealed by an X-ray crystal structure are two regions of subdomain I that contain four cysteine residues that are coordinated to a zinc ion, and this is vital for replication [108]. Additionally, subdomain II contains a disulphide link between two cysteine residues, and together forms a dimeric structure with a configuration described by a ‘claw-like’ surface protein that accommodates the viral genome, which is hypothesized to protect the RNA from degradation.

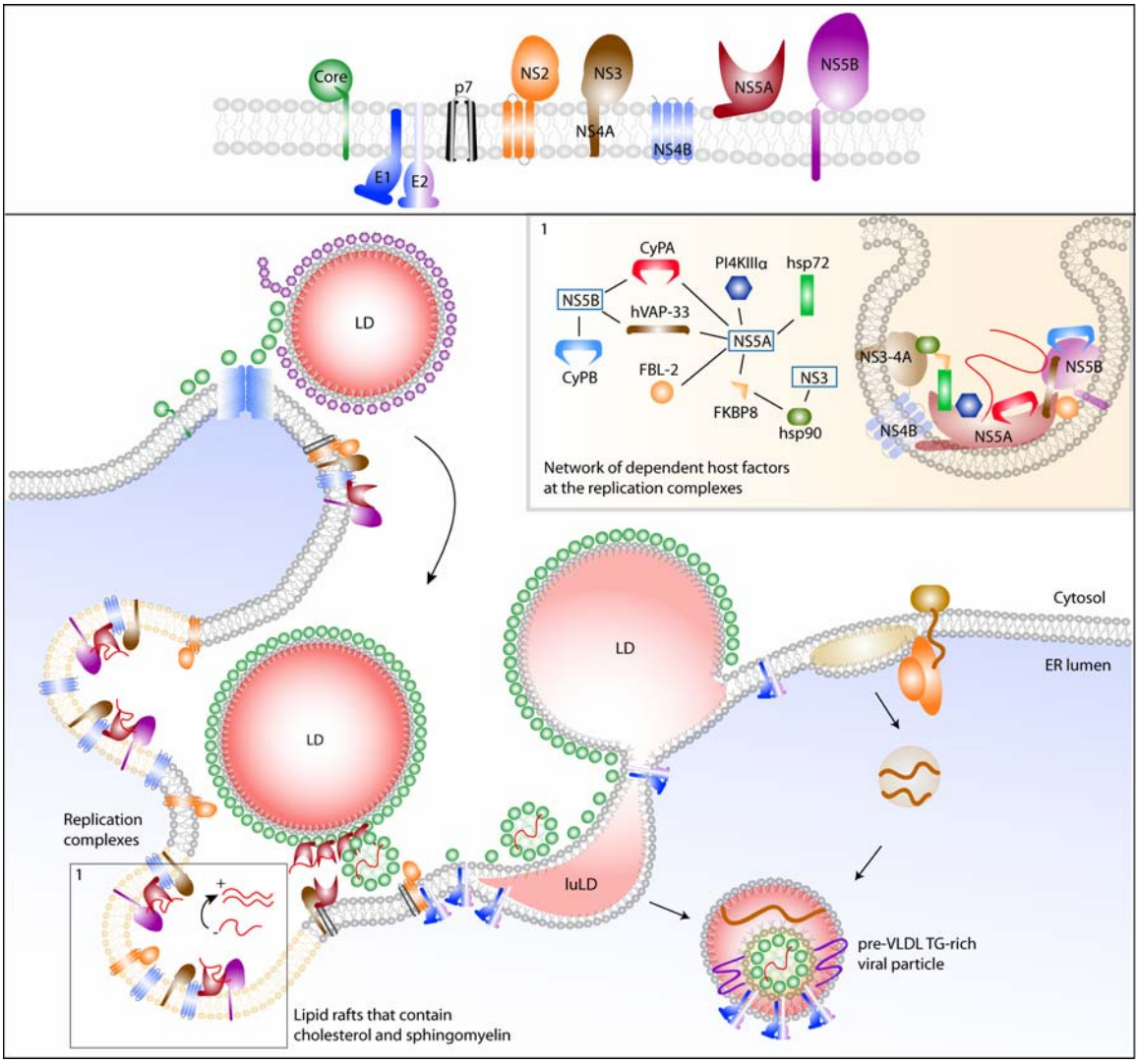

Schematic 1.3: Model depicting host and viral factors required for HCV replication in the viral lifecycle. A legend is provided (top) to match the identified shapes that correspond accordingly to viral proteins shown in the depiction (bottom). Replication complexes are located within altered membranes (highly curved membranes) that closely associate with LDs. The replication complexes contain a large abundance of sphingolipids and cholesterol within the membranes. The ratio of positive to negative strand HCV RNA is approximately 10:1. A magnified portion of a replication complex, inset 1, is a representative model that includes active host proteins required for viral replication. Overlapping of host and viral proteins are modeled together to depict direct interactions at the replication complex, respectively. Specifically, inhibiting the function of any of these host factor proteins can sufficiently block HCV replication. Non-structural proteins (NS3-NS5B) are outlined in greater detail because they represent viral proteins that are required to initiate and sustain replication. Included in this scheme is a general illustrative network for direct interactions between

viral proteins and host factors, respectively. Refer to Table 1.1 for host protein abbreviations. LuLD: Luminal lipid droplets; VLDL: very-low density lipoproteins; ER: Endoplasmic reticulum.

While subdomain III is less conserved and can accommodate partial deletions or insertions at permissive sites without sacrificing replication, this domain has increasingly been shown to participate in viral assembly [109, 110]. NS5A exists under two forms, identified as a hyperphosphorylated (58kDa) or hypophosphorylated (56kDa) state [111, 112]. It is conceivable that conversion between these two states may regulate HCV replication [111, 112]. Evidently, reducing hyperphosphorylated forms of NS5A has been shown to enhance HCV genome replication [109, 113]. The phosphorylated levels of NS5A was hypothesized to be an intrinsic mechanism that may bridge the transition between replication and assembly [112]. On the molecular level, NS5A was visualized to comprise of two distinct populations within the cytoplasm, both of which are dynamically mobile [114]. Live-cell imaging has demonstrated that a successful green fluorescent protein fusion tag encoded in NS5A of the viral genome showed variable mobility that is dependent on the cluster size of NS5A. The authors suggested that large and static clusters were representative of the replication complexes at the membranous webs. On the other hand, the smaller clusters displayed long-range mobility and saltatory movements at variable speeds along the network of microtubules [114].

As the last non-structural protein encoded in the viral genome, NS5B is the central catalytic component for HCV RNA replication and functions as a RNA-dependent RNA polymerase (RdRp). It is anchored at the ER membrane through its C-terminal transmembrane domain [115]. The finger, thumb, and palm subdomains, which are also common features of polymerases in other viruses, recognizes the negative-strand RNA as a template for RNA replication to generate the positive-strand [116]. Nucleotide triphosphates (NTPs) enter the active site by an alternative positively-charged tunnel [117].

More in depth on the molecule level of an HCV replication complex, the ratio of HCV proteins in comparison to positive and negative strand RNA was a >1000-fold in excess [118]. Of this, only a fraction of total processed non-structural proteins expressed within a cell are involved in RNA replication. It is estimated that a few hundred copies of non-structural proteins, one negative-strand HCV RNA, and two to ten copies of positive-strand HCV RNA are found within one single replication complex [118].

Host lipids that support viral replication

Intracellular host lipids are obligate factors that are required in almost every step of the HCV lifecycle [2]. For replication, the host lipidome is largely diverted by infection to support the integrity of the viral replication complexes, as well as, post-translationally modulate replicase viral proteins that facilitate HCV replication. In particular, HCV infection induces higher lipogenesis, silences compensatory mechanisms that are regularly active during a homeostatic response due to an accumulation of lipids, and retains lipid accumulation by preventing its export out of the cell [119-121]. Gene expression profiles of infected chimpanzees demonstrate a marked increase in expression of lipid metabolic genes [122]. Depending on the genotype, specific polymorphisms encoded in viral proteins are responsible for differential magnitudes in lipid up-regulation [123]. Importantly, HCV induced lipid accumulation is the result of *de novo* biosynthesis of cholesterol and fatty acids [122, 124] [120]. Specifically, saturated and monounsaturated fatty acids (MUFAs) have proven to be proviral, while polyunsaturated fatty acids (PUFAs) are unfavourable for HCV replication [124]. The authors of these findings describe that the benefits and consequences are related to differential degrees of fatty acid unsaturation that may be required to maintain a suitable level of membrane fluidity [124]. As such, host lipids may contribute to the biophysical properties that are required to generate replication complexes by modifying membranes of the ER that ultimately form an array of web-like membranous structures (Schematic 1.3; altered membranes are discussed more in detail in chapter 5) [124]. On the other hand, PUFAs affect the hydrophobic packing of ER membranes and in turn disrupt

membrane integrity [124]. Since HCV is highly dependent on host lipids, the use of statins such as fluvastatin (Schematic 1.5 D), has shown to be antiviral against HCV replication [125]. Statins are small molecule inhibitors that target 3-hydroxy-3-methyl-glutaryl-CoA (HMG-CoA) reductase, which is the rate-limiting step of cholesterol biosynthesis [126]. The products of HMG-CoA reductase include sterol intermediates involved in viral protein prenylation required for replication. For example, an F-box protein, FBL-2, was shown to be a crucial host factor that is prenylated by a geranylgeraniol lipid anchor and this post-translational modification is required to be both membrane bound, as well as, bound to NS5A at the replication sites [127, 128]. The complex formed between FBL-2 and NS5A on the membrane is required for RNA replication. By contrast, farnesol biogenesis, which is also linked on the same mevalonate pathway as geranylgeraniol biosynthesis and involved in protein prenylation of cellular proteins, showed no effects on enhancing HCV replication [127].

The architecture and composition of the HCV replication complexes is critical for replication. They assemble on lipid rafts that take place in the golgi, and also on subcellular membranous lipid compartments at the ER [105, 129, 130]. This was revealed when viral RNA at these membranous compartments, closely associated with LDs, was resistant to nucleases in the cytoplasm but failed to be resistant in the presence of a non-ionic detergent, nonident P-40 [130]. Additionally, the authors demonstrated that when non-structural proteins located only on the cytosolic face were solubilized by proteinase K treatment, the viral RNA remained intact [130]. Sphingolipids and cholesterol are abundant at these lipid rafts [131]. An inhibitor that targets serine palmitoyltransferase, which is required for sphingolipid synthesis, caused a decrease in HCV replication and disrupted the localization of NS5B, without altering the location other non-structural proteins [131]. A follow-up study identified that, of the abundant intracellular sphingomyelin derivatives, the molecular species of *d*18:1-16:0 and *d*18:1-24:0 (classification represents the number of carbons and unsaturations) are predominant in these HCV-induced lipid rafts [132].

The aforementioned examples have illustrated selective host proteins and lipids that are differentially regulated under HCV infection. Several attempts were made to identify lipid kinases in

the human kinome that are HCV dependent by using RNA interference (RNAi) screens for several HCV models [133, 134]. One study included a genomic wide screen using a library containing 21,093 small-interfering RNAs (siRNAs), and identified, consistent with other studies, a phosphatidylinositol (PI) 4-kinase (PI4K) that converts PI to PI-4-phosphate, to be an important factor for HCV replication [134, 135]. Predominantly localized at the ER, the silencing of PI4K was shown to significantly inhibit viral replication [136]. Also known as PI4KIIIα, which is the only kinase within its class amongst three other kinases that also synthesize PI4P, was found to be selective for HCV replication [137]. The first hypothesized role that suggested that PI4KIIIα is required at the replication complexes was elucidated when immunofluorescence imaging identified that PI4KIIIα colocalized with NS5A [138]. By contrast, silencing PI4KIIIα produced an abnormal NS5A clustering and localization. Electron microscopy further confirmed the presence of these abnormal NS5A clusters suggesting that the activity of PI4KIIIα, which was rescued by overexpression of active wt-PI4KIIIα but not its inactive mutant, has a role in maintaining the integrity of NS5A at replication complexes [136]. Notably, this was further supported by observations that the product of PI4KIIIα activity, PI4P, is also localized at these replication complexes, and that PI4Ps may structurally contribute to physical membrane properties required for efficient HCV replication [136].

Host factors that support the complexes of viral replication

This following section now shifts the focus towards host-virus interactions that are independent of the lipid biosynthetic pathway. As such, host-viral interacting partners that are also representative candidates as targets for pharmaceutical intervention are pertinently described (Table 1.1 & Schematic 1.3, inset 1). Among the host factors is a human vesicle-associated membrane protein-associated protein of 33 kDa (hVAP-33) that, in the absence of infection, normally aids in synaptic vesicles and plasma membrane fusion [139]. In HCV, hVAP-33, alternatively known as hVAP-A, complexes with NS5A and NS5B and has been suggested to be involved in the structural formation of the viral replication complexes [140, 141]. Concomitantly, inhibiting hVAP-33 with small

Host Protein	Influence on HCV replication
microRNA-122 [143, 144]	Enhances and regulates translation of viral RNA
Cyclophilin A and B [145-148]	Interacts with NS5A and NS5B and is required for replication
Hsp90 [149]	Essential co-factor for stabilizing the NS3 helicase domain and interacts with NS5A by forming a complex with FKBP8
FKBP8 [150, 151]	Binds to NS5A and Hsp90 and is required for replication
hVAP-33 [141]	Interacts with both NS5A and NS5B and is necessary for efficient replication
FBL-2 [127]	Geranylgeranylated F-box protein that is required for replication by binding to NS5A
PI4KIIIα [136, 138]	Binds to NS5A and phosphorylates PIP to PI4P, which is a phospholipid substrate required for stabilizing replication complexes
Rab5 [152]	Interacts with NS4B and plays a functional role in HCV RNA synthesis
Sphingomyelin [131]	Enhances replication by binding to NS5B
SYNCRIP [153]	Increases replication by binding to HCV RNA
CES1 [154]	Lipid enzyme that loads triglycerides into LDs at the replication complexes

Table 1.1: Host factors involved in HCV replication.

Abbreviations: Hsp90: Heat shock protein 90; FKBP8: FK506-binding protein 8; hVAP-33: Human vesicle-associated membrane protein-associated protein of 33 kDa; PI4KIIIα: Phosphatidylinositol 4-kinase type IIIα; SYNCRIP: Synamptotagmin-binding, cytoplasmic RNA-interacting protein; CES1: Carboxylesterase 1.

interfering RNA (siRNA) negatively affects HCV replication [141]. By suppressing the function of hVAP-33, NS5B had dispersed away from replication complexes, which suggests that proper anchoring of NS5B at sites of replication is dependent upon hVAP-33 [141]. Moreover, an additional isoform among the VAP proteins, VAP-B, was identified to form heterodimers with hVAP-A, and

that this interaction was required for HCV replication [142]. Interestingly, binding between hVAP-33 and NS5A, and RNA replication are restricted by the hyperphosphorylated state of NS5A [113].

Replication is also known to be affected by liver specific microRNAs. These are non-coding RNAs with a size between 21-23 nucleotides in length [143]. Mammalian microRNAs are well-known for their involvement in repressing genes by binding to the 3'UTR region of messenger RNAs. Its role in HCV, however, has been shown that when a liver specific microRNA-122 is a bound to the 5'UTR end, its binding stimulates HCV translation and replication [143, 144].

Heat shock proteins (hsp) are also critical in HCV replication. Hsps are molecular chaperone proteins mainly required for proper folding and stability of newly synthesized proteins. In one study, co-immunoprecipitation identified both heat shock cognate 70 (hsc70) and heat shock protein 72 (hsp72) as NS5A interacting partners [155]. The participatory roles in replication for the former are less clear, however, the latter protein is involved in either stabilizing more replicase viral components within the replication complexes, or potentially increase the translational efficiency as shown by enhancement of IRES mediated activity [155]. This mechanism was supported by observing the accumulation of viral proteins concentrated in the replication complexes, detected by immunofluorescence upon hsp72 overexpression [155]. Together, the chaperone activity by both families may be required to enhance proper folding of rapidly synthesized viral proteins during HCV infection to avoid a build-up of improperly folded viral proteins. As an additional co-chaperone, heat shock protein 90 (hsp90) was identified to play a role in HCV when bound to NS3 [149]. Despite that it is a clear NS3 binding partner, it also controls for preferential degradation of NS3 [149]. Inhibitors that target hsp90 resulted in decreased NS3 protein levels without perturbation of other HCV non-structural proteins [149]. At the same time, knockdown and inhibition of hsp90 by siRNAs and small molecule inhibitors in HCV-infected chimeric mice also showed dose-dependent suppression of HCV replication [156]. Concomitantly, hsp90 was also identified to indirectly interact with NS5A through a homomultimer complex formed by FKBP8, which is a member of an FK506-binding protein family [150]. Also, mutations that affect hsp90's ability to bind to the FKBP8 complex also diminished RNA

replication without modifying FKBP8's interaction with NS5A [151]. Similar to hsp72's role in stabilizing newly synthesized viral proteins, the interaction between FKBP8 and NS5A's role in recruiting co-chaperone, hsp90, is likely required for similar stabilizing functions.

The preceding examples illustrate a list of important host-viral ectopic protein-protein interactions (Schematic 1.3). To further evaluate other viral dependent host-processes, enzymatic activity of host proteins is equally required for efficient HCV replication. Categorized as immunophilins, cyclophilins are peptidyl-prolyl cis-trans isomerases (PPIase) involved in the stereochemical conversion of prolyl peptide bonds at the primary amino acid level [145, 146, 157]. Cyclophilins are abundantly expressed in all tissues and are inhibited by nanomolar concentrations of cyclosporine A [158]. A change in protein conformation aided by cyclophilins is proposed to help assist cellular protein interactions [158]. There is circumstantial evidence illustrating that NS5A and NS5B are cyclophilin binding partners and that cyclophilins are required to modulate proper conformational changes of viral proteins [148, 159]. Because there are two cyclophilin isoforms, cyclophilin B (CyPB) emerged as a candidate for facilitating HCV RNA and NS5B interactions at the replication complexes [145]. On the other hand, cyclophilin A (CyPA) was shown to interact with NS5A [147, 148, 159, 160]. It is accepted that both cyclophilin isoforms A and B are active but do not necessarily play equal roles in HCV replication.

Viral particle assembly

HCV core protein and the lipid droplet

Models of viral particle assembly currently focus on regions of LD-associated ER membranes as the pivotal location for assembling the viral particle (Schematic 1.4). At this location, HCV core protein is predominantly responsible for influencing LD localization and dynamically recruits viral proteins that initiate the early stages of assembly [161, 162].

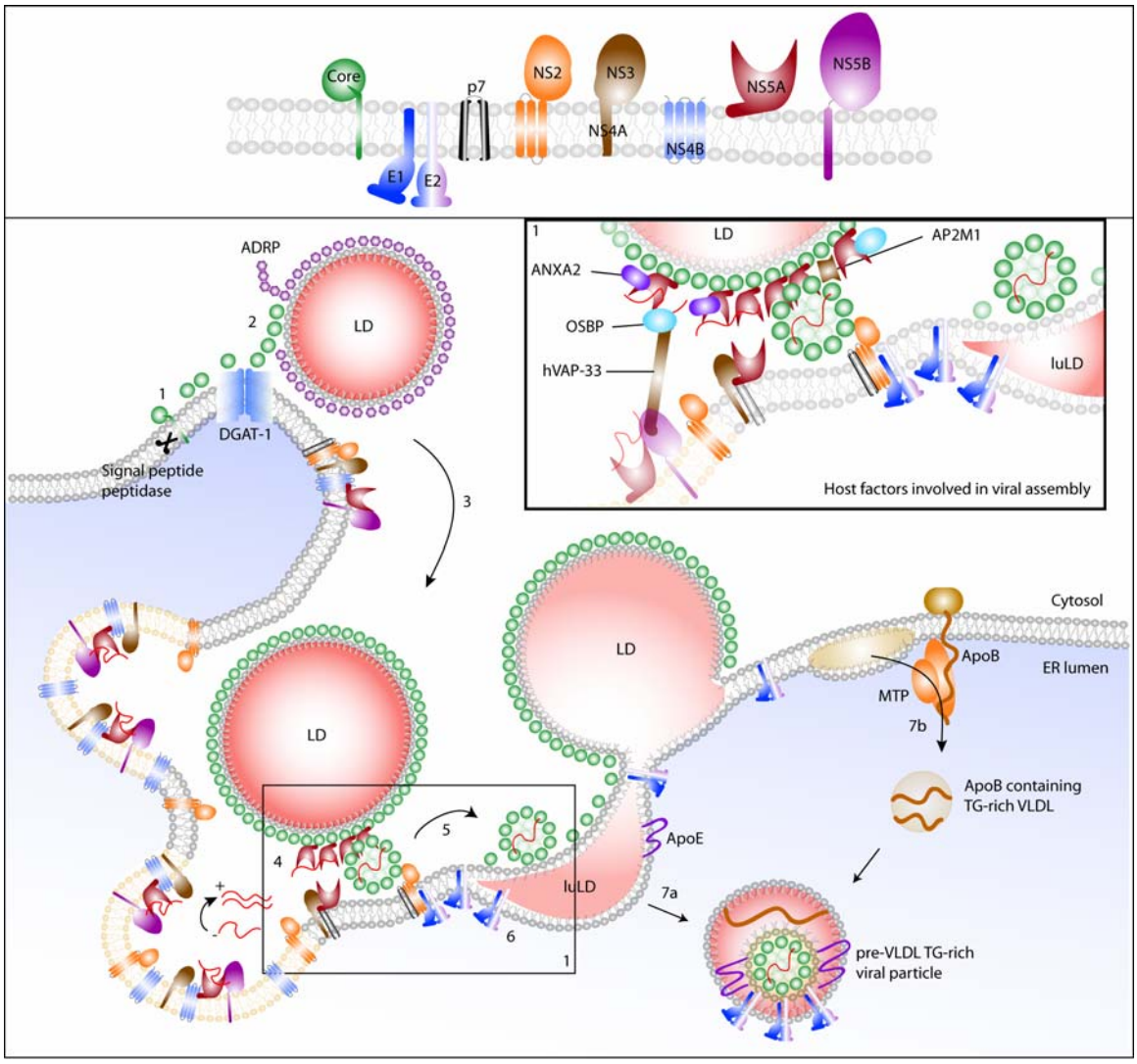

Schematic 1.4: Depicting critical steps in viral assembly. (1) Maturation of HCV core protein occurs via enzymatic cleavage by two host proteases. (2) Active DGAT-1 is required for core to bind to the LD surface. As core protein hijacks the LD surface, naïve LD-binding proteins, such as ADRP, are displaced. (3) Core induces LD localization to the perinuclear region of altered membranes where replication complexes are known to reside, effectively forming a LD-associated membrane environment tightly linked to the ER. (4) Binding between core and LDs is required to recruit NS5A to the surface of the LD and in turn, recruit viral RNA. Core-containing particles that represent the formation of the nucleocapsid that surrounds HCV viral RNA is formed by protein-protein interactions that involve NS3. (5) NS2 may orchestrate the final assembly stages by mediating the interaction of core-containing particles with (6) envelope proteins, E1 and E2, which form the shell of the viral particle. The late stages of budding and release involve the secretory pathway of VLDL. (7a) Luminal LDs (luLD) that comprise of TGs from cytoplasmic LDs may aid in the budding process of

the viral particle, meanwhile it is plausible that apoE is attached to the membrane at this site. (7b) An apoB-rich VLDL particle formed via enzymatic activity of MTP may further associate with the nascent viral particle to form a lipoviroparticle that requires further maturation in the golgi before it exits the cell. Inset 1 is a magnified portion of the assembly site and provides a greater in-depth view that includes host factor proteins that interact with viral proteins required to facilitate viral assembly. Overlapping of host and viral proteins are modeled to depict direct interactions, respectively. Refer to Table 1.2 for host protein abbreviations. VLDL: very-low density lipoproteins; ER: Endoplasmic reticulum; DGAT-1: Diacylglycerol acyltransferase 1; ADRP: Adipose differentiation-related protein; MTP: Microsomal triglyceride transfer protein; apoB/E: apolipoprotein A/E; TG: Triglyceride.

Previously identified as a benign storage organelle, the LD has increasingly been shown to contain greater functional roles and has gained attention by its involvement in many host cell functions that include signaling, membrane organization, and trafficking [163-165]. Lipids that form the LD are also important for protein prenylation, membrane fatty-acyl chains, and rich energy sources upon catabolism [166-168]. *De novo* LD biosynthesis occurs in the ER and its late stages are linked to the activities of diacylglycerol acyltransferase 1 (DGAT-1), DGAT-2, and acetyl-CoA acyltransferase (ACAT) enzymes, whereby DGAT-1 catalyzes the last step of triglycerides (TGs) by linking individual fatty acids to glycerol backbones, while ACAT is involved in esterifying cholesterol intermediates by converting the sterol to a neutral form (Regulation of these pathways is further discussed in chapter 3) [164, 167-169]. Together, TGs and cholesterol esters make up the bulk of neutral lipids stored in the inner core of the LD [163, 164]. Its formation is orchestrated by the build-up of neutral lipids between the cytosolic and luminal ER bilayer [170, 171]. A nascent LD organelle is then generated when the build-up of neutral lipids in the ER bilayer bud towards the cytosolic leaflet, which then extracts only the cytosolic phospholipids of the bilayer [170, 171]. Consistent with this, the outer layer of the LD is comprised of a phospholipid monolayer. These organelles, which range from 1-100 μm as detected by electron microscopy, are also surrounded by LD binding proteins, known as the PAT

family of proteins. They consist of perilipin, adipose differentiation-related protein (ADRP), and tail-interacting protein 47 (TIP47) [172, 173]. Generally, these proteins are required to maintain the integrity of the LD, facilitate cellular signaling interactions, and control the access of metabolic enzymes for oxidation [172, 173]. More than 200 mammalian LD-associated proteins have been identified, including soluble N-ethylmaleimide-sensitive factor attachment protein receptors (SNAREs), which are required for LD fusion [174]. These reasons strongly highlight that the dynamic nature of these organelles are simply far from being static [173].

Supported by multiple independent studies, evidence has shown that HCV assembly strongly requires core protein bound-LDs localized directly or juxtaposed to regions of viral particle assembly [13, 77, 175-177]. To illustrate this, for example, sphere-like particles representing HCV lipoviroparticles that contain HCV RNA, core protein, triglycerides, and apolipoproteins, have been found close in proximity to LDs [13]. Moreover, the HCV RNA minus and plus-strands were also found localized close to LDs suggesting that HCV replication complexes also localize to LDs [13]. Additionally, a rich source of TGs involved in the assembly of VLDL particles are extracted by luminal LDs that is, in part, derived from cytosolic LDs (Schematic 1.4). While core protein may also be located at the ER, the assembly of the nucleocapsid is likely derived from the population of core protein bound to LDs (discussed more in detail in the next section). This was illustrated when mutations that abolished core protein's ability to bind to LDs, also abrogated viral assembly [73, 77]. Furthermore, an active DGAT-1 is also required for core to translocate from the ER to LDs [178]. Cell culture studies demonstrated that DGAT-1, but not its alternative isoform, DGAT-2, strongly binds to core protein as observed by co-immunoprecipitation studies. Abolishing the activity of DGAT-1 prevents core localization to the LD and significantly impaired the production of infectious virus (Schematic 1.4, steps 1-2) [178]. Despite inhibiting the activity of DGAT-1, core protein remained bound to the enzyme, suggesting that active DGAT-1 is required to release core from the ER to the LD surface [178].

A combination of viral and host proteins facilitate viral particle assembly

It is becoming clearer that viral proteins, once thought to play an exclusive role for a single step in the viral lifecycle, are multifunctional across multiple stages. This has largely increased the complexity of current models of assembly. For example, data has shown that non-structural proteins required for replication and excluded from the structure of the viral particle are required for the assembly process [14]. For simplicity, before we include the details by which non-structural proteins were uncovered to be involved in assembly, there are general observations that occur sequentially [15]. First, LDs that play a crucial role in assembly are recruited, once bound to the mature form of core protein, towards areas of replication and assembly (Schematic 1.4, steps 1-3). Secondly, NS5A proteins are recruited to sites of core bound to LDs, creating a favourable core, NS5A, and LD complex (Schematic 1.4, step 4). Thirdly, core-containing intracellular particles with encapsulated HCV RNA (nucleocapids) are brought to sites of assembly (Schematic 1.4, step 5). Fourth, it is clear that core-containing intracellular particles must interact with envelope glycoproteins, E1 and E2, in order to form the viral particle (Schematic 1.4, step 6). Additionally, the budding and release of viral particles involves the secretory pathway by which lipoproteins are normally cleared from the liver. While the general steps in viral assembly are clear, the following sections will focus on uncovering the specific roles by which non-structural proteins aid in the transitioning between these steps. Further, in order to better provide a fundamental understanding of the mechanism of assembly, I show how non-structural proteins are also involved in the formation of the viral particle.

The interactions of HCV core, NS5A, and LDs are crucial for viral particle assembly

As previously discussed, viral assembly is managed by host and viral factors and is supported by LDs and their associated membranes at ER compartments. In agreement with the data, a core and LD association remains crucial and central to the initial stages of viral assembly. Once the core bound LD reaches the replication sites, it is logical that newly synthesized viral RNA must be transported

towards the core protein to initiate the formation of the nucleocapsid in which the viral RNA will be contained [15]. But before this occurs, NS5A is recruited to the core-bound LD surface to form a crucial complex between core, NS5A, and LDs that is required for assembly [13, 15]. In particular, domain III of NS5A is responsible for binding to core [13, 87]. In fact, mutations in domain I and III of NS5A that abolishes its interaction with core, subsequently abolishes further downstream recruitment of other non-structural proteins [13, 87]. A triple alanine substitution in the region of domain I of NS5A failed to recruit other non-structural proteins, indicating that this domain is responsible for subsequent viral protein interactions with NS5A [13]. Meanwhile, it has also been demonstrated that this critical interaction may also be dependent on the level of NS5A phosphorylation [112]. Taken together, the NS5A interaction with core-bound LDs initiates the recruitment of replicase viral proteins (NS4B & NS5B) in addition to NS3 and NS2 [13, 87, 179, 180]. This provides a plausible explanation by which newly synthesized HCV RNA is recruited to the surface of the core-bound LD via NS5A [13]. Nevertheless, at this stage in the assembly process, the complex formed by HCV RNA, NS5A and core -bound LDs is required to initiate assembly (Schematic 1.4, step 4).

Viral proteins NS2, NS3, and p7 aid in viral particle formation and budding

In the next stage of assembly, there are data to support that while p7, NS2, and NS3 are dispensable for viral replication, they are fundamental to virion assembly [80, 86, 181, 183]. NS3's unsuspecting role in assembly was first identified by using a cell-culture chimeric strain, HJ3, which contained genome segments from two different strains that were capable of producing infectious viral particles [30, 181]. This chimeric strain comprised of regions spanning core-NS2 from an H77c genotype 1a strain, and NS3-NS5B from JFH1 genotype 2a [30]. HJ3 was observed to contain deficiencies in the production of infectious viruses, unlike both its parental strains, although no shortcomings were demonstrated in viral replication [181]. Evidently, the association of core, NS5A and LDs remained intact in HJ3 expressing cells. However, a delay of infectious particles appeared 9 days post

transfection with HJ3, in comparison to JFH1, which produces infectious particles 2 days post transfection [181]. Upon sequencing the HJ3 genome once it was capable of producing infectious viruses after 9 days, the sequence revealed an appearance of a compensatory mutation at the Q221L position of NS3 [181]. This prompted Yi and colleagues to introduce Q221L into the parental HJ3 strain, and remarkably it produced infectious virus only 2 days post transfection [181]. Furthermore, core-containing intracellular particles (nucleocapsids) were not detected in the absence of this mutation [181]. It is plausible to suggest that NS3's role may participate at the initial step of assembly that allows nascent core-containing intracellular particles to be generated (Schematic 1.4, step 4) [181, 183, 184]. This is likely due to new protein-protein interactions initiated by a compensatory mutation at Q221L that rescued defective production of progeny infectious virus [181, 183].

With regard to p7, cell culture studies have demonstrated that mutations or full deletions of p7 in viral RNA genomes abolished the production of infectious particles [80, 185]. Consistently, p7 deletions in viral RNA mimicked these consequences in chimpanzees [186]. It has yet to be elucidated, however, whether its role in assembly is dependent on its viroporin capability or its direct cross-talk with other viral proteins [80, 185].

After the assembly of core-containing intracellular particles is complete, the next step in assembly has been shown to be highly dependent upon p7 and NS2 (Schematic 1.4, step 5) [80, 182, 185, 187]. Recently, core's redistribution from the LD surface to the ER was discovered to be mediated by the interaction of p7 and NS2, with the aid of additional host proteins [188]. Interestingly, a single serine mutation to glycine or alanine at position 168 of NS2 abolished the production of infectious viral particles, even though core-containing intracellular particles remained present (which was dependent on NS3 as previously discussed). The physiology of these core-containing intracellular particles in the presence of NS2 mutations is evidently similar to those produced by wild-type [184]. Moreover, NS2 was also observed to interact with both E1 and E2, ultimately forming a complex that includes p7 and NS3 (Schematic 1.4, steps 5-6) [86, 184]. Consistently, immunofluorescence studies illustrated that, in addition to E1 and E2, NS2 colocalized with NS5A, and was observed in close in proximity to core-

bound LDs [87]. For the complex involving core, NS5A, and LDs, mutations on NS5A that abolish phosphorylation rendered NS2 incapable of binding to NS5A, suggesting that phosphorylated NS5A plays a role in viral particle assembly [87]. It is possible that this interaction may be required to initiate the transfer of core-containing intracellular particles from the LD to the ER for the assembly (Schematic 1.4, step 5) [87]. This data provides a plausible mechanism by which NS2 is involved in bridging the gap between core-containing intracellular particles, NS5A, E1, and E2 proteins at the stage just prior to budding. Taken together, the evidence supports NS2's dynamic capability to initiate late stages of assembly by recruiting the intermediate core-containing intracellular particles containing HCV RNA to sites of E1 and E2 proteins (Schematic 1.4, steps 5-6). From these interactions at the apex of where the particle buds inwards to the ER lumen, the viral particle is then further matured via the VLDL secretory pathway (Schematic 1.4, steps 6-7) [15, 179, 180].

HCV hijacks the VLDL secretory pathway for viral particle release

There is a strong link between clearance of lipids through the VLDL secretory pathway in the liver, and HCV particle maturation and exit from the cell. Correspondingly, the circulating viral particle associates with VLDL particles to create a lower buoyant density particle that is higher in infectivity [26]. By contrast, in the absence of fusion with VLDL, the viral particle remains higher in buoyant density and has reduced infectivity, suggesting that the VLDL pathway enhances virion infectivity [189, 190]. The fusion mechanism between VLDLs and the viral particle are not well understood, however, it is clear that apolipoproteins (apo), apo E and apo B are included as part of the complete virion topology [191, 192]. In addition to the viral particle, VLDLs also require further maturation by incorporating with TGs, which may be derived by luminal LDs (Schematic 1.4, steps 7a & 7b) [193]. This is one plausible mechanism by which apoE is incorporated into the viral particle. On the other hand, it is hypothesized that apoB, which requires MTP activity and is derived away from the site of assembly, then fuses with the viral particle already containing apoE (Figure 1.4, step 7b) [194]. These observations were drawn together when it was shown that MTP activity was reported to

be a requirement for assembly, although other studies have indicated conflicting reports by demonstrating that MTP is dispensable; nevertheless, it is possible that these results may depend on the particular host that is being studied [192, 195, 196]. Moreover, it is clear that the viral particle is covered in a lipid-rich layer composed of cholesterol and sphingolipids that together enrich infectivity, and were independently isolated from HCV particles [197]. Nonetheless, it is accepted that the last step in the viral lifecycle is dependent upon VLDL, cholesterol, triglycerides, apoB, and apoE to orchestrate the maturation of the viral particle [190-192, 195].

Host proteins involved in assembly

Many viral and host protein-protein interactions at various steps in viral assembly have been identified (Table 1.2). Most protein-protein interactions were shown to be critical at the early stages of viral assembly by aiding the interactions of core, NS5A and the LD. Proteomic analysis identified an NS5A interacting host protein, Annexin A2, which is important within the inclusions of membranous webs [198]. Annexin A2 belong to a family of proteins that are Ca^{+}-dependent and binds to negatively charged phospholipids. These proteins recognize domains rich in cholesterol and specifically interacts with phosphatidylinositol-4,5-bisphosphate, and colocalizes with replication complexes as visualized by microscopy. From studies where Annexin A2 is knocked-down by siRNA, replication was not affected, but instead viral assembly process was altered [198]. This was concluded since low levels of infectious virus was detected in the supernatant, supported by low intracellular viral titres, suggesting that assembly rather than release was modulated upon Annexin A2 silencing [198].

A similar proteomics approach identified oxysterol binding protein (OSBP) as a host factor within ER altered replication complexes [199]. Its main function as a sterol sensor is to regulate cholesterol homeostasis, in part, by binding to hydroxycholesterol for transport to the golgi [199]. Interestingly, OSBP does not act alone and has many functions linked to other host obligate processes in HCV replication and assembly. For example, it binds to hVAP-33 [200], and contains binding sites

Host Protein	Influence on HCV viral assembly
MTP [192]	Participates in luLD formation and apoB transfer to form the viral particle
DGAT-1 [178]	Permits core localization to LDs and is required at the early stages of assembly
OSBP [199]	Binds VAP-A and NS5A and is involved in transport from ER to the golgi network for virion secretion
CKII [112]	Phosphorylates NS5A and regulates virion production
apoE and apoB [189, 204]	Apolipoproteins in pre-VLDL associated particles interact with the viral particle before further maturation in the golgi
ANXA2 [198]	Binds to domain III of NS5A and in turn may stabilize microdomains for virion morphogenesis
PKD [203]	Phosphorylates and controls activity of OSBP
AP2M1 [205]	Interacts with core protein at sites of assembly via phosphorylation by AAK1 and GAK

Table 1.2: Host factors involved in HCV viral assembly.

Abbreviations: MTP: Microsomal triglyceride transfer protein; DGAT-1: Diacylglycerol acyltransferase 1; OSBP: Oxysterol binding protein; CKII: Casein kinase II; apoE/B: apolipoproteins A/B; ANXA2: Annexin A2; PDK: Protein kinase D; AP2M1: adaptor-related protein complex 2 μ 1 subunit; AAK1: Adaptor-associated kinase 1; GAK: Cyclin G-associated kinase.

for PI4P [201]. OSBP was also demonstrated to bind to the N-terminal domain I of NS5A [199]. In addition, it is also involved in transporting ceramide to the golgi for *de novo* lipid biosynthesis of sphingomyelin and diacylglycerol, both of which are significant substrates important within the viral lifecycle [202]. Silencing OSBP showed partial inhibition of replication, but more significantly, impaired the release of virion secretion [199]. The authors further assessed this by using deleterious mutations at sites required for OSBP to localize at the golgi, which also impaired release of virions, suggesting that it may play a role in transporting pre-VLDL associated virions to the golgi for

maturation in the final stages of assembly. Furthermore, OSBP functions together with ceramide transfer protein at the golgi to enable transport of ceramide [203]. The same research group identified that protein kinase D (PKD) regulated the function of OSBP [203]. PKD is also involved in phosphorylating serine residues in both OSBP and ceramide transfer protein, attenuating their localization to the golgi, and in turn limit sphingomyelin biosynthesis [203]. By contrast, suppression of PKD rescued and enhanced the effects of HCV secretion [203]. Collectively, OSBP, which is controlled by PKD, is an important host protein that may provide a plausible link in facilitating direct or indirect interactions of pre-VLDL viral particles in the ER and its translocation towards the golgi where the viral particle is matured before exiting the cell.

Infectivity corresponds directly to viral particle density

Depending on the host from which the virus is derived, the viral particle varies in composition [14, 206]. For example, viral particles extracted from the plasma of infected patients range in density from 1.25g/mL to less than 1.06g/mL [25-27, 189, 190]. Within this range, lower density particles corresponded to several magnitudes greater in infectivity [207]. In addition to the viral proteins, core, E1, and E2, the composition of triglyceride rich viral particles also includes apoB, apoE, and in some cases apoC1-3 [189, 204, 208]. Viral particles derived from cultured human hepatoma cells have an average density of 1.14g/mL [209] and apoB has been found to be excluded in the lipoprotein portion of these viral particles [206 40 192]. Furthermore, when using a cell-culture strain to infect chimpanzees, viruses recovered from sustained infection, *in vivo,* was reported to be higher in infectivity than what is normally observed in cell-culture infectious models [209]. The buoyant density of these viral particles extracted from chimpanzees, on average, was calculated to be lower than 1.10 g/mL [209]. Taken together, these data suggest that HCV can exist as a lipo-viro-particle that is highly infectious.

Current Therapies for Treating HCV

Improving the standard of care: Emergence of the first generation of DAAs

Up until early 2011, the current standard of care for chronic HCV infections was a combination therapy that included peg-IFN combined with RBV. During this time, no other treatment alternatives existed, in spite of the fact that peg-IFN and RBV was burdened by high treatment costs, introduced lengthy therapy for a duration of up to 48 weeks, and induced adverse side effects that caused patients to voluntarily withdrawal from treatment [10]. Even so, the cure rate was approximately 50% measured by rates of sustained virologic response (SVR). Achieving a high SVR rate is a therapeutic goal and is reached when HCV RNA titer levels is undetected for 24 weeks after the end of treatment [210].

More recently, however, the first generation of approved direct-acting antivirals (DAAs) have improved SVR rates when combined with our current standard of care. They include peptidomimetic NS3-4A protease inhibitors boceprevir and telaprevir (Schematic 1.5 B & C). By comparison to when peg-IFN and RBV are administered alone, the addition of DAA's has significantly improved the SVR from 50% to approximately 67- 75% for genotype 1 [211, 212]. This achievement marks a significant milestone for HCV therapy. The triple treatment combination also shortens the duration of therapy to almost half the time length in comparison to the standard of care. Both telaprevir and boceprevir belong to linear ketoamide derivatives that bind the small active site, covalently, but reversibly [213]. In addition to linear protease inhibitors, macrocyclic inhibitors that also target the NS3-4A active site, but non-covalently, are currently being developed in clinical trials, and this includes danoprevir (Schematic 1.5 E) [214]. Examples of non-protease targets that are being developed in the clinic include nucleoside inhibitors (NIs) and non-nucleoside inhibitors (NNIs) that bind to the NS5B RdRp enzyme. NIs bind the catalytic active site that contains the typical palm, finger, and thumb region, by competing with nucleoside triphosphates that are incorporated into the growing HCV RNA chain [10]. Mericitabine is an example of an NI and is currently in clinical trials

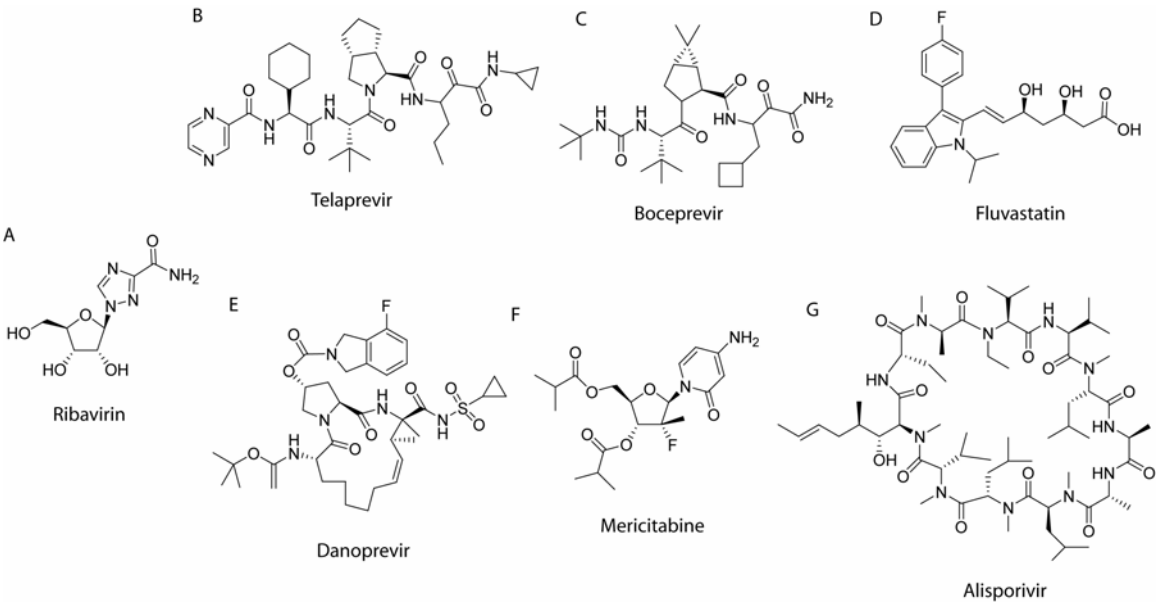

Schematic 1.5: Classes of small molecule inhibitors as therapeutics against HCV. (A) Non specific nucleoside inhibitor that is currently used in combination with Peg-IFN as the standard of care in HCV therapy. (B & C) First generation of direct-acting enzyme inhibitors that belong to ketoamide derivatives, target the NS3 protease. (D) Statin inhibitor that targets the rate-limiting step of cholesterol biosynthesis, HMG-CoA reductase, has demonstrated antiviral effects in clinical studies. (E) Macrocyclic class inhibitor targets NS3 protease, similar to (B & C). (F) Nucleoside inhibitor that targets NS5B RNA-dependent RNA polymerase is currently in clinical trials. (G) An analogue of cyclosporine A is used to target cyclophilins that are known to interact with NS5A and NS5B and functions as a peptide-peptidyl cis/trans isomerase. This compound is currently in Phase III of clinical trials.

(Schematic 1.5 F) [215]. By contrast, NNIs are involved in targeting adjacent regions other than the catalytic site and modulates conformational changes to the enzyme, which consequently blocks chain elongation [10]. NNI inhibitors, however, do not necessarily impede the activity of the enzyme and therefore confers to lower barrier of resistance [213].

Current limitations of DAAs

There are several reasons why targeting the host to treat HCV infections is a viable alternative. Some of which are stemmed by the drawbacks from the first generation of DAAs. Foremost, while the goal for HCV therapy is to eliminate peg-IFN and RBV from our current treatment regiments, the newly approved DAAs must be used in combination because they possess low genetic barrier to resistance. For example, monotherapy with telaprevir showed that resistant viruses quickly emerged within 14 days of treatment [216]. Most strikingly, monotherapy introduces the emergence of single amino acid mutations in viral RNA, escape mutants, that are highly resistant without a detrimental cost to viral fitness [217]. Of such, the sequence of emerging resistant strains is primarily caused by independent single and double mutations that conferred low and high resistance against telaprevir [217, 218]. These consistent reoccurring mutations enable them to be predictable in drug resistance [217, 218]. Thus, patients who cannot tolerate of peg-IFN and RBV treatments have no other options, and cannot be supplemented with DAA monotherapy due to the risk of sequestering highly drug-resistant genomes. Additionally, the harsh side effects encountered by DAAs add to the side effects already observed with peg-IFN and RBV [9]. These factors, although not exclusively, are unfavourable for patients, whom may perceive that the long-term benefits of treatment may not outweigh the immediate adverse effects, which can lead to the risk of treatment withdrawal. Moreover, the DAAs that were originally tailored against genotype 1 are variably effective across all genotypes [219]. The geographical population of those infected with genotype 1 is largely isolated to North America and parts of Europe, limiting DAAs capacity to be an effective global therapeutic option [6]. These reasons alone are circumstantial in attracting the search for therapeutics that is better suited against HCV. As previously mentioned, a strategy to effectively manage these problems is to target the host as an alternative therapeutic regiment. The goal is to decrease the resistance and increase cross-genotype potency. Conceivably, by targeting important viral dependent host interactions, the barrier to develop mutations to compensate for the change in the host is rather more

difficult for the virus to adapt to, rather than relying on mutations within its own viral genome. By moving away from peg-IFN and RBV therapy, targeting the host is an appealing option as a potential monotherapeutic intervention, or viable as a co-treatment regiment with DAAs. Expanding more options for therapy is still needed. While the current focus for novel inhibitors in the expanding drug pipeline are DAAs, it is attractive to shift focus towards identifying targets that disrupt host-virus interactions.

Viral-dependent host proteins are valid host targets

Amongst an expanding list of host factors involved in the HCV lifecycle, novel inhibitors at the clinical level that currently target these factors include host cyclophilins (CyPs) [220]. A direct CyP binding small molecule, Debio-025 (Schematic 1.5 G, Alisporivir), which is currently in phase III clinical trials, has shown potent antiviral activity with a high barrier of viral resistance [160, 221]. At the early stages in elucidating CyPs as host targets, inhibitors that suppressed its function were determined to be potent HCV inhibitors in *in vitro* and *in vivo* studies. This prompted further assessment to identify the synergism between Debio-025 with current therapies [221, 222]. While CyPs represent effective targets, it is unknown which CyP isoform, CyPA or CyPB, is responsible for conferring antiviral effects. CyPA binds to NS5A, and CyPB binds to NS5B [145, 146, 223], and both isoforms have been shown to be equally important for HCV replication [145, 223]. As a prominent therapeutic, human trials with Debio-025 was first conducted in co-infected HCV/HIV-1 patients [224]. CyPA is an important co-factor for HIV replication and interacts with the HIV viral capsid protein and HIV replication is also inhibited by Debio-025 treatment *in vitro* [225]. Its ability to potentially target both viruses is novel when considering the fact that nearly one-third of those infected with HIV in the United States are co-infected with HCV, bringing a total of approximately 7 million people harbouring both infections [226]. The result in treating co-infected patients during a 14-day oral treatment study demonstrated a large reduction in HCV viral loads that was observed across all three

genotypes tested (genotypes 1, 3, and 4) and remarkably, no rebounds in HCV RNA levels was detected [224]. In this trial, however, due to the inability to measure changes in intracellular CyPA levels, it was undetermined whether antiviral effects were dependent on its action against CyPA or CyPB, although CyPB levels were shown to be reduced [224]. Similarly, a follow-up clinical study conducted by the same research group investigated potential synergism effects across genotypes 1-4 with the addition of peg-IFNα [227]. Debio-025 monotherapy induced antiviral effects comparable to when peg-IFNα 2a was administered alone, and this was effective across the genotypes tested [227]. On the other hand, when administered in combination with peg-IFNα 2a, a synergy effect that reduced viral levels was reported [227]. The number of patients showing reduced HCV levels to below the limit of HCV RNA detection increased 2-fold and side effects were limited to those typically caused by peg-IFNα 2a [227]. The potency of Debio-025 when combined with a DAA was also evaluated. Based on this evaluation, *in vitro* studies observed a synergistic effect when Debio-025 was co-administered with either telaprevir or other DAA inhibitors [228]. Remarkably, when predicted resistant replicons common to DAAs emerged, mono-treated Debio-025 remained active against these resistance replicons [228]. Furthermore, low concentrations of Debio-025 combined with telaprevir delayed the development of resistant genomic mutations that are commonly observed by telaprevir monotherapy [228]. However, Debio-025 could also induce resistant viruses. Although the development of resistant replicons against Debio-025 was difficult and slow to emerge, nevertheless, Coelmont *et al*. reported that a single amino acid mutation at the CyPA binding sites of domain II of NS5A was responsible for resistance to Debio-025 [160]. This reported mutation (D230E) required an average of 20 weeks for resistant strains to emerge. By contrast, resistant strains emerged as early as two weeks with DAA treatment [160].

Further assessing the relationship between CyPA and NS5A, it was hypothesized that Debio-025's antiviral activity interfered with CyPA's isomerase activity to induce a proper conformational change of domain II of NS5A, and as a result, this region of NS5A can no longer interact with NS5B at their co-binding sites as required for replication [160]. Moreover, structural analysis of domain II in

NS5A in the resistant stain (D230E) showed a dominant trans configuration that is unusual in the wild-type (wt) [160]. By comparison, the wt conformer normally contains a dominant cis configuration that is otherwise dependent on CyPA's activity to convert it to the less dominant trans conformer [160]. In this case, the resistant strain to Debio-025 is less dependent on the isomerase activity of CyPA. Because the virus requires a mutation that renders it less dependent on the host, this may explain, in part, Debio-025's higher barrier of viral resistance. Taken together, Debio-025 represents an active candidate that holds promise for the development of other host-targeted antivirals. This focus can amend the strategy by which therapy is tailored against HCV [9, 220].

Inhibitors of microRNA-122 is currently a target for therapy undergoing phase I studies in chimpanzees. Miravirsen (SPC3649) is a locked nucleic acid that sequesters microRNA-122 [229]. The remarkable potency of microRNA-122 inhibition was observed when microRNA-122 suppression in chimps infected with chronic HCV showed prolonged suppression of viraemia [229].

For host lipid enzymes involved in viral assembly, DGAT-1 remains a prominent host target. HCV Core protein is required to localize onto LDs as a mechanism of recruiting these LDs towards replication complexes and sites of assembly, and because this is dependent on active DGAT-1, inhibiting its activity will hinder the early stages of viral assembly. Prominently, Herker *et al.* demonstrated that a small molecule inhibitor that targets DGAT-1 showed a promising reduction in the assembly of infectious virions [178]. Further studies are required to evaluate DGAT-1 as a potential clinical therapeutic.

There is an urgent need to broaden the scope of alternative HCV therapeutics by focusing on relevant host lipid metabolic pathways that, in the future, can be co-administered with DAAs and move towards the elimination of peg-IFN and RBV treatments. Along this line, the administered combination of statins with DAAs that independently target different viral and host processes was reported to induce a synergistic anti-HCV effect [127, 230-232]. Addressing viral-dependent associated pathways is suitable for intervention and can raise the barrier of viral resistance. Although DAAs hold dominance amongst the arsenal of drugs in the current clinical therapeutic pipeline, these

therapies can be optimized by adopting research efforts to uncover the biology of host-virus interactions and shift focus in developing inhibitors of these host targets.

References

1. Randall, G.; Panis, M.; Cooper, J. D.; Tellinghuisen, T. L.; Sukhodolets, K. E.; Pfeffer, S.; Landthaler, M.; Landgraf, P.; Kan, S.; Lindenbach, B. D.; Chien, M.; Weir, D. B.; Russo, J. J.; Ju, J.; Brownstein, M. J.; Sheridan, R.; Sander, C.; Zavolan, M.; Tuschl, T.; Rice, C. M., Cellular cofactors affecting hepatitis C virus infection and replication. *Proc. Natl. Acad. Sci. U. S. A.* **2007**, 104, 12884-12889.

2. Syed, G. H.; Amako, Y.; Siddiqui, A., Hepatitis C virus hijacks host lipid metabolism. *Trends Endocrinol. Metab.* **2010**, 21, 33-40.

3. Wise, M.; Bialek, S.; Finelli, L.; Bell, B.; Sorvillo, F., Changing trends in hepatitis C-related mortality in the United States, 1995-2004. *Hepatology* **2008**, 47, 1128-1135.

4. Tang, H.; Grisé, H., Cellular and molecular biology of HCV infection and hepatitis. *Clin. Sci.* **2009**, 117, 49-65.

5. Lavanchy, D., Evolving epidemiology of hepatitis C virus. *Clin. Microbiol. Infect.* **2011**, 17, 107-115.

6. Gravitz, L., Introduction: A smouldering public-health crisis. *Nature* **2011**, 474, S2-S4.

7. Simmonds, P.; Bukh, J.; Combet, C.; Deléage, G.; Enomoto, N.; Feinstone, S.; Halfon, P.; Inchauspé, G.; Kuiken, C.; Maertens, G.; Mizokami, M.; Murphy, D. G.; Okamoto, H.; Pawlotsky, J.-M.; Penin, F.; Sablon, E.; Shin-I, T.; Stuyver, L.; Thiel, H.-J.; Viazov, S.; Weiner, A.; Widell, A., Consensus proposals for a unified system of nomenclature of hepatitis C virus genotypes. *Hepatology* **2005**, 42, 962-973.

8. Moradpour, D.; Penin, F.; Rice, C., Replication of hepatitis C virus. *Nat. Rev. Microbiol.* **2007**, 5, 453-463.

9. Salloum, S.; Tai, A., Treating hepatitis C infection by targeting the host. *Transl. Res.* **2012**, 159, 421-429.

10. Thompson, A.; McHutchison, J., Antiviral resistance and specifically targeted therapy for HCV (STAT-C). *J. Viral Hepat.* **2009**, 16, 377-387.

11. Susser, S.; Vermehren, J.; Forestier, N.; Welker, M. W.; Grigorian, N.; Füller, C.; Perner, D.; Zeuzem, S.; Sarrazin, C., Analysis of long-term persistence of resistance mutations within the hepatitis C virus NS3 protease after treatment with telaprevir or boceprevir. *J. Clin. Virol.* **2011**, 52, 321-327.

12. Susser, S.; Welsch, C.; Wang, Y.; Zettler, M.; Domingues, F. S.; Karey, U.; Hughes, E.; Ralston, R.; Tong, X.; Herrmann, E.; Zeuzem, S.; Sarrazin, C., Characterization of resistance to the protease inhibitor boceprevir in hepatitis C virus–infected patients. *Hepatology* **2009**, 50, 1709-1718.

13. Miyanari, Y.; Atsuzawa, K.; Usuda, N.; Watashi, K.; Hishiki, T.; Zayas, M.; Bartenschlager, R.; Wakita, T.; Hijikata, M.; Shimotohno, K., The lipid droplet is an important organelle for hepatitis C virus production. *Nat. Cell Biol.* **2007**, 9, 1089-1097.

14. Popescu, C.-I.; Rouillé, Y.; Dubuisson, J., Hepatitis C virus assembly imaging. *Viruses* **2011**, 3, 2238-2254.

15. Jones, D.; McLauchlan, J., Hepatitis C virus: assembly and release of virus particles. *J. Biol. Chem.* **2010**, 285, 22733-22739.

16. Pegoraro, A. F.; Ridsdale, A.; Moffatt, D. J.; Jia, Y.; Pezacki, J. P.; Stolow, A., Optimally chirped multimodal CARS microscopy based on a single Ti:sapphireoscillator. *Opt. Express* **2009**, 17, 2984-2996.

17. Pezacki, J. P.; Blake, J. A.; Danielson, D. C.; Kennedy, D. C.; Lyn, R. K.; Singaravelu, R., Chemical contrast for imaging living systems: molecular vibrations drive CARS microscopy. *Nat. Chem. Biol.* **2011**, 7, 137-145.

18. Evans, C. L.; Potma, E. O.; Puoris'haag, M.; Côté, D.; Lin, C. P.; Xie, X. S., Chemical imaging of tissue in vivo with video-rate coherent anti-Stokes Raman scattering microscopy. *Proc. Natl. Acad. Sci. U. S. A.* **2005**, 102, 16807-16812.

19. Bassendine, M. F.; Sheridan, D. A.; Felmlee, D. J.; Bridge, S. H.; Toms, G. L.; Neely, R. D. G., HCV and the hepatic lipid pathway as a potential treatment target. *J. Hepatol.* **2011**, 55, 1428-1440.

20. Perz, J. F.; Armstrong, G. L.; Farrington, L. A.; Hutin, Y. J. F.; Bell, B. P., The contributions of hepatitis B virus and hepatitis C virus infections to cirrhosis and primary liver cancer worldwide. *J. Hepatol.* **2006**, 45, 529-538.

21. Zou, S.; Tepper, M.; El Saadany, S., Prediction of hepatitis C burden in Canada. *Can. J. Gastroenterol.* **2000**, 14, 575-580.

22. Forman, L.; Lewis, J.; Berlin, J.; Feldman, H.; Lucey, M., The association between hepatitis C infection and survival after orthotopic liver transplantation. *Gastroenterology* **2002**, 122, 889-896.

23. Lohmann, V., Replication of subgenomic hepatitis C virus RNAs in a hepatoma cell line. *Science* **1999**, 285, 110-113.

24. Blight, K.; Kolykhalov, A.; Rice, C., Efficient initiation of HCV RNA replication in cell culture. *Science* **2000**, 290, 1972-1974.

25. Wakita, T.; Pietschmann, T.; Kato, T.; Date, T.; Miyamoto, M.; Zhao, Z.; Murthy, K.; Habermann, A.; Kräusslich, H.-G.; Mizokami, M.; Bartenschlager, R.; Liang, T., Production of infectious hepatitis C virus in tissue culture from a cloned viral genome. *Nat. Med.* **2005**, 11, 791-796.

26. Lindenbach, B.; Evans, M.; Syder, A.; Wölk, B.; Tellinghuisen, T.; Liu, C.; Maruyama, T.; Hynes, R.; Burton, D.; McKeating, J.; Rice, C., Complete replication of hepatitis C virus in cell culture. *Science* **2005**, 309, 623-626.

27. Zhong, J.; Gastaminza, P.; Cheng, G.; Kapadia, S.; Kato, T.; Burton, D.; Wieland, S.; Uprichard, S.; Wakita, T.; Chisari, F., Robust hepatitis C virus infection in vitro. *Proc. Natl. Acad. Sci. U. S. A.* **2005**, 102, 9294-9299.

28. Zhong, J.; Gastaminza, P.; Chung, J.; Stamataki, Z.; Isogawa, M.; Cheng, G.; McKeating, J.; Chisari, F., Persistent hepatitis C virus infection in vitro: coevolution of virus and host. *J. Virol.* **2006**, 80, 11082-11093.

29. Delgrange, D.; Pillez, A.; Castelain, S.; Cocquerel, L.; Rouillé, Y.; Dubuisson, J.; Wakita, T.; Duverlie, G.; Wychowski, C., Robust production of infectious viral particles in Huh-7 cells by introducing mutations in hepatitis C virus structural proteins. *J. Gen. Virol.* **2007**, 88, 2495-2503.

30. Yi, M.; Ma, Y.; Yates, J.; Lemon, S., Compensatory mutations in E1, p7, NS2, and NS3 enhance yields of cell culture-infectious intergenotypic chimeric hepatitis C virus. *J. Virol.* **2007**, 81, 629-638.

31. Bowen, D. G.; Walker, C. M., Adaptive immune responses in acute and chronic hepatitis C virus infection. *Nature* **2005**, 436, 946-952.

32. Vachon, M.-L.; Dieterich, D., The era of direct-acting antivirals has begun: the beginning of the end for HCV? *Semin. Liver Dis.* **2011**, 31, 399-409.

33. Tsukiyama-Kohara, K.; Iizuka, N.; Kohara, M.; Nomoto, A., Internal ribosome entry site within hepatitis C virus RNA. *J. Virol.* **1992**, 66, 1476-1483.

34. Pezacki, J. P.; Singaravelu, R.; Lyn, R. K., Host-virus interactions during hepatitis C virus infection: a complex and dynamic molecular biosystem. *Mol. Biosyst.* **2010**, 6, 1131-1142.

35. Diamond, D.; Syder, A.; Jacobs, J.; Sorensen, C.; Walters, K.-A.; Proll, S.; McDermott, J.; Gritsenko, M.; Zhang, Q.; Zhao, R.; Metz, T.; Camp, D.; Waters, K.; Smith, R.; Rice, C.; Katze, M., Temporal proteome and lipidome profiles reveal hepatitis C virus-associated reprogramming of hepatocellular metabolism and bioenergetics. *PLoS. Pathog.* **2010**, 6, e1000719.

36. Helle, F.; Dubuisson, J., Hepatitis C virus entry into host cells. *Cell. Mol. Life Sci.* **2008**, 65, 100-112.

37. Blanchard, E.; Belouzard, S.; Goueslain, L.; Wakita, T.; Dubuisson, J.; Wychowski, C.; Rouillé, Y., Hepatitis C virus entry depends on clathrin-mediated endocytosis. *J. Virol.* **2006**, 80, 6964-6972.

38. Meertens, L.; Bertaux, C.; Dragic, T., Hepatitis C virus entry requires a critical postinternalization step and delivery to early endosomes via clathrin-coated vesicles. *J. Virol.* **2006**, 80, 11571-11578.

39. Ploss, A.; Evans, M., Hepatitis C virus host cell entry. *Curr. Opin. Virol.* **2012**, 2, 14-19.

40. Owen, D.; Huang, H.; Ye, J.; Gale, M., Apolipoprotein E on hepatitis C virion facilitates infection through interaction with low-density lipoprotein receptor. *Virology* **2009**, 394, 99-108.

41. Chung, N.; Wasan, K., Potential role of the low-density lipoprotein receptor family as mediators of cellular drug uptake. *Adv. Drug Deliv. Rev.* **2004**, 56, 1315-1334.

42. Agnello, V.; Abel, G.; Elfahal, M.; Knight, G.; Zhang, Q., Hepatitis C virus and other flaviviridae viruses enter cells via low density lipoprotein receptor. *Proc. Natl. Acad. Sci. U. S. A.* **1999**, 96, 12766-12771.

43. Scarselli, E.; Ansuini, H.; Cerino, R.; Roccasecca, R.; Acali, S.; Filocamo, G.; Traboni, C.; Nicosia, A.; Cortese, R.; Vitelli, A., The human scavenger receptor class B type I is a novel candidate receptor for the hepatitis C virus. *EMBO J.* **2002**, 21, 5017-5025.

44. Pileri, P.; Uematsu, Y.; Campagnoli, S.; Galli, G.; Falugi, F.; Petracca, R.; Weiner, A.; Houghton, M.; Rosa, D.; Grandi, G.; Abrignani, S., Binding of hepatitis C virus to CD81. *Science* **1998**, 282, 938-941.

45. Evans, M.; von Hahn, T.; Tscherne, D.; Syder, A.; Panis, M.; Wölk, B.; Hatziioannou, T.; McKeating, J.; Bieniasz, P.; Rice, C., Claudin-1 is a hepatitis C virus co-receptor required for a late step in entry. *Nature* **2007**, 446, 801-805.

46. Liu, S.; Yang, W.; Shen, L.; Turner, J.; Coyne, C.; Wang, T., Tight junction proteins claudin-1 and occludin control hepatitis C virus entry and are downregulated during infection to prevent superinfection. *J. Virol.* **2009**, 83, 2011-2014.

47. Burlone, M.; Budkowska, A., Hepatitis C virus cell entry: role of lipoproteins and cellular receptors. *J. Gen. Virol.* **2009**, 90, 1055-1070.

48. Harris, H.; Farquhar, M.; Mee, C.; Davis, C.; Reynolds, G.; Jennings, A.; Hu, K.; Yuan, F.; Deng, H.; Hubscher, S.; Han, J.; Balfe, P.; McKeating, J., CD81 and claudin 1 coreceptor association: role in hepatitis C virus entry. *J. Virol.* **2008**, 82, 5007-5020.

49. Harris, H.; Davis, C.; Mullins, J.; Hu, K.; Goodall, M.; Farquhar, M.; Mee, C.; McCaffrey, K.; Young, S.; Drummer, H.; Balfe, P.; McKeating, J., Claudin association with CD81 defines hepatitis C virus entry. *J. Biol. Chem.* **2010**, 285, 21092-21102.

50. Krieger, M., Scavenger receptor class B type I is a multiligand HDL receptor that influences diverse physiologic systems. *J. Clin. Invest.* **2001**, 108, 793-797.

51. Suzuki, T.; Ishii, K.; Aizaki, H.; Wakita, T., Hepatitis C viral life cycle. *Adv. Drug Deliv. Rev.* **2007**, 59, 1200-1212.

52. Bartosch, B.; Vitelli, A.; Granier, C.; Goujon, C.; Dubuisson, J.; Pascale, S.; Scarselli, E.; Cortese, R.; Nicosia, A.; Cosset, F.-L., Cell entry of hepatitis C virus requires a set of co-receptors that include the CD81 tetraspanin and the SR-B1 scavenger receptor. *J. Biol. Chem.* **2003**, 278, 41624-41630.

53. Bartosch, B.; Dubuisson, J.; Cosset, F. L., Infectious Hepatitis C Virus Pseudo-particles Containing Functional E1-E2 Envelope Protein Complexes. *J. Exp. Med.* **2003**, 197. 633-642.

54. Zeisel, M.; Koutsoudakis, G.; Schnober, E.; Haberstroh, A.; Blum, H.; Cosset, F.-L.; Wakita, T.; Jaeck, D.; Doffoel, M.; Royer, C.; Soulier, E.; Schvoerer, E.; Schuster, C.; Stoll-Keller, F.; Bartenschlager, R.; Pietschmann, T.; Barth, H.; Baumert, T., Scavenger receptor class B type I is a key host factor for hepatitis C virus infection required for an entry step closely linked to CD81. *Hepatology* **2007**, 46, 1722-1731.

55. Flint, M.; Thomas, J.; Maidens, C.; Shotton, C.; Levy, S.; Barclay, W.; McKeating, J., Functional analysis of cell surface-expressed hepatitis C virus E2 glycoprotein. *J Virol.* **1999**, 73, 6782-6790.

56. Sainz, B.; Barretto, N.; Martin, D.; Hiraga, N.; Imamura, M.; Hussain, S.; Marsh, K.; Yu, X.; Chayama, K.; Alrefai, W.; Uprichard, S., Identification of the Niemann-Pick C1-like 1 cholesterol absorption receptor as a new hepatitis C virus entry factor. *Nat. Med.* **2012**, 18, 281-285.

57. Goffard, A.; Dubuisson, J., Glycosylation of hepatitis C virus envelope proteins. *Biochimie* **2003**, 85, 295-301.

58. Tscherne, D.; Jones, C.; Evans, M.; Lindenbach, B.; McKeating, J.; Rice, C., Time- and temperature-dependent activation of hepatitis C virus for low-pH-triggered entry. *J Virol.* **2006**, 80, 1734-1741.

59. Marsh, M.; Helenius, A., Virus entry: open sesame. *Cell* **2006**, 124, 729-740.

60. Rosa, D.; Campagnoli, S.; Moretto, C.; Guenzi, E.; Cousens, L.; Chin, M.; Dong, C.; Weiner, A.; Lau, J.; Choo, Q.; Chien, D.; Pileri, P.; Houghton, M.; Abrignani, S., A quantitative test to estimate neutralizing antibodies to the hepatitis C virus: cytofluorimetric assessment of envelope glycoprotein 2 binding to target cells. *Proc. Natl. Acad. Sci. U. S. A.* **1996**, 93, 1759-1763.

61. Yagnik, A.; Lahm, A.; Meola, A.; Roccasecca, R.; Ercole, B.; Nicosia, A.; Tramontano, A., A model for the hepatitis C virus envelope glycoprotein E2. *Proteins* **2000**, 40, 355-366.

62. Lescar, J.; Roussel, A.; Wien, M.; Navaza, J.; Fuller, S.; Wengler, G.; Rey, F., The Fusion glycoprotein shell of Semliki Forest virus: an icosahedral assembly primed for fusogenic activation at endosomal pH. *Cell* **2001**, 105, 137-148.

63. Vieyres, G.; Thomas, X.; Descamps, V.; Duverlie, G.; Patel, A.; Dubuisson, J., Characterization of the envelope glycoproteins associated with infectious hepatitis C virus. *J. Virol.* **2010**, 84, 10159-10168.

64. Bukh, J.; Purcell, R.; Miller, R., Sequence analysis of the 5' noncoding region of hepatitis C virus. *Proc. Natl. Acad. Sci. U. S. A.* **1992**, 89, 4942-4946.

65. Lukavsky, P.; Otto, G.; Lancaster, A.; Sarnow, P.; Puglisi, J., Structures of two RNA domains essential for hepatitis C virus internal ribosome entry site function. *Nat. Struct. Biol.* **2000**, 7, 1105-1110.

66. Ji, H.; Fraser, C.; Yu, Y.; Leary, J.; Doudna, J., Coordinated assembly of human translation initiation complexes by the hepatitis C virus internal ribosome entry site RNA. *Proc. Natl. Acad. Sci. U. S. A.* **2004**, 101, 16990-16995.

67. Otto, G.; Puglisi, J., The pathway of HCV IRES-mediated translation initiation. *Cell* **2004**, 119, 369-380.

68. Chisari, F., Unscrambling hepatitis C virus-host interactions. *Nature* **2005**, 436, 930-932.

69. Takamizawa, A.; Mori, C.; Fuke, I.; Manabe, S.; Murakami, S.; Fujita, J.; Onishi, E.; Andoh, T.; Yoshida, I.; Okayama, H., Structure and organization of the hepatitis C virus genome isolated from human carriers. *J. Virol.* **1991**, 65, 1105-1113.

70. Hope, R.; McLauchlan, J., Sequence motifs required for lipid droplet association and protein stability are unique to the hepatitis C virus core protein. *J. Gen. Virol.* **2000**, 81, 1913-1925.

71. Boulant, S.; Vanbelle, C.; Ebel, C.; Penin, F., Hepatitis C virus core protein is a dimeric alpha-helical protein exhibiting membrane protein features. *J. Virol.* **2005**, 79, 11353-11365.

72. Hope, R.; Murphy, D.; McLauchlan, J., The domains required to direct core proteins of hepatitis C virus and GB virus-B to lipid droplets share common features with plant oleosin proteins. *J. Biol. Chem.* **2002**, 277, 4261-4270.

73. Boulant, S.; Montserret, R.; Hope, R.; Ratinier, M.; Targett-Adams, P.; Lavergne, J.-P.; Penin, F.; McLauchlan, J., Structural determinants that target the hepatitis C virus core protein to lipid droplets. *J. Biol. Chem.* **2006**, 281, 22236-22247.

74. McLauchlan, J.; Lemberg, M.; Hope, G.; Martoglio, B., Intramembrane proteolysis promotes trafficking of hepatitis C virus core protein to lipid droplets. *EMBO J.* **2002**, 21, 3980-3988.

75. Shavinskaya, A.; Boulant, S.; Penin, F.; McLauchlan, J.; Bartenschlager, R., The lipid droplet binding domain of hepatitis C virus core protein is a major determinant for efficient virus assembly. *J. Biol. Chem.* **2007**, 282, 37158-37169.

76. Targett-Adams, P.; Hope, G.; Boulant, S.; McLauchlan, J., Maturation of hepatitis C virus core protein by signal peptide peptidase is required for virus production. *J. Biol. Chem.* **2008**, 283, 16850-16859.

77. Boulant, S.; Targett-Adams, P.; McLauchlan, J., Disrupting the association of hepatitis C virus core prtein with lipid droplets correlates with a loss in production of infectious virus. *J. Gen. Virol.* **2007**, 88, 2204-2213.

78. Op De Beeck, A.; Cocquerel, L.; Dubuisson, J., Biogenesis of hepatitis C virus envelope glycoproteins. *J. Gen. Virol.* **2001**, 82, 2589-2595.

79. Luik, P.; Chew, C.; Aittoniemi, J.; Chang, J.; Wentworth, P.; Dwek, R.; Biggin, P.; Vénien-Bryan, C.; Zitzmann, N., The 3-dimensional structure of a hepatitis C virus p7 ion channel by electron microscopy. *Proc. Natl. Acad. Sci. U. S. A.* **2009**, 106, 12712-12716.

80. Steinmann, E.; Penin, F.; Kallis, S.; Patel, A.; Bartenschlager, R.; Pietschmann, T., Hepatitis C virus p7 protein is crucial for assembly and release of infectious virions. *PLoS Pathog.* **2007**, 3, e103.

81. Steinmann, E.; Pietschmann, T., Hepatitis C virus p7-a viroporin crucial for virus assembly and an emerging target for antiviral therapy. *Viruses* **2010**, 2, 2078-2095.

82. Carrére-Kremer, S.; Montpellier-Pala, C.; Cocquerel, L.; Wychowski, C.; Penin, F.; Dubuisson, J., Subcellular Localization and Topology of the p7 Polypeptide of Hepatitis C Virus. *J. Virol.* **2002**, 76, 3720-3730.

83. Pallaoro, M.; Lahm, A.; Biasiol, G.; Brunetti, M.; Nardella, C.; Orsatti, L.; Bonelli, F.; Orrù, S.; Narjes, F.; Steinkühler, C., Characterization of the hepatitis C virus NS2/3 processing reaction by using a purified precursor protein. *J. Virol.* **2001**, 75, 9939-9946.

84. Lorenz, I.; Marcotrigiano, J.; Dentzer, T.; Rice, C., Structure of the catalytic domain of the hepatitis C virus NS2-3 protease. *Nature* **2006**, 442, 831-835.

85. Franck, N.; Le Seyec, J.; Guguen-Guillouzo, C.; Erdtmann, L., Hepatitis C virus NS2 protein is phosphorylated by the protein kinase CK2 and targeted for degradation to the proteasome. *J. Virol.* **2005**, 79, 2700-2708.

86. Stapleford, K.; Lindenbach, B., Hepatitis C virus NS2 coordinates virus particle assembly through physical interactions with the E1-E2 glycoprotein and NS3-NS4A enzyme complexes. *J. Virol.* **2011**, 85, 1706-1717.

87. Popescu, C.-I.; Callens, N.; Trinel, D.; Roingeard, P.; Moradpour, D.; Descamps, V.; Duverlie, G.; Penin, F.; Héliot, L.; Rouillé, Y.; Dubuisson, J., NS2 protein of hepatitis C virus interacts with structural and non-structural proteins towards virus assembly. *PLoS Pathog.***2011**, 7, e1001278.

88. Tomei, L.; Failla, C.; Santolini, E.; De Francesco, R.; La Monica, N., NS3 is a serine protease required for processing of hepatitis C virus polyprotein. *J. Virol.* **1993**, 67, 4017-4026.

89. Kim, J.; Morgenstern, K.; Griffith, J.; Dwyer, M.; Thomson, J.; Murcko, M.; Lin, C.; Caron, P., Hepatitis C virus NS3 RNA helicase domain with a bound oligonucleotide: the crystal structure provides insights into the mode of unwinding. *Structure* **1998**, 6, 89-100.

90. Saalau-Bethell, S.; Woodhead, A.; Chessari, G.; Carr, M.; Coyle, J.; Graham, B.; Hiscock, S.; Murray, C.; Pathuri, P.; Rich, S.; Richardson, C.; Williams, P.; Jhoti, H., Discovery of an allosteric mechanism for the regulation of HCV NS3 protein function. *Nat. Chem. Biol.* **2012**, 8, 920-925.

91. Failla, C.; Tomei, L.; De Francesco, R., Both NS3 and NS4A are required for proteolytic processing of hepatitis C virus nonstructural proteins. *J. Virol.* **1994**, 68, 3753-3760.

92. Wölk, B.; Sansonno, D.; Kräusslich, H.; Dammacco, F.; Rice, C.; Blum, H.; Moradpour, D., Subcellular localization, stability, and trans-cleavage competence of the hepatitis C virus NS3-NS4A complex expressed in tetracycline-regulated cell lines. *J. Virol.* **2000**, 74, 2293-2304.

93. Kim, J.; Morgenstern, K.; Lin, C.; Fox, T.; Dwyer, M.; Landro, J.; Chambers, S.; Markland, W.; Lepre, C.; O'Malley, E.; Harbeson, S.; Rice, C.; Murcko, M.; Caron, P.; Thomson, J., Crystal structure of the hepatitis C virus NS3 protease domain complexed with a synthetic NS4A cofactor peptide. *Cell* **1996**, 87, 343-355.

94. Love, R.; Parge, H.; Wickersham, J.; Hostomsky, Z.; Habuka, N.; Moomaw, E.; Adachi, T.; Hostomska, Z., The crystal structure of hepatitis C virus NS3 proteinase reveals a trypsin-like fold and a structural zinc binding site. *Cell* **1996**, 87, 331-342.

95. Bartenschlager, R.; Ahlborn-Laake, L.; Mous, J.; Jacobsen, H., Kinetic and structural analyses of hepatitis C virus polyprotein processing. *J. Virol.* **1994**, 68, 5045-5055.

96. Failla, C.; Tomei, L.; De Francesco, R., An amino-terminal domain of the hepatitis C virus NS3 protease is essential for interaction with NS4A. *J. Virol.* **1995**, 69, 1769-1777.

97. Lin, C.; Prágai, B.; Grakoui, A.; Xu, J.; Rice, C., Hepatitis C virus NS3 serine proteinase: trans-cleavage requirements and processing kinetics. *J. Virol.* **1994**, 68, 8147-8157.

98. Tanji, Y.; Hijikata, M.; Hirowatari, Y.; Shimotohno, K., Hepatitis C virus polyprotein processing: kinetics and mutagenic analysis of serine proteinase-dependent cleavage. *J. Virol.* **1994**, 68, 8418-8422.

99. Gouttenoire, J.; Penin, F.; Moradpour, D., Hepatitis C virus nonstructural protein 4B: a journey into unexplored territory. *Rev. Med. Virol.* **2010**, 20, 117-129.

100. Gouttenoire, J.; Castet, V.; Montserret, R.; Arora, N.; Raussens, V.; Ruysschaert, J.-M.; Diesis, E.; Blum, H.; Penin, F.; Moradpour, D., Identification of a novel determinant for membrane association in hepatitis C virus nonstructural protein 4B. *J. Virol.* **2009**, 83, 6257-6268.

101. Lundin, M.; Monné, M.; Widell, A.; von Heijne, G.; Persson, M. A. A., Topology of the Membrane-Associated Hepatitis C Virus Protein NS4B. *J. Virol.* **2003**, 77, 5428-5438.

102. Yu, G.-Y.; Lee, K.-J.; Gao, L.; Lai, M., Palmitoylation and polymerization of hepatitis C virus NS4B protein. *J. Virol.* **2006**, 80, 6013-6023.

103. Einav, S.; Gerber, D.; Bryson, P.; Sklan, E.; Elazar, M.; Maerkl, S.; Glenn, J.; Quake, S., Discovery of a hepatitis C target and its pharmacological inhibitors by microfluidic affinity analysis. *Nat. Biotechnol.* **2008**, 26, 1019-1027.

104. Egger, D.; Wölk, B.; Gosert, R.; Bianchi, L.; Blum, H. E.; Moradpour, D.; Bienz, K., Expression of hepatitis C virus proteins induces distinct membrane alterations including a candidate viral replication complex. *J. Virol.* **2002**, 76, 5974-5984.

105. Aizaki, H.; Lee, K.-J.; Sung, V.; Ishiko, H.; Lai, M., Characterization of the hepatitis C virus RNA replication complex associated with lipid rafts. *Virology* **2004**, 324, 450-461.

106. Brass, V.; Bieck, E.; Montserret, R.; Wölk, B.; Hellings, J.; Blum, H.; Penin, F.; Moradpour, D., An amino-terminal amphipathic alpha-helix mediates membrane association of the hepatitis C virus nonstructural protein 5A. *J. Biol. Chem.* **2002**, 277, 8130-8139.

107. Penin, F.; Brass, V.; Appel, N.; Ramboarina, S.; Montserret, R.; Ficheux, D.; Blum, H.; Bartenschlager, R.; Moradpour, D., Structure and function of the membrane anchor domain of hepatitis C virus nonstructural protein 5A. *J. Biol. Chem.* **2004**, 279, 40835-40843.

108. Tellinghuisen, T.; Marcotrigiano, J.; Rice, C., Structure of the zinc-binding domain of an essential component of the hepatitis C virus replicase. *Nature* **2005**, 435, 374-379.

109. Moradpour, D.; Evans, M.; Gosert, R.; Yuan, Z.; Blum, H. E.; Goff, S. P.; Lindenbach, B. D.; Rice, C. M., Insertion of green fluorescent protein into nonstructural protein 5A allows direct visualization of functional hepatitis C virus replication complexes. *J. Virol.* **2004**, 78, 7400-7409.

110. Appel, N.; Pietschmann, T.; Bartenschlager, R., Mutational analysis of hepatitis C virus nonstructural protein 5A: potential role of differential phosphorylation in RNA replication and identification of a genetically flexible domain. *J. Virol.* **2005**, 79, 3187-3194.

111. Tanji, Y.; Kaneko, T.; Satoh, S.; Shimotohno, K., Phosphorylation of hepatitis C virus-encoded nonstructural protein NS5A. *J. Virol.* **1995**, 69, 3980-3986.

112. Tellinghuisen, T.; Foss, K.; Treadaway, J., Regulation of hepatitis C virion production via phosphorylation of the NS5A protein. *PLoS Pathog.* **2008**, 4, e1000032.

113. Evans, M.; Rice, C.; Goff, S., Phosphorylation of hepatitis C virus nonstructural protein 5A modulates its protein interactions and viral RNA replication. *Proc. Natl. Acad. Sci. U. S. A.* **2004**, 101, 13038-13043.

114. Wölk, B.; Büchele, B.; Moradpour, D.; Rice, C., A dynamic view of hepatitis C virus replication complexes. *J. Virol.* **2008**, 82, 10519-10531.

115. Lee, K.; Choi, J.; Ou, J.-H.; Lai, M., The C-terminal transmembrane domain of hepatitis C virus (HCV) RNA polymerase is essential for HCV replication in vivo. *J. Virol.* **2004**, 78, 3797-3802.

116. Lesburg, C.; Cable, M.; Ferrari, E.; Hong, Z.; Mannarino, A.; Weber, P., Crystal structure of the RNA-dependent RNA polymerase from hepatitis C virus reveals a fully encircled active site. *Nat. Struct. Biol.* **1999**, 6, 937-943.

117. Bressanelli, S.; Tomei, L.; Roussel, A.; Incitti, I.; Vitale, R.; Mathieu, M.; De Francesco, R.; Rey, F., Crystal structure of the RNA-dependent RNA polymerase of hepatitis C virus. *Proc. Natl. Acad. Sci. U. S. A.* **1999**, 96, 13034-13039.

118. Quinkert, D.; Bartenschlager, R.; Lohmann, V., Quantitative analysis of the hepatitis C virus replication complex. *J. Virol.* 2005, 79, 13594-13605.

119. Harris, C.; Herker, E.; Farese, R. V.; Ott, M., Hepatitis C Virus Core Protein Decreases Lipid Droplet Turnover. *J. Biol. Chem.* **2011**, 286, 42615-42625.

120. Jackel-Cram, C.; Babiuk, L. A.; Liu, Q., Up-regulation of fatty acid synthase promoter by hepatitis C virus core protein: Genotype-3a core has a stronger effect than genotype-1b core. *J. Hepatol.* **2007**, 46, 999-1008.

121. Perlemuter, G.; Sabile, A.; Letteron, P.; Vona, G.; Topilco, A.; Chretien, Y.; Koike, K.; Pessayre, D.; Chapman, J.; Barba, G.; Brechot, C., Hepatitis C virus core protein inhibits microsomal triglyceride transfer protein activity and very low density lipoprotein secretion: a model of viral-related steatosis. *FASEB J*. **2002**, 16, 185-194.

122. Su, A.; Pezacki, J.; Wodicka, L.; Brideau, A.; Supekova, L.; Thimme, R.; Wieland, S.; Bukh, J.; Purcell, R.; Schultz, P.; Chisari, F., Genomic analysis of the host response to hepatitis C virus infection. *Proc. Natl. Acad. Sci. U. S. A.* **2002**, 99, 15669-15674.

123. Jhaveri, R.; McHutchison, J.; Patel, K.; Qiang, G.; Diehl, A., Specific polymorphisms in hepatitis C virus genotype 3 core protein associated with intracellular lipid accumulation. *J. Infect. Dis.* **2008**, 197, 283-374.

124. Kapadia, S.; Chisari, F., Hepatitis C virus RNA replication is regulated by host geranylgeranylation and fatty acids. *Proc. Natl. Acad. Sci. U. S. A* **2005**, 102, 2561-2566.

125. Bader, T.; Fazili, J.; Madhoun, M.; Aston, C.; Hughes, D.; Rizvi, S.; Seres, K.; Hasan, M., Fluvastatin Inhibits Hepatitis C Replication in Humans. *Am. J. Gastroenterol.* **2008**, 103, 1383-1389.

126. Takemoto, M.; Liao, J. K., Pleiotropic Effects of 3-Hydroxy-3-Methylglutaryl Coenzyme A Reductase Inhibitors. *Arterioscler. Thromb. Vasc. Biol.* **2001**, 21, 1712-1719.

127. Wang, C.; Gale, M.; Keller, B.; Huang, H.; Brown, M.; Goldstein, J.; Ye, J., Identification of FBL2 as a geranylgeranylated cellular protein required for hepatitis C virus RNA replication. *Mol. Cell* **2005**, 18,425-434.

128. Ye, J.; Wang, C.; Sumpter, R.; Brown, M.; Goldstein, J.; Gale, M., Disruption of hepatitis C virus RNA replication through inhibition of host protein geranylgeranylation. *Proc. Natl. Acad. Sci. U. S. A* **2003**, 100, 15865-15870.

129. Shi, S. T.; Lee, K.-J.; Aizaki, H.; Hwang, S. B.; Lai, M. M. C., Hepatitis C Virus RNA Replication Occurs on a Detergent-Resistant Membrane That Cofractionates with Caveolin-2. *J. Virol.* **2003**, 77, 4160-4168.

130. Miyanari, Y.; Hijikata, M.; Yamaji, M.; Hosaka, M.; Takahashi, H.; Shimotohno, K., Hepatitis C virus non-structural proteins in the probable membranous compartment function in viral genome replication. *J. Biol. Chem.* **2003**, 278, 50301-50308.

131. Sakamoto, H.; Okamoto, K.; Aoki, M.; Kato, H.; Katsume, A.; Ohta, A.; Tsukuda, T.; Shimma, N.; Aoki, Y.; Arisawa, M.; Kohara, M.; Sudoh, M., Host sphingolipid biosynthesis as a target for hepatitis C virus therapy. *Nat. Chem. Biol.* **2005**, 1, 333-337.

132. Hirata, Y.; Ikeda, K.; Sudoh, M.; Tokunaga, Y.; Suzuki, A.; Weng, L.; Ohta, M.; Tobita, Y.; Okano, K.; Ozeki, K.; Kawasaki, K.; Tsukuda, T.; Katsume, A.; Aoki, Y.; Umehara, T.; Sekiguchi, S.; Toyoda, T.; Shimotohno, K.; Soga, T.; Nishijima, M.; Taguchi, R.; Kohara, M., Self-enhancement of hepatitis C virus replication by promotion of specific sphingolipid biosynthesis. *PLoS Pathog.* 2012, 8, e1002860.

133. Li, Q.; Brass, A.; Ng, A.; Hu, Z.; Xavier, R.; Liang, T.; Elledge, S., A genome-wide genetic screen for host factors required for hepatitis C virus propagation. *Proc. Natl. Acad. Sci. U. S. A.* **2009**, 106, 16410-16415.

134. Tai, A.; Benita, Y.; Peng, L.; Kim, S.-S.; Sakamoto, N.; Xavier, R.; Chung, R., A functional genomic screen identifies cellular cofactors of hepatitis C virus replication. *Cell Host Microbe* **2009**, 5, 298-307.

135. Balla, A.; Balla, T., Phosphatidylinositol 4-kinases: old enzymes with emerging functions. *Trends Cell Biol.* **2006**, 16, 351-361.

136. Reiss, S.; Rebhan, I.; Backes, P.; Romero-Brey, I.; Erfle, H.; Matula, P.; Kaderali, L.; Poenisch, M.; Blankenburg, H.; Hiet, M.-S.; Longerich, T.; Diehl, S.; Ramirez, F.; Balla, T.; Rohr, K.; Kaul, A.; Bühler, S.; Pepperkok, R.; Lengauer, T.; Albrecht, M.; Eils, R.; Schirmacher, P.; Lohmann, V.; Bartenschlager, R., Recruitment and activation of a lipid

kinase by hepatitis C virus NS5A is essential for integrity of the membranous replication compartment. *Cell Host Microbe* **2011**, 9, 32-45.

137. D'Angelo, G.; Vicinanza, M.; Di Campli, A.; De Matteis, M., The multiple roles of PtdIns(4)P -- not just the precursor of PtdIns(4,5)P2. *J. Cell Sci.* **2008**, 121, 1955-1963.

138. Berger, K. L.; Cooper, J. D.; Heaton, N. S.; Yoon, R.; Oakland, T. E.; Jordan, T. X.; Mateu, G.; Grakoui, A.; Randall, G., Roles for endocytic trafficking and phosphatidylinositol 4-kinase III alpha in hepatitis C virus replication. *Proc. Natl. Acad. Sci. U. S. A.* **2009**, 106, 7577-7582.

139. Skehel, P.; Fabian-Fine, R.; Kandel, E., Mouse VAP33 is associated with the endoplasmic reticulum and microtubules. *Proc. Natl. Acad. Sci. U. S. A.* **2000**, 97, 1101-1106.

140. Tu, H.; Gao, L.; Shi, S.; Taylor, D.; Yang, T.; Mircheff, A.; Wen, Y.; Gorbalenya, A.; Hwang, S.; Lai, M., Hepatitis C virus RNA polymerase and NS5A complex with a SNARE-like protein. *Virology* **1999**, 263, 30-41.

141. Gao, L.; Aizaki, H.; He, J.-W.; Lai, M., Interactions between viral nonstructural proteins and host protein hVAP-33 mediate the formation of hepatitis C virus RNA replication complex on lipid raft. *J. Virol.* **2004**, 78, 3480-3488.

142. Hamamoto, I.; Nishimura, Y.; Okamoto, T.; Aizaki, H.; Liu, M.; Mori, Y.; Abe, T.; Suzuki, T.; Lai, M.; Miyamura, T.; Moriishi, K.; Matsuura, Y., Human VAP-B is involved in hepatitis C virus replication through interaction with NS5A and NS5B. *J. Virol.* **2005**, 79, 13473-13482.

143. Jopling, C.; Yi, M.; Lancaster, A.; Lemon, S.; Sarnow, P., Modulation of hepatitis C virus RNA abundance by a liver-specific MicroRNA. *Science* **2005**, 309, 1577-1581.

144. Jopling, C.; Schütz, S.; Sarnow, P., Position-dependent function for a tandem microRNA miR-122-binding site located in the hepatitis C virus RNA genome. *Cell Host Microbe* **2008**, 4, 77-85.

145. Watashi, K.; Ishii, N.; Hijikata, M.; Inoue, D.; Murata, T.; Miyanari, Y.; Shimotohno, K., Cyclophilin B is a functional regulator of hepatitis C virus RNA polymerase. *Mol. Cell* **2005**, 19, 111-122.

146. Hanoulle, X.; Badillo, A. l.; Wieruszeski, J.-M.; Verdegem, D.; Landrieu, I.; Bartenschlager, R.; Penin, F.; Lippens, G., Hepatitis C virus NS5A protein is a substrate for the peptidyl-prolyl cis/trans isomerase activity of cyclophilins A and B. *J. Biol. Chem.* **2009**, 284, 13589-13601.

147. Yang, F.; Robotham, J.; Nelson, H.; Irsigler, A.; Kenworthy, R.; Tang, H., Cyclophilin A is an essential cofactor for hepatitis C virus infection and the principal mediator of cyclosporine resistance in vitro. *J. Virol.* **2008**, 82, 5269-5278.

148. Chatterji, U.; Bobardt, M.; Selvarajah, S.; Yang, F.; Tang, H.; Sakamoto, N.; Vuagniaux, G.; Parkinson, T.; Gallay, P., The isomerase active site of cyclophilin A is critical for hepatitis C virus replication. *J. Biol. Chem.* **2009**, 284, 16998-17005.

149. Ujino, S.; Yamaguchi, S.; Shimotohno, K.; Takaku, H., Heat-shock protein 90 is essential for stabilization of the hepatitis C virus nonstructural protein NS3. *J. Biol. Chem.* **2009**, 284, 6841-6846.

150. Okamoto, T.; Omori, H.; Kaname, Y.; Abe, T.; Nishimura, Y.; Suzuki, T.; Miyamura, T.; Yoshimori, T.; Moriishi, K.; Matsuura, Y., A single-amino-acid mutation in hepatitis C virus NS5A disrupting FKBP8 interaction impairs viral replication. *J. Virol* **2008**, 82, 3480-3489.

151. Okamoto, T.; Nishimura, Y.; Ichimura, T.; Suzuki, K.; Miyamura, T.; Suzuki, T.; Moriishi, K.; Matsuura, Y., Hepatitis C virus RNA replication is regulated by FKBP8 and Hsp90. *EMBO J.* **2006**, 25, 5015-5025.

152. Stone, M.; Jia, S.; Heo, W. D.; Meyer, T.; Konan, K. V., Participation of Rab5, an Early Endosome Protein, in Hepatitis C Virus RNA Replication Machinery. *J. Virol.* **2007**, 81, 4551-4563.

153. Liu, H. M.; Aizaki, H.; Choi, K. S.; Machida, K.; Ou, J. J. H.; Lai, M. M. C., SYNCRIP (synaptotagmin-binding, cytoplasmic RNA-interacting protein) is a host factor involved in hepatitis C virus RNA replication. *Virology* **2009**, 386, 249-256.

154. Blais, D. R.; Lyn, R. K.; Joyce, M. A.; Rouleau, Y.; Steenbergen, R.; Barsby, N.; Zhu, L.-F.; Pegoraro, A. F.; Stolow, A.; Tyrrell, D. L.; Pezacki, J. P., Activity-based Protein Profiling Identifies a Host Enzyme, Carboxylesterase 1, Which Is Differentially Active during Hepatitis C Virus Replication. *J. Biol. Chem.* **2010**, 285, 25602-25612.

155. Chen, Y.-J.; Chen, Y.-H.; Chow, L.-P.; Tsai, Y.-H.; Chen, P.-H.; Huang, C.-Y. F.; Chen, W.-T.; Hwang, L.-H., Heat shock protein 72 is associated with the hepatitis C virus replicase complex and enhances viral RNA replication. *J. Biol. Chem.* **2010**, 285, 28183-28190.

156. Nakagawa, S.; Umehara, T.; Matsuda, C.; Kuge, S.; Sudoh, M.; Kohara, M., Hsp90 inhibitors suppress HCV replication in replicon cells and humanized liver mice. *Biochem. Biophys. Res. Commun.* **2007**, 353, 882-888.

157. Fischer, G.; Wittmann-Liebold, B.; Lang, K.; Kiefhaber, T.; Schmid, F., Cyclophilin and peptidyl-prolyl cis-trans isomerase are probably identical proteins. *Nature* **1989**, 337, 476-478.

158. Göthel, S.; Marahiel, M., Peptidyl-prolyl cis-trans isomerases, a superfamily of ubiquitous folding catalysts. *Cell. Mol. Life Sci.* ***1*****999**, 55, 423-436.

159. Kaul, A.; Stauffer, S.; Berger, C.; Pertel, T.; Schmitt, J.; Kallis, S.; Zayas, M.; Lopez, M.; Lohmann, V.; Luban, J.; Bartenschlager, R., Essential role of cyclophilin A for hepatitis C virus replication and virus production and possible link to polyprotein cleavage kinetics. *PLoS Pathog.* **2009**, 5, e1000546.

160. Coelmont, L.; Hanoulle, X.; Chatterji, U.; Berger, C.; Snoeck, J.; Bobardt, M.; Lim, P.; Vliegen, I.; Paeshuyse, J.; Vuagniaux, G. g.; Vandamme, A.-M.; Bartenschlager, R.; Gallay, P.; Lippens, G.; Neyts, J., DEB025 (Alisporivir) inhibits hepatitis C virus replication by preventing a cyclophilin A induced cis-trans isomerisation in domain II of NS5A. *PloS One* **2010**, 5, e13687.

161. McLauchlan, J., Properties of the hepatitis C virus core protein: a structural protein that modulates cellular processes. *J. Viral Hepat.* **2000**, 7, 2-14.

162. Saka, H.; Valdivia, R., Emerging Roles for Lipid Droplets in Immunity and Host-Pathogen Interactions. *Annu. Rev. Cell Dev. Biol.* **2012**, 28, 411-437.

163. Martin, S.; Parton, R., Lipid droplets: a unified view of a dynamic organelle. *Nat. Rev. Mol. Cell Biol.* **2006**, 7, 373-378.

164. Farese, R.; Walther, T., Lipid droplets finally get a little R-E-S-P-E-C-T. *Cell* **2009**, 139, 855-860.

165. Walther, T.; Farese, R., Lipid droplets and cellular lipid metabolism. *Annu. Rev. Biochem.* **2012**, 81, 687-714.

166. Digel, M.; Ehehalt, R.; Füllekrug, J., Lipid droplets lighting up: insights from live microscopy. *FEBS Lett.* **2010**, 584, 2168-2175.

167. Murphy, D.; Vance, J., Mechanisms of lipid-body formation. *Trends Biochem. Sci.* **1999**, 24, 109-115.

168. Olofsson, S.-O.; Boström, P.; Andersson, L.; Rutberg, M.; Perman, J.; Borén, J., Lipid droplets as dynamic organelles connecting storage and efflux of lipids. *Biochim. Biophys. Acta.* **2009**, 1791, 448-458.

169. Yen, C.-L. E.; Stone, S.; Koliwad, S.; Harris, C.; Farese, R., Thematic review series: glycerolipids. DGAT enzymes and triacylglycerol biosynthesis. *J. Lipid Res.* **2008**, 49, 2283-2301.

170. Robenek, H.; Hofnagel, O.; Buers, I.; Robenek, M.; Troyer, D.; Severs, N., Adipophilin-enriched domains in the ER membrane are sites of lipid droplet biogenesis. *J. Cell Sci.* **2006**, 119, 4215-4224.

171. Murphy, D., The biogenesis and functions of lipid bodies in animals, plants and microorganisms. *Prog. Lipid Res.* **2001**, 40, 325-438.

172. Brasaemle, D., Thematic review series: adipocyte biology. The perilipin family of structural lipid droplet proteins: stabilization of lipid droplets and control of lipolysis. *J. Lipid Res.* **2007**, 48, 2547-2559.

173. Bickel, P.; Tansey, J.; Welte, M., PAT proteins, an ancient family of lipid droplet proteins that regulate cellular lipid stores. *Biochim. Biophys. Acta.* **2009**, 1791, 419-440.

174. Boström, P.; Andersson, L.; Rutberg, M.; Perman, J.; Lidberg, U.; Johansson, B.; Fernandez-Rodriguez, J.; Ericson, J.; Nilsson, T.; Borén, J.; Olofsson, S.-O., SNARE proteins mediate fusion between cytosolic lipid droplets and are implicated in insulin sensitivity. *Nat. Cell Biol.* **2007**, 9, 1286-1293.

175. Barba, G.; Harper, F.; Harada, T.; Kohara, M.; Goulinet, S.; Matsuura, Y.; Eder, G.; Schaff, Z.; Chapman, M. J.; Miyamura, T.; Bréchot, C., Hepatitis C virus core protein shows a cytoplasmic localization and associates to cellular lipid storage droplets. *Proc. Natl. Acad. Sci. U. S. A.* **1997**, *94*, 1200-1205.

176. Sato, S.; Fukasawa, M.; Yamakawa, Y.; Natsume, T.; Suzuki, T.; Shoji, I.; Aizaki, H.; Miyamura, T.; Nishijima, M., Proteomic profiling of lipid droplet proteins in hepatoma cell lines expressing hepatitis C virus core protein. *J. Biochem.* **2006**, 139, 921-930.

177. Depla, M.; Uzbekov, R.; Hourioux, C.; Blanchard, E.; Le Gouge, A. l.; Gillet, L.; Roingeard, P., Ultrastructural and quantitative analysis of the lipid droplet clustering induced by hepatitis C virus core protein. *Cell. Mole. Life Sci.* **2010**, 67, 3151-3161.

178. Herker, E.; Harris, C.; Hernandez, C. l.; Carpentier, A.; Kaehlcke, K.; Rosenberg, A.; Farese, R.; Ott, M., Efficient hepatitis C virus particle formation requires diacylglycerol acyltransferase-1. *Nat. Med.* **2010**, 16, 1295-1298.

179. Jirasko, V.; Montserret, R.; Lee, J.; Gouttenoire, J.; Moradpour, D.; Penin, F.; Bartenschlager, R., Structural and functional studies of nonstructural protein 2 of the hepatitis C virus reveal its key role as organizer of virion assembly. *PLoS Pathog.* **2010**, 6, e1001233.

180. Ma, Y.; Anantpadma, M.; Timpe, J.; Shanmugam, S.; Singh, S.; Lemon, S.; Yi, M., Hepatitis C virus NS2 protein serves as a scaffold for virus assembly by interacting with both structural and nonstructural proteins. *J. Virol.* **2010**, 85, 86-97.

181. Ma, Y.; Yates, J.; Liang, Y.; Lemon, S.; Yi, M., NS3 helicase domains involved in infectious intracellular hepatitis C virus particle assembly. *J. Virol.* **2008**, 82, 7624-7639.

182. Counihan, N. A.; Rawlinson, S. M.; Lindenbach, B. D., Trafficking of Hepatitis C Virus Core Protein during Virus Particle Assembly. *PLoS Pathog.* **2011**, 7, e1002302.

183. Phan, T.; Beran, R.; Peters, C.; Lorenz, I.; Lindenbach, B., Hepatitis C virus NS2 protein contributes to virus particle assembly via opposing epistatic interactions with the E1-E2 glycoprotein and NS3-NS4A enzyme complexes. *J. Virol.* **2009**, 83, 8379-8395.

184. Yi, M.; Ma, Y.; Yates, J.; Lemon, S., Trans-complementation of an NS2 defect in a late step in hepatitis C virus (HCV) particle assembly and maturation. *PLoS Pathog.* **2009**, 5, e1000403.

185. Jones, C.; Murray, C.; Eastman, D.; Tassello, J.; Rice, C., Hepatitis C virus p7 and NS2 proteins are essential for production of infectious virus. *J. Virol.* **2007**, 81, 8374-8383.

186. Sakai, A.; Claire, M.; Faulk, K.; Govindarajan, S.; Emerson, S.; Purcell, R.; Bukh, J., The p7 polypeptide of hepatitis C virus is critical for infectivity and contains functionally important genotype-specific sequences. *Proc. Natl. Acad. Sci. U. S. A.* **2003**, 100, 11646-11651.

187. Jirasko, V.; Montserret, R.; Appel, N.; Janvier, A.; Eustachi, L.; Brohm, C.; Steinmann, E.; Pietschmann, T.; Penin, F.; Bartenschlager, R., Structural and functional characterization of nonstructural protein 2 for its role in hepatitis C virus assembly. *J. Biol. Chem.* **2008**, 283, 28546-28562.

188. Boson, B.; Granio, O. l.; Bartenschlager, R.; Cosset, F.-L, A concerted action of hepatitis C virus p7 and nonstructural protein 2 regulates core localization at the endoplasmic reticulum and virus assembly. *PLoS Pathog.* 2011, 7, e1002144.

189. André, P.; Komurian-Pradel, F.; Deforges, S.; Perret, M.; Berland, J.; Sodoyer, M.; Pol, S.; Bréchot, C.; Paranhos-Baccalà , G.; Lotteau, V., Characterization of low- and very-low-density hepatitis C virus RNA-containing particles. *J. Virol.* **2002**, 76, 6919-6928.

190. Nielsen, S.; Bassendine, M.; Burt, A.; Martin, C.; Pumeechockchai, W.; Toms, G., Association between hepatitis C virus and very-low-density lipoprotein (VLDL)/LDL analyzed in iodixanol density gradients. *J. Virol.* **2006**, 80, 2418-2428.

191. Nielsen, S.; Bassendine, M.; Martin, C.; Lowther, D.; Purcell, P.; King, B.; Neely, D.; Toms, G., Characterization of hepatitis C RNA-containing particles from human liver by density and size. *J. Gen. Virol.* **2008**, 89, 2507-2517.

192. Huang, H.; Sun, F.; Owen, D.; Li, W.; Chen, Y.; Gale, M.; Ye, J., Hepatitis C virus production by human hepatocytes dependent on assembly and secretion of very low-density lipoproteins. *Proc. Natl. Acad. Sci. U. S. A.* **2007**, 104, 5848-5853.

193. Mensenkamp, A.; Havekes, L.; Romijn, J.; Kuipers, F., Hepatic steatosis and very low density lipoprotein secretion: the involvement of apolipoprotein E. *J. Hepatol.* **2001**, 35, 816-822.

194. Bartenschlager, R.; Penin, F.; Lohmann, V.; André, P., Assembly of infectious hepatitis C virus particles. *Trends Microbiol.* **2011**, 19, 95-103.

195. Gastaminza, P.; Cheng, G.; Wieland, S.; Zhong, J.; Liao, W.; Chisari, F. V., Cellular Determinants of Hepatitis C Virus Assembly, Maturation, Degradation, and Secretion. *J. Virol.* **2008**, 82, 2120-2129.

196. Jiang, J.; Luo, G., Apolipoprotein E but Not B Is Required for the Formation of Infectious Hepatitis C Virus Particles. *J. Virol.* **2009**, 83, 12680-12691.

197. Aizaki, H.; Morikawa, K.; Fukasawa, M.; Hara, H.; Inoue, Y.; Tani, H.; Saito, K.; Nishijima, M.; Hanada, K.; Matsuura, Y.; Lai, M.; Miyamura, T.; Wakita, T.; Suzuki, T., Critical role of virion-associated cholesterol and sphingolipid in hepatitis C virus infection. *J. Virol.* **2008**, 82, 5715-5724.

198. Backes, P.; Quinkert, D.; Reiss, S.; Binder, M.; Zayas, M.; Rescher, U.; Gerke, V.; Bartenschlager, R.; Lohmann, V., Role of annexin A2 in the production of infectious hepatitis C virus particles. *J. Virol.* **2010**, 84, 5775-5789.

199. Amako, Y.; Sarkeshik, A.; Hotta, H.; Yates, J.; Siddiqui, A., Role of oxysterol binding protein in hepatitis C virus infection. *J. Virol.* **2009**, 83, 9237-9246.

200. Wyles, J.; McMaster, C.; Ridgway, N., Vesicle-associated membrane protein-associated protein-A (VAP-A) interacts with the oxysterol-binding protein to modify export from the endoplasmic reticulum. *J. Biol. Chem.* **2002**, 277, 29908-29918.

201. Levine, T.; Munro, S., Targeting of Golgi-specific pleckstrin homology domains involves both PtdIns 4-kinase-dependent and -independent components. *Curr. Biol.* **2002**, 12, 695-704.

202. Perry, R.; Ridgway, N., Oxysterol-binding protein and vesicle-associated membrane protein-associated protein are required for sterol-dependent activation of the ceramide transport protein. *Mol. Biol Cell* **2006**, 17, 2604-2616.

203. Amako, Y.; Syed, G.; Siddiqui, A., Protein kinase D negatively regulates hepatitis C virus secretion through phosphorylation of oxysterol-binding protein and ceramide transfer protein. *J. Biol. Chem.* **2011**, 286, 11265-11274.

204. Chang, K.-S.; Jiang, J.; Cai, Z.; Luo, G., Human apolipoprotein e is required for infectivity and production of hepatitis C virus in cell culture. *J. Virol.* **2007**, 81, 13783-13793.

205. Neveu, G.; Barouch-Bentov, R.; Ziv-Av, A.; Gerber, D.; Jacob, Y.; Einav, S., Identification and Targeting of an Interaction between a Tyrosine Motif within Hepatitis C Virus Core Protein and AP2M1 Essential for Viral Assembly. *PLoS Pathog.* **2012**, 8, e1002845.

206. Merz, A.; Long, G.; Hiet, M.-S.; BrÃ¼gger, B.; Chlanda, P.; Andre, P.; Wieland, F.; Krijnse-Locker, J.; Bartenschlager, R., Biochemical and morphological properties of hepatitis C virus particles and determination of their lipidome. *J. Biol. Chem.* **2011**, 286, 3018-3032.

207. Hijikata, M.; Shimizu, Y.; Kato, H.; Iwamoto, A.; Shih, J.; Alter, H.; Purcell, R.; Yoshikura, H., Equilibrium centrifugation studies of hepatitis C virus: evidence for circulating immune complexes. *J. Virol.* **1993**, 67, 1953-1958.

208. Meunier, J-C.; Russell, R. S.; Engle, R. E.; Faulk, K. N.; Purcell, R. H.; Emerson, S. U., Apolipoprotein c1 association with hepatitis C virus. *J. Virol.* **2008**, 82, 9647-9656.

209. Lindenbach, B. D.; Meuleman, P.; Ploss, A.; Vanwolleghem, T.; Syder, A. J.; McKeating, J. A.; Lanford, R. E.; Feinstone, S. M.; Major, M. E.; Leroux-Roels, G.; Rice, C. M., Cell culture-grown hepatitis C virus is infectious in vivo and can be recultured in vitro. *Proc. Natl. Acad. Sci. U. S. A.* **2006**, 103, 3805-3809.

210. Fusco, D. N.; Chung, R. T., Novel Therapies for Hepatitis C: Insights from the Structure of the Virus. *Annu. Rev. Med.* **2012**, 63, 373-387.

211. Jacobson, I.; McHutchison, J.; Dusheiko, G.; Di Bisceglie, A.; Reddy, K.; Bzowej, N.; Marcellin, P.; Muir, A.; Ferenci, P.; Flisiak, R.; George, J.; Rizzetto, M.; Shouval, D.; Sola, R.; Terg, R.; Yoshida, E.; Adda, N.; Bengtsson, L.; Sankoh, A.; Kieffer, T.; George, S.; Kauffman, R.; Zeuzem, S.; Team, A. S., Telaprevir for previously untreated chronic hepatitis C virus infection. *N. Engl. J Med.* **2011**, 364, 2405-2416.

212. Poordad, F.; McCone, J.; Bacon, B.; Bruno, S.; Manns, M.; Sulkowski, M.; Jacobson, I.; Reddy, K.; Goodman, Z.; Boparai, N.; DiNubile, M.; Sniukiene, V.; Brass, C.; Albrecht, J.; Bronowicki, J.-P.; Investigators, S.-. Boceprevir for untreated chronic HCV genotype 1 infection. *N. Engl. J Med.* **2011**, 364, 1195-1206.

213. Lange, C.; Sarrazin, C.; Zeuzem, S., Review article: specifically targeted anti-viral therapy for hepatitis C - a new era in therapy. *Aliment. Pharmacol. Ther.* **2010**, 32, 14-28.

214. Forestier, N.; Larrey, D.; Guyader, D.; Marcellin, P.; Rouzier, R. g.; Patat, A.; Smith, P.; Bradford, W.; Porter, S.; Blatt, L.; Seiwert, S.; Zeuzem, S., Treatment of chronic hepatitis C patients with the NS3/4A protease inhibitor danoprevir (ITMN-191/RG7227) leads to robust reductions in viral RNA: a phase 1b multiple ascending dose study. *J. Hepatol.* **2011**, 54, 1130-1136.

215. McCown, M. F.; Rajyaguru, S.; Le Pogam, S.; Ali, S.; Jiang, W.-R.; Kang, H.; Symons, J.; Cammack, N.; Najera, I., The Hepatitis C Virus Replicon Presents a Higher Barrier to

Resistance to Nucleoside Analogs than to Nonnucleoside Polymerase or Protease Inhibitors. *Antimicrob. Agents Chemother.* **2008**, 52, 1604-1612.

216. Reesink, H.; Zeuzem, S.; Weegink, C.; Forestier, N.; van Vliet, A.; van de Wetering de Rooij, J.; McNair, L.; Purdy, S.; Kauffman, R.; Alam, J.; Jansen, P., Rapid decline of viral RNA in hepatitis C patients treated with VX-950: a phase Ib, placebo-controlled, randomized study. *Gastroenterology* **2006**, 131, 997-1002.

217. Sarrazin, C.; Kieffer, T.; Bartels, D.; Hanzelka, B.; Müh, U.; Welker, M.; Wincheringer, D.; Zhou, Y.; Chu, H.-M.; Lin, C.; Weegink, C.; Reesink, H.; Zeuzem, S.; Kwong, A., Dynamic hepatitis C virus genotypic and phenotypic changes in patients treated with the protease inhibitor telaprevir. *Gastroenterology* **2007**, 132, 1767-1777.

218. Kieffer, T. L.; Sarrazin, C.; Miller, J. S.; Welker, M. W.; Forestier, N.; Reesink, H. W.; Kwong, A. D.; Zeuzem, S., Telaprevir and pegylated interferon–alpha-2a inhibit wild-type and resistant genotype 1 hepatitis C virus replication in patients. *Hepatology* **2007**, 46, 631-639.

219. Schlutter, J., Therapeutics: New drugs hit the target. *Nature* **2011**, 474, S5-S7.

220. Flisiak, R.; Jaroszewicz, J.; Flisiak, I.; Łapiński, T., Update on alisporivir in treatment of viral hepatitis C. *Expert Opin. Investig. Drugs* **2012**, 21, 375-382.

221. Paeshuyse, J.; Kaul, A.; De Clercq, E.; Rosenwirth, B.; Dumont, J.-M.; Scalfaro, P.; Bartenschlager, R.; Neyts, J., The non-immunosuppressive cyclosporin DEBIO-025 is a potent inhibitor of hepatitis C virus replication in vitro. *Hepatology* **2006**, 43, 761-770.

222. Inoue, K.; Umehara, T.; Ruegg, U.; Yasui, F.; Watanabe, T.; Yasuda, H.; Dumont, J.-M.; Scalfaro, P.; Yoshiba, M.; Kohara, M., Evaluation of a cyclophilin inhibitor in hepatitis C virus-infected chimeric mice in vivo. *Hepatology* **2007**, 45, 921-928.

223. Nakagawa, M.; Sakamoto, N.; Tanabe, Y.; Koyama, T.; Itsui, Y.; Takeda, Y.; Chen, C.-H.; Kakinuma, S.; Oooka, S.; Maekawa, S.; Enomoto, N.; Watanabe, M., Suppression of hepatitis C virus replication by cyclosporin a is mediated by blockade of cyclophilins. *Gastroenterology* **2005**, 129, 1031-1041.

224. Flisiak, R.; Horban, A.; Gallay, P.; Bobardt, M.; Selvarajah, S.; Wiercinska-Drapalo, A.; Siwak, E.; Cielniak, I.; Higersberger, J.; Kierkus, J.; Aeschlimann, C.; Grosgurin, P.; Nicolas-Métral, V.; Dumont, J.-M.; Porchet, H.; Crabbé, R.; Scalfaro, P., The cyclophilin inhibitor Debio-025 shows potent anti–hepatitis C effect in patients coinfected with hepatitis C and human immunodeficiency virus. *Hepatology* **2008**, 47, 817-826.

225. Chatterji, U.; Bobardt, M. D.; Stanfield, R.; Ptak, R. G.; Pallansch, L. A.; Ward, P. A.; Jones, M. J.; Stoddart, C. A.; Scalfaro, P.; Dumont, J.-M.; Besseghir, K.; Rosenwirth, B.; Gallay, P. A., Naturally Occurring Capsid Substitutions Render HIV-1 Cyclophilin A Independent in Human Cells and TRIM-cyclophilin-resistant in Owl Monkey Cells. *J. Biol. Chem.* **2005**, 280, 40293-40300.

226. Taylor, L. E.; Swan, T.; Mayer, K. H., HIV Coinfection With Hepatitis C Virus: Evolving Epidemiology and Treatment Paradigms. *Clin. Infect. Dis.* **2012**, 55, S33-S42.

227. Flisiak, R.; Feinman, S. V.; Jablkowski, M.; Horban, A.; Kryczka, W.; Pawlowska, M.; Heathcote, J. E.; Mazzella, G.; Vandelli, C.; Nicolas-Métral, V.; Grosgurin, P.; Liz, J. S.; Scalfaro, P.; Porchet, H.; Crabbé, R., The cyclophilin inhibitor Debio 025 combined with PEG IFNα2a significantly reduces viral load in treatment-naïve hepatitis C patients. *Hepatology* **2009**, 49, 1460-1468.

228. Coelmont, L.; Kaptein, S.; Paeshuyse, J.; Vliegen, I.; Dumont, J.-M.; Vuagniaux, G.; Neyts, J., Debio 025, a Cyclophilin Binding Molecule, Is Highly Efficient in Clearing Hepatitis C Virus (HCV) Replicon-Containing Cells When Used Alone or in Combination with Specifically Targeted Antiviral Therapy for HCV (STAT-C) Inhibitors. *Antimicrob. Agents Chemother.* **2009**, 53, 967-976.

229. Lanford, R.; Hildebrandt-Eriksen, E.; Petri, A.; Persson, R.; Lindow, M.; Munk, M.; Kauppinen, S.; Ørum, H., Therapeutic silencing of microRNA-122 in primates with chronic hepatitis C virus infection. *Science* **2010**, 327, 198-201.

230. Ikeda, M.; Abe, K.; Yamada, M.; Dansako, H.; Naka, K.; Kato, N., Different anti-HCV profiles of statins and their potential for combination therapy with interferon. *Hepatology* **2006**, 44, 117-125.

231. Delang, L.; Paeshuyse, J.; Vliegen, I.; Leyssen, P.; Obeid, S.; Durantel, D.; Zoulim, F.; Op de Beeck, A.; Neyts, J., Statins potentiate the in vitro anti-hepatitis C virus activity of selective hepatitis C virus inhibitors and delay or prevent resistance development. *Hepatology* **2009**, 50, 6-16.

232. Sheridan, D.; Neely, R.; Bassendine, M., Hepatitis C virus and lipids in the era of direct acting antivirals (DAAs). *Clin. Res. Hepatol. Gastroenterol.* **2012**, http://dx.doi.org/10.1016/j.clinre.2012.07.002

2

Direct imaging of the disruption of hepatitis C virus replication complexes by inhibitors of lipid metabolism

Introduction

HCV remains to be a global health problem with currently no cure [1]. The virus' error prone mechanism and high genetic heterogeneity significantly adds to the challenge for developing a vaccine [2, 3]. Since, its first discovery in 1975, HCV infections have mostly been treated with non-specific antivirals and therapy to boost the immune response [4-6]. Recent approvals of DAAs, which have aided the effectiveness when co-administered with ribavirin and peg-IFN, do not preclude the harsh side effects of treatment and remain a costly option [7-9]. There is an urgent need to discover alternative novel therapeutics. Like all viruses, HCV requires a host for propagation [10]. Given that the host contains a large network that is exploited by the virus, we have shifted our approach from directly targeting the virus, to focus on investigating specific viral-dependent host interactions [11-14]. Targeting host pathways that are differentially regulated during HCV infection, and hijacked by the virus, are suitable candidates [12, 15]. Currently, a leading drug candidate in clinical trials, Alisporivir, which targets cyclophilins, confirms the effectiveness for targeting the host for HCV therapy [16, 17].

For these reasons, targeting the host as an alternative to DAAs may potentially play a role in the future of HCV treatment.

One host pathway in particular that is utilized by HCV is the regulation of lipid biosynthesis [2, 18, 19]. The liver is the biosynthetic site for intracellular lipids, which are aliphatic biomolecules that form higher ordered structures such as sterol esters, triglycerides and phospholipids [20, 21]. Lipids are required for cell signaling, and act as substrates for lipid-rich organelles created for energy stores [20-22]. HCV upregulates intracellular lipids and alters lipid-rich environments throughout its entire lifecycle [23, 24]. HCV hijacks the pathways in host lipid biosynthesis and metabolism [23, 24]. Two particular pathways that involve cholesterol biosynthesis and lipid homeostasis will be investigated in this chapter. We focus on using small molecule inhibitors to disrupt lipid metabolism and homeostasis. Firstly, we used a benzamide analogue to target the peroxisome proliferator-activated receptor (PPAR) pathway in order to assess antagonistic effects on transcription of genes involved in lipid regulation (Fig. 2.1 A). Secondly, we used a statin inhibitor, lovastatin, which targets HMG-CoA reductase in order to assess the blockade of cholesterol biosynthesis (Fig. 2.1 B). Molecular imaging was also applied to directly visualize the antiviral cell alterations that are induced by perturbing lipid metabolism.

Statins

Statins have been developed to treat hypercholestermia, and its side effects are quite minimal [25]. The target for statins is 3-hydroxy-3-methylglutaryl coenzyme A (HMG-CoA) reductase enzyme, which is the rate-limiting step of cholesterol biosynthesis involved in converting HMG-CoA to mevalonate [26]. Inhibiting HMG-CoA reductase effectively depletes downstream biosynthesis of sterol lipids [27]. As previously mentioned in the chapter 1, sterols are involved in protein prenylation and are present in the membrane, which are both important for HCV viral replication and assembly [24, 28-31]. The use of statins has been shown to exhibit antiviral activity against HCV [25]. Notably, a study using

an *in situ* model assessed a range of statins, which included atorvastatin, fluvastatin, pravastatin, simvastatin, and lovastatin [25]. Variable anti-HCV properties were observed, with fluvastastin resulting in the highest potency, and displayed a synergistic effect when combined with peg-IFNα [25]. Another study along the same methodology reported similar antiviral properties with these statin inhibitors, which also showed synergistic effects when co-administered with peg-IFN [32]. Furthermore, a clinical study had observed that treating HCV infected patients for 2-5 weeks at a tolerable dosage of fluvastatin, resulted in a decrease in viral loads [33]. These authors hypothesize that fluvastatin may bind to newly created viral particles, which may prevent a host-induced immune response [33]. More recently, a clinical study showed that, the combination of fluvastatin, in addition with peg-IFN and RBV, significantly improved the SVR rate, suggesting that the use of statins may be more effective as a co-administered therapy [34]. Nonetheless, inhibiting cholesterol biosynthesis remains to be an important therapeutic target to combat HCV.

Nuclear receptors in lipid metabolism

Peroxisome proliferator-activated receptors (PPAR) are nuclear receptors that control a variety of roles both in homeostasis and in diseased states [35]. PPARs are ligand-activated by fatty acids and prostaglandins, and are responsible for transcription of regulatory genes at peroxisome proliferator response element (PPRE) domains [36-38]. Binding to PPREs are aided by co-factors, and for transcription to occur, PPARs must heterodimerize with the retinoid X receptor (RXR, Schematic 2.1) [38, 39]. PPARs ubiquitously contain four distinct domains, which generally include a ligand binding domain that is responsible for binding to RXR, a target domain for phosphorylation, and a DNA binding domain that contains two zinc fingers that bind to the PPRE [35]. Three isoforms represent the subfamily of PPAR nuclear receptors: α, γ, δ. Because of its pleiotropic roles, there are several tissues in the body that express all three PPAR isoforms that differentially target several

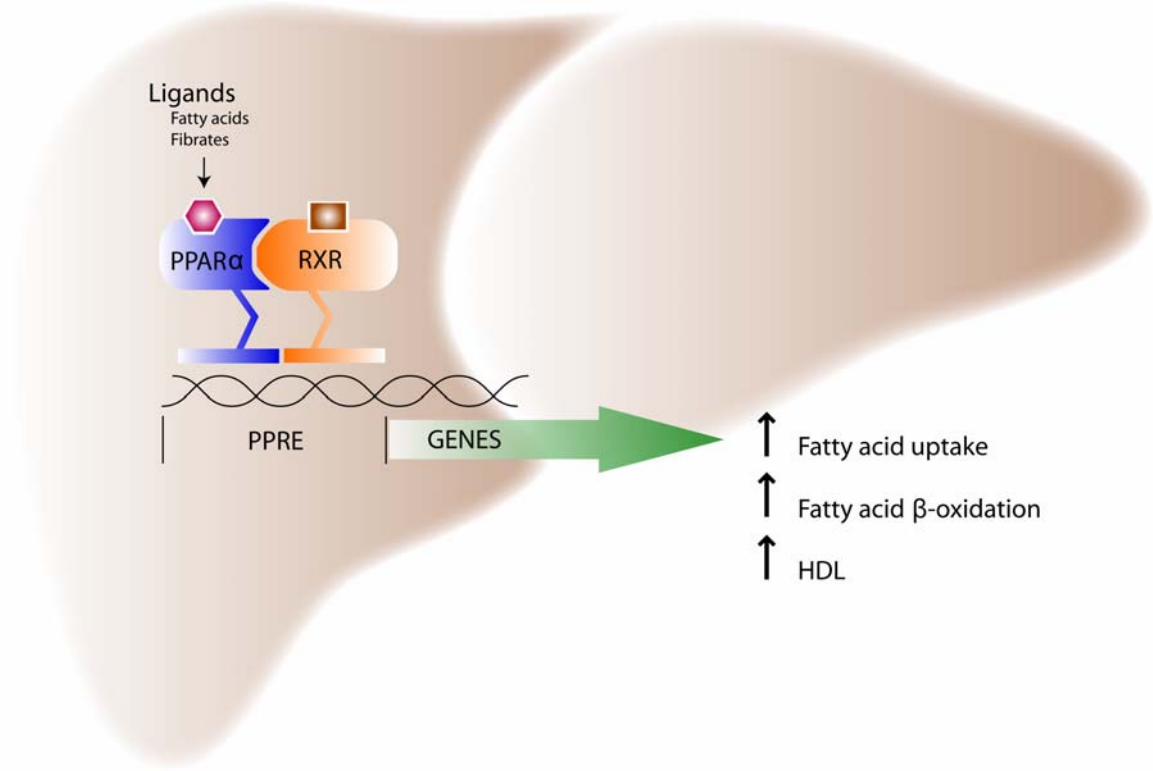

Schematic 2.1: Effects of PPARα activation in the liver. Functional PPARα is ligand activated and heterodimerizes with RXR in the nucleus. The PPARα and RXR complex binds to PPRE that encode for genes involved in lipid catabolism, such as, increasing FATP for fatty acid uptake, and fatty acid β-oxidation. Additionally, genes that upregulate HDL biosynthesis for lipid clearance is also controlled by PPARα.

genes in lipid metabolism [36, 37, 40]. For regulation of glucose and lipid metabolism in the liver, PPARα and PPARγ are responsible for these roles, while PPARδ manages this in the skeletal muscle [41]. More specifically, a critical function of PPARα is to regulate intracellular levels of fatty acids by activating fatty acid catabolism [36]. This is accomplished by PPARα-induced expression of genes at the PPREs, which encode for enzymes of fatty acid β-oxidation in the mitochondria and peroxisomes (Schematic 2.1) [36, 37, 40]. It is well documented that enzymes, acyl-CoA oxidase (ACO) and ω-hydroxylase, are

involved in β-oxidation of acyl-CoA esters [39]. For this to occur fatty acids must first be transported to sites where catabolism takes place. For example, a PPARα-induced gene, fatty acid transport protein (FATP), can increase fatty acid uptake through the plasma membrane, which in turn, are activated into acyl-CoA esters that are further sequestered for β-oxidation (Schematic 2.1) [39, 42]. Similarly, carnitine palmitoyl transferase I (CPTI) is also induced by PPARα, and is upregulated to aid in translocating acyl-CoAs into the mitochondria for mitochondrial β-oxidation [43]. Although PPARγ similarly modulates lipid metabolism, this isoform is predominantly expressed in adipose tissues and less in the liver [40].

Agonists of PPARα has been shown to lower triglyceride levels, increase high density lipoprotein (HDL) synthesis, and increase insulin sensitivity [44, 45]. For example, in a human trial study, fibrates that are a PPARα agonists, such as bezafibrate, have been shown to reduce triglyceride levels after treatment [46, 47]. Additionally, in mice, bezafibrate has been shown to activate PPARα-induced lipid catabolic genes, but had also affected PPARδ to a lesser extent [48]. By contrast, PPARγ agonist, such as, thiazolidinediones (TZDs), suppressed glucose uptake, and showed promising results to treat patients with type II diabetes [49]. While more research is required to assess long-term safety profile for these inhibitors, dual agonists that bind both PPARα and PPARγ equally are actively being researched [45, 50].

Molecular imaging: CARS Microscopy as a novel chemical imaging tool

Investigating the dynamics of cellular lipids can yield new interesting insights into their behaviour and biological function in the cell, and importantly, provide information about how lipids are misregulated in the context of viral infection [24, 51-53]. For example, the LD organelle has been shown to be a critical interacting partner with HCV viral proteins, and this host-virus interaction may mediate the connection between different stages of the viral lifecycle [24, 54-56]. However, these

interactions have primarily been explored by static imaging, which does not capture the dynamics of these processes [51, 57, 58]. Included in these methods are fixation or immunofluorescence staining, which may alter cellular functions, and this would exclude its application for *in vivo* experimentation. To effectively visualize dynamics, however, new techniques for molecular imaging requires live-cell and label-free methodologies [53, 59]. Molecular imaging can effectively aid in early stages of drug discovery [54, 60]. But importantly, imaging methods can provide high contrast for the intended targets, such as, viral or host proteins. Therefore, to selectively image with high specificity, optical methods based on Raman scattering, such as coherent anti-Stokes Raman scattering (CARS) microscopy, offers visualization of specific chemical environments in the cell, and in a label-free manner [61-64].

In principle, Raman scattering is a powerful spectroscopic technique that probes for chemical vibrations that are intrinsic in organic biomolecules [65, 66]. In biological specimens, the Raman spectrum for organic molecules is situated in regions of 3100-2700 cm^{-1} and 1800-500 cm^{-1}, which can provide the signatures of biomolecules, such as, phospholipids, sugars, nucleic acids, and ribosomal proteins [61, 67]. The Raman spectrum in between regions, less than 1800 cm^{-1}, however, is identified to be the fingerprint region where molecular vibrations correspond to specific chemical functional groups [61, 68]. Based on Raman scattering, CARS microscopy employs multi-photon absorption, which in comparison to traditional Raman techniques, can enhance the rate of imaging from hours to milliseconds, and can improve the signal by a 1000-fold [61, 64]. The signal is generated when CARS tunes to the frequency of an inherent vibrating chemical bond in a biological specimen, but unlike in Raman scattering, the signal is resonantly enhanced with CARS [59, 61, 67]. This is accomplished by using three input beams to generate a blue-shifted, higher energy photon, and excludes contamination of fluorescence signals observed in the red-shifted range [59]. When the frequency difference (ω_p - ω_s) between the pump (ω_p) and stokes (ω_s) equals and matches the frequency that of the molecular vibration of a chemical bond (Ω), the vibration of the chemical bonds will oscillate coherently with the applied field [61] (Schematic 2.2). An additional probe beam, which is generated by the pump ω_p, then resonantly enhances the coherently driven Raman vibration,

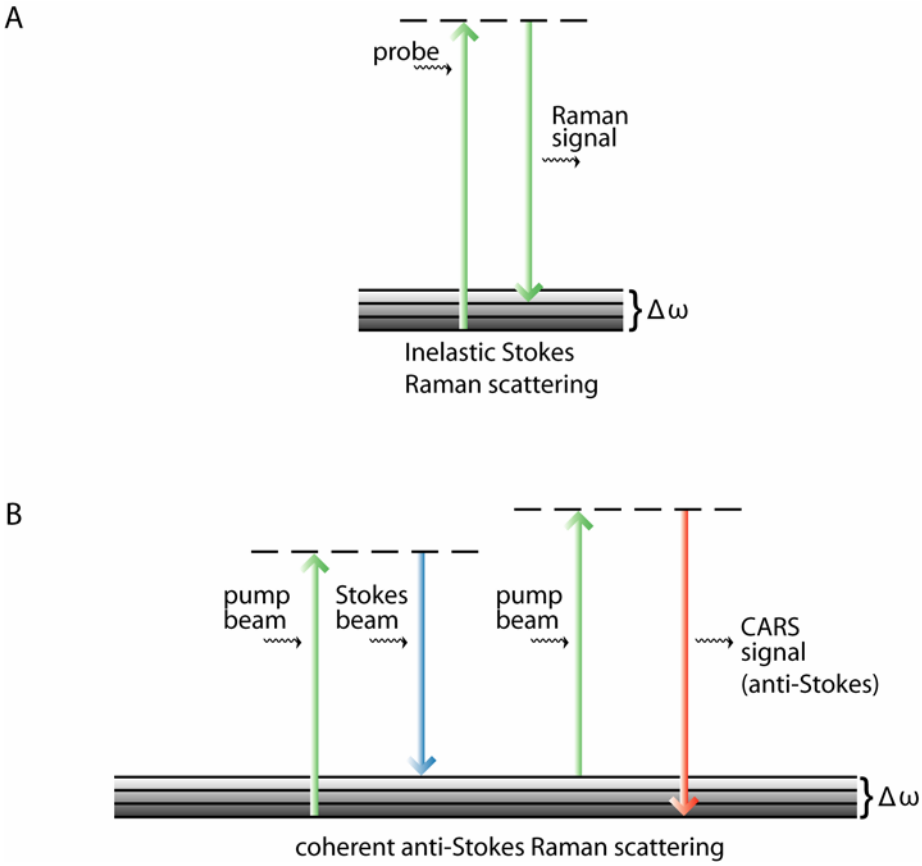

Schematic 2.2: Transitions in Raman and CARS spectroscopy. (A) The Raman signal is generated by inelastic scattering of photons resulting in a red-shifted emission. (B) In CARS, the signal is generated when the sample is irradiated by the pump (ω_p) and Stokes (ω_s) beam. The molecular vibration ($\Delta\omega$) of the intended target oscillates coherently when the frequency difference between the pump (ω_p) and Stokes (ω_s), matches the molecular vibration ($\Delta\omega$). A second pump (ω_p) beam will resonantly enhance the signal to generate a higher-energy, anti-Stokes, emission ($\omega_{as} = 2\omega_p - \omega_s$).

generating the anti-Stokes photons ($\omega_{as} = 2\omega_p - \omega_s$), which provides the CARS signal [61, 62, 69]. With the capabilities of video-rate imaging with high specificity and 3-dimensional spatial resolution without chemical labeling, CARS is a novel imaging technique that can be used to study the dynamics of cells in a diseased or a non-diseased state [59, 63, 70]. As labeling often perturbs biological specimens, CARS

offers to circumvent these problems [53]. Although lipid imaging is most commonly employed using CARS, its range in applications is far from limited, since dysregulation of lipid biosynthesis and metabolism can give rise to multiple diseased states, such as, diabetes, cardiovascular diseases, and cancer [61, 63, 67, 71-74].

In this chapter, we used a combination of microscopy techniques to visualize HCV RNA and intracellular LDs in human hepatoma cells (Huh-7). By using a femtosecond excitation laser source, two-photon excited fluorescence (TPF) imaging can simultaneously be combined with CARS [62, 69]. With this capability for noninvasive lipid imaging, we explored the use of lipid metabolic inhibitors that target specific host lipid pathways that are vital for HCV. We used lovastatin, which inhibits the HMG-CoA reductase, as well as a PPARα antagonist benzamide analogue. Despite their known potency against HCV, their mechanisms at the cellular level remain unexplored. To investigate this, we required a method to visualize HCV RNA in the cell. We accomplished this by employing an Alexa Fluor-488 probe, which covalently binds to the 5' end of the HCV RNA subgenomic replicon [75]. When applied *in situ,* the probe can allow us to track HCV RNA localization. We also focused on applying CARS to study changes in LDs by treatment with lovastatin and a 2-chloro-5-nitro-N-(pyridyl) benzamide (BA) analogue to examine whether changes in LDs and viral inhibition both correlate in a temporal manner. Our aim was to identify whether live-cell visualization of HCV RNA and LDs can probe for the mechanisms in which blockade of lipid metabolism corresponds directly to antiviral activity.

Hypothesis

Live cell simultaneous two-photon and CARS microscopies has the ability to visualize labeled RNA localized in its replication sites, and monitor the effects of lipid metabolism inhibitors on the RNA dissociation and degradation.

Results

PPARα antagonism with BA results in rapid hyperlipidemia in Huh-7.5 cells

To characterize the effects of inhibitors of lipid metabolism on cellular lipid storage and LD phenotype, CARS microscopy was used to analyze the LD phenotype of human hepatoma cells (Huh-7.5) upon treatment with the PPARα antagonist, BA (Fig. 2.1). The CARS microscope was selectively tuned to image LDs by adjusting the frequency difference between the two input laser pulses derived from one light source combined with a photonic crystal fiber to match the inherent Raman vibration of C-H bond stretching at 2850 cm^{-1}, which is highly concentrated in lipids [62]. The lipid phenotype observed after treatment showed dramatic hyperlipidemia induced by 75 μM treatment with BA, a concentration known to significantly reduce HCV replication in cell culture (Fig. 2.1 C) [76]. The inhibition of HCV replication was confirmed by Western and Northern blots as well as a luciferase assay, as previously described [76].

After a 6 h treatment with BA, we observed that a significant accumulation of LDs was mainly localized around the perinuclear region of the cell, appearing as larger LD aggregates (Fig. 1 D). We quantified the lipid volume per cell using voxel analysis [71, 77, 78]. Voxel analysis determines the number of 3-dimensional pixels that are present in a defined region of interest above a set threshold. Voxel analysis can be performed using signals such as fluorescence or CARS within a given cell image. This analysis, which was performed for at least 20 different cells per replicate, provides quantitative data as previously reported [71, 77, 78]. The high volume and density of these LDs resulted in hyperlipidemia, forming LD aggregates that can be described as a group of LDs fused together or tightly grouped in a particular region of the cell with a roughly 5- to 15-fold increase in the lipid density by volume (Fig. 2.1, Appendix 2.1 & 2.2). We observed that the increase in LDs and LD aggregates first occurred as early as 3 h after treatment. In the absence of treatment, a low abundance of small LDs (~1 μm in diameter) were mainly distributed throughout the cell, indicative

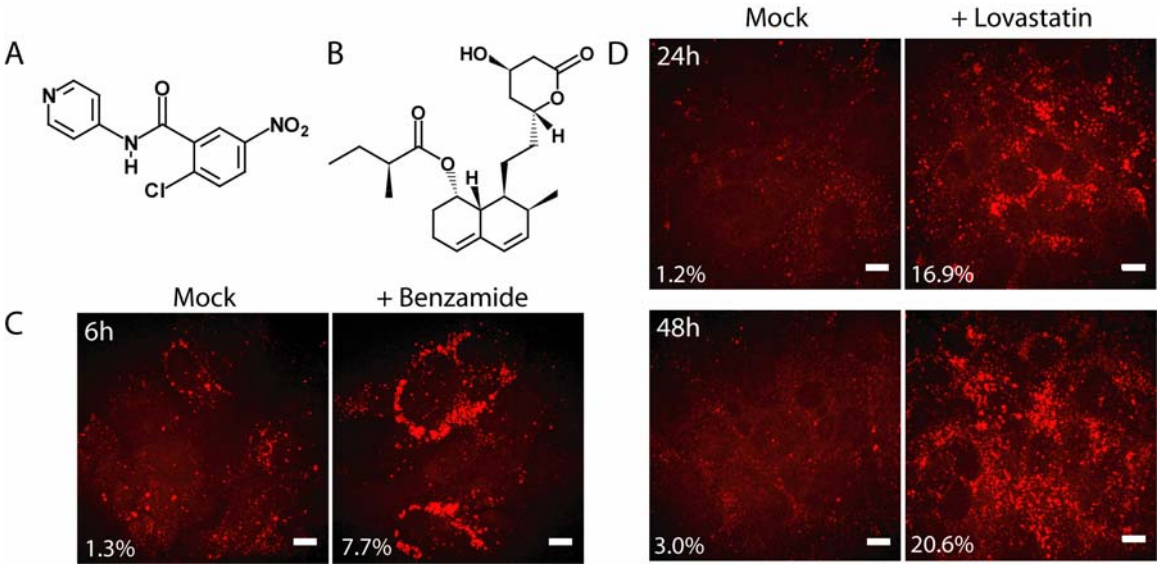

Figure 2.1: CARS images show changes in lipids observed in Huh-7.5 cells treated with BA and lovastatin. (A) Structure of 2-Chloro-5-nitro-N-(pyridyl) benzamide (BA). (B) Structure of lovastatin. (C) The effects of 75 μM BA on Huh-7.5 cells incubated in culture for 6 h. (D) The effects of 50 μM lovastatin treated Huh-7.5 cells for either 24 or 48 h. Values on the bottom left corner of the CARS images represent voxel analysis indicating the lipid droplet volume per cell (average of 5 cells per sample). Scale bars: 10 μm.

of naïve cellular lipid levels. These levels were similar in the mock-treatment and resulted in minimal variance at all time-points, as observed by CARS microscopy, in contrast to the BA-treated cells (Appendix 2.1 & 2.2). Similar results were obtained in serum-depleted media, suggesting that increases in lipid storage are not dependent on lipid content in the media (Appendix 2.1 & 2.3). Using low concentrations of serum in the cell culture medium presumably limits the amount of lipids that can be absorbed by the Huh-7.5 cells in culture. At a serum concentration of 2%, a condition where fatty acid content is reduced ~ 5-fold, hyperlipidemia was observed by CARS microscopy upon treatment with 75μM of BA, which are similar to the effects observed under normal (10%) serum levels. These results suggest that BA directly influences lipid metabolic pathways that regulate *de novo* lipid synthesis.

Inhibition of HMG-CoA reductase with lovastatin results in hyperlipidema

Next we investigated whether lovastatin would induce similar changes in LDs as observed in BA treated cells, although the mechanisms of action are quite different. Huh-7.5 cells treated with lovastatin displayed similar total levels of lipid density at 48 h as did BA-treated cells at the 6 h timepoint. Increases in lipids were first observed at 24 h and continued to increase through to the 72 h time point (Fig. 2.1 D, Appendix 2.2 B). In addition, in cells treated with lovastatin, LD complexes localized in the perinuclear region of the cell were first observed at 24 h. These complexes then diffused from the ER region into the cytoplasm resulting in a random scattering of LDs at 48 h. Although changes of LD density were observed as early as 3 h for BA-treated cells, this was not the case for lovastatin treatment, which first demonstrated detectable changes in lipid density at the 24 h time point in huh-7.5 cells. Since BA is a transcriptional antagonist of the entire PPARα pathway, while lovastatin only inhibits a single enzyme in the mevalonate pathway, this may account for the large difference in kinetics observed for these two molecules for the induction of hyperlipidemia [36, 79-81]. Lovastatin treatment took approximately 8-fold longer to induce the same hyperlipidemic effect as

BA treatment, and continued exposure resulted in sub-cellular re-organization of the LDs that was not observed with BA at any time. The levels of lovastatin used were significantly higher than those used clinically to lower serum cholesterol levels [82]. We show that while lovastatin is used to reduce cholesterol levels, it can also induce hyperlipidemia in hepatocytes, resulting in a similar lipid phenotype in cells as observed with BA treatment. Again we limited exogenous lipids in cell culture media by depleting the serum concentration (~2%) and observed similar results (Appendix 2.2 & 2.3).

Bezafibrate reduces hyperlipidemia by activating PPARα

PPARα is a global regulator of directly or indirectly controlling lipid metabolism through a complex network of transcriptionally regulated pathways [36, 79, 80]. After demonstrating through CARS microscopy that the PPARα antagonist, BA, increases lipid storage by altering cellular lipid metabolism, we hypothesized that bezafibrate (BF, Fig. 2.2 A), a PPARα agonist, should reverse the effects of BA treatment by inducing PPAR binding to the peroxisome proliferators response elements (PPREs) that control the transcription of PPRE regulated genes. Since BA is an antagonist of the PPARα pathway, treatment with an agonist should have a minimal effect on LDs in their naïve state that is already at a low LD level, and the cellular lipid levels should remain similar to the mock-treated samples. As expected, BF treatment alone did not alter lipid levels and the cellular LD phenotype remained similar to that of the mock-treated samples (Fig. 2.2 B). To confirm that the effects of BA treatment was due to PPARα antagonism, we carried out a complementation experiment in which cells were first induced by BA to a state of hyperlipidemia, followed by the treatment with BF, which should reverse the effects. Since the IC_{50} of BF is similar to BA [83], we evaluated the effects of 75 μM PPARα agonist, BF, on Huh-7.5 cells (Fig. 2.2 C).

CARS imaging and voxel analysis confirmed an increase in cellular lipid volume after 6 h of BA treatment, and remained at a high lipid volume level after undergoing a wash and incubation with culture media in the absence of BA for another 6 h (Fig. 2.2 C, left panel; Appendix 2.4). Next, we

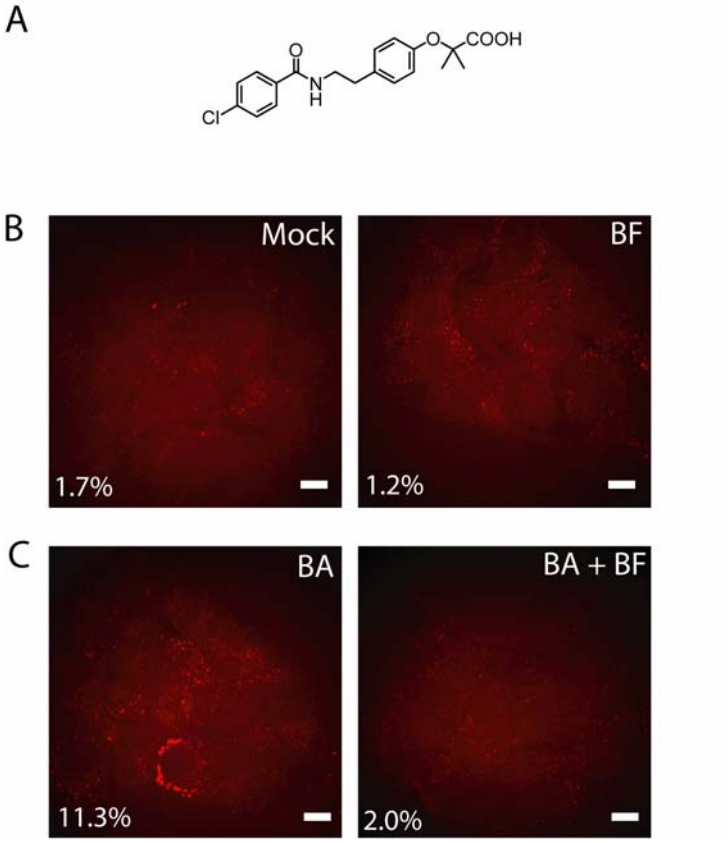

Figure 2.2: Bezafibrate rescues cells from hyperlipidemia after the treatment with benzamide. (A) Structure of bezafibrate. (B) Huh-7.5 cells were fixed without any treatment at 12 h (left panel) and treated with 75μM BF for 6 h (right panel). (C) Huh-7.5 cells were treated with BA for 6 h and washed with PBS buffer followed by the addition of regular media (left panel) or 75 μM of bezafibrate treatment (right panel) for 6 h and was fixed. Values on the bottom left corner of the CARS images represent voxel analysis indicating the lipid droplet volume per cell (average of 5 cells per sample). Scale bars: 10 μm.

investigated whether a reversal effect is observed with BF treatment. Following the 6 h BA incubation, the cells were washed and treated with BF for a subsequent 6 h treatment to reverse the effects of BA induced hyperlipidemia. We then measured the effects of treatment with BF (Fig. 2.2 C, right panel) by CARS microscopy. Voxel analysis shows that the lipid density significantly decreased and returned to normal levels, approximately 2% lipid volume per cell which is consistent with naïve cells only fixed at 12 h (Fig. 2.2 B, left panel; Appendix 2.4). The results from BF treatment clearly demonstrate a rescue effect on BA induced hyperlipidemia.

Larger LDs formed after BA treatment are partially the result of lipid fusion events

To further characterize lipid aggregate formation, we applied CARS microscopy and scanned regions containing multiple cells during the first 6 h of treatment with BA (Fig. 2.3). The hyperlipidemia previously observed in BA-treated cells can either result from de novo LD biosynthesis, or LD fusion events where smaller LDs combine to form larger LDs. While monitoring the same cell over a 6 h time course, we observed a fusion event involving three independent LDs in close proximity that fused over several hours during BA treatment. This suggests that lipid fusion proteins may play a role in facilitating this process. Since BA treatment results in a dramatic increase in both the size and number of LDs and many LDs become closely associated, it is impossible to quantify the contribution of LD fusion to the formation of larger LDs. Therefore, we cannot rule out LD fusion as a contributing mechanism to hyperlipidemia in Huh-7.5 cells treated with BA.

Imaging of HCV replicon harbouring cells treated with BA and lovastatin

Once we established that CARS microscopy could be used to quantify changes in lipid metabolism and that this can be used to observe LD fusion events, we next wanted to apply this

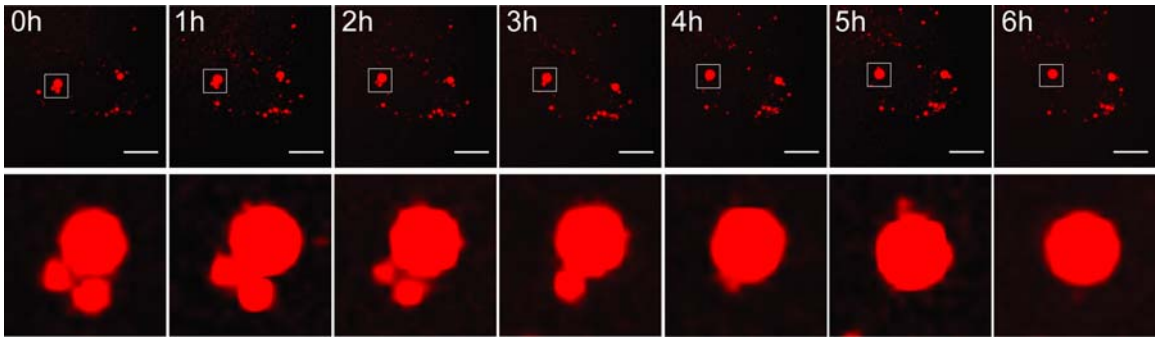

Figure 2.3: Demonstration during live cell imaging of an independent lipid fusion event observed over 6 h with BA treatment. Bottom panels are high magnification representations of cropped inset shown in the upper panel. Scale bars: 10 μm.

technique to examine the effects of BA and lovastatin on cell culture models for HCV. In this approach, we used Huh-7 cells that stably harbour a subgenomic HCV replicon (Fig. 2.4 A). Since BA and lovastatin are both known to inhibit HCV replication, we wanted to test whether HCV influences the ability of either BA or lovastatin to induce hyperlipidemia in Huh-7 cells. Here, we show that HCV replicon harbouring cells treated with BA and lovastatin responded similarly to naïve Huh-7.5 cells. This suggests that HCV does not prevent hyperlipidemia, but rather is inhibited by the results of the changes to cellular lipid metabolism, which is consistent with previous findings [76, 84].

Having demonstrated that CARS can effectively monitor changes in lipid phenotypes upon treatment with known lipid metabolism inhibitors we next sought to probe the effects of these compounds on HCV RNA localization while simultaneously observing their effects on lipid metabolism. Upon treatment with BA or lovastatin, changes in LD accumulation and localization may affect HCV replication complexes and changes in neutral lipid levels may also influence viral replication. To explore the direct effect of these compounds on HCV RNA, we used two-photon fluorescence (TPF) microscopy to visualize labeled HCV RNA simultaneously with CARS microscopy in order to monitor changes in lipid phenotype. Naïve Huh-7.5 cells were electroporated with subgenomic HCV replicon RNA that was covalently labeled at the 5' end with an Alexa Fluor-488 fluorescent tag (Fig. 2.5 A) [75, 78]. Our previous studies indicated that 5'labeled HCV RNA is replication-competent [75, 78, 85]. Although this approach does not give any information about location of progeny RNA that are replicated from the template, it is a very useful technique to track RNA localization while simultaneously evaluating the lipid content and storage in the form of LDs.

By combining CARS and TPF microscopies, we have observed simultaneously the development of hyperlipidemia and localization of a fluorophore tagged HCV RNA as described previously [78]. Treatment with BA and lovastatin commenced 24 h after electroporation of labeled replicon RNA into cell in order to allow cells to recover and to permit viral translation and establishment of HCV replication complexes. It was generally observed that upon electroporation of Huh-7.5 cells with subgenomic HCV replicon RNA covalently labeled at the 5'-end with Alex Fluor-

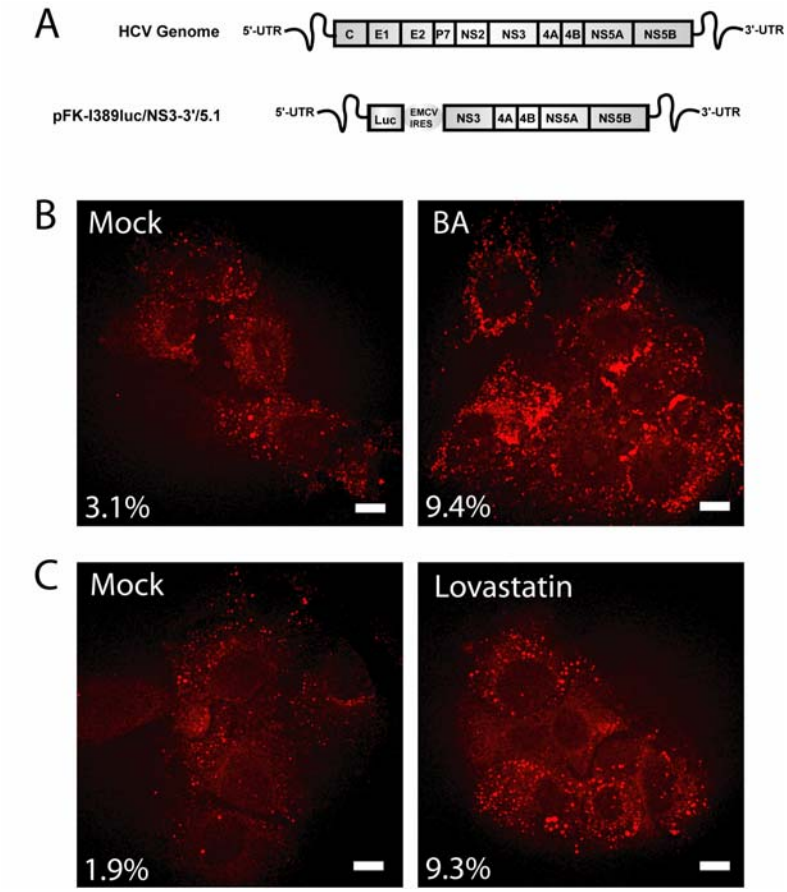

Figure 2.4: CARS images demonstrating lipid droplet distribution in BA and lovastatin treated Huh-7 cells stably harboring an HCV subgenomic replicon. (A) Schematic representation of full length HCV genomic RNA and the subgenomic replicon containing non-structural proteins in the genomic RNA sequence with the addition of a luciferase reporter gene located at the 5' region. (B) The effects of 75 μM BA on Huh-7 cells stably harboring an HCV subgenomic replicon incubated in culture for 6 h (C) The effects of 50 μM lovastatin on Huh-7 cells stably harboring an HCV subgenomic replicon incubated in culture for 24 h. Values on the bottom left corner of the CARS images represent voxel analysis indicating the lipid droplet volume per cell (average of multiple cells per sample). Scale bars: 10 μm.

488, hundreds of copies of fluorescently tagged RNA were visible following a 24-h recovery and just prior to treatment.

We observed a similar change in the LD phenotype after treatment with BA over 6 h as previously observed in naïve Huh-7.5 cells. With lovastatin, changes in LD phenotype were also observed, but not until 24 h after treatment. Since, hyperlipidemia is only observed after 24 h and that the half-life of the fluorophore conjugated RNA is approximately 12 h in Huh-7.5 cells [75, 78], we are unable to observe significant levels of RNA at the timepoints where lovastatin is active. Accordingly, we observed weak fluorescence signals that are highly dispersed in the control cells after 48 h, irrespective of treatment. Therefore we are unable to evaluate the effects of lovastatin on HCV RNA at the replication sites by this technique. By contrast, the rapid kinetics of BA is compatible with the lifetime of the Alexa Fluor-488 conjugated HCV RNA and therefore allowed us to track changes in localization of HCV RNA.

BA disrupts HCV replication complexes

At the start-time of imaging, the labeled replicon RNA was found to be localized in tightly associated bright punctate spots, which are likely to contain hundreds of copies of labeled RNA, in distinct areas of the cells mostly localized to the perinuclear region. Smaller punctate spots were also observed residing a little farther away from the nucleus. Rapid changes were observed within the first hour of treatment, with BA showing a more diffuse pattern for the labeled HCV RNA (green) surrounding what originally were punctate spots (Fig. 2.5 A). This dispersion of smaller clusters of RNA becomes more apparent with time, diffusing to the rest of the cytoplasm in a progressive manner and eventually levels off at the 5–6 h time point (Fig. 2.5 A). We hypothesize that dispersed RNA is no longer undergoing active translation or replication. This is supported by previous work that indicated a significant decrease in levels of HCV proteins and RNA upon treatment with BA at

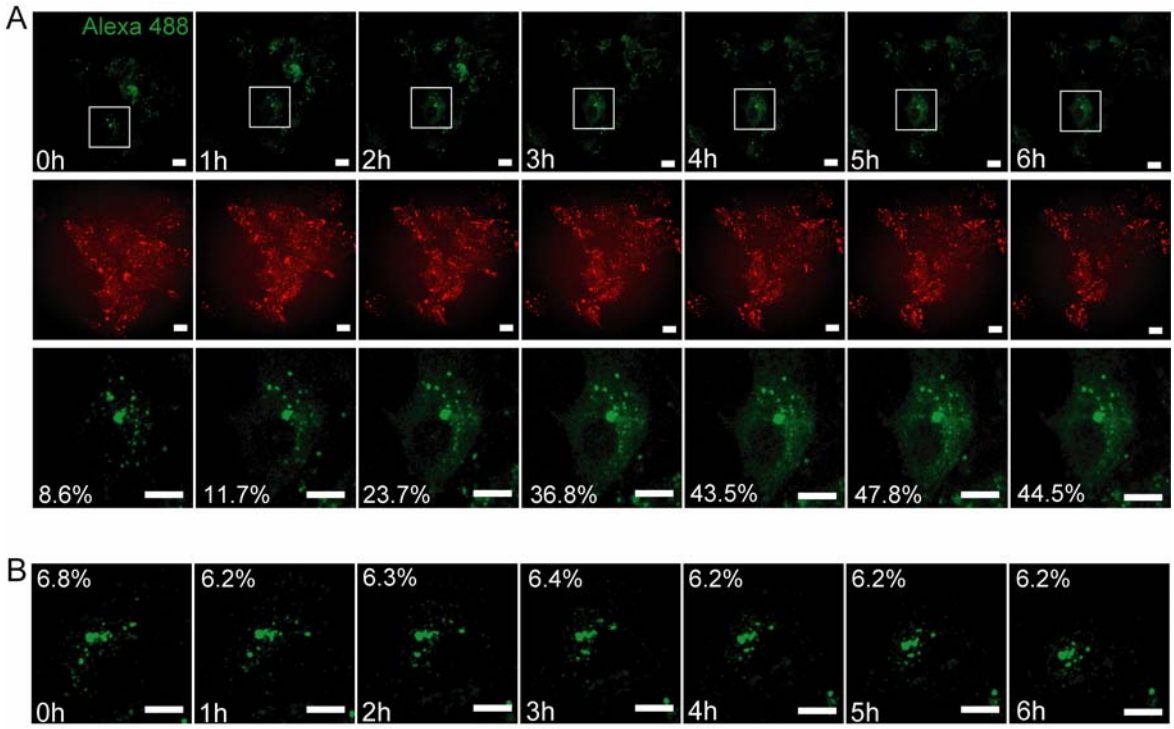

Figure 2.5: Live Cell Imaging of Huh-7.5 cells electroporated with a replicon HCV genomic RNA tagged with a 5' Alexa Fluor 488 label and treated with 75 μM of BA over 6 h. **(A-B)** After observing more than 40 independent areas of BA treated cells in each sample with more than 6 replicates (240 independent areas), shown here are the images of two-photon fluorescence (upper panel), CARS channel images (middle panel), and a magnified view indicated by the boxes of the upper panel of one cell expressing labeled HCV RNA (lower panel). Scale bars: 10 μm. **(A)** The effects of 75 μM BA disrupting the replication complex of HCV 488-RNA. **(B)** Cells imaged without BA treatment. Values on the magnified images represent voxel analysis that measures the volume of dispersion throughout the entire cell of the 5' fluorescently tagged RNA label from a tightly compact localization within replication complexes. Scale bars: 10 μm.

these time points [76]. Under the same conditions but without BA treatment, fluorescently labeled HCV replicon RNA retained a punctate pattern demonstrating that the observed RNA dispersion is caused by the action of BA (Fig. 2.5 B). Voxel analysis allowed us to quantify the dispersion of the HCV RNA as a function of cell volume. We observed that in the absence of BA, the fluorophore-labeled HCV RNA occupies roughly 6%–8% of the total cell volume. When BA is added this volume increases to ~40%. This is consistent with our hypothesis that BA treatment results in the disruption of HCV RNA replication complexes.

Detection of HCV dsRNA reveals a disrupted replication complex

To confirm the dispersion of HCV RNA that was actively replicating in its replication complexes, we next used an antibody that was specific for dsRNA in cells stably replicating subgenomic HCV replicons. Imaging was performed to capture changes in dsRNA intermediates as a function of time. To observe a change in localization, from punctate to diffuse localization, we treated the cell line stably harboring an HCV subgenomic replicon with BA (Fig. 2.6). By using a monoclonal antibody that specifically recognizes dsRNA in replication complexes based on previous studies, we observe a typical punctate fluorescence pattern in HCV replicon cells detected by immunofluorescence (Fig. 2.6 B) [86, 87]. Our observations using this approach were consistent with results seen in live cell imaging of Alexa Fluor-tagged HCV RNA (no BA treatment) as the labeled HCV RNA was highly concentrated in the replication complexes known to reside in the perinuclear region of the cell [87]. We observed that after a corresponding treatment with BA for 6 h (Fig. 2.6 C&D), the detection of HCV dsRNA was more diffuse, which confirms our results for labeled subgenomic HCV replicon. Voxel analysis indicated a greater than 60-fold increase in the dispersion of the ds-RNA relative to control cells, and the dispersed RNA occupied ~30%, and ~50% of the cell volume after BA treatment (Fig. 2.6). Control samples validate the specificity of the dsRNA antibody

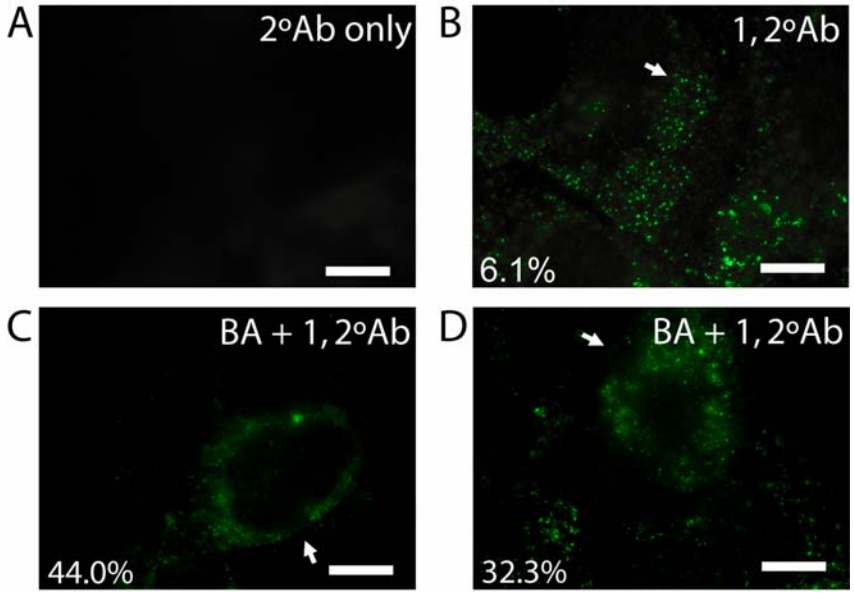

Figure 2.6: Immunofluorescence detection of HCV dsRNA in Huh-7 cells stably harboring subgenomic replicons after the treatment with BA. All samples were imaged as described in the materials and methods, to detect Cy2 tagged secondary antibody using the fitc channel on the confocal microscopy. (A) A control sample includes cells stained with Cy2 tagged secondary antibody in the absence of primary antibody that recognizes HCV dsRNA. (B-D) shows Huh-7 cells harbouring a subgenomic replicon was labeled for HCV dsRNA with a monoclonal primary antibody and Cy2 conjugated secondary antibody with and without BA treatment. (B) Huh-7 cells harbouring a subgenomic replicon without treatment, (C-D) and cells treated with 75μM BA for 6 h. Values on the bottom left of the images represent voxel analysis that measures the volume of dispersion of HCV dsRNA throughout the cell (arrow) in the shown image. Scale bars: 10 μm.

in cells harboring the HCV replicon, which showed a punctate staining patter in the absence of BA treatment (Fig. 2.6 B). We also confirmed that there is no nonspecific fluorescence attributed to the secondary antibody and autofluorescence of the cells (Fig. 2.6 A). In addition, we do not see appreciable staining in naive Huh-7.5 cells with the same staining protocol confirming the specificity of the antibody to dsRNA intermediates of HCV over cellular RNA. Thus, the dsRNA imaging experiments confirm our hypothesis that BA is dispersing HCV RNA from functional replication complexes.

Upregulation of triglycerides is compensated with a decrease in cholesterol

Next we sought to understand the effects of these two inhibitors on cholesterol, cholesterol ester, and triglyceride levels in cells supporting HCV replication of subgenomic replicons. To evaluate the changes in neutral lipid components in the treated cells, we measured the cellular levels of cholesterol and cholesterol esters in HCV replicon harboring cells with or without BA or lovastatin treatment (Table 2.1). Given that lovastatin is a well-known HMG-CoA reductase inhibitor, which blocks the rate determining enzyme in the cholesterol pathway, it is not surprising that a significant decrease of cellular levels of cholesterol and cholesterol esters is observed upon treatment with lovastatin after 48 h (Table 2.1). Similarly, BA treated cells also showed a decrease in cholesterol levels; however, cholesterol ester levels, a major LD component, remain relatively constant throughout the course of treatment (Table 2.1). This is consistent with the observed upregulation in LD biogenesis and the induction of hyperlipidemia observed in Huh-7.5 cells treated with BA (Fig. 2.1). Although cholesterol ester levels are significantly decreased by lovastatin yet remain unchanged with BA treatment, with CARS microscopy a hyperlipidemic phenotype is consistently observed when treated with either of the small molecule inhibitors. Because LDs primarily contain a core of cholesterol esters and triglycerides, triglyceride levels must increase to compensate for the decrease in cholesterol ester levels. To confirm this hypothesis, we measured cellular levels of triglycerides

		Cholesterol[1]	Cholesterol Esters[1]	Triglycerides[1]
6 h	HCV + BA	- 1.65 (± 0.06)	- 1.09 (± 0.09)	+ 1.37 (± 0.11)
48 h	HCV + Lovastatin	- 2.72 (± 0.02)	- 3.04 (± 0.07)	+ 1.93 (±0.05)

[1] (-) Fold change represent reductions, whereas (+) fold changes represent increases.

Table 2.1: Fold change analysis of cholesterol, cholesterol esters, and triglycerides levels in Huh-7 cells stably harbouring subgenomic HCV replicons that are treated with BA and lovastatin.

from the same cellular extracts used to measure cholesterol ester levels. Upon treatment with BA (6 h), or lovastatin (48 h), an increase in triglyceride levels is observed compared with the levels in untreated cells (Table 2.1). These observations validate the hyperlipidemic effects observed under CARS microscopy and confirm that high levels of LDs observed are consistent with an upregulation of triglyceride levels induced by both small molecules.

Expression of HCV core protein does not modulate the effects of BA

The HCV core protein is a key building block for the viral nucleocapsid and is an essential protein for HCV infectivity [55, 88-91]. The core protein is known to colocalize with LDs and components of the very low density lipoprotein (VLDL) assembly pathway [55, 88, 92-94]. The core protein has also been established to induce fatty acid synthase (FAS) activity in cell culture and induce hyperlipidemia in both cells and animal models [95-97]. The HCV genotype 3a core protein is known to exert a stronger influence on lipid metabolism [55, 98]. We next decided to test the ability of core proteins from either genotype 1a or 3a to modulate the effects of BA on HCV RNA dispersion. To accomplish this, we used bicistronic plasmids expressing GFP and HCV core protein (Fig. 2.7 A) so that we could track individual cells expressing the core protein with GFP as a reporter, and observe changes in the cell by confocal microscopy. We chose to overexpress the core protein rather than use a genomic replicon because we wanted to test whether core has any influence on BA activity at maximal levels of core overexpression.

Hepatoma cells stably harboring an HCV subgenomic replicon were transfected with either the genotype 1a or 3a core protein and dsRNA localization was measured using immunofluorescence [99, 100]. Expression of the core protein was confirmed by Western blot (Fig. 2.7 B). Interestingly, HCV replicon harboring cells that were overexpressing the HCV core protein still showed a dramatic increase in RNA dispersion upon treatment with BA for 6 h (Fig. 2.7 C&D). Neither the overexpression of core 1a nor that of core 3a had an appreciable effect on the degree of HCV dsRNA

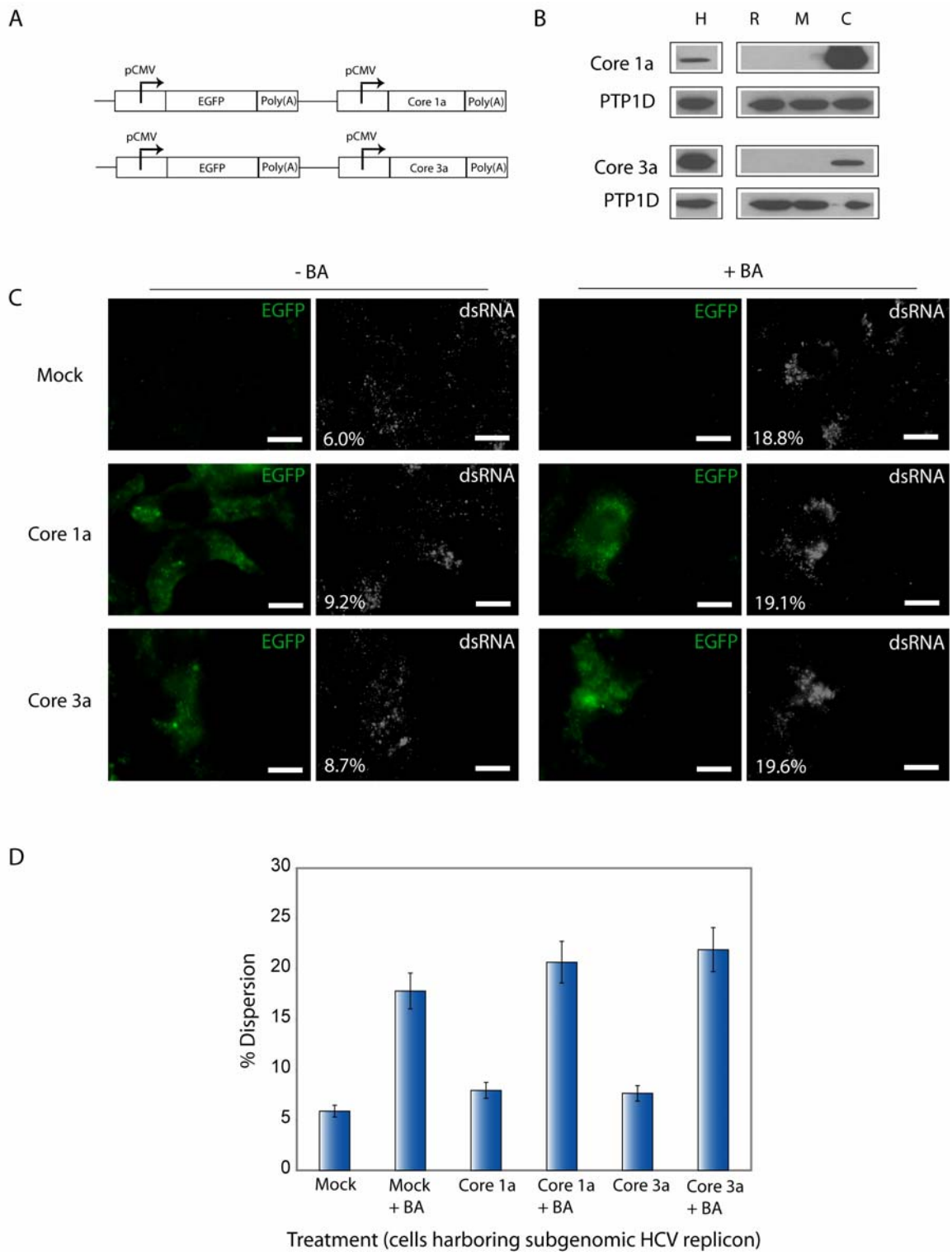

Figure 2.7: Immunofluorescence detection of HCV dsRNA in Huh-7 cells stably harboring subgenomic replicons that were expressing HCV core protein followed by BA treatment. All samples were imaged by confocal microscopy as described in the materials and methods, to detect Cy3 tagged

secondary antibody that binds to a primary dsRNA antibody(A) Schematic representation of bicistronic plasmids encoding EGFP and HCV core1a and core3a under different promoters and were used to transfect Huh-7 cells stably harboring subgenomic replicons. (B) Western blot expression levels of HCV core protein. Lanes are: R, Huh-7 cells stably harboring subgenomic replicons; M, mock of 15 μl of lipofectamine; C, 7.5 μg of bicistronic core plasmid transfection; H, Huh-7.5 cells expressing HCV core. (C) The effects of 75 μM BA on Huh-7 cells stably harboring subgenomic replicons that are expressing HCV core protein 1a and 3a. EGFP was detected in the fitc channel to monitor core expression and HCV dsRNA was detected in the tritc channel. Values on the bottom left of the images represent voxel analysis that measures the volume of dispersion of HCV dsRNA throughout the cell. Scale bars: 10 μm. (D) A graph quantifying the percentage of dispersion of dsRNA in Huh-7 cells stably harboring subgenomic replicons and expressing HCV core protein genotype 1a and 3a were treated with and without BA (average of at least 5 samples).

dispersion. It appears that neither protective effects nor synergistic effects were observed even with core 3a, which is well known to have a strong influence on sterol regulatory element binding protein (SREBP) and FAS activity. Rather, the effects of BA appear to dominate over any changes to the host cell that are induced by the HCV core protein.

Discussion

Host interactions and specific host factors play important roles in HCV replication [10, 11, 93]. Previously, it has been established that host cell lipid metabolism plays an important role in HCV propagation and that inhibitors of the mevalonate pathway and antagonists of PPARα-signaling block HCV replication [28, 76, 101]. In addition, eliminating cellular sphingolipids decreases HCV replication and the budding of infectious HCV particles involves association with apolipoprotein-dependent VLDL particles for viral assembly and egress [102-104]. In the case of inhibitors of the mevalonate pathway, it has been established that a geranylgeranylated host protein FBL2 is required for competent HCV replication complexes [84]. However, the correlation of changes in cellular lipid metabolism and simultaneous effects of HCV are difficult to measure. Coupled with TPF, CARS microscopy can measure effects on lipid metabolism while simultaneously tracking fluorescently tagged HCV RNA molecules. Herein, we show that HCV RNA is dispersed from replication complexes upon treatment with BA. This likely prevents HCV RNA from associating with host and viral proteins that are necessary for replication. Alternatively, membrane environments such as the membranous web that serve as a platform for HCV replication complexes may also be perturbed resulting in the observed decrease HCV replication. Also, it has recently been reported that LDs are important for viral replication and assembly of the replication complex in LD-associated membranes [51]. The changes we observed in viral RNA localization upon induction of a hyperlipidemic state in HCV replicon expressing cells supports these findings.

Herein, we have shown that treatment with lipid metabolic inhibitors resulted in perturbations in lipid phenotype over time, specifically changes in LD density and distribution. BA induces a rapid rate of hyperlipidemia with 6 hr of treatment, while lovastatin treatment results in the progressive build up of LDs from 24 h to 72 h. Upon these changes in lipid metabolism, we measured a significant increase in triglyceride levels, the other major component found within LDs, which shows that the overall composition of the droplets is likely changing as the hyperlipidemic state is induced since the ratios of cellular cholesterol esters and triglycerides are clearly altered during treatment with BA and lovastatin.

The biogenesis of triglycerides and cholesterol requires cellular acetate. As acetyl-CoA is formed, it enters either the mevalonate pathway or the malonyl-CoA pathway to form cholesterol for the former and triglycerides for the latter (Fig. 2.8 A). Our results suggest that inhibition of the mevalonate pathway with BA does not prevent triglyceride synthesis and may actually promote it as a homeostatic response to the decrease in cholesterol levels. Lovastatin may elicit a similar event through a homeostatic response to the blocking of the mevalonate pathway and cholesterol synthesis.

Because the timeline for the emergence of hyperlipidemia was observed to be similar to that of HCV RNA knockdown upon BA treatment, we monitored changes in HCV RNA localization in an attempt to visualize and understand the mechanism by which HCV replication is inhibited. After employing a 5'-Alexa fluor tagged HCV RNA that was electroporated into Huh-7.5 cells, we observed a punctate RNA staining localized in the perinuclear region where the replication complex is known to reside [2, 105-107]. Simultaneous TPF and CARS microscopy was used to capture the dynamics of RNA localization, and at the same time monitor changes in LD distribution. We have demonstrated that HCV RNA labeling is an effective tool to visualize dynamic processes and localization in living cells. In addition, this was confirmed by labeling for dsRNA (Fig. 2.6). Live cell imaging studies provide the means to understand changes in localization that are associated with changes in the host cell.

By combining the use of labeled RNA in live cell imaging, we find that modulating host metabolic processes indirectly induces changes in HCV RNA localization. Immediately after

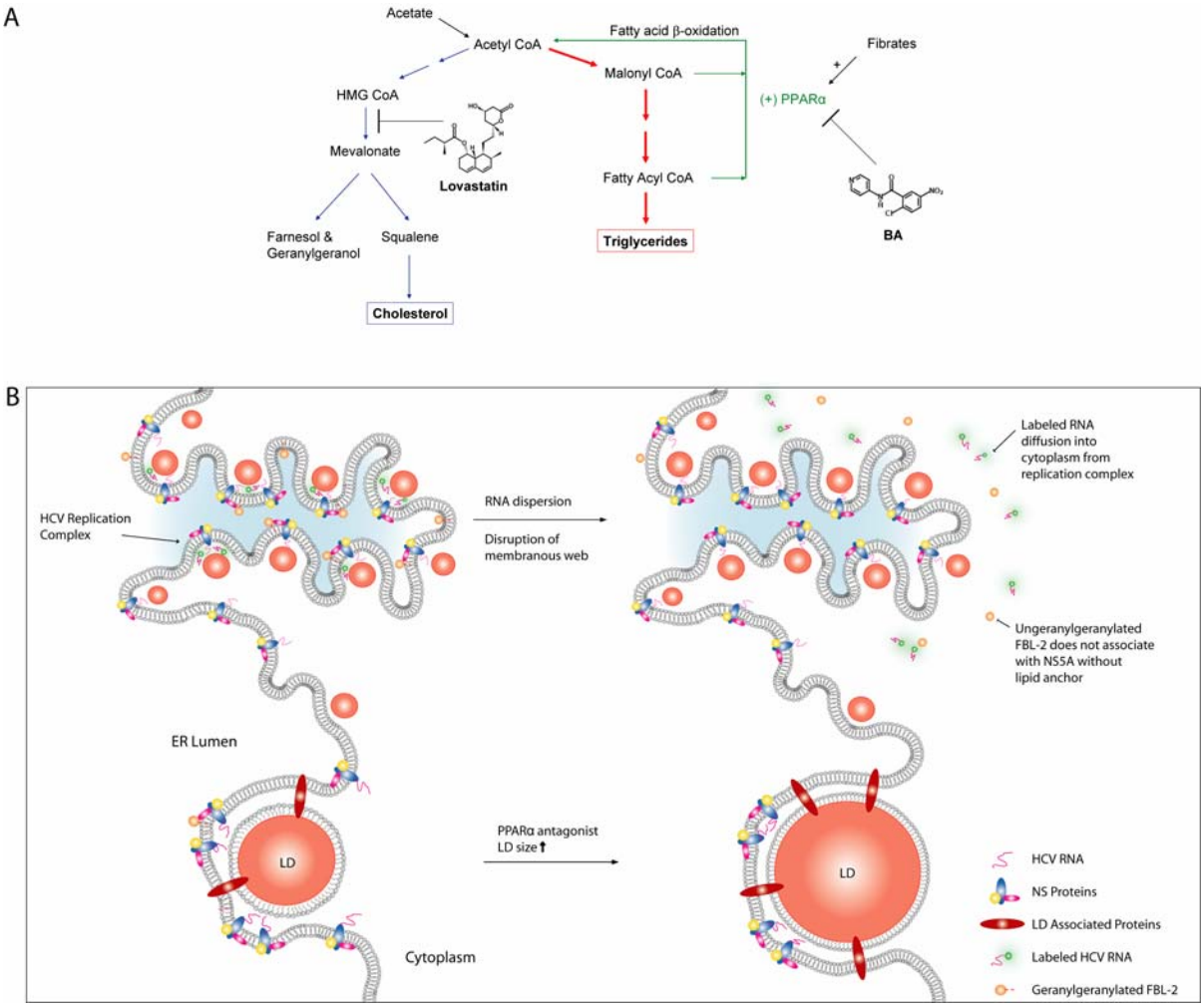

Figure 2.8: HCV replication complex relies on host metabolic processes. (A) Schematic of neutral lipid formation from the acetate pathway and the mode of inhibition with lovastatin and benzamide influencing the levels of mevalonate and malonyl-CoA. (B) A hypothetical model of HCV replication complex environment being disrupted by changes modulating host lipid metabolism. Both PPARα antagonism that results in larger lipid droplets and density, and inhibition of HMG-CoA reductase that prevents the necessary cholesterol substrates for HCV replication, are demonstrated in this schematic.

treatment with BA, TPF images show the rapid dispersion of labeled RNA in a diffuse pattern throughout the cytoplasmic space over 6 h. This coincides with changes in lipid dispersion in the cell that likely disrupts the replication complex to which the HCV RNA is associated in LD-associated membranes. This progressive diffusion of labeled RNA directly corresponded to the time points observed under changes in lipid phenotype. This is consistent with results, which previously demonstrated that BA decreases HCV RNA replication over a 6 h time course [76]. RNA dispersion from replication complexes was quantified using voxel analysis and showed a marked increase in RNA dispersion occupying greater than 40%, on average, of the cell after only a 6 h BA treatment.

While we observed an increase in hyperlipidemia as demonstrated by CARS microscopy, cells treated with either inhibitor consistently display LD aggregates accompanied by an increase in LD size and number. These large complexes are initially confined to the perinuclear region of the cells, although with lovastatin treatment, they diffuse into the cytoplasm slowly over time. LD fusion was observed to occur in live cells as demonstrated by CARS microscopy and is likely a source for the formation of larger LDs. An increase in LD size may also arise from increases in progressive TG loading into LD, as well as, an increase in *de novo* biosynthesis of lipids. The fact that we have observed some fusion events indicate that the SNARE system, which is known to have an important role in LD fusion, involving several proteins including NSF (N-ethylmaleimide-sensitive factor), α-SNAP (soluble NSF attachment protein) and the SNAREs (SNAP receptors), SNAP23 (synaptosomal-associated protein of 23 kDa), syntaxin-5, and VAMP4 (vesicle-associated membrane protein 4), may be modulated during treatment with BA [108, 109]. Previously it was shown that the knockdown of the genes for SNAP23, syntaxin-5, or VAMP4, decreases the rate of fusion and the size of the LDs observed in liver cells [108, 109]. The observation of LD fusion suggests that BA, and thus negative regulation of PPARα signaling, may stimulate the SNARE system to further aid in the storage of triglycerides and cholesterol esters.

The HCV core protein originating from genotype 3a, in particular, is well known to induce hyperlipidemia largely by activating SREBP-controlled genes as well as increasing FAS activity in

hepatoma cells [55, 95-97]. However, during overexpression of HCV core proteins, we do not observe dispersion of HCV RNA as measured using a dsRNA-specific antibody (Fig. 2.7). This implies that the effects of core protein alone are not sufficient to influence replication complex localization and stability. We also find that core protein does not contribute to the effects of BA on HCV RNA localization. The upregulation of FAS and ultimately VLDL secretion by the HCV core protein may be controlled evolutionarily in order to maximize infectious particle secretion but not so high as to cause changes in replication complex fidelity through altered localization.

Our observations of LD fusion may provide deeper insight for the importance of the local membrane environment necessary for HCV replication. We observed punctate RNA staining patterns consistent with localization at replication complexes in the interstitial space between the LD and the ER membrane forming an LD-associated membrane or membranous web as has been previously proposed [105-107, 110]. When hyperlipidemia is induced with the PPARα antagonist, BA, two possible pathways may lead to the dispersion of HCV RNA. First, BA has been shown to cause a rapid decrease in HMG-CoA reductase levels that likely results in the reduction in geranylgeranylation of FBL2, and, in turn, causes the release of HCV replicon RNA from the replication complexes [76, 84]. FBL2 interacts with NS5A at the site of the replication complex where the HCV NS proteins reside [84]. Second, it is possible that by increasing LD size via droplet fusion events there are also changes to the local environment around LDs and the membranous web that disrupts the replication complexes that would give rise to the rapid kinetics of the RNA dispersion observed.

In conclusion, we have shown that HCV RNA replication is disrupted by BA and lovastatin by altering host cell metabolism, and specifically, by causing a dispersion of the RNA from replication complexes. CARS and TPF can be used to measure dynamics and subcellular localization of HCV RNA while at the same time imaging changes in the host cell metabolism and alterations of LDs. This is particularly significant for HCV given that LDs are of such critical importance for the infectivity of the virus. CARS and TPF microscopy show a buildup of lipids and LDs upon treatment with BA, a PPAR antagonist, which is consistent with an impaired function of the PPARα receptor.

Simultaneous CARS and TPF experiments indicate that BA disperses HCV RNA and this is coincident with a decrease in HCV replication, suggesting that the HCV RNA is no longer located in replication complexes in the membranous web environment.

Materials and Methods

In vitro transcription

In vitro transcripts were generated using a MEGAscript™ (Ambion, Austin, Texas) according to the manufacturer's protocol. In brief, the template DNA was linearized with the restriction enzyme ScaI (New England BioLabs, Pickering, Ontario), precipitated for less than 30 min and resuspended in RNase-free water to a concentration of 0.5 μg/μl. The *in vitro* reaction was set up and incubated at 37 ºC for 2 h. To degrade the DNA template, 1 μl of DNaseI was added and incubated for another 15 min at 37 ºC. The *in vitro* transcripts were then cleaned using the MEGAclear kit from Ambion (Austin, Texas) according to the manufacturer's protocol. The concentration was determined by measurement the absorbance at 260 nm with a ND-1000 Spectrophotometer (NanoDrop Technologies, Rockland, DE) and RNA integrity was verified by electrophoresis using the Agilent 2100 bioanalyzer with the RNALabChip® kit according to the manufacturer's protocol.

5'-end labeling of RNA with Alexa Fluor 488® C_5 dye

RNA *in-vitro* transcripts were labeled with an Alexa Fluor 488® C_5 maleimide dye (Invitrogen, Burlington, ON) using the 5'-EndTag Nucleic Acid Labeling System™ from Vector Laboratories (Burlingame, CA). Briefly, 120 μg of HCV RNA were labeled with the thiol-reactive label, Alexa Fluor 488® C_5 maleimide. Briefly, a thiophosphate is transferred from ATPγS to the 5' hydroxyl group of the RNA by T4 polynucleotide kinase. After addition of the thiol functional group, a thiol-reactive label was chemically coupled to the 5' end of the RNA. Finally, the labeled RNA is purified by phenol-chloroform extraction and precipitated prior to quantification.

Simultaneous CARS and two-photon microscopy

The CARS microscopy system uses a single femtosecond Ti:sapphire oscillator (Spectra Physics Tsunami operating at 80 MHz) as the excitation source. The frequency difference between two input lasers, stokes and pump beam, is equal to that of the Raman resonance of interest. The second longer wavelength (Stokes beam) is generated through use of a photonic crystal fiber (PCF) which produces good power in the wavelength range of 1035 nm with negligible amplitude fluctuations [62]. When overlapped with the 800 nm (pump beam) from the Ti:sapphire laser, this corresponds to the 2850 cm^{-1} Raman resonance of the C-H stretch. A modified Olympus Fluoview 300 laser scanning system and IX71 inverted microscope was used to carry out all CARS and two-photon imaging. A 40X 1.15 NA UAPO water immersion lens with a cover slip collection was used as the objective and the 0.55 NA long working distance condenser lens for collection in the forward direction. Fluorescence signal was collected through the objective lens (epi-direction). A 400-700 nm filter (E700sp, Chroma Technology, VT) was used to discriminate fluorescence, and anti-stokes signals from the pump and stokes beams. Light was directed to photomultiplier tubes (PMT) with enhanced red sensitivity (Hamamatsu R3896) and operated at a gain of about 530 V. Imaging was completed when the combined average powers reached approximately 120 mW for the pump and the Stokes. Under live cell imaging, an incubator placed on top of the stage maintained conditions of 5% CO_2 at 37°C. Live and fixed cell samples were imaged in 4.2cm^2 Lab-Tek Chambers Slide System (NUNC, Rochester, NY). Optical sectioning of lipid droplets were imaged at 1 μm z-slices for a total z-stack analysis ranging from 7-12 μm depending on thickness of cell sample. Areas with cells expressing labeled HCV RNA were imaged by retrieving z-stacks for a 6 hour time course with images taken at each hour for control and BA treated cell samples. The same method was applied with lovastatin treated cells but with the specified time interval. Mock images were obtained to set the minimal threshold level of background fluorescence by adjusting the PMT levels.

Tissue culture

Human hepatoma cells (Huh-7.5) were grown in DMEM medium supplemented with 100 nM nonessential amino acids, 50 U/mL penicillin, 50 μg/mL streptomycin, and 10% FBS (CANSERA, Rexdale, ON). Huh-7 cells harboring the pFK-I389neo/NS3-3'/5.1 subgenomic replicon were maintained in the same culture medium supplemented with 250 μg/mL G418 Geneticin (GIBCO-BRL, Burlington, ON). The pFK-I389neo/NS3-3'/5.1 subgenomic replicon was kindly provided by Ralf Bartenschlager (Institute of Hygiene, University of Heidelberg, Germany).

Electroporation of labeled RNA in Huh-7.5 cells

Huh-7.5 cells were transfected with 488-labeled RNA through electroporation using a (BTX ECM830, Harvard Apparatus Inc., Holliston, MA). Briefly, cells were washed twice and resuspended with PBS. 5ug of labeled RNA was mixed with 80uL of washed cells with a density of $2.4x10^5$ cells in a 4mm gap cuvette and was pulsed five times at 820V, 99 μsec pulse length at 1.1 second intervals. After a 10 min recovery time, cells were resuspended in prewarmed DMEM and plated on the Lab-Tek Chambers.

BA and lovastatin treatment

Post 24 h electroporation of labeled RNA, cells at an approximate density of 70-90% confluency were treated with either 75 uM of benzamide (Calbiochem, San Diego, Calif.) or 50 uM of lovastatin (Cedarlane, Burlington, ON) for a total volume of 2 mL per Lab-Tek Chamber well. Benzamide was diluted in prewarmed antibiotic free DMEM and was added to the cellular sample prior to imaging with the specified time courses.

Fixed cell protocol

After the desired time interval of incubation of benzamide and lovastatin treatment in live cells culture, cells were washed twice with PBS, followed by a 15 minute incubation at room temperature

with fixing solution (4% formaldehyde, 4% sucrose, 1 mL). The fixed cells were washed twice with PBS for 3 minutes and then stored at 4°C in PBS prior to imaging.

Measurement of cellular triglyceride and cholesterol content

Huh-7 cells stably expressing an HCV subgenomic replicon, as previously described, were treated with BA and lovastatin for 6 h and 48 h respectively, after which lipids were extracted from 10^6 trypsinized cells. Triglyceride and cholesterol concentrations were analyzed directly by spectrophotometric analyses, using the triglyceride and cholesterol/cholesterol ester quantification kit (BioVision, Mountain View, CA) according to the manufacturer's instructions. Total protein levels were quantified with the BCA protein assay (Pierce, Rockford, IL). Triglyceride and cholesterol levels were expressed as nmol/mg protein and μg/mg protein, respectively.

Statistical analysis

Individual experiments in this study were performed in triplicate in order to confirm the reproducibility of the results. Values are represented as means ± standard deviations. The statistical significance of differences between two or more means was evaluated by using analysis of variance (ANOVA); P values of less than 0.05 (indicated by asterisks) were considered to be statistically significant

Rescue with Bezafibrate

Following 6 h of BA treatment, culture cells were washed 2X PBS, and then treated with either 75 μM bezafibrate (Cedarlane, Burlington, ON) in prewarmed DMEM (2 mL), or DMEM (2 mL) Cells were fixed in the same manner as previously described or used for live cell imaging.

Quantitative voxel analysis

Quantitative data from the CARS images was determined using ImageJ software. A voxel counting routine was used to determine the number of voxels in a defined region that meet a set threshold intensity. Using our software and conditions, this was set to 55, to eliminate all background signal. Using the ImageJ software the regions of interest (ROI) were defined by outlining the cell by autofluorescent images or by viewing z-stacks of the individual images. The voxels that met the threshold intensity were then counted in the ROI of a defined cell outline revealing the % volume of lipids. In each image, 5 cells were counted for a % lipid volume average.

Immunofluorescence analysis

Huh-7 cells harboring the HCV subgenomic replicon were seeded at 1.4 x 10^5 cells/well in DMEM on coverslips in a 12-well plate. After 24 h, at a confluency of 70-80%, cells were treated with 75 μM BA for the 3 and 6 h, and with 25 μM BA for the 18 h. After BA treatments, cells were washed once with 1X PBS pH 7.4 and fixed with pre-cooled 100% methanol for 10 min at -20^{o}C. Cells were washed three times with 1X PBS and incubated for 1 h at room temperature with a mouse monoclonal antibody specific for dsRNA (J2) (1:300 dilution in PBS, Scicons, Hungary). After three more washes with PBS, cells were incubated with Cy2-labeled donkey anti-mouse IgG secondary antibody (1:1000 dilution in PBS, Jackson ImmunoResearch Laboratories, Inc., Westgrove, PA) for 1 h at room temperature. Following three more washes with 1X PBS, cells were rinsed in H_2O before being mounted onto slides with 50% glycerol in PBS. Cells images were captured using an Olympus IX81 inverted microscope (Olympus America Inc.) and fluorescence was detected through a 100x NA 1.40 oil objective. The images were analyzed using ImagePro software (MediaCybernatics).

Overexpression of HCV core protein

Huh-7 cells harboring the HCV subgenomic replicon were seeded at 1.6 x 10^5 cells/well in Lab-Tek chambers. After 24 h, at a confluency of 60-70%, cells were then transfected with Core1a and Core3a expression plasmids [99, 100] suspended in transfection media comprised of DMEM without FBS, along

with lipofectamine 2000 (Invitrogen Canada Inc., Burlington, ON). After 4 h, DMEM in 20% FBS was added in equal volume to the transfection media already in the chambers. Core protein was then overexpressed for 48 h. Cells were then washed 1 x PBS and treated with BA in a similar manner as previously described. The cells were then fixed in the same manner as previously described in the fixed cell protocol. Immunofluorescence imaging was completed as described previously in the immunofluorescence analysis.

Immunoblot Analysis

Huh-7 cells harboring subgenomic replicons were seeded 8.0 x 10^5 cells in 60 mm dishes for preparation of Western blot lysates. After overexpression of HCV core protein and corresponding benzamide treatment as described previously, cells were washed and lysed with an SDS lysis buffer consisting of 50 mM Tris-HCl (pH 6.8), 2% SDS, 10% glycerol, 100 mM dithiothreitol (DTT), and 0.1% bromophenol blue (prepared without the DTT and bromophenol blue). A protease inhibitor cocktail mix (Roche Diagnostics, Penzberg, Germany) was added to each extract. The protein concentration of each sample was quantified by using the Bio-Rad DC Protein Assay according to the manufacturer's protocol. Prior to loading, 10% v/v of DTT and bromophenol blue (1:1) were added to each sample, and 35 mg/well was loaded onto a SDS-PAGE gel (12% resolving, 4% stacking gel). The resolved proteins were transferred to a Hybond-P (Amersham Biosciences, Piscataway, NJ) polyvinylidene difluoride membrane. The membrane was probed against HCV core protein by using a mouse anti-core 1º antibody (1:1000 dilution, Cedarlane, Burlington, ON) followed by a 2º (HRP)-conjugated goat anti-mouse IgG antibody (1:1000 dilution) obtained from Jackson ImmunoResearch Laboratories, Inc. (Westgrove, PA). As a loading control, a mouse PTP1D 1º antibody (1:2500 dilution; Sigma, Saint Louis, MO) was used with the same 2º antibody described above. Protein bands were visualized by Western Lightning Western Blot Chemiluminescence reagents (PerkinElmer Life and Analytical Sciences, Inc., Boston, MA) according to the manufacturer's protocol.

References

1. Gravitz, L., Introduction: A smouldering public-health crisis. *Nature* **2011,** 474, S2-S4.

2. Moradpour, D.; Penin, F.; Rice, C., Replication of hepatitis C virus. *Nat. Rev. Microbiol.* **2007,** 5, 453-463.

3. Simmonds, P.; Bukh, J.; Combet, C.; Deléage, G.; Enomoto, N.; Feinstone, S.; Halfon, P.; Inchauspé, G.; Kuiken, C.; Maertens, G.; Mizokami, M.; Murphy, D. G.; Okamoto, H.; Pawlotsky, J.-M.; Penin, F.; Sablon, E.; Shin-I, T.; Stuyver, L.; Thiel, H.-J.; Viazov, S.; Weiner, A.; Widell, A., Consensus proposals for a unified system of nomenclature of hepatitis C virus genotypes. *Hepatology* **2005**, 42, 962-973.

4. Feinstone, S. M.; Kapikian, A. Z.; Purcell, R. H.; Alter, H. J.; Holland, P. V., Transfusion-Associated Hepatitis Not Due to Viral Hepatitis Type A or B. *N. Engl. J. Med.* **1975,** 292, 767-770.

5. Webster, D. P.; Klenerman, P.; Collier, J.; Jeffery, K. J. M., Development of novel treatments for hepatitis C. *Lancet Infect. Dis.* **2009,** 9, 108-117.

6. Lange, C.; Sarrazin, C.; Zeuzem, S., Review article: specifically targeted anti-viral therapy for hepatitis C - a new era in therapy. *Aliment. Pharmacol. Ther.* **2010,** 32, 14-28.

7. Thompson, A.; McHutchison, J., Antiviral resistance and specifically targeted therapy for HCV (STAT-C). *J. Viral Hepat.* **2009,** 16, 377-387.

8. Jacobson, I.; McHutchison, J.; Dusheiko, G.; Di Bisceglie, A.; Reddy, K.; Bzowej, N.; Marcellin, P.; Muir, A.; Ferenci, P.; Flisiak, R.; George, J.; Rizzetto, M.; Shouval, D.; Sola, R.; Terg, R.; Yoshida, E.; Adda, N.; Bengtsson, L.; Sankoh, A.; Kieffer, T.; George, S.; Kauffman, R.; Zeuzem, S.; Team, A. S., Telaprevir for previously untreated chronic hepatitis C virus infection. *N. Engl. J. Med.* **2011,** 364, 2405-2416.

9. Poordad, F.; McCone, J.; Bacon, B.; Bruno, S.; Manns, M.; Sulkowski, M.; Jacobson, I.; Reddy, K.; Goodman, Z.; Boparai, N.; DiNubile, M.; Sniukiene, V.; Brass, C.; Albrecht, J.; Bronowicki, J.-P.; Investigators, S.-. Boceprevir for untreated chronic HCV genotype 1 infection. *N. Engl. J. Med.* **2011,** 364, 1195-1206.

10. Chisari, F., Unscrambling hepatitis C virus-host interactions. *Nature* **2005,** 436, 930-932.

11. Tai, A.; Benita, Y.; Peng, L.; Kim, S.-S.; Sakamoto, N.; Xavier, R.; Chung, R., A functional genomic screen identifies cellular cofactors of hepatitis C virus replication. *Cell Host Microbe* **2009,** 5, 298-307.

12. Bassendine, M. F.; Sheridan, D. A.; Felmlee, D. J.; Bridge, S. H.; Toms, G. L.; Neely, R. D. G., HCV and the hepatic lipid pathway as a potential treatment target. *J. Hepatol.* **2011,** 55, 1428-1440.

13. Salloum, S.; Tai, A., Treating hepatitis C infection by targeting the host. *Trans. Res.* **2012,** 159, 421-429.

14. Sheridan, D.; Neely, R.; Bassendine, M., Hepatitis C virus and lipids in the era of direct acting antivirals (DAAs). *Clin. Res. Hepatol. Gastroenterol.* **2012**, http://dx.doi.org/10.1016/j.clinre.2012.07.002

15. Fusco, D. N.; Chung, R. T., Novel Therapies for Hepatitis C: Insights from the Structure of the Virus. *Annu. Rev. Med.* **2012,** 63, 373-387.

16. Flisiak, R.; Feinman, S. V.; Jablkowski, M.; Horban, A.; Kryczka, W.; Pawlowska, M.; Heathcote, J. E.; Mazzella, G.; Vandelli, C.; Nicolas-Métral, V.; Grosgurin, P.; Liz, J. S.; Scalfaro, P.; Porchet, H.; Crabbé, R., The cyclophilin inhibitor Debio 025 combined with PEG IFNα2a significantly reduces viral load in treatment-naïve hepatitis C patients. *Hepatology* **2009,** 49, 1460-1468.

17. Flisiak, R.; Jaroszewicz, J.; Flisiak, I.; Łapiński, T., Update on alisporivir in treatment of viral hepatitis C. *Expert Opin. Investig. Drugs* **2012**, 21, 375-382.

18. Saka, H.; Valdivia, R., Emerging Roles for Lipid Droplets in Immunity and Host-Pathogen Interactions. *Annu. Rev. Cell Dev. Biol.* **2012**, 28, 411-437.

19. Diamond, D.; Syder, A.; Jacobs, J.; Sorensen, C.; Walters, K.-A.; Proll, S.; McDermott, J.; Gritsenko, M.; Zhang, Q.; Zhao, R.; Metz, T.; Camp, D.; Waters, K.; Smith, R.; Rice, C.; Katze, M., Temporal proteome and lipidome profiles reveal hepatitis C virus-associated reprogramming of hepatocellular metabolism and bioenergetics. *PLoS Pathog.* **2010,** 6, e1000719.

20. Martin, S.; Parton, R., Lipid droplets: a unified view of a dynamic organelle. *Nat. Rev. Mol. Cell Biol.* **2006,** 7, 373-378.

21. Farese, R.; Walther, T., Lipid droplets finally get a little R-E-S-P-E-C-T. *Cell* **2009,** 139, (5), 855-860.

22. Murphy, D., The biogenesis and functions of lipid bodies in animals, plants and microorganisms. *Prog. Lipid Res.* **2001,** 40, 325-438.

23. Herker, E.; Ott, M., Unique ties between hepatitis C virus replication and intracellular lipids. *Trends Endocrin. Metab.* **2011,** 22, 241-249.

24. Syed, G.; Amako, Y.; Siddiqui, A., Hepatitis C virus hijacks host lipid metabolism. *Trends Endocrin. Metab.* **2010,** 21, 33-40.

25. Ikeda, M.; Abe, K.; Yamada, M.; Dansako, H.; Naka, K.; Kato, N., Different anti-HCV profiles of statins and their potential for combination therapy with interferon. *Hepatology* **2006,** 44, 117-125.

26. Friesen, J.; Rodwell, V., The 3-hydroxy-3-methylglutaryl coenzyme-A (HMG-CoA) reductases. *Genome Biol.* **2004,** 5, 248.

27. Goldstein, J. L.; Brown, M. S., Regulation of the mevalonate pathway. *Nature* **1990,** 343, 425-430.

28. Su, A.; Pezacki, J.; Wodicka, L.; Brideau, A.; Supekova, L.; Thimme, R.; Wieland, S.; Bukh, J.; Purcell, R.; Schultz, P.; Chisari, F., Genomic analysis of the host response to hepatitis C virus infection. *Proc. Natl. Acad. Sci. U. S. A.* **2002,** 99, 15669-15674.

29. Targett-Adams, P.; Boulant, S.; Douglas, M.; McLauchlan, J., Lipid metabolism and HCV infection. *Viruses* **2010,** 2, 1195-1217.

30. Ye, J.; Wang, C.; Sumpter, R.; Brown, M.; Goldstein, J.; Gale, M., Disruption of hepatitis C virus RNA replication through inhibition of host protein geranylgeranylation. *Proc. Natl. Acad. Sci. U. S. A.* **2003,** 100, 15865-15870.

31. Kapadia, S.; Chisari, F., Hepatitis C virus RNA replication is regulated by host geranylgeranylation and fatty acids. *Proc. Natl. Acad. Sci. U. S. A.* **2005,** 102, 2561-2566.

32. Delang, L.; Paeshuyse, J.; Vliegen, I.; Leyssen, P.; Obeid, S.; Durantel, D.; Zoulim, F.; Op de Beeck, A.; Neyts, J., Statins potentiate the in vitro anti-hepatitis C virus activity of selective hepatitis C virus inhibitors and delay or prevent resistance development. *Hepatology* **2009,** 50, 6-16.

33. Bader, T.; Fazili, J.; Madhoun, M.; Aston, C.; Hughes, D.; Rizvi, S.; Seres, K.; Hasan, M., Fluvastatin inhibits hepatitis C replication in humans. *Am. J. Gastroenterol.* **2008,** 103, 1383-1389.

34. Kondo, C.; Atsukawa, M.; Tsubota, A.; Itokawa, N.; Fukuda, T.; Matsushita, Y.; Kidokoro, H.; Kobayashi, T.; Narahara, Y.; Nakatsuka, K.; Kanazawa, H.; Sakamoto, C., An open-label randomized controlled study of pegylated interferon/ribavirin combination therapy for chronic hepatitis C with versus without fluvastatin. *J. Viral Hepat.* **2012,** 19, 615-622.

35. Giguère, V., Orphan Nuclear Receptors: From Gene to Function. *Endocr. Rev.* **1999,** 20, 689-725.

36. Berger, J.; Moller, D. E., The mechanism of action of PPARs. *Annu. Rev. Med.* **2002,** 53, 409-435.

37. Berger, J.; Akiyama, T.; Meinke, P., PPARs: therapeutic targets for metabolic disease. *Trends Pharmacol. Sci.* **2005,** 26, 244-251.

38. Torra, I. P.; Chinetti, G.; Duval, C.; Fruchart, J.-C.; Staels, B., Peroxisome proliferator-activated receptors: from transcriptional control to clinical practice. *Curr. Opin. Lipidol.* **2001,** 12, 245-254.

39. van Raalte, D.; Li, M.; Pritchard, P.; Wasan, K., Peroxisome proliferator-activated receptor (PPAR)-alpha: a pharmacological target with a promising future. *Pharm. Res.* **2004,** 21, 1531-1538.

40. Cho, M.-C.; Lee, K.; Paik, S.-G.; Yoon, D.-Y., Peroxisome Proliferators-Activated Receptor (PPAR) Modulators and Metabolic Disorders. *PPAR Res.* **2008,** 2008, 14 pages. doi:10.1155/2008/679137.

41. Kota, B.; Huang, T.; Roufogalis, B., An overview on biological mechanisms of PPARs. *Pharm. Res.* **2005,** 51, 85-94.

42. Mascaró, C.; Acosta, E.; Ortiz, J. A.; Marrero, P. F.; Hegardt, F. G.; Haro, D., Control of Human Muscle-type Carnitine Palmitoyltransferase I Gene Transcription by Peroxisome Proliferator-activated Receptor. *J. Biol. Chem.* **1998,** 273, 8560-8563.

43. Barrero, M. J.; Camarero, N.; Marrero, P. F.; Haro, D., Control of human carnitine palmitoyltransferase II gene transcription by peroxisome proliferator-activated receptor through a partially conserved peroxisome proliferator-responsive element. *Biochem. J.* **2003,** 369, 721-729.

44. Schoonjans, K.; Staels, B.; Auwerx, J., Role of the peroxisome proliferator-activated receptor (PPAR) in mediating the effects of fibrates and fatty acids on gene expression. *J. Lipid Res.* **1996,** 37, 907-25.

45. Tenenbaum, A.; Motro, M.; Fisman, E., Dual and pan-peroxisome proliferator-activated receptors (PPAR) co-agonism: the bezafibrate lessons. *Cardiovasc. Diabetol.* **2005,** 4, 14. doi:10.1186/1475-2840-4-14

46. Group, B. I. P. S., Secondary Prevention by Raising HDL Cholesterol and Reducing Triglycerides in Patients With Coronary Artery Disease: The Bezafibrate Infarction Prevention (BIP) Study. *Circulation* **2000,** 102, 21-27.

47. Staels, B.; Fruchart, J.-C., Therapeutic Roles of Peroxisome Proliferator-Activated Receptor Agonists. *Diabetes* **2005,** 54, 2460-2470.

48. Peters, J. M.; Aoyama, T.; Burns, A. M.; Gonzalez, F. J., Bezafibrate is a dual ligand for PPARα and PPARβ: studies using null mice. *Biochim. Biophys. Acta.* **2003,** 1632, 80-89.

49. Sears, D. D.; Hsiao, G.; Hsiao, A.; Yu, J. G.; Courtney, C. H.; Ofrecio, J. M.; Chapman, J.; Subramaniam, S., Mechanisms of human insulin resistance and thiazolidinedione-mediated insulin sensitization. *Proc. Natl. Acad. Sci. U. S. A.* **2009,** 106, 18745-18750.

50. Fievet, C.; Fruchart, J.-C.; Staels, B., PPARα and PPARβ dual agonists for the treatment of type 2 diabetes and the metabolic syndrome. *Curr. Opin. Pharmacol.* **2006,** 6, 606-614.

51. Miyanari, Y.; Atsuzawa, K.; Usuda, N.; Watashi, K.; Hishiki, T.; Zayas, M.; Bartenschlager, R.; Wakita, T.; Hijikata, M.; Shimotohno, K., The lipid droplet is an important organelle for hepatitis C virus production. *Nat. Cell Biol.* **2007,** 9, 1089-1097.

52. Counihan, N. A.; Rawlinson, S. M.; Lindenbach, B. D., Trafficking of Hepatitis C Virus Core Protein during Virus Particle Assembly. *PLoS Pathog.* **2011**, 7, e1002302.

53. Schnell, U.; Dijk, F.; Sjollema, K. A.; Giepmans, B. N. G., Immunolabeling artifacts and the need for live-cell imaging. *Nat. Methods* **2012,** 9, 152-158.

54. Pezacki, J. P.; Singaravelu, R.; Lyn, R. K., Host-virus interactions during hepatitis C virus infection: a complex and dynamic molecular biosystem. *Mol. BioSyst.* **2010,** 6, 1131-1142.

55. McLauchlan, J., Lipid droplets and hepatitis C virus infection. *Biochim.Biophys. Acta* **2009,** 1791, 552-561.

56. Popescu, C.-I.; Rouillé, Y.; Dubuisson, J., Hepatitis C virus assembly imaging. *Viruses* **2011**, 3, 2238-2254.

57. Jackel-Cram, C.; Babiuk, L. A.; Liu, Q., Up-regulation of fatty acid synthase promoter by hepatitis C virus core protein: Genotype-3a core has a stronger effect than genotype-1b core. *J. Hepatol.* **2007,** 46, 999-1008.

58. Barba, G.; Harper, F.; Harada, T.; Kohara, M.; Goulinet, S.; Matsuura, Y.; Eder, G.; Schaff, Z.; Chapman, M. J.; Miyamura, T.; Bréchot, C., Hepatitis C virus core protein shows a cytoplasmic localization and associates to cellular lipid storage droplets. *Proc. Natl. Acad. Sci. U. S. A.* **1997**, *94*, 1200-1205.

59. Evans, C. L.; Xie, X. S., Coherent Anti-Stokes Raman Scattering Microscopy: Chemical Imaging for Biology and Medicine. *Annu. Rev. Anal. Chem.* **2008,** 1, 883-909.

60. Willmann, J. K.; van Bruggen, N.; Dinkelborg, L. M.; Gambhir, S. S., Molecular imaging in drug development. *Nat. Rev. Drug Discov.* **2008,** 7, 591-607.

61. Cheng, J.-X.; Xie, X. S., Coherent Anti-Stokes Raman Scattering Microscopy: Instrumentation, Theory, and Applications. *J. Phys. Chem. B.* **2004,** 108, 827-840.

62. Pegoraro, A.; Ridsdale, A.; Moffatt, D.; Jia, Y.; Pezacki, J.; Stolow, A., Optimally chirped multimodal CARS microscopy based on a single Ti:sapphire oscillator. *Opt. Express* **2009,** 17, 2984-3080.

63. Pezacki, J. P.; Blake, J. A.; Danielson, D. C.; Kennedy, D. C.; Lyn, R. K.; Singaravelu, R., Chemical contrast for imaging living systems: molecular vibrations drive CARS microscopy. *Nat. Chem. Biol.* **2011,** 7, 137-145.

64. Wachsmann-Hogiu, S.; Weeks, T.; Huser, T., Chemical analysis in vivo and in vitro by Raman spectroscopy - from single cells to humans. *Curr. Opin. Biotechnol.* **2009,** 20, 63-73.

65. Chan, J.; Fore, S.; Wachsmann-Hogiu, S.; Huser, T., Raman spectroscopy and microscopy of individual cells and cellular components. *Laser Photon. Rev.* **2008,** 2, 325-349.

66. Das, R. S.; Agrawal, Y. K., Raman spectroscopy: Recent advancements, techniques and applications. *Vib. Spectrosc.* **2011,** 57, 163-176.

67. Rodriguez, L. G.; Lockett, S. J.; Holtom, G. R., Coherent anti-stokes Raman scattering microscopy: A biological review. *Cytometry A* **2006,** 69, 779-791.

68. Hashimoto, M.; Araki, T.; Kawata, S., Molecular vibration imaging in the fingerprint region by use of coherent anti-Stokes Raman scattering microscopy with a collinear configuration. *Opt. Lett.* **2000,** 25, 1768-1770.

69. Pegoraro, A.; Ridsdale, A.; Moffatt, D.; Pezacki, J.; Thomas, B.; Fu, L.; Dong, L.; Fermann, M.; Stolow, A., All-fiber CARS microscopy of live cells. *Opt. Express* **2009,** 17, 20700-20706.

70. Silberberg, Y., Quantum Coherent Control for Nonlinear Spectroscopy and Microscopy. *Annu. Rev. Phys. Chem.* **2009,** 60, 277-292.

71. Hellerer, T.; Axäng, C.; Brackmann, C.; Hillertz, P.; Pilon, M.; Enejder, A., Monitoring of lipid storage in Caenorhabditis elegans using coherent anti-Stokes Raman scattering (CARS) microscopy. *Proc. Natl. Acad. Sci. U. S. A.* **2007,** 104, (37), 14658-14663.

72. Cheng, J.-X.; Volkmer, A.; Book, L. D.; Xie, X. S., Multiplex Coherent Anti-Stokes Raman Scattering Microspectroscopy and Study of Lipid Vesicles. *J. Phys. Chem. B* **2002,** 106, 8493-8498.

73. Le, T. T.; Yue, S.; Cheng, J.-X., Shedding new light on lipid biology with coherent anti-Stokes Raman scattering microscopy. *J. Lipid Res.* **2010,** 51, 3091-3102.

74. Wang, H.-W.; Fu, Y.; Huff, T. B.; Le, T. T.; Wang, H.; Cheng, J.-X., Chasing lipids in health and diseases by coherent anti-Stokes Raman scattering microscopy. *Vib. Spectrosc.* **2009,** 50, 160-167.

75. Noestheden, M.; Hu, Q.; Tonary, A. M.; Tay, L.-L.; Pezacki, J. P., Evaluation of chemical labeling strategies for monitoring HCV RNA using vibrational microscopy. *Org. Biomol. Chem.* **2007,** 5, 2380-2389.

76. Rakic, B.; Sagan, S. M.; Noestheden, M.; Bélanger, S.; Nan, X.; Evans, C. L.; Xie, X. S.; Pezacki, J. P., Peroxisome Proliferator-Activated Receptor α Antagonism Inhibits Hepatitis C Virus Replication. *Chem. Biol.* **2006,** 13, 23-30.

77. Kennedy, D. C.; Lyn, R. K.; Pezacki, J. P., Cellular Lipid Metabolism Is Influenced by the Coordination Environment of Copper. *J. Am. Chem. Soc.* **2009,** 131, 2444-2445.

78. Nan, X.; Tonary, A. M.; Stolow, A.; Xie, X. S.; Pezacki, J. P., Intracellular Imaging of HCV RNA and Cellular Lipids by Using Simultaneous Two-Photon Fluorescence and Coherent Anti-Stokes Raman Scattering Microscopies. *ChemBioChem* **2006,** 7, 1895-1897.

79. Anderson, S. P.; Dunn, C.; Laughter, A.; Yoon, L.; Swanson, C.; Stulnig, T. M.; Steffensen, K. R.; Chandraratna, R. A.; Gustafsson, J. A.; Corton, J. C., Overlapping Transcriptional Programs Regulated by the Nuclear Receptors Peroxisome Proliferator-Activated Receptor α, Retinoid X Receptor, and Liver X Receptor in Mouse Liver. *Mol. Pharmacol.* **2004,** 66, 1440-1452.

80. Auboeuf, D.; Rieusset, J.; Fajas, L.; Vallier, P.; Frering, V.; Riou, J. P.; Staels, B.; Auwerx, J.; Laville, M.; Vidal, H., Tissue Distribution and Quantification of the Expression of mRNAs of Peroxisome Proliferator-Activated Receptors and Liver X Receptor-α in Humans: No Alteration in Adipose Tissue of Obese and NIDDM Patients. *Diabetes* **1997,** 46, 1319-1327.

81. Guzmán, M.; Cortés, J.; Castro, J., Effects of lovastatin on hepatic fatty acid metabolism. *Lipids* **1993,** 28, 1087-1093.

82. O'Leary, J.; Chan, J.; McMahon, C.; Chung, R., Atorvastatin does not exhibit antiviral activity against HCV at conventional doses: a pilot clinical trial. *Hepatology* **2007,** 45, 895-898.

83. Haubenwallner, S.; Essenburg, A. D.; Barnett, B. C.; Pape, M. E.; DeMattos, R. B.; Krause, B. R.; Minton, L. L.; Auerbach, B. J.; Newton, R. S.; Leff, T., Hypolipidemic activity of

select fibrates correlates to changes in hepatic apolipoprotein C-III expression: a potential physiologic basis for their mode of action. *Journal of Lipid Research* **1995,** 36, (12), 2541-51.

84. Wang, C.; Gale, M.; Keller, B.; Huang, H.; Brown, M.; Goldstein, J.; Ye, J., Identification of FBL2 as a geranylgeranylated cellular protein required for hepatitis C virus RNA replication. *Mol. Cell* **2005,** 18, 425-434.

85. Tonary, A. M.; Pezacki, J. P., Simultaneous quantitative measurement of luciferase reporter activity and cell number in two- and three-dimensional cultures of hepatitis C virus replicons. *Anal. Biochem.* **2006,** 350, 239-248.

86. Schönborn, J.; Oberstrass, J.; Breyel, E.; Tittgen, J.; Schumacher, J.; Lukacs, N., Monoclonal antibodies to double-stranded RNA as probes of RNA structure in crude nucleic acid extracts. *Nucleic Acids Res.* **1991,** 19, 2993-3000.

87. Targett-Adams, P.; Boulant, S.; McLauchlan, J., Visualization of Double-Stranded RNA in Cells Supporting Hepatitis C Virus RNA Replication. *J. Virol.* **2008,** 82, 2182-2195.

88. Boulant, S.; Targett-Adams, P.; McLauchlan, J., Disrupting the association of hepatitis C virus core protein with lipid droplets correlates with a loss in production of infectious virus. *J. Gen. Virol.* **2007,** 88, 2204-2213.

89. Boulant, S.; Douglas, M.; Moody, L.; Budkowska, A.; Targett-Adams, P.; McLauchlan, J., Hepatitis C virus core protein induces lipid droplet redistribution in a microtubule- and dynein-dependent manner. *Traffic* **2008,** 9, 1268-1282.

90. McLauchlan, J., Properties of the hepatitis C virus core protein: a structural protein that modulates cellular processes. *J. Viral Hepat.* **2000,** 7, 2-14.

91. McLauchlan, J.; Lemberg, M.; Hope, G.; Martoglio, B., Intramembrane proteolysis promotes trafficking of hepatitis C virus core protein to lipid droplets. *EMBO J.* **2002,** 21, 3980-3988.

92. Gao, L.; Aizaki, H.; He, J.-W.; Lai, M., Interactions between viral nonstructural proteins and host protein hVAP-33 mediate the formation of hepatitis C virus RNA replication complex on lipid raft. *J. Virol.* **2004,** 78, 3480-3488.

93. Sato, S.; Fukasawa, M.; Yamakawa, Y.; Natsume, T.; Suzuki, T.; Shoji, I.; Aizaki, H.; Miyamura, T.; Nishijima, M., Proteomic profiling of lipid droplet proteins in hepatoma cell lines expressing hepatitis C virus core protein. *J. Biochem.* **2006,** 139, 921-930.

94. Shi, S. T.; Polyak, S. J.; Tu, H.; Taylor, D. R.; Gretch, D. R.; Lai, M. M. C., Hepatitis C Virus NS5A Colocalizes with the Core Protein on Lipid Droplets and Interacts with Apolipoproteins. *Virology* **2002,** 292, 198-210.

95. Moriya, K.; Yotsuyanagi, H.; Shintani, Y.; Fujie, H.; Ishibashi, K.; Matsuura, Y.; Miyamura, T.; Koike, K., Hepatitis C virus core protein induces hepatic steatosis in transgenic mice. *J. Gen. Virol.* **1997,** 78, 1527-1531.

96. Oem, J.-K.; Jackel-Cram, C.; Li, Y.-P.; Zhou, Y.; Zhong, J.; Shimano, H.; Babiuk, L. A.; Liu, Q., Activation of sterol regulatory element-binding protein 1c and fatty acid synthase transcription by hepatitis C virus non-structural protein 2. *J. Gen. Virol.* **2008,** 89, 1225-1230.

97. Yang, W.; Hood, B. L.; Chadwick, S. L.; Liu, S.; Watkins, S. C.; Luo, G.; Conrads, T. P.; Wang, T., Fatty acid synthase is up-regulated during hepatitis C virus infection and regulates hepatitis C virus entry and production. *Hepatology* **2008,** 48, 1396-1403.

98. Jackel-Cram, C.; Babiuk, L.; Liu, Q., Up-regulation of fatty acid synthase promoter by hepatitis C virus core protein: genotype-3a core has a stronger effect than genotype-1b core. *J. Hepatol.* **2007,** 46, 999-2007.

99. Abid, K.; Pazienza, V.; de Gottardi, A.; Rubbia-Brandt, L.; Conne, B.; Pugnale, P.; Rossi, C.; Mangia, A.; Negro, F., An in vitro model of hepatitis C virus genotype 3a-associated triglycerides accumulation. *J. Hepatol.* **2005,** 42, 744-751.

100. Pazienza, V.; Clément, S.; Pugnale, P.; Conzelman, S.; Foti, M.; Mangia, A.; Negro, F., The hepatitis C virus core protein of genotypes 3a and 1b downregulates insulin receptor substrate 1 through genotype-specific mechanisms. *Hepatology* **2007,** 45, 1164-1171.

101. Sagan, S. M.; Rouleau, Y.; Leggiadro, C.; Supekova, L.; Schultz, P. G.; Su, A. I.; Pezacki, J. P., The influence of cholesterol and lipid metabolism on host cell structure and hepatitis C virus replication. *Biochem. Cell Biol.* **2006,** 84, 67-79.

102. Sakamoto, H.; Okamoto, K.; Aoki, M.; Kato, H.; Katsume, A.; Ohta, A.; Tsukuda, T.; Shimma, N.; Aoki, Y.; Arisawa, M.; Kohara, M.; Sudoh, M., Host sphingolipid biosynthesis as a target for hepatitis C virus therapy. *Nat. Chem. Biol.* **2005,** 1, 333-337.

103. Gastaminza, P.; Cheng, G.; Wieland, S.; Zhong, J.; Liao, W.; Chisari, F. V., Cellular Determinants of Hepatitis C Virus Assembly, Maturation, Degradation, and Secretion *J. Virol.* **2008,** 82, 2120-2129.

104. Huang, H.; Sun, F.; Owen, D.; Li, W.; Chen, Y.; Gale, M.; Ye, J., Hepatitis C virus production by human hepatocytes dependent on assembly and secretion of very low-density lipoproteins. *Proc. Natl. Acad. Sci. U. S. A.* **2007,** 104, 5848-5853.

105. Moradpour, D.; Brass, V.; Bieck, E.; Friebe, P.; Gosert, R.; Blum, H. E.; Bartenschlager, R.; Penin, F.; Lohmann, V., Membrane Association of the RNA-Dependent RNA Polymerase Is Essential for Hepatitis C Virus RNA Replication. *J. Virol.* **2004,** 78, 13278-13284.

106. Moradpour, D.; Gosert, R.; Egger, D.; Penin, F. o.; Blum, H. E.; Bienz, K., Membrane association of hepatitis C virus nonstructural proteins and identification of the membrane alteration that harbors the viral replication complex. *Antiviral Research* **2003,** 60, (2), 103-109.

107. Wölk, B.; Büchele, B.; Moradpour, D.; Rice, C., A dynamic view of hepatitis C virus replication complexes. *J. Virol.* **2008**, 82, 10519-10531.

108. Boström, P.; Andersson, L.; Rutberg, M.; Perman, J.; Lidberg, U.; Johansson, B.; Fernandez-Rodriguez, J.; Ericson, J.; Nilsson, T.; Borén, J.; Olofsson, S.-O., SNARE proteins mediate fusion between cytosolic lipid droplets and are implicated in insulin sensitivity. *Nat. Cell Biol.* **2007**, 9, 1286-1293.

109. Olofsson, S.-O.; Boström, P.; Andersson, L.; Rutberg, M.; Perman, J.; Borén, J., Lipid droplets as dynamic organelles connecting storage and efflux of lipids. *Biochim. Biophys. Acta.* **2009**, 1791, 448-458.

110. Egger, D.; Wölk, B.; Gosert, R.; Bianchi, L.; Blum, H. E.; Moradpour, D.; Bienz, K., Expression of hepatitis C virus proteins induces distinct membrane alterations including a candidate viral replication complex. *J. Virol.* **2002**, 76, 5974-5984.

3

Investigating dynamics of lipid droplets induced by HCV core protein

Introduction

Liver steatosis occurs in more than half the cases of chronic HCV infections [1-4]. Steatosis is a histopathologic phenotype that is described as a dense accumulation of cellular triglycerides and cholesterol esters in the form of cytoplasmic LDs [2, 3, 5]. HCV-induced steatosis is linked to quicker development of fibrosis and hepatocellular carcinoma, and increases the chance for developing type II diabetes and atherosclerotic complications [1, 6, 7]. As the prevalence of steatosis in HCV-related cases range from 40-70% [2, 8], its severity varies by genotype, particularly with genotype 3 accounting for the highest number of cases [1, 5, 9-12].

Genotype dependency for HCV-associated steatosis

The development of steatosis in individuals infected with genotypes other than genotype 3, is strongly related to host-associated factors, insulin resistance and metabolic changes [13-16]. On

the other hand, development of steatosis in genotype 3 infected patients has been strongly linked to be a viral-induced manifestation. This link was first evident in patients infected with genotype 3a, who, when treated with peg-IFN and RBV therapy had successfully cleared the virus, which correlated to marked improvements or a complete reversal of steatosis [11]. In the same experiment, genotype 3 infected patients who were non-responders to therapy, however, continued to exhibit steatosis. For non-genotype 3 patients, steatosis remained, despite the outcome of viral clearance [11, 17, 18]. While it appears that HCV-associated steatosis is dependent on host factors for non-genotype 3 infected patients, there are specific viral proteins that globally contribute to enhancing lipogenic pathways that favour the biosynthesis and accumulation of host lipids, and thus, contribute to clinical steatosis [16, 19, 20].

The link between HCV core protein and steatosis

Multiple viral proteins including the structural protein, core, and non-structural proteins, NS2, NS4B, and NS5A, are responsible for the misregulation of host lipid pathways [21-24]. Among these proteins, HCV core is likely to have the largest contribution, and has been well documented to perturb host lipid metabolism by a multifactorial process [25]. In cell-culture models, the expression of core protein has been shown to differentially enhance transcription of lipogenic genes, and produce an accumulation of LDs, similarly observed by the histopathological description of steatosis [10, 26, 27]. Indeed, LDs are required at the replication complexes and assembly sites, and virus exploitation of these lipid-rich organelles is likely a strategy employed by the virus [21, 28, 29]. An early link between HCV core protein and LDs was demonstrated when core was shown to bind to the surface of the LD [30]. Since then, assessing the expression of core protein in various methods that include cell culture, transgenic mice, and liver serum, showed a marked upregulation of intracellular triglycerides and cholesterol [3, 10, 26, 31, 32]. This is mainly accomplished by core-induced enhancement of transcription factors that target lipogenic genes,

and further increases the expression of multiple host lipid enzymes that accumulate a build-up of cytoplasic LDs [5, 25-27, 33-35]. Based on this evidence, HCV core protein, although not exclusively, is linked to the development of liver steatosis. To better understand how host metabolic pathways are misregulated by core it is crucial to understand the mechanisms of host *de novo* biosynthesis of triglycerides and cholesterol[36].

SREBPs are master regulators of lipid metabolism

Regulation of fatty acid and cholesterol biosynthesis in the liver is largely controlled by sterol regulatory element binding proteins (SREBPs) [36-39]. Upon ligand-induced activation, they enter the nucleus as nuclear transcription factors that bind to sterol regulatory elements (SREs) at promoter regions that regulate lipogenic genes [38, 40]. Research on SREBPs was mostly pioneered by Goldstein and colleagues [38, 41]. Their work led to the discovery of a family of SREBPs that comprise of three isoforms: SREBP-1a, SREBP-1c, and SREBP-2 [42]. The first isoform, SREBP-1c, plays a predominant role in activating fatty acid biosynthesis, with the latter of the family involved in activating cholesterol biosynthesis [40, 43]. Meanwhile, SREBP-1a is capable of controlling both pathways [40, 43]. Each of these transcription factors are organized into three domains. The N-terminus includes a cluster of acidic residues that mediate translocation across the nuclear membrane, and contains a basic-helix-loop-helix leucine zipper (bHLH-zip) that is responsible for binding to the promoter regions at the SREs. The C-terminus regulatory tail binds to SREBP cleavage activating protein (SCAP, Schematic 3.1) [38, 39, 43]. Importantly, SCAP functions as a sensory domain that measures intracellular levels of fatty acids and sterols that, under low level of lipids, for example, enables translocation of the SREBP- SCAP complex to the golgi, and is further cleaved by host proteases at this site [43, 45, 48, 49]. Transport of the SREBP-SCAP complex is aided by COPII proteins [43]. Following cleavage of SREBP, the bHLH-zip domain is released into the nucleus and induces transcription of lipogenic genes that include a

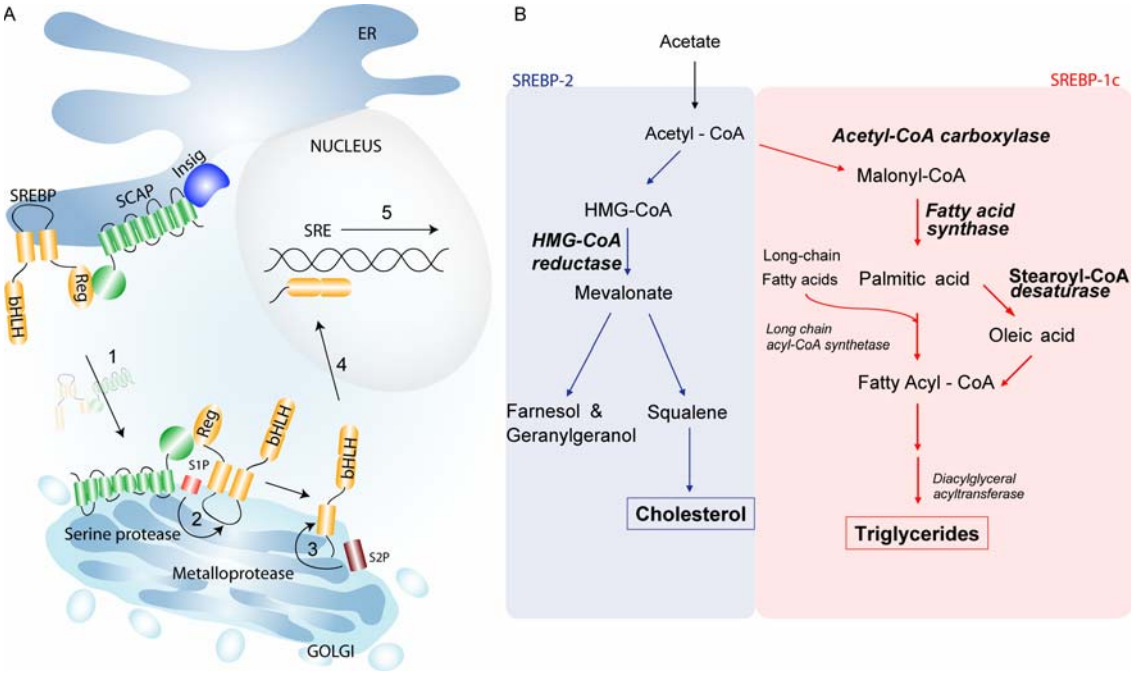

Schematic 3.1: Regulation of SREBPs. (A) Activation of SRE target genes by SREBP occurs as a response after sensing intracellular levels of fatty acids and sterols. This is followed by proteolytic cleavage, and transcriptional binding in the nucleus. The N and C-terminal domains of SREBP are separated by two hydrophobic transmembrane domains, with a hydrophilic loop in the middle, which allows anchorage to the ER membrane [41, 44]. (Step 1) SCAP is composed of eight transmembrane domains, with domains II to VI containing a sterol sensing domain, and functions as an escort protein by binding onto COPII proteins that facilitate its translocation towards the golgi [43]. The complex formed by SREBP-SCAP is further controlled by an insulin induced gene (insig), which in the presence of high sterol levels, can bind to the SREBP-SCAP complex and prevents it from translocating from the ER to the golgi [45]. By contrast, Insig is released from the SREBP-SCAP complex when SCAP senses low levels of sterols [43, 45]. Upon translocation to the golgi, the SREBP-SCAP complex is further cleaved by two site proteases [43]. (Step 2) The first protease, site-1 protease (S1P), cleaves SREBP at the hydrophobic loop via a serine protease [46]. (Step 3) From there a metalloprotease of site-2 protease (S2P), further cleaves a membrane spanning region and releases the bHLH domain into the nucleus where it binds to the targeted SRE genes [47]. (Step 4) The activated bHLH domain of SREBP is then released and enters the nucleus. (Step 5) The DNA binding domain of the bHLH recognizes promoter regions that initiate the transcription of lipogenic genes at the SREs. (B) SREBPs control cholesterol and fatty acid biosynthesis by regulating the expression of HMG-CoA reductase, ACC, FAS, and SCD

(highlighted in bold). The rate-limiting step for cholesterol and fatty acid biosynthesis is HMG-CoA reductase for the former, and ACC for the latter.

wide range of downstream enzymatic processes involved in cholesterol biosynthesis via HMG-CoA reductase, and fatty acid biosynthesis via acetyl-CoA carboxylase, fatty acid synthase, and stearoyl-CoA desaturase-1 (Schematic 3.1 B) [38, 50-52].

Mechanisms of HCV core-induced lipogenesis

HCV core protein is a multifunctional protein that, on one hand, is a component of the viral particle that forms the nucleocapsid, but is also capable of enhancing lipogenesis by hijacking metabolic pathways [16, 53, 54]. A link between HCV core and SREBP was elucidated in cell culture when expression of HCV core protein from genotypes 1b and 3a enhanced proteolytic cleavage of SREBP, which promoted lipogenesis by a core-induced SREBP-dependent manner [55]. Consistently, SREBP target genes were also observed to be upregulated at early stages of HCV infection [56]. Furthermore, *in vivo* and *in vitro* studies further show that HCV core protein binds directly with retinoid X receptor-α (RXRα), which is a ligand-induced transcription factor highly expressed in the liver, and is involved in activating genes in lipid metabolism and differentiation [57]. Interestingly, core protein expression enhanced transcriptional activity of RXRα target genes, likely as an RXRα binding co-factor. Given these observations, a core-induced enhancement of RXRα-DNA transcriptional activity is hypothesized as a potential mechanism that could lead to the development of steatosis [34]. In the context of transcriptional regulation by core protein, PPARα was also downregulated in mice expressing core protein [58]. While the function of PPARs are known to be disrupted by HCV, as previously discussed in chapter 2, the blockade of fatty acid β-oxidation may play a role in mediating an accumulation of intracellular triglycerides [59, 60]. Additionally, HCV core protein expressed in transgenic mice was shown to up-regulate

transcription of SREBP-1c and genes at the SREBP-1c promoter region that include fatty acid synthase (FAS), acetyl-CoA carboxylase (ACC), and stearoyl-CoA desaturase (SCD) [61] (Schematic 3.1). This enhancement, however, was not observed in mice containing a proteasome activator (PA28γ) knockout gene, suggesting that its effects were dependent on PA28γ [61]. In the liver, PA28γ mediates degradation of proteins, and more specifically, can degrade HCV core protein in a ubiquitin-dependent manner [35]. It was hypothesized that PA28γ-induced degradation may alter the folding of core protein, which may increase its binding affinity to RXRα and activate *srebp-1c* [61].

An alternative mechanism for core-induced steatosis, however, may not be linked to an increase in lipogenesis, but rather occurs through a mechanism that prevents lipolysis upon core binding to intracellular LDs [62]. Harris and colleagues studied this by using radiolabeled oleate as a measurement of LDs and observe its turnover rate [62]. They reported that in core expressing cells, TG turnover was delayed by correlation to retained amounts of radiolabeled oleate, which was not observed in non-core expressing cells [62]. As such, the authors demonstrate that core prevents access of lipolytic enzymes to LDs when bound to the LD surface, which is a plausible mechanism of retaining intracellular levels of LDs in the cytoplasm [62]. Supporting this, they also found that when core is unable to bind to LDs due to mutations in core that are non-permissive to SP cleavage, this did not prevent LD turnover [62]. Consistently, retention of TGs and TG-rich VLDLs was also observed when HCV core protein was overexpressed in transgenic mice [63]. These authors demonstrate that core protein expression was directly linked to a decreased level of MTP activity without perturbing MTP expression levels [63]. Based on this, an inability to secrete TG-rich VLDLs was hypothesized to lead to the development of steatosis [63].

HCV core-3a polymorphisms

There is a direct relationship between steatosis and HCV core derived from genotype 3a. Although steatosis observed in genotypes other than 3a are less severe, core protein modulation of host lipid metabolism does not appear to be entirely genotype specific. Its severity, however, may be reflected from specific sequences that appear in the core protein region of genotype 3a [1, 5, 10, 26, 27, 31]. Numerous polymorphisms in the core-3a sequence has been identified that are responsible for a build-up of intracellular LDs in cell culture studies, reflective to what is observed in core-3a-induced clinical steatosis [10, 31]. This was identified when a difference in amino acid sequence at the position of ^{164}YATG^{167} in genotype 1b in comparison to ^{164}FATG^{167} in genotype 3a was observed [26]. This single amino acid mutation correlated with stronger upregulation of FAS for the latter [26]. This was confirmed when high levels of FAS activity for genotype-3a was reduced to genotype-1a levels, which occurred after phenylalanine (P) at position 164 of genotype 3a was mutated to tyrosine (Y), which is normally observed in genotype 1a [26]. In a similar study, the authors reported similar findings and postulated that, because a phenylalanine residue is greater in hydrophobicity by comparison to tyrosine, that an enhancement of FAS activity may have correlated with higher binding affinity of core protein to the LD surface [31]. Furthermore, serum samples collected from 8 genotype 3a infected patients showed that, specific polymorphisms at position 182 and 186, such as a phenylalanine-valine or leucine-isoleucine pair at this less conserved region, resulted in differential intrahepatic steatosis [10]. This was characterized by measuring intracellular levels of LDs in cells expressing the polymorphic core genotype 3a clones from steatotic and non-steatotic patients [10]. Numerous studies have supported that core genotype 3a-induced effects are mediated by directly binding of core to transcriptional regulators [26, 33, 55, 58, 59, 61, 64, 65]. It is less clear, however, whether secondary effects mediated by core can exert an equal level of enhanced lipogenesis. For example, one pathway related to core genotype 3a-induced steatosis may be mediated by core inhibiting translation of phosphatase tensin homolog deleted on chromosome 10 (PTEN) without altering the levels of PTEN mRNA [66]. PTEN functions as a negative regulator for insulin signalling [67].

Clement and colleagues observed that PTEN blockade by core3a expression resulted in the accumulation of large LDs, which evidently, was also shown in PTEN knockout model in mice [68]. From these observations, PTEN is a possible general host factor in the primary cause of liver steatosis. Although post-translational modifications can control PTEN stability, core 3a exerted no effects upon PTEN modifications. However, the authors conclude from their studies that core induces expression of currently unidentified microRNAs that can repress PTEN mRNA translation [66]. A summary of the different mechanisms of core3a-induced lipogenesis is summarized in schematic 3.2.

Taken together, core is capable of modulating host lipid metabolism by a synergy of factors that include up-regulating lipogenesis, suppressing fatty-acid β-oxidation, and impairing lipoprotein secretion [34, 63, 69, 70]. These factors may be implicated in core-induced or core-associated involvement for the development of steatosis. To further identify host-virus interactions that proceed after *de novo* LD biosynthesis, in this chapter, we quantified LDs in core genotype 3a expressing Huh-7 cells. We approached this by using a bicistronic vector expressing a green fluorescent protein (GFP), which acts as a transfection reporter, that correspondingly expresses core by the same promoter region of the vector. Using this construct, we demonstrate that live-cell imaging is capable of monitoring differential changes in LD mobility and directionality in Huh-7 cells expressing and non-expressing HCV core-3a protein. Simultaneous TPF and CARS microscopy allows for a novel imaging modality that can visualize the LD dynamics in a label-free mode.

Hypothesis

HCV core protein modulates cellular LD metabolism and speed and directionality of LD movement within in human hepatoma cells.

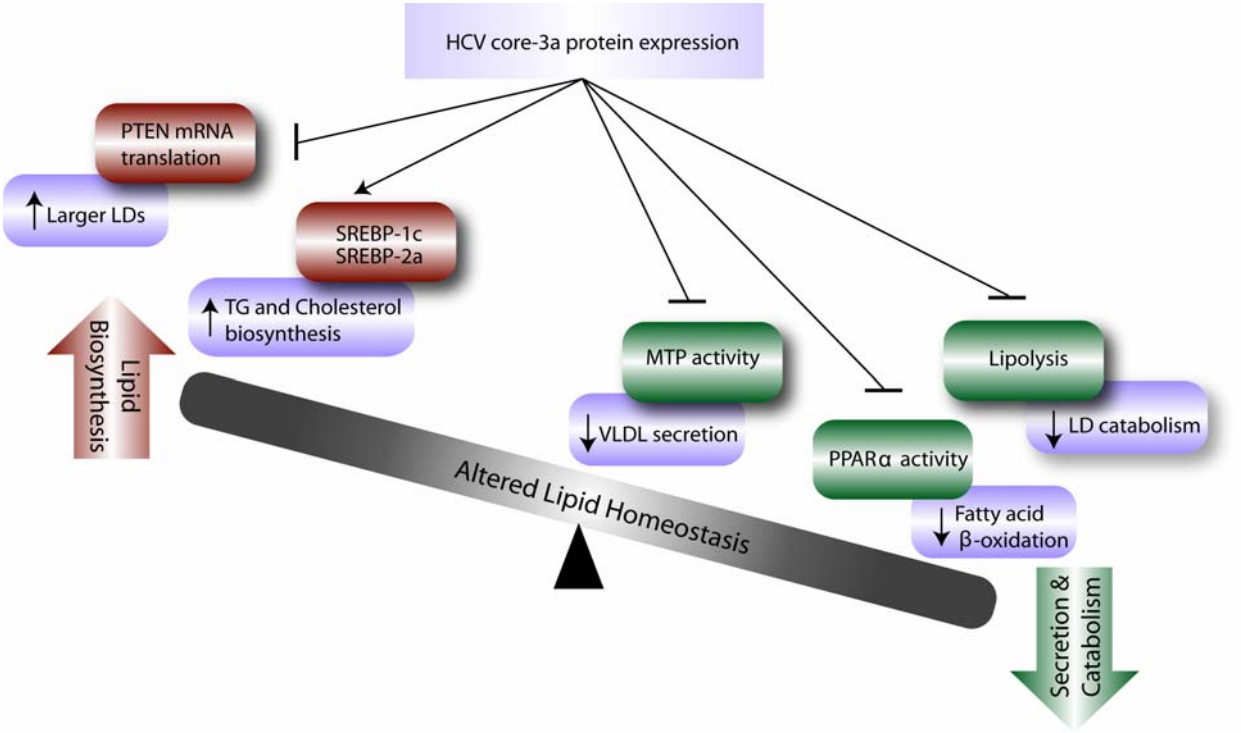

Schematic 3.2: Mechanisms for core genotype-3a induced altered lipid homeostasis. An imbalance of lipid homeostasis during core protein expression includes upregulation of lipid biosynthesis (red boxes) and downregulation of lipid secretion and catabolism (green boxes). HCV core protein promotes tryglyceride and cholesterol biosynthesis by increasing proteolytic cleavage of SREBPs [55]. Core-3a promotes larger LDs by downregulating PTEN mRNA translation without affecting levels of PTEN mRNA [66]. HCV core prevents VLDL secretion by inhibiting MTP activity [63]. Catabolism of LDs is reduced by core-3a modulation of PPARα function, which is involved in fatty-acid β-oxidation [58]. Catabolism of LDs is reduced when core protein prevents lipolytic enzymes from accessing the LD surface [62]. Together these mechanisms are involved in core-3a induced upregulation of triglyceride-rich LDs. These pathways may potentially play a role in the development of HCV genotype-3a induced steatosis. This schematic was adapted from *Syed, G., Amako, Y., Siddiqui, A. Trend Endocrin. Met.* ***21****, 2010* [16].

Results

HCV core genotype 3a expression induces LD biosynthesis

To determine whether core-3a expression enhanced LD biosynthesis in Huh-7.5 cells, we used CARS microscopy to evaluate changes to cytoplasmic LDs. We transfected a bicistronic vector expressing HCV core genotype 3a and EGFP, with separate reading frames so that EGFP marks cells that are successfully transfected and expressing HCV core protein, into Huh-7.5 cells. Using simultaneous CARS and TPF microscopies, we were able to image cells overexpressing EGFP and HCV core proteins and measure changes to LD density and localization (Fig. 3.1). In comparison to mock transfected samples, cells that selectively express EGFP along with core protein, showed a large increase in LD size and density. The changes to LD size occurred rapidly and synchronously with the appearance of EGFP signal, typically within 8 h of transfection of the plasmid expressing the core protein. The increase in LDs as a result of core expression was quantified by using voxel analysis [71], which measures the amount of lipid volume per cell, and was determined to be ~7.6 ± 1.0 % (n=12), a 7-fold difference in the volume of LDs per cell. By contrast, the total lipid content in naïve cells is lower than with core induced levels of LDs with voxel analysis yielding the lipid volume per cell to be ~1.2 ± 0.2 % (n=12). Additionally, the LDs in cells lacking EGFP expression, but in cells adjacent to cells expressing EGFP and core, resemble LD size and density of mock transfected cells (Fig. 3.1). After core protein has been expressed for 48 h, we observed that LDs appear to completely localize in the perinuclear region, where HCV replication complexes and assembly sites are typically found, and amass particularly close together in tight LD aggregates (Fig. 3.1) [72, 73].

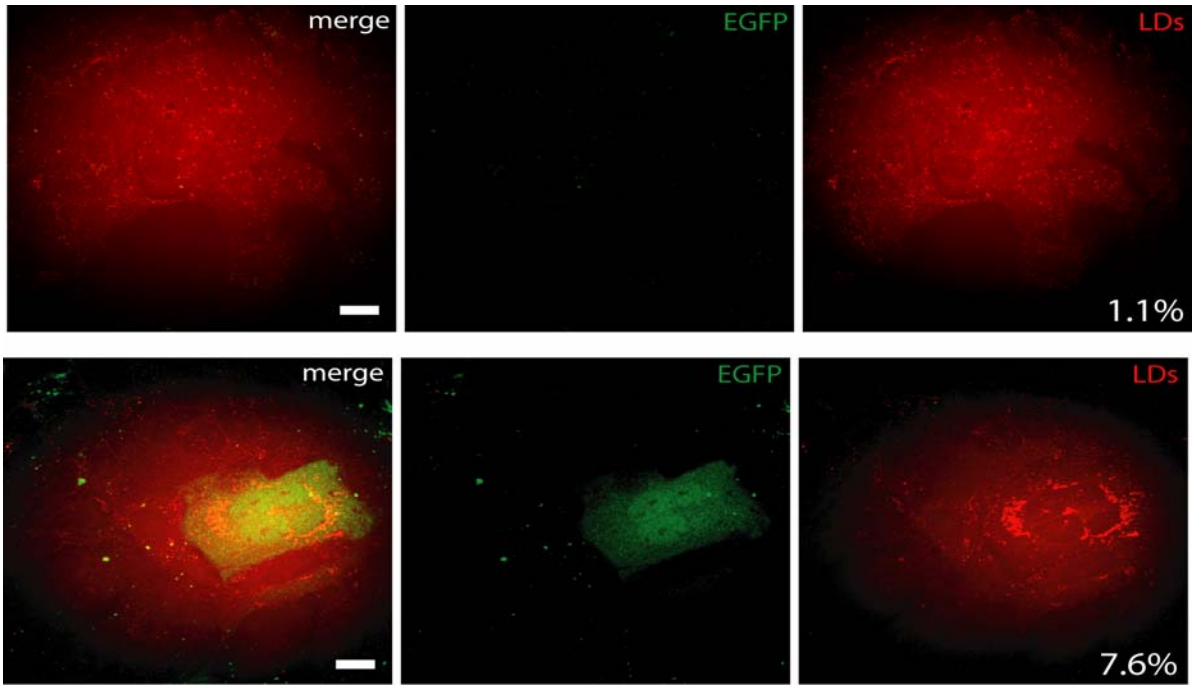

Figure 3.1: Live-cell CARS microscopy imaging of lipid droplet size, density and redistribution in HCV core protein expressing Huh-7.5 cells. A bicistronic plasmid encoding HCV core and EFGP was transfected into Huh-7.5 cells. EGFP was used as a cellular marker for expression of core. Mock samples were incubated with lipofectamine transfection reagent without the plasmid (upper panel) and cells transfected with the bicistronic plasmid (lower panel). CARS was used to measure LDs while TPF to measure EGFP. Values on the bottom of the CARS images represent voxel analysis indicating the lipid droplet volume per cell (average of 12 samples); Scale bars, 10μm.

Live-cell imaging captures LD migration towards the perinuclear region

In order to perform more detailed studies of the dynamics of LD localization, we developed a new method that combines CARS, TPF and differential interference contrast (DIC) microscopies. We developed this method because we found that DIC was able to capture the movement of LDs over very long time courses (many days) without photodamaging the cells. Because LDs have a greater index of refraction than the surrounding cytosol, they can be viewed by DIC with high contrast and can be discriminated from the other organelles in the cell. We used DIC to track single LD particles and to perform kinetic measurements regarding their movement during core protein expression. To confirm that features being observed by DIC were in fact LDs, we first imaged by CARS, and then superimposed those images with DIC images to identify which features in the DIC image were LDs (Fig. 3.2). Here, we clearly observed a direct correlation between CARS signal corresponding to the C-H stretching frequency from neutral lipids contained in LDs with high contrast features captured by DIC (Fig. 3.2).

Next we used DIC combined with CARS and TPF microscopies to capture the movements of LDs, as they migrate towards the perinuclear region of the cell. Following the same approach, we transfected the bicistronic vector in Huh-7.5 cells and applied live-cell DIC and TPF imaging. Importantly, the appearance of EGFP expression should precede that of LD migration towards the perinuclear region in order to identify which cells are expressing core protein so that we can monitor the change in LD localization. We imaged many different cells with DIC right after detectable levels of EGFP expression was observed (by TPF), typically ~20 h after transfection (Fig. 3.1). Notably, we were able to visualize an increase in the number and size of LDs before their localization at the perinuclear region (Fig. 3.3 A). To capture LD movement we monitored LD redistribution with DIC for 12 h by collecting images at regular intervals (1.65s/frame). During these time course measurements, the LDs appear to migrate from peripheral regions of the cell, slowly towards the perinuclear region in a period of 7 h (Fig. 3.3

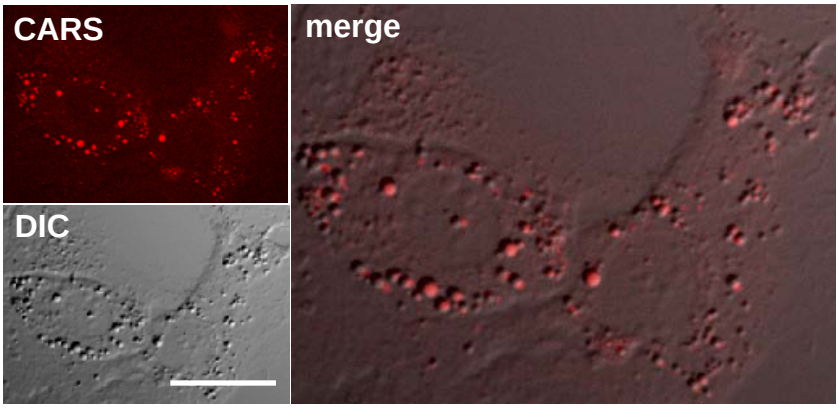

Figure 3.2: Live-cell CARS and DIC microscopy imaging of HCV core protein expressing Huh-7.5 cells. CARS and DIC microscopy were used to identify features that display high differential interference contrast that are rich in lipids as determined by the C-H resonance signal from CARS, shown as a merged image. The individual CARS and DIC channels are also shown; Scale bars, 10μm.

A). These data suggest that there is a directed movement of LDs that is initiated by the HCV core protein, and that this change occurs sequentially after LD biogenesis.

LDs in Huh-7.5 human hepatoma cells travel on microtubules

Previous studies have shown that LDs move via a microtubule-dependant mechanism [29, 74, 75]. LDs also can increase in size by a microtubule-dependent mechanism or through enzymatic loading of LDs [76, 77]. To confirm that core gives rise to changes in localization of LDs by affecting their movement along microtubules, we repeated the experiments in the presence of nocodazole, which interferes with the polymerization of microtubules [29]. First we examined LD movement of naïve Huh-7.5 cells. Here, we observed that LDs move rapidly and randomly without a clear defined path. After 2 h of imaging, the same samples were treated with nocodazole. Less than 30 min after treatment, the LDs had ceased moving. To confirm that LDs are transported along microtubules, we assessed this by using a live-cell dye for labeling microtubules. We applied the same continuous scanning approach (1.65s/frame) using CARS and TPF microscopy, and demonstrated rapid movement of LDs along microtubule networks (Fig. 3.3 B). For experiments involving HCV core protein expression and nocodazole treatment we observed that the LDs increased in size due to core expression as expected but did not move to the perinuclear region as previously observed. This demonstrates that core directs the movement of randomly scattered LDs to the perinuclear region along microtubules, to where HCV replication complexes are known to reside [72, 73].

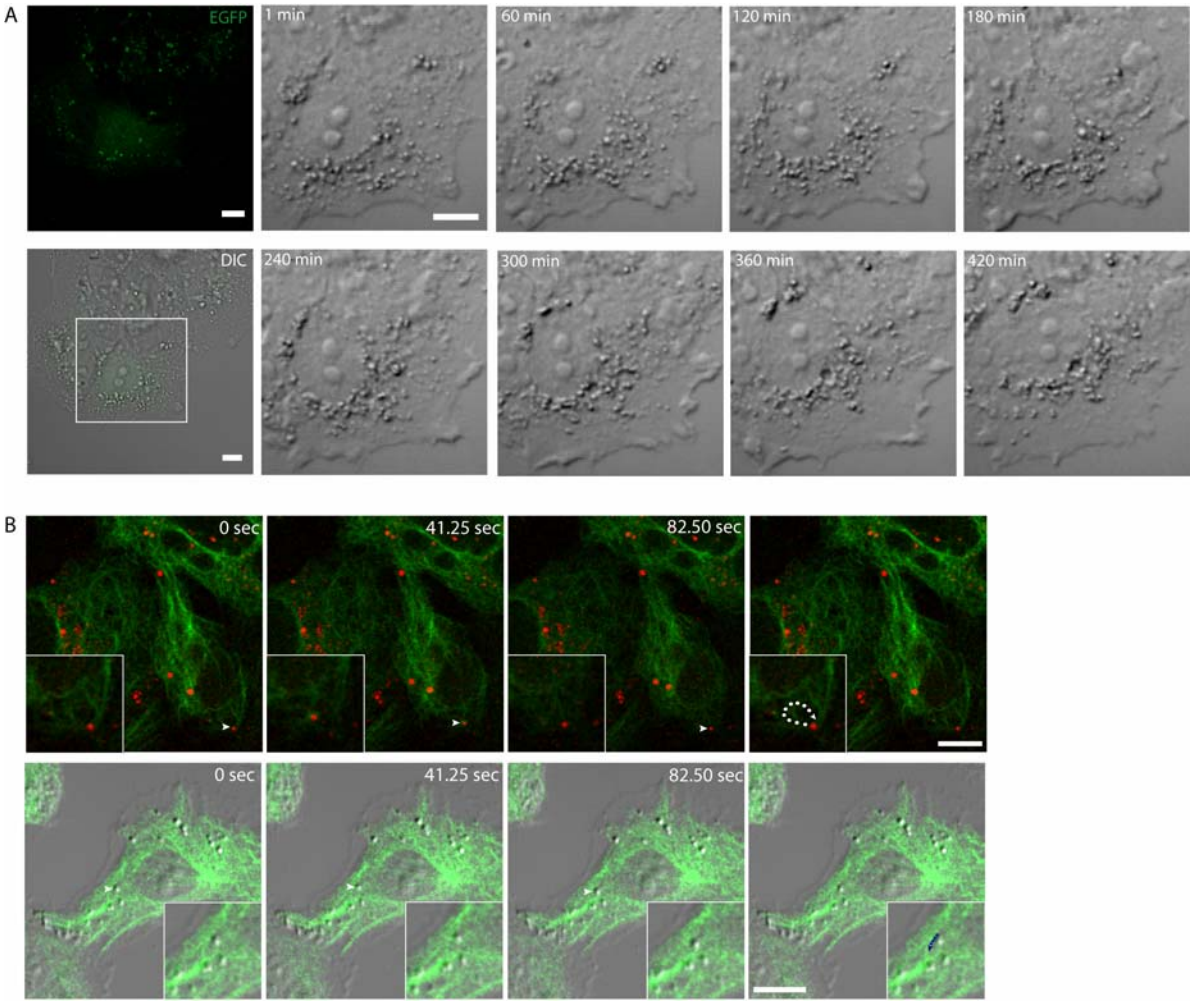

Figure 3.3: Live-cell CARS, TPF and DIC microscopies were used for imaging of lipid droplet size, density and redistribution in HCV core protein expressing Huh-7.5 cells. **(**A) Migration of LDs to the perinuclear region were monitored after transfection with the bicistronic plasmid. Shown are the simultaneous TPF (upper left panel) and DIC (bottom left panel) images. The eight images are a magnified view of the white box measuring LD redistribution towards the perinuclear region within the time points indicated. (B) Huh-7.5 cells were stained with tubulin tracker (green). Simultaneous TPF and CARS (upper panel) and TPF and DIC (lower panel) microscopy were used to capture LD movement along microtubules. The white box indicates the region that is subsequently shown as a magnified view containing a region of interest with a tracked LD marked by a white arrow. The dotted line shows trajectory. Scale bars, 10μm.

LDs in core-3a expressing cells travel at half the distances

It is well known that cargo movement along microtubules requires the molecular motor proteins dynein and kinesin that both anchor the cargo to microtubule tracks and move the cargo by taking step-wise movements [29, 74, 75, 78]. LDs, like many organelles, are cargo that is transported to meet cellular demands. In order to determine the roles of the molecular motor proteins on core-mediated LD movement, we further investigated the distances traveled by LDs, under time-lapsed microscopy using DIC. Quantitative analysis was obtained via particle tracking using pixel resolution of ~350 nm x 350 nm [79, 80]. We tracked LD motion in naïve and HCV core protein expressing Huh-7.5 cells, irrespective of directionality to assess how changes to the LD cargo may alter its motility.

It is possible that movement of LD cargo along microtubules may vary according to LD size and the capacity for molecular motors to take sizeable steps before falling off the microtubule. Consistent with previous studies, we find that both the rate and average length of movement did not vary according to LD size in naïve Huh-7.5 cells [29, 74, 75]. To assess LD motion, particle tracking was used to follow the LDs in the DIC images [80-82]. Next, changes in pixel positions in subsequent scans, 1.65s apart, were used to project the LDs travel distance that were subsequently added together over the entire scan time (Fig. 3.2 B). Typical experiments during live-cell imaging were conducted by monitoring the changes in displacement of a single LD throughout a 4 minute continuous time course with the delay of 1.65 seconds per scan (Fig. 3.3 B). We observed that in naïve Huh-7.5 cells as well as Huh-7.5 cells without the expression of HCV core (internal control) LDs move on average 17.8 ± 0.8 μm over the time course with an average speed of 74.4 ± 3 nm/s (n= 55). By contrast, when core is expressed in these cells, the LDs move approximately half the travel distance with an average of 9.4 ± 1 μm over this time period with an average speed of 39.1 ± 4 nm/s (n= 51, Fig. 3.4). In comparison, LD movement in

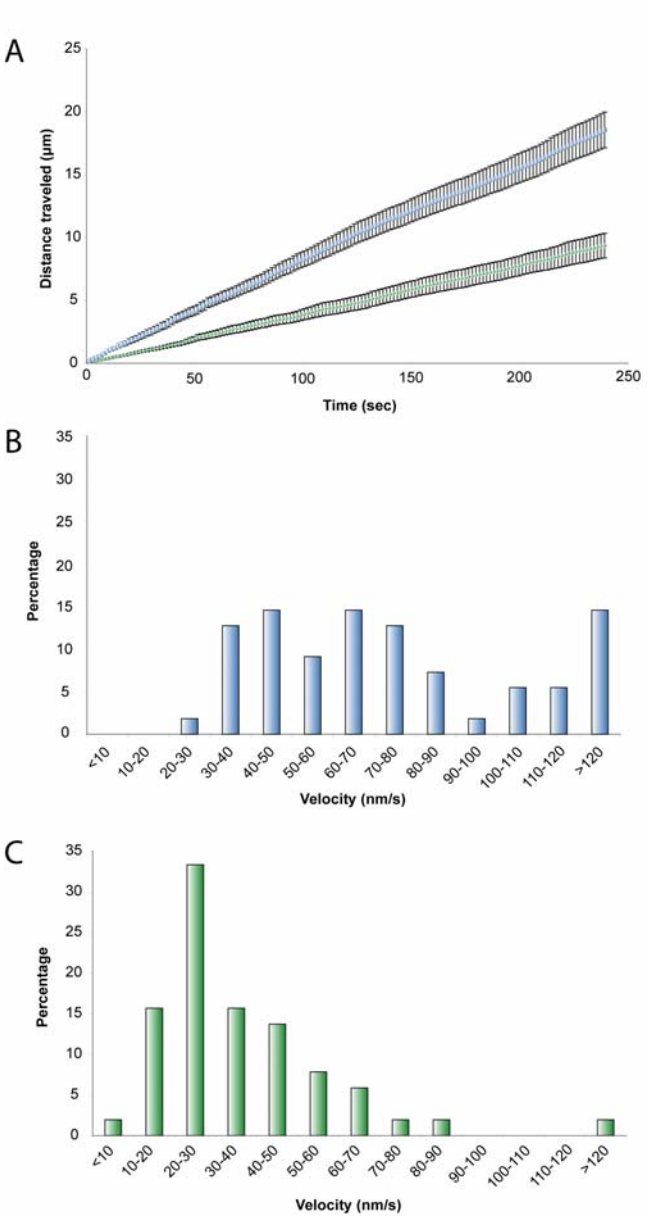

Figure 3.4: Particle tracking data shows changes in speed and distance travelled by lipid droplets induced by the HCV core protein. Particle tracking of LDs was conducted using ImageJ software in Huh-7.5 cells and Huh-7.5 cells expressing the HCV core protein. LD movement in core expressing cells (green data points, n=51) and naïve Huh-7.5 cells (blue data points, n=55) was assessed by measuring the average travel distance as a function of time, A. Particle tracking data were also plotted by using bins to represent the speed of individual LDs in naïve (B) and HCV core expressing (C) Huh-7.5 cells. The binned data are for different speed increments and are expressed as a percentage relative to the sample size.

Huh-7.5 cells treated with 3.3 μM nocodazole was even more hampered with the average distance traveled being only 3.7 ± 0.1 μm with an average speed of 15.5±0.4 nm/s (n= 49). Taken together these data indicate that core protein expression significantly affects LD motility.

Discussion

CARS microscopy is a convenient imaging modality for imaging changes in LD size and abundance in living cells in real time and has previously been successfully applied to the study of HCV host-virus interactions [71, 83-90]. Here we used CARS microscopy to measure changes in LDs induced by the expression of HCV core (genotype 3a) in Huh-7.5 human hepatoma cells. We showed that LDs increase in size and density after measuring the LD volume in cells expressing core-3a and compared it to mock transfected cells (Fig. 3.1). Similarly, non core-3a expressing cells that are adjacent to core-3a expressing cells under the same field of view showed a similar phenotype (Fig. 3.1). This increase in both LD size and density is most likely the result of core-mediated stimulation of LD biogenesis. This is consistent with cell-culture studies that visualized an abundance and enlargement of LDs in core-3a expressing cells [27, 31, 66]. Furthermore, Jackel-Cram et al. showed that a phenylalanine amino acid at the 164 position of Domain II found in core-3a, but is absent in other genotypes, induced an upregulation of FAS that was mediated by an SREBP-dependent manner [26, 64]. Consistently, our core-3a sequence contains the same phenylalanine at position 164. It is likely that an imbalance between lipid catabolism and lipid biosynthesis contributes to the abundance and enlargement of LDs as observed by CARS microscopy (Schematic 3.2).

In core-3a expressing cells, it appears that LDs have completely migrated towards the perinuclear region. We observed that this change in localization, however, occurred only after core induced the upregulation of LD biogenesis (Fig. 3.3). Since the core protein is required for

new viral particle assembly, eventually HCV RNA, and HCV envelope proteins must colocalize with core. Interestingly, it appears that the HCV core protein has evolved a molecular mechanism that stimulates core-associated LDs to move towards the sites of replication where new HCV RNA is produced. Here we show that this can occur very rapidly especially in the context of a real infection where viral titres can take days or weeks to reach detectable levels post-infection [28, 56, 91]. When HCV core protein is translocated to LDs it forms oligomers on the LD surface and displaces LD binding proteins such as those of the PAT family, including the adipose differentiation related protein (ADRP) [25]. Movement of LD cargo on microtubules requires that molecular motor proteins dynein and kinesin bind to both the LD and the microtubule and that these molecular motor proteins are functional so that transport can take place [29, 74, 75]. Interactions of the core protein with the LD surface, as well as other LD-binding proteins, likely modulate the ability of dynein and kinesin to function as motor proteins [92-94]. It is likely then that this change in molecular environment at the surface changes the docking environment of the LD cargo with the microtubules and gives rise to differences in speed and the overall distance travelled for the LD cargo (Fig 3.4).

Previously, McLauchlan and coworkers hypothesized that correlated core-dependant LD movement may be the result of an imbalance of dynein and kinesin motors that facilitate retrograde transport, possibly migrating towards the microtubule organizing center (MTOC) [25, 29]. The speed measurements here show a decrease in molecular motor activity when the HCV core protein is expressed and binds to LDs. Since LDs are likely undergoing core-dependant retrograde transport, preferential molecular motor activity of dynein over kinesin may be taking place. There are a number of possibilities for how this could occur, however, the fact that we observe a significant decrease in the distance travelled and the speed of the LDs suggests that core is significantly reducing or eliminating the kinesin motor activity on LDs. Core may accomplish this by displacing kinesin proteins from the surface of the LDs or it may simply

deactivate the kinesin through protein-protein interactions, via an allosteric mechanism. Displacing kinesin might allow for more dynein motor activity, however, our observations show that core likely eliminates half the motor protein activity, resulting in directed motion of LDs towards the perinuclear region. It is also possible that core effects the rate of movement and localization, independent of motor proteins, an alternative idea further explained in Chapter 4.

Our results from imaging and particle tracking studies provide evidence that the HCV core protein controls the directionality and speed of LD movement as part of a critical step in the viral lifecycle. This represents a highly novel mechanism for viral protein-induced LD translocation to sites where viral particle assembly is known to take place. We have shown in this chapter that CARS microscopy is a suitable tool to capture viral-induced steatosis, and study the mechanisms that contribute to its development in the liver. Importantly, we have developed a new method for particle tracking LDs that combines DIC, TPF, and CARS microscopies. The core-mediated translocation of LDs also represents a novel host-HCV interaction for therapeutic intervention.

Future Directions

While we have reported in this chapter that, the interactive environment between molecular motors and LDs are likely modified when core protein hijacks the LD surface, it would be interesting to identify the fate of LD-associated binding proteins that normally encapsulate the LD. With our imaging set-up, we can approach this by intrinsically encoding a fluorescent protein fusion tag, as a contrast reporter, to LD-associated binding proteins, such as TIP47 or ADRP, and monitor whether a change in localization occurs during core protein expression. In theory, this live-cell imaging approach could identify two potential LD populations. For example, the first LD population may have a high coverage of LD-binding associated proteins, as measured by the

fluorescence intensity, and secondly, a LD population with low coverage of LD-associated binding proteins. By measuring the dynamics for both populations, we could identify whether displacement of LD-associated binding proteins on the LD surface by core, correlates to a loss in speed and travel distances for LDs in core-expressing Huh-7 cells. Furthermore, with two fluorescent proteins expressed in this model (GFP as a reporter for core expression, and a LD-associated binding protein fused to a fluorescent protein), the emission wavelength for both fluorescent proteins can be separated by dichroic mirrors, as long as the peak emission wavelengths for each protein do not overlap. Applying live-cell imaging methods to monitor kinetics may ultimately provide greater insight into the potential mechanism in which core protein can induce a change in LD transport that is highly beneficial to HCV. The next approach would be to identify a method that would render HCV core protein to be tracked for live-cell imaging. The combination of core and LD imaging in live-cells is a powerful combination that would serve as a unique model to provide further understanding of core-induced modulation of LD dynamics.

Materials and Methods

Overexpression of HCV core protein

Huh-7.5 cells were seeded at 1.0 x 10^5 cells/well in borosilicate Lab-Tek chambers (VWR, Mississauga, ON). After 24 h, at a confluency of 60-70%, cells were then transfected with core-3a plasmid suspended in transfection media that includes lipofectamine 2000 (Invitrogen Canada Inc., Burlington, ON). After 4 h, DMEM in 20% FBS was added in equal volume to the chambers.

Simultaneous coherent anti-Stokes Raman scattering and two-photon fluorescence microscopies

The CARS microscopy system uses a single femtosecond Ti:sapphire oscillator as the excitation source, as previously described [95, 96].

Laser scanning simultaneous two-photon excited fluorescence and differential interference contrast microscopies

An Olympus FV300 laser scanning microscopy system on an IX71 inverted microscope was used for imaging experiments. A 40X Uapo 1.15NA water immersion objective and a long working distance 0.55 NA condenser were used. The FV300 was adapted for two photon fluorescence. Source was a Coherent Mira 900 Ti:sapphire laser producing pulses of approximately 100 femto-seconds at 800 nm wavelength with an 80 MHz repetition rate. Laser scanning microscopy can be readily adapted to DIC by taking advantage of the high inherent polarization in most laser sources. The DIC optics was adjusted as they would typically be for transmitted light use: with the prisms removed the condenser polarizer is adjusted to cross with the objective polarizer. For laser scanning, the analyzer, which is in a fluorescence cube in the IX71, is removed from the beam path. To optimally align the polarization of the laser with that of the microscope optics, a 700-1000 nm achromatic half wave plate (WPA1212 Casix) was placed in the laser path before entering the FV300 scan-box. The polarization of the laser was adjusted by rotating this wave plate to minimize the amount of light collected through the condenser polarizer. The DIC prisms are inserted and the path and the bias of the objective prism adjusted to the optimal image.

Quantitative voxel analysis

Quantitative data from the CARS images was determined using a voxel counting routine in ImageJ as previously described [71]. In each image, multiple cells were counted to obtain an average percentage lipid volume.

Particle tracking of lipid droplets in Huh-7.5 cells

Particle tracking of lipid droplet motion for both speed and distance was captured using spot tracker add-on with ImageJ, as previously described [80-82, 97]. The spot tracker followed the light shaded halo contrast of lipid droplets as a result of changes in refractive index with DIC imaging.

References

1. Adinolfi, L.; Gambardella, M.; Andreana, A.; Tripodi, M.; Utili, R.; Ruggiero, G., Steatosis accelerates the progression of liver damage of chronic hepatitis C patients and correlates with specific HCV genotype and visceral obesity. *Hepatology* **2001,** 33, 1358-1364.

2. Goodman, Z.; Ishak, K., Histopathology of hepatitis C virus infection. *Semin. Liver Dis.* **1995,** 15, 70-81.

3. Moriya, K.; Yotsuyanagi, H.; Shintani, Y.; Fujie, H.; Ishibashi, K.; Matsuura, Y.; Miyamura, T.; Koike, K., Hepatitis C virus core protein induces hepatic steatosis in transgenic mice. *J. Gen. Virol.* **1997,** 78, 1527-1531.

4. Alvisi, G.; Madan, V.; Bartenschlager, R., Hepatitis c virus and host cell lipids: An intimate connection. *RNA Biol.* **2011,** 8, 258-269.

5. Rubbia-Brandt, L.; Quadri, R.; Abid, K.; Giostra, E.; Malé, P.-J.; Mentha, G.; Spahr, L.; Zarski, J.-P.; Borisch, B.; Hadengue, A.; Negro, F., Hepatocyte steatosis is a cytopathic effect of hepatitis C virus genotype 3. *J. Hepatol.* **2000,** 33, 106-115.

6. Pekow, J. R.; Bhan, A. K.; Zheng, H.; Chung, R. T., Hepatic steatosis is associated with increased frequency of hepatocellular carcinoma in patients with hepatitis C-related cirrhosis. *Cancer* **2007,** 109, 2490-2496.

7. Ohata, K.; Hamasaki, K.; Toriyama, K.; Matsumoto, K.; Saeki, A.; Yanagi, K.; Abiru, S.; Nakagawa, Y.; Shigeno, M.; Miyazoe, S.; Ichikawa, T.; Ishikawa, H.; Nakao, K.; Eguchi, K., Hepatic steatosis is a risk factor for hepatocellular carcinoma in patients with chronic hepatitis C virus infection. *Cancer* **2003,** 97, 3036-3043.

8. Lok, A.; Everhart, J.; Chung, R.; Padmanabhan, L.; Greenson, J.; Shiffman, M.; Everson, G.; Lindsay, K.; Bonkovsky, H.; Di Bisceglie, A.; Lee, W.; Morgan, T.; Ghany, M.; Morishima, C.; Group, H.-C. T., Hepatic steatosis in hepatitis C: comparison of diabetic and nondiabetic patients in the hepatitis C antiviral long-term treatment against cirrhosis trial. *Clin. Gastroenterol. Hepatol.* **2007,** 5, 245-254.

9. Moriya, K.; Fujie, H.; Shintani, Y.; Yotsuyanagi, H.; Tsutsumi, T.; Ishibashi, K.; Matsuura, Y.; Kimura, S.; Miyamura, T.; Koike, K., The core protein of hepatitis C virus induces hepatocellular carcinoma in transgenic mice. *Nat. Med.* **1998,** 4, 1065-1067.

10. Jhaveri, R.; McHutchison, J.; Patel, K.; Qiang, G.; Diehl, A., Specific polymorphisms in hepatitis C virus genotype 3 core protein associated with intracellular lipid accumulation. *J. Infect. Dis.* **2008,** 197, 283-374.

11. Kumar, D.; Farrell, G. C.; Fung, C.; George, J., Hepatitis C virus genotype 3 is cytopathic to hepatocytes: Reversal of hepatic steatosis after sustained therapeutic response. *Hepatology* **2002,** 36, 1266-1272.

12. Negro, F.; Sanyal, A., Hepatitis C virus, steatosis and lipid abnormalities: clinical and pathogenic data. *Liver Int.* **2009,** 29, 26-63.

13. Fartoux, L.; Poujol-Robert, A.; Guéchot, J.; Wendum, D.; Poupon, R.; Serfaty, L., Insulin resistance is a cause of steatosis and fibrosis progression in chronic hepatitis C. *Gut* **2005,** 54, 1003-1008.

14. Moucari, R.; Asselah, T.; Cazals-Hatem, D.; Voitot, H.; Boyer, N.; Ripault, M. P.; Sobesky, R.; Martinot-Peignoux, M.; Maylin, S.; Nicolas-Chanoine, M. H.; Paradis, V.; Vidaud, M.; Valla, D.; Bedossa, P.; Marcellin, P., Insulin Resistance in Chronic Hepatitis C: Association With Genotypes 1 and 4, Serum HCV RNA Level, and Liver Fibrosis. *Gastroenterology* **2008,** 134, 416-423.

15. Zekry, A.; McHutchison, J. G.; Diehl, A. M., Insulin resistance and steatosis in hepatitis C virus infection. *Gut* **2005,** 54, 903-906.

16. Syed, G.; Amako, Y.; Siddiqui, A., Hepatitis C virus hijacks host lipid metabolism. *Trends Endocrinol. Metab.* **2010,** 21, 33-73.

17. Patton, H. M.; Patel, K.; Behling, C.; Bylund, D.; Blatt, L. M.; Vallée, M.; Heaton, S.; Conrad, A.; Pockros, P. J.; McHutchison, J. G., The impact of steatosis on disease progression and early and sustained treatment response in chronic hepatitis C patients. *J. Hepatol.* **2004,** 40, 484-490.

18. Poynard, T.; Ratziu, V.; McHutchison, J.; Manns, M.; Goodman, Z.; Zeuzem, S.; Younossi, Z.; Albrecht, J., Effect of treatment with peginterferon or interferon alfa-2b and ribavirin on steatosis in patients infected with hepatitis C. *Hepatology* **2003,** 38, (1), 75-85.

19. Ferré, P.; Foufelle, F., Hepatic steatosis: a role for de novo lipogenesis and the transcription factor SREBP-1c. *Diabetes Obes. Metab.* **2010,** 12, 83-92.

20. Blackham, S.; Baillie, A.; Al-Hababi, F.; Remlinger, K.; You, S.; Hamatake, R.; McGarvey, M. J., Gene Expression Profiling Indicates the Roles of Host Oxidative Stress, Apoptosis, Lipid Metabolism, and Intracellular Transport Genes in the Replication of Hepatitis C Virus. *J. Virol.* **2010,** 84, 5404-5414.

21. Herker, E.; Ott, M., Emerging role of lipid droplets in host/pathogen interactions. *J. Biol. Chem.* **2012,** 287, 2280-2287.

22. Oem, J.-K.; Jackel-Cram, C.; Li, Y.-P.; Zhou, Y.; Zhong, J.; Shimano, H.; Babiuk, L. A.; Liu, Q., Activation of sterol regulatory element-binding protein 1c and fatty acid synthase transcription by hepatitis C virus non-structural protein 2. *J. Gen. Virol.* **2008,** 89, 1225-1230.

23. Park, C.-Y.; Jun, H.-J.; Wakita, T.; Cheong, J. H.; Hwang, S. B., Hepatitis C Virus Nonstructural 4B Protein Modulates Sterol Regulatory Element-binding Protein Signaling via the AKT Pathway. *J. Biol. Chem.* **2009,** 284, 9237-9246.

24. Kim, K.; Kim, K. H.; Ha, E.; Park, J. Y.; Sakamoto, N.; Cheong, J., Hepatitis C virus NS5A protein increases hepatic lipid accumulation via induction of activation and expression of PPARgamma. *FEBS Lett.* **2009,** 583, 2720-2726.

25. McLauchlan, J., Lipid droplets and hepatitis C virus infection. *Biochim. Biophys. Acta.* **2009,** 1791, 552-561.
26. Jackel-Cram, C.; Babiuk, L.; Liu, Q., Up-regulation of fatty acid synthase promoter by hepatitis C virus core protein: genotype-3a core has a stronger effect than genotype-1b core. *J. Hepatol.* **2007,** 46, 999-2007.

27. Abid, K.; Pazienza, V.; de Gottardi, A.; Rubbia-Brandt, L.; Conne, B.; Pugnale, P.; Rossi, C.; Mangia, A.; Negro, F., An in vitro model of hepatitis C virus genotype 3a-associated triglycerides accumulation. *J. Hepatol.* **2005,** 42, 744-751.

28. Miyanari, Y.; Atsuzawa, K.; Usuda, N.; Watashi, K.; Hishiki, T.; Zayas, M.; Bartenschlager, R.; Wakita, T.; Hijikata, M.; Shimotohno, K., The lipid droplet is an important organelle for hepatitis C virus production. *Nat. Cell Biol.* **2007,** 9, 1089-1186.

29. Boulant, S.; Douglas, M.; Moody, L.; Budkowska, A.; Targett-Adams, P.; McLauchlan, J., Hepatitis C virus core protein induces lipid droplet redistribution in a microtubule- and dynein-dependent manner. *Traffic* **2008,** 9, 1268-1282.

30. Barba, G.; Harper, F.; Harada, T.; Kohara, M.; Goulinet, S.; Matsuura, Y.; Eder, G.; Schaff, Z.; Chapman, M. J.; Miyamura, T.; Brechot, C., Hepatitis C virus core protein shows a cytoplasmic localization and associates to cellular lipid storage droplets. *Proc. Natl. Acad. Sci. U. S. A.* **1997,** 94, 1200-1205.

31. Hourioux, C.; Patient, R.; Morin, A.; Blanchard, E.; Moreau, A.; Trassard, S.; Giraudeau, B.; Roingeard, P., The genotype 3-specific hepatitis C virus core protein residue phenylalanine 164 increases steatosis in an in vitro cellular model. *Gut* **2007,** 56, 1302-1310.

32. Koike, K., Steatosis, liver injury, and hepatocarcinogenesis in hepatitis C viral infection. *J. Gastroenterol.* **2009,** 44, 82-90.

33. Raglow, Z.; Thoma-Perry, C.; Gilroy, R.; Wan, Y.-J. Y., The interaction between HCV and nuclear receptor-mediated pathways. *Pharmacol. Ther.* **2011,** 132, 30-38.

34. Tsutsumi, T., Interaction of hepatitis C virus core protein with retinoid X receptor α modulates its transcriptional activity. *Hepatology* **2002,** 35, 937-946.

35. Moriishi, K.; Shoji, I.; Mori, Y.; Suzuki, R.; Suzuki, T.; Kataoka, C.; Matsuura, Y., Involvement of PA28γ in the propagation of hepatitis C virus. *Hepatology* **2010,** 52, 411-420.

36. Horton, J.; Goldstein, J.; Brown, M., SREBPs: activators of the complete program of cholesterol and fatty acid synthesis in the liver. *J. Clin. Invest.* **2002,** 109, 1125-1131.

37. Eberlé, D.; Hegarty, B.; Bossard, P.; Ferré, P.; Foufelle, F., SREBP transcription factors: master regulators of lipid homeostasis. *Biochimie* **2004,** 86, 839-848.

38. Brown, M. S.; Goldstein, J. L., The SREBP Pathway: Regulation of Cholesterol Metabolism by Proteolysis of a Membrane-Bound Transcription Factor. *Cell* **1997,** 89, 331-340.

39. Shimano, H., Sterol regulatory element-binding proteins (SREBPs): transcriptional regulators of lipid synthetic genes. *Prog. Lipid Res.* **2001**, 40, 439-452.

40. Shao, W.; Espenshade, P. J., Expanding Roles for SREBP in Metabolism. *Cell Metab.* **2012,** 16, 414-419.

41. Goldstein, J. L.; Brown, M. S., Regulation of the mevalonate pathway. *Nature* **1990,** 343, 425-430.

42. Yokoyama, C.; Wang, X.; Briggs, M. R.; Admon, A.; Wu, J.; Hua, X.; Goldstein, J. L.; Brown, M. S., SREBP-1, a basic-helix-loop-helix-leucine zipper protein that controls transcription of the low density lipoprotein receptor gene. *Cell* **1993,** 75, 187-197.

43. Goldstein, J. L.; DeBose-Boyd, R. A.; Brown, M. S., Protein Sensors for Membrane Sterols. *Cell* **2006,** 124, 35-46.

44. Wang, X.; Sato, R.; Brown, M. S.; Hua, X.; Goldstein, J. L., SREBP-1, a membrane-bound transcription factor released by sterol-regulated proteolysis. *Cell* **1994,** 77, 53-62.

45. Yang, T.; Espenshade, P. J.; Wright, M. E.; Yabe, D.; Gong, Y.; Aebersold, R.; Goldstein, J. L.; Brown, M. S., Crucial Step in Cholesterol Homeostasis: Sterols Promote Binding of SCAP to INSIG-1, a Membrane Protein that Facilitates Retention of SREBPs in ER. *Cell* **2002,** 110, 489-500.

46. Sakai, J.; Rawson, R. B.; Espenshade, P. J.; Cheng, D.; Seegmiller, A. C.; Goldstein, J. L.; Brown, M. S., Molecular Identification of the Sterol-Regulated Luminal Protease that Cleaves SREBPs and Controls Lipid Composition of Animal Cells. *Mol. Cell* **1998,** 2, 505-514.

47. Rawson, R. B.; Zelenski, N. G.; Nijhawan, D.; Ye, J.; Sakai, J.; Hasan, M. T.; Chang, T. Y.; Brown, M. S.; Goldstein, J. L., Complementation Cloning of S2P, a Gene Encoding a Putative Metalloprotease Required for Intramembrane Cleavage of SREBPs. *Mol. Cell* **1997,** 1, 47-57.

48. Radhakrishnan, A.; Ikeda, Y.; Kwon, H. J.; Brown, M. S.; Goldstein, J. L., Sterol-regulated transport of SREBPs from endoplasmic reticulum to Golgi: Oxysterols block transport by binding to Insig. *Proc. Natl. Acad. Sci. U. S. A.* **2007,** 104, 6511-6518.

49. Sun, L.-P.; Seemann, J.; Goldstein, J. L.; Brown, M. S., Sterol-regulated transport of SREBPs from endoplasmic reticulum to Golgi: Insig renders sorting signal in Scap inaccessible to COPII proteins. *Proc. Natl. Acad. Sci. U. S. A.* **2007,** 104, 6519-6526.

50. Magaña, M. M.; Osborne, T. F., Two Tandem Binding Sites for Sterol Regulatory Element Binding Proteins Are Required for Sterol Regulation of Fatty-acid Synthase Promoter. *J. Biol. Chem.* **1996,** 271, 32689-32694.

51. Lopez, J. M.; Bennett, M. K.; Sanchez, H. B.; Rosenfeld, J. M.; Osborne, T. E., Sterol regulation of acetyl coenzyme A carboxylase: a mechanism for coordinate control of cellular lipid. *Proc. Natl. Acad. Sci. U. S. A.* **1996,** 93, 1049-1053.

52. Clément, S.; Negro, F., Hepatitis C virus: the viral way to fatty liver. *J. Hepatol.* **2007,** 46, 985-992.

53. Targett-Adams, P.; Boulant, S.; Douglas, M.; McLauchlan, J., Lipid metabolism and HCV infection. *Viruses* **2010,** 2, 1195-1412.

54. Herker, E.; Ott, M., Unique ties between hepatitis C virus replication and intracellular lipids. *Trends Endocrinol. Metab.* **2011,** 22, 241-249.

55. Waris, G.; Felmlee, D. J.; Negro, F.; Siddiqui, A., Hepatitis C Virus Induces Proteolytic Cleavage of Sterol Regulatory Element Binding Proteins and Stimulates Their Phosphorylation via Oxidative Stress. *J. Virol.* **2007,** 81, 8122-8130.

56. Su, A.; Pezacki, J.; Wodicka, L.; Brideau, A.; Supekova, L.; Thimme, R.; Wieland, S.; Bukh, J.; Purcell, R.; Schultz, P.; Chisari, F., Genomic analysis of the host response to hepatitis C virus infection. *Proc. Natl. Acad. Sci. U. S. A.* **2002,** 99, 15669-15743.

57. Mangelsdorf, D. J.; Evans, R. M., The RXR heterodimers and orphan receptors. *Cell* **1995,** 83, 841-850.

58. Yamaguchi, A.; Tazuma, S.; Nishioka, T.; Ohishi, W.; Hyogo, H.; Nomura, S.; Chayama, K., Hepatitis C Virus Core Protein Modulates Fatty Acid Metabolism and Thereby Causes Lipid Accumulation in the Liver. *Dig. Dis. Sci.* **2005,** 50, 1361-1371.

59. Dharancy, S.; Malapel, M.; Perlemuter, G.; Roskams, T.; Cheng, Y.; Dubuquoy, L.; Podevin, P.; Conti, F.; Canva, V.; Philippe, D.; Gambiez, L.; Mathurin, P.; Paris, J.-C.; Schoonjans, K.; Calmus, Y.; Pol, S.; Auwerx, J.; Desreumaux, P., Impaired expression of the peroxisome proliferator-activated receptor alpha during hepatitis C virus infection. *Gastroenterology* **2005,** 128, 334-342.

60. Agriesti, F.; Tataranni, T.; Ruggieri, V.; Capitanio, N.; Piccoli, C., PPARs and HCV-Related Hepatocarcinoma: A Mitochondrial Point of View. *PPAR Res,* **2012,** 2012, doi:10.1155/2012/605302.

61. Moriishi, K.; Mochizuki, R.; Moriya, K.; Miyamoto, H.; Mori, Y.; Abe, T.; Murata, S.; Tanaka, K.; Miyamura, T.; Suzuki, T.; Koike, K.; Matsuura, Y., Critical role of PA28gamma in hepatitis C virus-associated steatogenesis and hepatocarcinogenesis. *Proc. Natl. Acad. Sci. U. S. A.* **2007,** 104, 1661-1666.

62. Harris, C.; Herker, E.; Farese, R. V.; Ott, M., Hepatitis C Virus Core Protein Decreases Lipid Droplet Turnover. *J. Biol. Chem.* **2011,** 286, 42615-42625.

63. Perlemuter, G.; Sabile, A.; Letteron, P.; Vona, G.; Topilco, A.; Chrétien, Y.; Koike, K.; Pessayre, D.; Chapman, J.; Barba, G.; Bréchot, C., Hepatitis C virus core protein inhibits microsomal triglyceride transfer protein activity and very low density lipoprotein secretion: a model of viral-related steatosis. *FASEB J.* **2002,** 16, 185-279.

64. Jackel-Cram, C.; Qiao, L.; Xiang, Z.; Brownlie, R.; Zhou, Y.; Babiuk, L.; Liu, Q., Hepatitis C virus genotype-3a core protein enhances sterol regulatory element-binding protein-1 activity through the phosphoinositide 3-kinase-Akt-2 pathway. *J. Gen. Virol.* **2010,** 91, 1388-1395.

65. Garcia-Mediavilla, M. V.; Pisonero-Vaquero, S.; Lima-Cabello, E.; Benedicto, I.; Majano, P. L.; Jorquera, F.; González-Gallego, J.; Sánchez-Campos, S., Liver X receptor α-mediated regulation of lipogenesis by core and NS5A proteins contributes to HCV-induced liver steatosis and HCV replication. *Lab Invest.* **2012,** 92, 1191-1202.

66. Clément, S.; Peyrou, M.; Sanchez-Pareja, A.; Bourgoin, L.; Ramadori, P.; Suter, D.; Vinciguerra, M.; Guilloux, K.; Pascarella, S.; Rubbia-Brandt, L.; Negro, F.; Foti, M., Down-regulation of phosphatase and tensin homolog by hepatitis C virus core 3a in hepatocytes triggers the formation of large lipid droplets. *Hepatology* **2011,** 54, 38-49.

67. Stiles, B.; Wang, Y.; Stahl, A.; Bassilian, S.; Lee, W. P.; Kim, Y.-J.; Sherwin, R.; Devaskar, S.; Lesche, R.; Magnuson, M. A.; Wu, H., Live-specific deletion of negative regulator Pten results in fatty liver and insulin hypersensitivity. *Proc. Natl. Acad. Sci. U. S. A.* **2004,** 101, 2082-2087.

68. Vinciguerra, M.; Veyrata-Durebex, C.; Moukil, M. A.; Rubbia-Brandt, L.; Rohner-Jeanrenaud, F.; Foti, M., PTEN Down-Regulation by Unsaturated Fatty Acids Triggers Hepatic Steatosis via an NF-kappaBp65/mTOR-Dependent Mechanism. *Gastroenterology* **2008,** 134, 268-280.

69. McPherson, S.; Jonsson, J.; Barrie, H.; O'Rourke, P.; Clouston, A.; Powell, E., Investigation of the role of SREBP-1c in the pathogenesis of HCV-related steatosis. *J. Hepatol.* **2008,** 49, 1046-1100.

70. Diamond, D.; Syder, A.; Jacobs, J.; Sorensen, C.; Walters, K.-A.; Proll, S.; McDermott, J.; Gritsenko, M.; Zhang, Q.; Zhao, R.; Metz, T.; Camp, D.; Waters, K.; Smith, R.; Rice, C.; Katze, M., Temporal proteome and lipidome profiles reveal hepatitis C virus-associated reprogramming of hepatocellular metabolism and bioenergetics. *PLoS Pathog.* **2010,** 6, e1000719.

71. Lyn, R. K.; Kennedy, D. C.; Sagan, S. M.; Blais, D. R.; Rouleau, Y.; Pegoraro, A. F.; Xie, X. S.; Stolow, A.; Pezacki, J. P., Direct imaging of the disruption of hepatitis C virus replication complexes by inhibitors of lipid metabolism. *Virology* **2009,** 394, 130-172.

72. Moradpour, D.; Penin, F.; Rice, C., Replication of hepatitis C virus. *Nat. Rev. Microbiol.* **2007,** 5, 453-463.

73. Wölk, B.; Büchele, B.; Moradpour, D.; Rice, C., A dynamic view of hepatitis C virus replication complexes. *J. Virol.* **2008**, 82, 10519-10531

74. Gross, S. P.; Welte, M. A.; Block, S. M.; Wieschaus, E. F., Dynein-Mediated Cargo Transport in Vivo: A Switch Controls Travel Distance. *J. Cell Biol.* **2000,** 148, 945-956.

75. Shubeita, G. T.; Tran, S. L.; Xu, J.; Vershinin, M.; Cermelli, S.; Cotton, S. L.; Welte, M. A.; Gross, S. P., Consequences of Motor Copy Number on the Intracellular Transport of Kinesin-1-Driven Lipid Droplets. *Cell* **2008,** 135, 1098-1107.

76. Boström, P.; Rutberg, M.; Ericsson, J.; Holmdahl, P.; Andersson, L.; Frohman, M. A.; Borén, J.; Olofsson, S.-O., Cytosolic Lipid Droplets Increase in Size by Microtubule-Dependent Complex Formation. *Arterioscler. Thromb. Vasc. Biol.* **2005,** 25, 1945-1951.

77. Blais, D. R.; Lyn, R. K.; Joyce, M. A.; Rouleau, Y.; Steenbergen, R.; Barsby, N.; Zhu, L.-F.; Pegoraro, A. F.; Stolow, A.; Tyrrell, D. L.; Pezacki, J. P., Activity-based Protein Profiling Identifies a Host Enzyme, Carboxylesterase 1, Which Is Differentially Active during Hepatitis C Virus Replication. *J. Biol. Chem.* **2010,** 285, 25602-25612.

78. Hirokawa, N., Kinesin and Dynein Superfamily Proteins and the Mechanism of Organelle Transport. *Science* **1998,** 279, 519-526.

79. Thompson, R. E.; Larson, D. R.; Webb, W. W., Precise Nanometer Localization Analysis for Individual Fluorescent Probes. *Biophys. J* **2002,** 82, 2775-2783.

80. Kuo, S. C.; McGrath, J. L., Steps and fluctuations of Listeria monocytogenes during actin-based motility. *Nature* **2000,** 407, 1026-1029.

81. Feder, T. J.; Brust-Mascher, I.; Slattery, J. P.; Baird, B.; Webb, W. W., Constrained diffusion or immobile fraction on cell surfaces: a new interpretation. *Biophys. J.* **1996,** 70, 2767-2773.

82. Ghosh, R. N.; Webb, W. W., Automated detection and tracking of individual and clustered cell surface low density lipoprotein receptor molecules. *Biophys. J.* **1994,** 66, 1301-1318.

83. Evans, C. L.; Xie, X. S., Coherent Anti-Stokes Raman Scattering Microscopy: Chemical Imaging for Biology and Medicine. *Annu. Rev. Anal. Chem.* **2008,** 1, 883-909.

84. Cheng, J.-X.; Xie, X. S., Coherent Anti-Stokes Raman Scattering Microscopy: Instrumentation, Theory, and Applications. *J. Phys. Chem. B* **2003,** 108, 827-840.

85. Evans, C. L.; Potma, E. O.; Puoris'haag, M.; Côté, D.; Lin, C. P.; Xie, X. S., Chemical imaging of tissue in vivo with video-rate coherent anti-Stokes Raman scattering microscopy. *Proc. Natl. Acad. Sci. U. S. A.* **2005,** 102, 16807-16812.

86. Freudiger, C. W.; Min, W.; Saar, B. G.; Lu, S.; Holtom, G. R.; He, C.; Tsai, J. C.; Kang, J. X.; Xie, X. S., Label-Free Biomedical Imaging with High Sensitivity by Stimulated Raman Scattering Microscopy. *Science* **2008,** 322, 1857-1861.

87. Nan, X.; Tonary, A. M.; Stolow, A.; Xie, X. S.; Pezacki, J. P., Intracellular Imaging of HCV RNA and Cellular Lipids by Using Simultaneous Two-Photon Fluorescence and Coherent Anti-Stokes Raman Scattering Microscopies. *ChemBioChem* **2006,** 7, 1895-1897.

88. Rakic, B.; Sagan, S. M.; Noestheden, M.; Bélanger, S.; Nan, X.; Evans, C. L.; Xie, X. S.; Pezacki, J. P., Peroxisome Proliferator-Activated Receptor α Antagonism Inhibits Hepatitis C Virus Replication. *Chem. Biol.* **2006,** 13, 23-30.

89. Robinson, I.; Ochsenkühn, M. A.; Campbell, C. J.; Giraud, G.; Hossack, W. J.; Arlt, J.; Crain, J., Intracellular imaging of host-pathogen interactions using combined CARS and two-photon fluorescence microscopies. *J. Biophotonics* **2010,** 3, 138-146.

90. Hellerer, T.; Axäng, C.; Brackmann, C.; Hillertz, P.; Pilon, M.; Enejder, A., Monitoring of lipid storage in Caenorhabditis elegans using coherent anti-Stokes Raman scattering (CARS) microscopy. *Proc. Natl. Acad. Sci. U. S. A.* **2007,** 104, 14658-14663.

91. Ogawa, K.; Hishiki, T.; Shimizu, Y.; Funami, K.; Sugiyama, K.; Miyanari, Y.; Shimotohno, K., Hepatitis C virus utilizes lipid droplet for production of infectious virus. *Proc. Jpn. Acad. Ser. B Phys. Biol. Sci.* **2009,** 85, 217-228.

92. Hourioux, C.; Ait-Goughoulte, M.; Patient, R.; Fouquenet, D.; Arcanger-Doudet, F.; Brand, D.; Martin, A.; Roingeard, P., Core protein domains involved in hepatitis C virus-like particle assembly and budding at the endoplasmic reticulum membrane. *Cellular Microbiol.* **2007,** 9, 1014-1027.

93. Roingeard, P.; Hourioux, C., Hepatitis C virus core protein, lipid droplets and steatosis. *J. Viral Hepat.* **2008,** 15, 157-164.

94. Rouillé, Y.; Helle, F.; Delgrange, D.; Roingeard, P.; Voisset, C.; Blanchard, E.; Belouzard, S.; McKeating, J.; Patel, A. H.; Maertens, G.; Wakita, T.; Wychowski, C.; Dubuisson, J., Subcellular Localization of Hepatitis C Virus Structural Proteins in a Cell Culture System That Efficiently Replicates the Virus. *J. Virol.* **2006,** 80, 2832-2841.

95. Pegoraro, A. F.; Ridsdale, A.; Moffatt, D. J.; Jia, Y.; Pezacki, J. P.; Stolow, A., Optimally chirped multimodal CARS microscopy based on a single Ti:sapphire oscillator. *Opt. Express* **2009,** 17, 2984-3080.

96. Pegoraro, A. F.; Ridsdale, A.; Moffatt, D. J.; Pezacki, J. P.; Thomas, B. K.; Fu, L.; Dong, L.; Fermann, M. E.; Stolow, A., All-fiber CARS microscopy of live cells. *Opt. Express* **2009,** 17, 20700-20706.

97. Sims, P. A.; Xie, X. S., Probing Dynein and Kinesin Stepping with Mechanical Manipulation in a Living Cell. *ChemPhysChem* **2009,** 10, 1511-1516.

4

Bidirectional lipid droplet velocities are controlled by differential binding strengths of HCV core DII protein

Introduction

Host microtubule and associated molecular motor proteins are responsible for delivering cytoplasmic cargo throughout the cell, and to do so, they must efficiently navigate through a dense cytoplasmic environment [1]. Motor proteins, such as dynein and kinesin travel specifically on microtubules that are composed of dimers of tubulin protein arranged as a long polymeric track [1-4]. Additional proteins are recruited to form larger motor protein complexes that regulate cargo transport and microtubule binding [4]. While a wide range of cellular organelles represent typical cytoplasmic cargo that are moved in the cell, in chapter 3 we have shown that LD organelles behave in a similar fashion and are quite mobile in hepatocytes, as similarly observed herein and by Boulant *et al* [5, 6]. Indeed, LD mobility induced by HCV core protein in the viral lifecycle plays a crucial role for viral assembly [5, 7]. However, there are limited studies that have fundamentally evaluated how core protein affects LD dynamics. Imaging techniques applied to simultaneously study the association between

core protein and LDs, to date, have involved only static imaging. For this reason, our aim is to track LDs and domain II (DII) of core protein in live-cells and monitor speed and directionality using particle tracking methods. The use of multi-modal imaging in this chapter has provided an insightful look at how LDs are modulated by core protein on a spatial and temporal level, and importantly, aids in understanding early stages of viral particle assembly.

Formation of mature core protein

HCV core protein is composed of three domains (Schematic 4.1 A) [8]. Upon translation of the HCV polyprotein, a signal sequence in the C-terminal region of core protein and E1 directs the polyprotein to the ER for protease processing [9]. As briefly mentioned in chapter 1, host proteases located at the ER lumen and bilayer are required to cleave each of the structural proteins (core, E1, E2) [10-12]. This begins with signal peptidase (SP) at the ER lumen that first cleaves core from the N-terminus of E1 to generate an immature form of core (Schematic 4.1 A) [10-13]. Next, there is a sequential cleavage by signal peptide peptidase (SPP), which releases the mature form (composed of DI and DII) that further translocates from the ER to the LD surface [12]. The mature form is a component used for virion assembly [5, 8, 14-19]. DI largely exhibits a basic domain that is highly folded in an α-helical form, and this region is responsible for binding to HCV RNA [20]. On the other hand, DII is highly hydrophobic and binds to lipid rich membranes, such as the ER and the LD [20, 21]. Although both domains have distinct functions, the proper folding of DI is dependent on the presence of DII [20]. Finally, DIII is the SP recognition domain, and is retained in the ER following the release of the mature form of core [22, 23]. The transfer of core to the surface of the LD is dependent on diacylglycerol acyltransferase-1 (DGAT1) enzyme [24]. This enzyme is responsible for the final catalyzing step in triglyceride biogenesis, but more recently, has been elucidated to play a fundamental role in viral particle assembly [24]. To date, much of the research

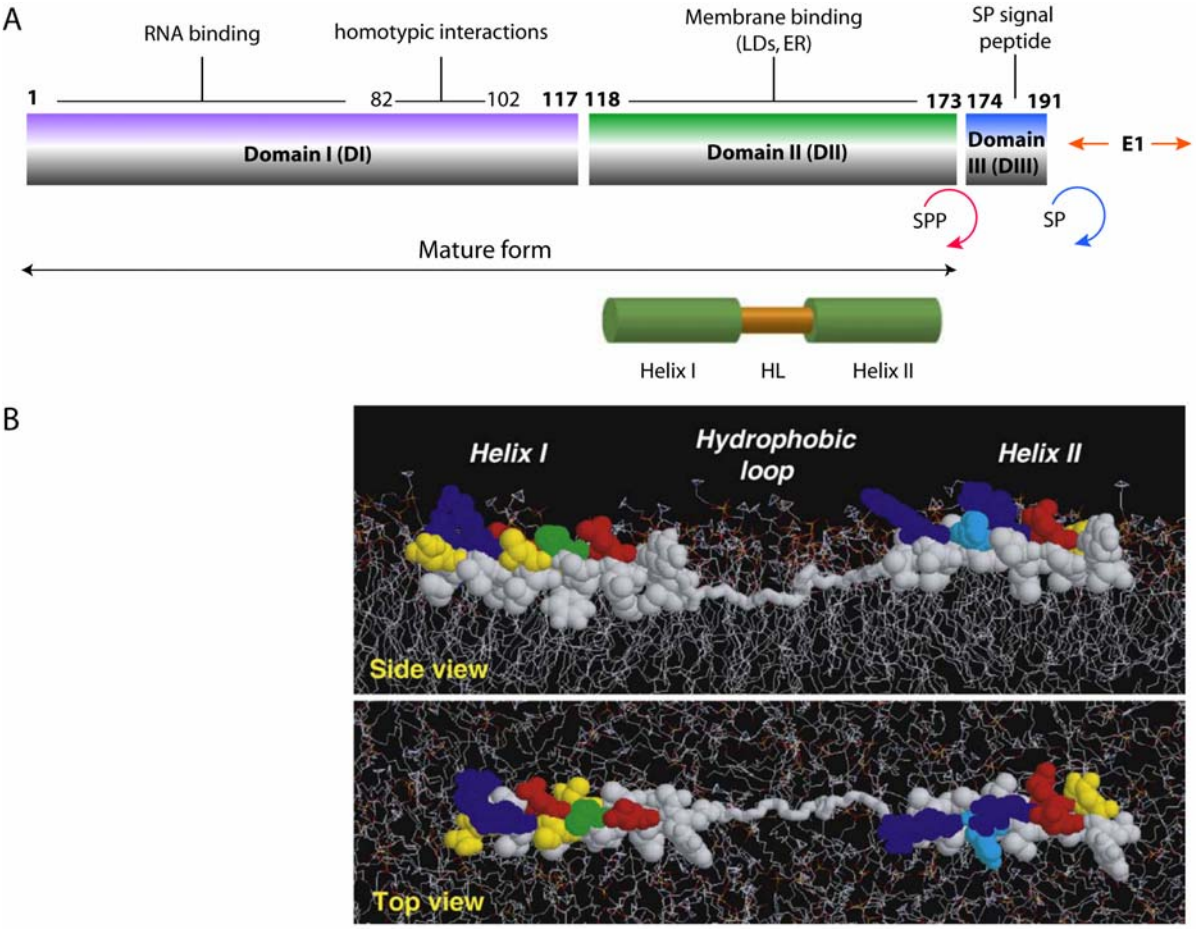

Schematic 4.1: Membrane interactions of Domain II of HCV core protein. (A) Distinct interactions belong to each of the three core protein domains. The mature and immature forms are also shown, and are generated by the two host proteases: signal peptidase (SP, blue), and signal peptide peptidase (SPP, red). Domain II contains two α-amphipathic helices that are separated by a hydrophobic loop. (B) Model of DII shows that this region sits in-plane with the surface of the lipid droplet. The grey regions represent hydrophobic amino acid residues, and the coloured (blue, green, red, yellow) regions represent hydrophilic amino acid residues. The depiction of DII on the surface of the LD is also shown for the side and top view. This schematic was adapted from McLauchlan, J. [9].

that has evaluated the critical binding properties of core and LDs has been pioneered by John McLauchlan and colleagues [8, 21, 25]. HCV core protein must interact with cytoplasmic LDs for viral assembly to occur in the viral lifecycle [9, 14, 26]. This was illustrated when specific mutations within the core region that render it unrecognizable by SP and SPP proteases, abolish assembly of the viral particle [10, 23, 24]. This effect was also mimicked upon inhibiting the activity of DGAT-1 in cell culture studies [24]. Moreover, single amino acid mutations that disrupt the core and LD binding interface also eliminate viral particle assembly [7, 13, 17, 27].

The topology of the LD binding domain of core protein, DII, is composed of two amphipathic α-helices that are separated by a hydrophobic loop (Schematic 4.1 A). Both α-helices lie between regions 119-136 and 148-164, respectively (Schematic 4.1 A) [14]. These amphipathic helices are arranged so that the hydrophobic amino acids are pointed towards the inner core of the LD. When these hydrophobic residues are mutated to hydrophilic residues, core has less binding strength to LD [7, 13, 14, 17]. Although DII is mostly hydrophobic, the few hydrophilic residues within these amphipathic helices are positioned opposite to the hydrophobic face [9, 14]. The observations support an interaction between the polar heads groups of the phospholipid monolayer and the hydrophilic face of the helix, while the opposite hydrophobic face interacts with the inner hydrophobic core of the LD. It is conceivable that both amphipathic helices and the hydrophobic loop sit, in-plane, with the LD surface (Schematic 4.1 B) [9, 14].

Dimerization of core protein

The propensity to dimerize is a structural feature of core protein [28, 29]. Dimerization is required to properly form protein-protein interactions at important steps of viral assembly [20, 28, 29]. In particular, dimerization of core enhances binding with NS3 – which is required to mediate the formation of core-containing particles that contain HCV RNA – prior to interacting with

glycoproteins at sites of viral assembly [28]. Because these interactions are critical, core dimerization is a suitable target for pharmacological blockade.

To effectively measure core dimerization, Förster resonance energy transfer (FRET) was employed as reporter in a bioassay that measured dimerization [30]. As such, Kota *et al.* identified that core dimerization can effectively be monitored by the presence of FRET between europium cryptate and allophycocyanin fluorescent probes that label core protein via a glutathione-S-transferase (GST) tag or a Flag peptide [30]. This technique was proven to be a suitable tool to identify inhibitors of core dimerization [30]. More recently, small molecule inhibitors have been developed to abolish core dimerization (Schematic 4.2) [31-33]. The first lead compound was an indoline alkaloid-type analogue (SL209), which inhibited dimerization of core, with an EC_{50} reported to be 1.4 μM (Schematic 4.2 A)[32]. Furthermore, direct binding of this analogue with core protein was visualized when SL209 was biotinylated and conjugated to a fluorescent probe for molecular imaging. Concurrently, it was also used for immunoprecipitation studies to assess direct interactions of core with non-structural viral proteins that are known core binding partners [31]. Importantly, this core-bound analogue effectively pulled-down non-structural proteins, notably NS3 and NS5A, which are expected binding partners [31].

A new approach to target dimerization of core protein was employed when a dimer of SL209 was introduced (Schematic 4.2 B) [33, 34]. This dimeric inhibitor was postulated to be more effective against protein-protein interactions of core protein that are crucial for HCV. Based on this, an alkyl ether linkage was used to connect two subunits of SL209 to form SL231, which resulted in a magnitude higher of inhibition by comparison to its monomeric form, with an EC_{50} reported to be 98 nM (Schematic 4.2 B) [33]. While several groups have shown that it is effective to target capsid proteins in other viruses, these small molecule inhibitors that target core dimerization may represent a new and promising class of antivirals [35]. This is novel, considering that core protein is the most conserved protein of the HCV genome [36]. Importantly, this suggests that inhibitors of core protein dimerization can potentially target a broad spectrum of HCV genotypes [31, 33].

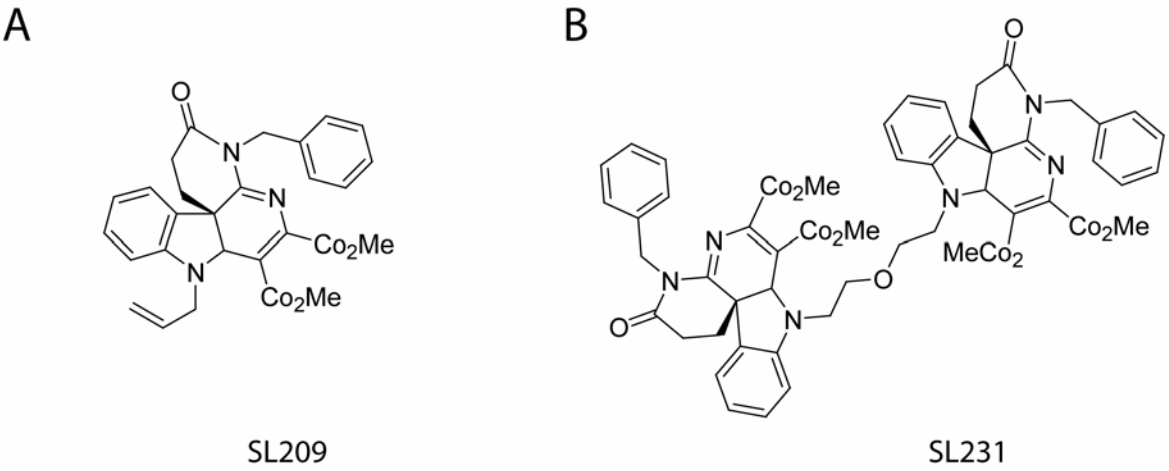

Schematic 4.2: Chemical structures of small molecule inhibitors developed to target HCV core dimerization. (A) SL209 was the first lead compound with an EC_{50} reported to 1.4 μM. (B) A dimer of SL209 (A) was synthesized to increase potency of inhibiting core-core interactions. The EC_{50} reported for SL231 was 98 nM.

Core-induced LD movement and trafficking in hepatocytes

It is clear that core upregulates *de novo* biosynthesis of lipids that virtually contribute in almost every single step of the viral lifecycle, and also serves to lipidate host and viral proteins [37-41]. Additionally, core must also bind to LDs to control its intracellular distribution towards distinct locations that are important for replication and assembly. Likely as a viral adapted mechanism to control LD migration, there are multiple reasons why this may occur. First, evidence has shown that LDs may play a role in providing a surface for viral replication and assembly [18, 26]. Second, LDs may be limiting factors that can provide triglyceride-rich VLDL particles via MTP activity [41, 42], which are required for virion particle maturation at the late stages of assembly. Third, since core protein recruits multiple non-structural proteins to its surface, a high local concentration of viral proteins may be required to provide the necessary environment for propagation of the viral lifecycle [26]. However, the

mechanisms that control core-induced changes to LD distribution are not well understood [26, 43]. Essentially, to reach their destination, core protein that is bound to the surface of LDs must be involved in modulating the movement on microtubules to control for directional transport [5, 6, 16]. We have previously shown in chapter 3 that core-induced LD biogenesis occur before LDs migrate towards the perinuclear region adjacent to replication complexes. McLauchlan *et al.* had also suggested that, by core displacing naïve LD-binding proteins, such as ADRP, the molecular motor dynein may have a higher binding affinity for core, therefore facilitating core-induced transport towards the microtubule organizing center (MTOC) [5].

The mobility of naïve LDs in different animal models reflect bi-directional movements that appear to be motile with very little coordination [1, 6]. However, studies have shown that cytoplasmic cargos, which include the LD, are highly coordinated through cross-talk between motor proteins and their accessory proteins that form larger motor complexes [1, 3, 4, 44-48]. Microtubules radiate from the MTOC outwards to the cell periphery [49]. Cargo is shuttled towards the MTOC in a dynein-mediated retrograde (minus-end motion) manner [2, 3, 50]. By contrast, kinesin motors transport cargo away from the MTOC in an anterograde manner (plus-end motion) [50]. Immunofluorescence studies that label peroxisomes in *Drosophila* have shown that both motors are likely localized on cargo at the same time [51]. To date, the dynamics of LD transport has been widely studied in *Drosophila* but studies are limited for hepatocytes [44].

To explore core-induced LD controlled mobility, it is favourable to use non-disruptive fluorescent markers to track core protein. In the literature, tracking HCV core protein has relied heavily on immunofluorescence staining, which requires the cells to be fixed [14, 16, 23, 26]. Additionally, these procedures render static images and do not provide information about the dynamics, in which, core protein controls LD mobility. More recently, Brett Lindenbach and colleagues incorporated a tetracysteine tag encoded within the core sequence that did not affect its functionality [19]. Using FlAsH reagents, this has provided a unique method of tracking HCV core protein in cell culture.

However, this technique is prone to toxicity, and additive reagents may disrupt biological process involved in mobility. Furthermore, this tag is incapable of long-term imaging due to photobleaching [19]. For imaging LDs, methods from the literature involve BODIPY dyes or indirectly measuring LDs by immunostaining for LD-binding proteins, such as ADRP [24, 26]. Since DII of core protein belongs to the region that binds to LDs, in this chapter, we hypothesized that a green fluorescent protein (GFP) fused to this domain would provide a suitable, and functional method to visualize core-induced LD mobility [17]. We observed by microscopy that DII-core retained colocalization with LDs, and showed that its binding induced LD migration towards sites of replication and assembly at the perinuclear region. As such, we decided to particle track DII-core^{wt} bound LDs, along with LDs in non-DII-core expressing cells, and followed their rates of transport in the cell. Because DII-core^{wt} coated LDs led to slower mean speeds and shorter mean travel distances, we decided to measure whether single amino acid substitutions that affect binding strengths with LDs can differentially modulate LD mobility by comparison to DII-core^{wt}. We showed that the changes in LD velocities and pauses contribute to the overall mean speeds and mean travel distances. By evaluating LD transport that is specific for each direction, our observations show that mechanisms other than a molecular motor imbalance are involved in shuttling LDs towards pertinent sites of replication and assembly.

Hypothesis

Single amino acid mutations in the LD binding domain of the core protein will affect their binding strengths and differentially affect LD dynamics measured in velocity and overall travel distances.

Results

GFP-tagged DII-core^{wt} colocalizes with LDs and upregulates LD *de novo* biosynthesis

To date, monitoring HCV core protein on LDs by adding a fusion protein at the N-terminus of core has been unsuccessful. Attempts to express the GFP-core fusion protein have resulted in unusual localization, and non-specific binding that is potentially caused by irregular protein folding. In order to circumvent this, we employed a construct that expressed a GFP encoded fusion to the N-terminus of DII- core protein from the JFH1 strain (Fig. 4.1 A). Importantly, this construct preserved the LD binding domain, and therefore highlights its potential use for evaluating core's effects of LD dynamics. Essentially, this would allow us to visualize DII-core localization via a GFP marker, while simultaneously monitoring its effects on LD mobility dynamics.

To ensure that a GFP tag, fused to DII-core did not hinder DII-core's ability to bind to LDs, we imaged Huh-7 cells expressing the GFP-tagged DII-core wild-type (DII-core^{wt}) by simultaneous two-photon fluorescence and CARS microscopy (Fig. 4.1 A-C). The methodology of CARS microscopy was explained in chapter 2 [52, 53]. As expected, DII-core^{wt} expression retained a colocalized pattern with intracellular LDs (Fig. 4.1 C). While it appears that not all of the cells are expressing DII-core^{wt}, this provides an advantage for directly measuring qualitative and quantitative comparisons between LD dynamics in DII-core^{wt} expressing and non-expressing cells under one single field of view (Fig. 4.1 C). Upon further evaluation, we observed a distinct change in LD density for cells expressing DII-core^{wt} by comparison to the intracellular distribution of LDs in non DII-core^{wt} expressing cells within the same field of view (Fig. 4.1 C, asterisks vs. double asterisks). This suggests that the expression of DII-core^{wt} in Huh-7 cells is inducing *de novo* LD biosynthesis. Furthermore, as an additional control, the cells that are not expressing DII-core^{wt} consistently showed a similar amount of LDs compared to mock Huh-7 cells (Fig. 4.1 B). Next, we used voxel analysis to

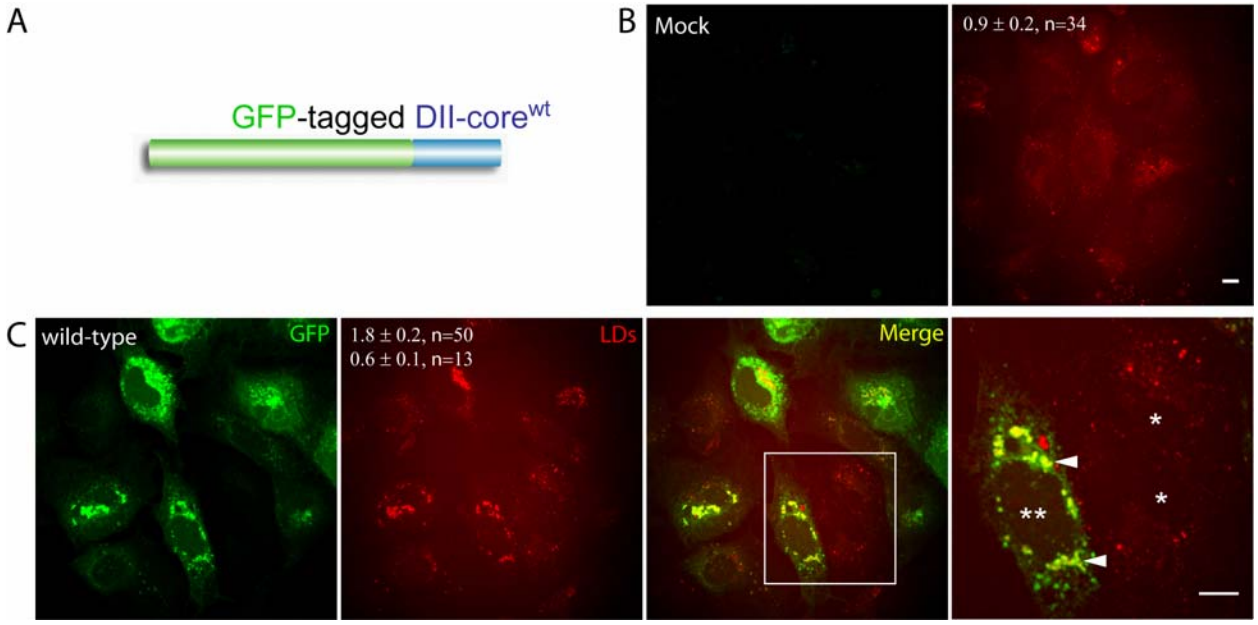

Figure 4.1: CARS microscopy imaging of LDs in Huh-7 cells expressing GFP-tagged DII-core^{wt}. All images were collected approximately 20 hours after Huh-7 cells were transfected with (C) DII-core^{wt} (B) and without DII-core^{wt}, which contained only the lipofectamine transfection reagent. (B) Lipid volumes measured by voxel analysis for mock Huh-7 cells are shown in the CARS image. (C) CARS imaging captures DII-core^{wt} induced LD biogenesis and redistribution towards the perinuclear region (panel 4, arrowheads). The two values in panel 2 represent the average LD volume for cells expressing DII-core^{wt} (top value, double asterisks in panel 4) and non-expressing DII-core cells (single asterisks in panel 4) within the same field of view (bottom value) as measured by voxel analysis. The n represents the number of cells quantified for LD density. This experiment was conducted under two biological replicates. Panel 4 is a magnified image selected by a region of interest from the merged image to project a clearer view of colocalization between DII-core mutants and LDs. All scale bars represent 10μm.

calculate the LD density, and determined that, LD density of DII-core expressing cells have increased by approximately 3-fold by comparison to non DII-core expressing cells under the same fields of view (Fig. 4.1 C). Similarly, the amount of LDs observed in non-DII core expressing cells was also consistent with mock Huh-7 cells (Fig. 4.1 B vs. 4.1 C, single asterisk). From DII-core^{wt} expressing cells, we also observed a change in LD localization, which appeared to form large LD dense inclusions at the perinuclear region (Fig. 4.1 C, arrowhead). This suggests that DII-core^{wt} is capable of inducing LD migration towards the perinuclear region, likely by affecting interactions with motor proteins that are involved in LD motility. Importantly, we observed that GFP did not disrupt DII-core from binding to LDs, indicating that this GFP-tagged DII-core is a suitable method to study the dynamics of LD mobility.

DII-core^{wt} modulates LD dynamics when it is bound to the LD surface

We have shown that DII-core^{wt} remains functional by achieving similar properties known for naïve full-length core protein. Next, we focused on assessing whether the interaction between DII-core^{wt} and LDs affect LD mobility, before it is fully transported to the perinuclear region. For DII-core^{wt} expressing cells, there are LDs that are unbound or bound to DII-core protein. By simultaneous TPF and DIC imaging, we can track the trajectories of LDs from both populations by following LD movements that are overlapped by the fluorescent GFP marker of DII-core. Therefore, these LDs that are bound to DII-core (fluorescence overlap) can be distinguished from those that are unbound (absence of fluorescence overlap). It is important to note that LD mobility may potentially be affected by factors, such as the cell passage number, cells cultured from different days, and cell confluency. To circumvent this, in every experiment that was conducted, the LD measurements acquired from Huh-7 cells expressing a DII-core^{wt} was directly compared with LD measurements from a mock sample of cells that were seeded on the same day. In chapter 3, we showed that LDs in full-length core expressing cells are motile but travel at half the speeds by comparison to mock LDs. With GFP-

tagged DII-core^{wt} expressing cells, we observed a similar pattern, and showed that DII-core^{wt} coated LDs traveled at approximately 40.3nm/sec by comparison to LDs in mock-treated Huh-7 cells, which traveled at 67.2nm/sec (Table 4.1). To compare these values, we divided the average speeds of DII-core^{wt} coated LDs by LDs in mock cells and observed a ratio of 0.60. To illustrate these changes more clearly, figure 4.2 is a representative image that was fragmented from a time-course movie that tracked (Fig. 4.2 A-C, arrowheads) spatially unique LDs under different expression conditions within the same field of view. For example, the trajectories of LD mobility for individual DII-core^{wt} coated LDs and non DII-core^{wt} coated LDs in the same cell are illustrated (Fig. 4.2 D, box 1 vs. box 2, inset 1 vs. inset 2). As expected we observed that the distance traveled was larger in the latter. Additionally, we monitored LDs in an adjacent cell that is not expressing DII-core^{wt} and showed that it also traveled further than LDs that are bound to DII-core^{wt} (Fig. 4.2 D, box 3 & inset 3).

HCV non-structural proteins (NS3-NS5B) bind to LDs when it is recruited by core protein. Because DI of core contains the binding sequences for non-structural proteins, DI`s absence should have no effect on DII-core induced changes to LD dynamics. We confirmed this by demonstrating that, DII-core^{wt} expression in Huh-7 cells stably expressing an HCV subgenomic replicon, colocalized with LDs and also induced a migration of LDs towards the perinuclear region (Fig. 4.3 A). Additionally, the average speed of DII-core^{wt} coated LDs by comparison to LDs of mock cells was observed to be a ratio 0.69 (Fig. 4.3 B). These observations suggest that the presence of non-structural proteins does not affect DII-core^{wt} induced modulation of LD mean speeds and mean LD travel distances. Thus, the effects of DII-core^{wt} on LD movement occur independently of non-structural proteins and of replication complexes.

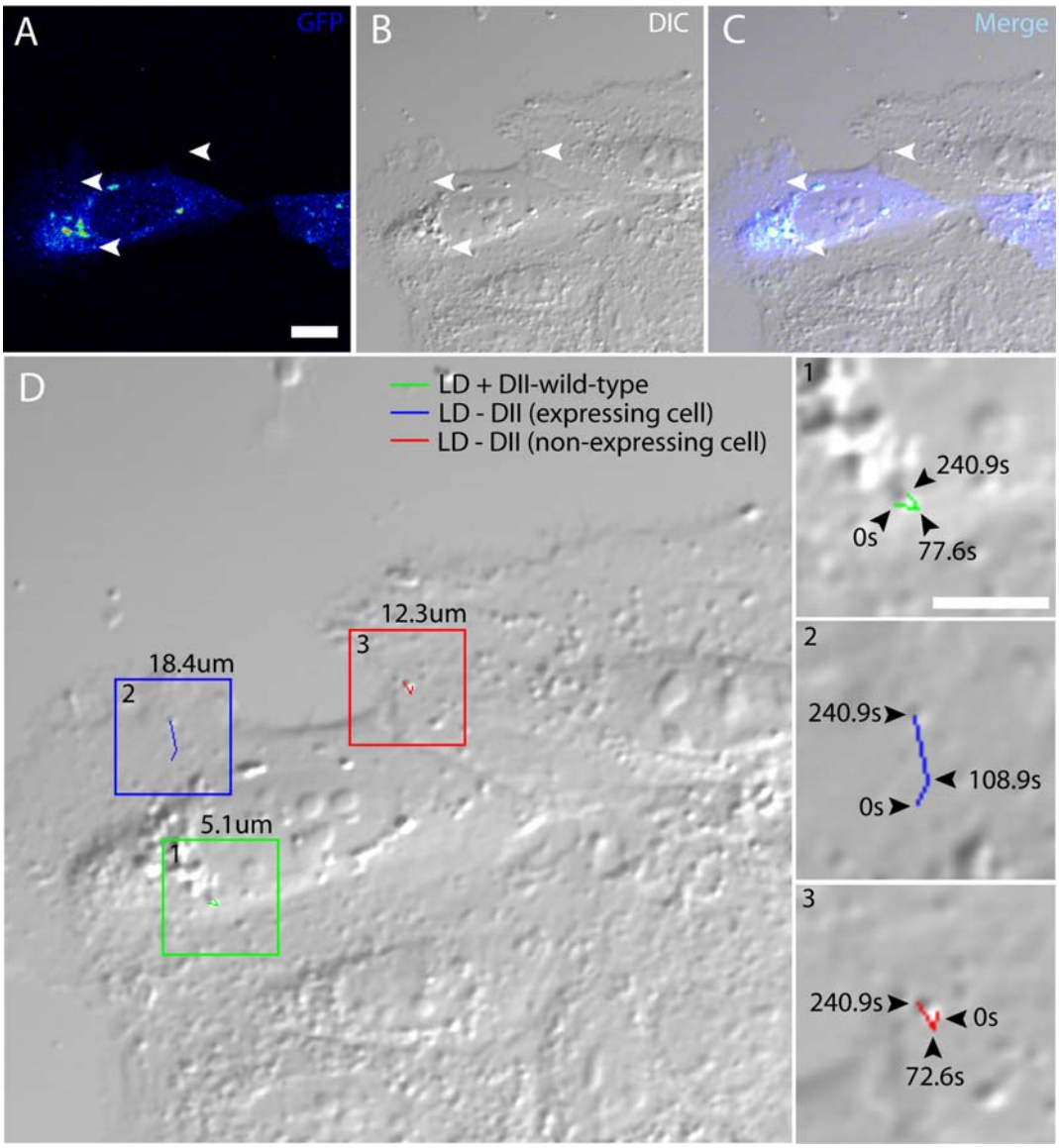

Figure 4.2: DII-core^{wt} coated LDs are particle tracked using simultaneous TPF and DIC microscopy. This is a representative image of DII-core^{wt} expressed in Huh-7 cells. Three individual LDs with dissimilar environments were selected (A-C, white arrows), and their trajectories were measured to calculate the overall distances traveled. (D) A larger DIC image of (B) includes boxes to identify each LD trajectory (inset 1-3). The value above each box (D) indicates their overall travel distances for (1) DII-core^{wt} coated LD, (2) non DII-core^{wt} coated LD within the same cell, (3) and a LD in an adjacent cell not expressing DII-core^{wt}**.** Each LD trajectory is magnified to demonstrate the LD track with selective freeze frame time-intervals representing the LD position at their indicated times. All of the LDs are tracked according to the same start and end time. All scale bars represent 10µm.

A

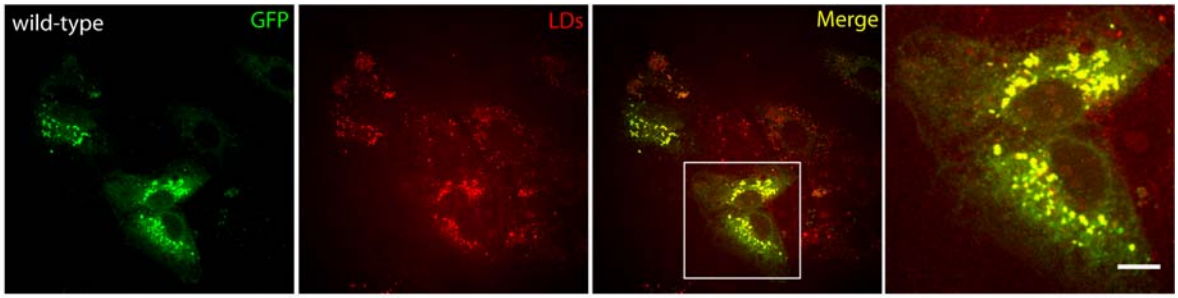

B

Construct	Distance traveled (μm)	Mean speed (nm/sec)	Ratio
Mock (n=61)	11 ± 0.6	47 ± 3	
Wild-type (n=84)	8 ± 0.4	32 ± 2	0.69

Figure 4.3: Particle tracking DII-core^{wt} coated LDs in Huh-7 cells stably expressing an HCV subgenomic replicon. (A) CARS and TPF microscopy captures colocalization between DII-core^{wt} and LDs, and captures DII-core^{wt}-induced LD localization at the perinuclear region. Panel 4 is a magnified image selected by a region of interest from the merged image to project a clearer view of colocalization between DII-core^{wt} and LDs. (B) Particle tracking DII-core^{wt} coated LDs and LDs in mock cells not expressing DII-core^{wt}. The overall mean travel distance and mean speeds were measured. The ratio is calculated by dividing the mean speed of DII-core^{wt} coated LDs by LDs from the mock sample. The n represents the number of LDs that were particle tracked. Live-cell imaging was conducted for duration of four minutes with each frame interval acquired at 1.5 sec/frame. All scale bars represent 10μm.

DII-core protein's binding strength to LDs dictate the overall LD mean speeds and travel distances

Based on the above results, the binding of DII-core^{wt} to LDs is enough to hijack LD dynamic mobility. Here, we postulated that Huh-7 cells expressing DII-core that contained single amino acid modifications at the region of the DII-core and LD interface can variably affect the dynamic mobility of LDs (Fig. 4.4). To evaluate this, the wt-glycine residue at position 161, which is located in the second α-helix of DII was mutated [9, 14, 20]. This gave a range of mutants that altered the hydrophobicity (phenylalanine, leucine, alanine, serine) profile for DII-core. McLauchlan and colleagues have shown that mutations, which increase the hydrophobicity at the 161 position, had also increased the binding strength to LDs. In contrast, a hydrophilic substitution decreased its binding strength to the LD (unpublished results, Fig. 4.4). To ensure that these mutations in DII-core^{161} did not disrupt its functional capabilities that would normally be observed for core protein, we first evaluated whether these DII-core^{161} mutants colocalized with LDs in Huh-7 cells. By microscopy, we showed that these constructs colocalized with LDs, and induced LD migration to the perinuclear region, as similarly observed by expression of DII-core^{wt} (Fig. 4.5 A-D). Consistently, the expression of these mutants had also increased *de novo* LD biosynthesis, and the LD volumes had increased in a range from approximately 3-5 fold.

After applying the same particle tracking methods used to analyze DII-core^{wt}, the mean speeds and overall travel distances measured for DII-core^{161} mutants, gave rise to a general trend that was observed to be dependent upon their binding strengths with LDs (Table 4.1 & Fig. 4.5). We noticed that the mutations, which ranged in hydrophobicity directly correlated to an increase in mean speed, although, overall, they were consistently lower than the mean LD speeds from their mocks samples. For example, the most hydrophobic substitution, DII-core^{G161F}, with the highest binding strength had decreased the mean LD speed to less than half the mean LD speed of the mock, with a

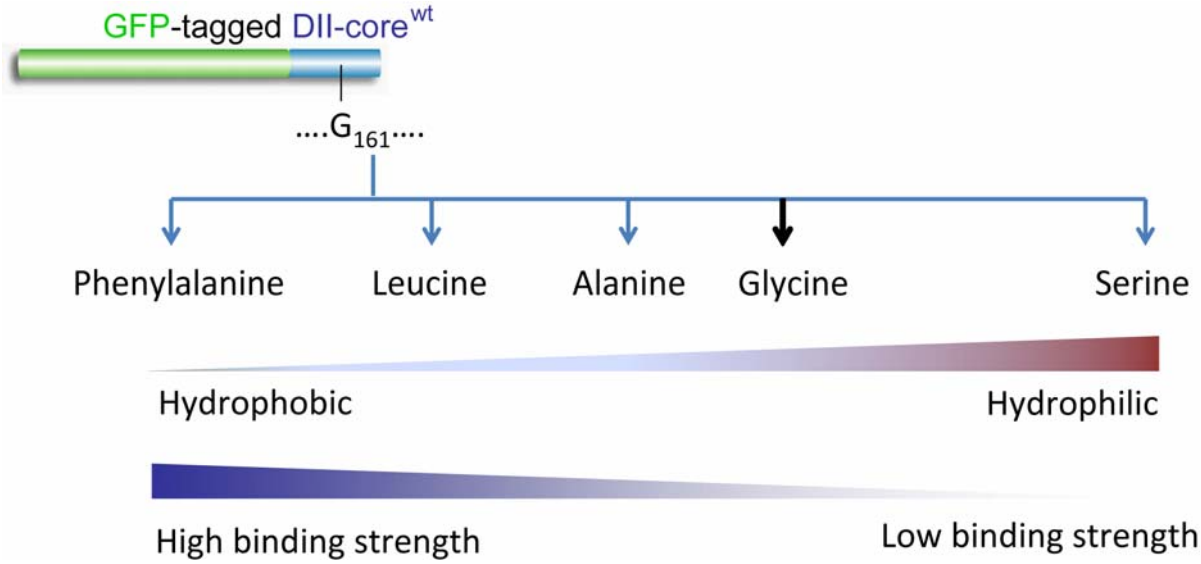

Figure 4.4: Single amino acid mutations at the 161 position of GFP-tagged DII-core^{wt}. The wt-glycine residue at position 161 was replaced with four amino acids that vary in the degree of hydrophobicity, as indicated, and were used for particle tracking experiments. A gradient that shows relative binding strengths of the DII-core mutants on the LD surface are also illustrated.

Construct	Distance traveled (um)	Mean speed (nm/sec)	Ratio
Mock (n=138)	16 ± 0.6	67 ± 2	
Wild-type (n=39)	10 ± 1	40 ± 3	0.60
Mock (n=53)	12 ± 0.7	52 ± 3	
G161F (n=51)	6 ± 0.4	24 ± 2	0.47
Mock (n=60)	13 ± 0.8	53 ± 3	
G161L (n=19)	7 ± 0.8	31 ± 3	0.58
Mock (n=46)	12 ± 0.6	48 ± 3	
G161S (n=39)	9 ± 0.7	37 ± 3	0.77
Mock (n=50)	13 ± 0.8	55 ± 3	
G161A (n=51)	10 ± 0.9	42 ± 4	0.77

Table 4.1: Mean LD speeds and travel distances. The mean speeds and overall travel distances of LDs are compared in DII-core expressing Huh-7 cells and LDs in mock cells. The n represents the number of LDs assessed by particle tracking. Live-cell imaging was conducted for duration of four minutes with each frame interval acquired at 1.65 sec/frame. To avoid variability for LD speeds that is contributed by cellular confluency and passage number, all of the experiments that directly compared DII-core coated LDs to LDs in a mock sample, which contained a vehicle transfection reagent only were observed by cells seeded on the same day. The ratio is calculated by dividing the mean speed of DII-core coated LDs by LDs in the mock cells.

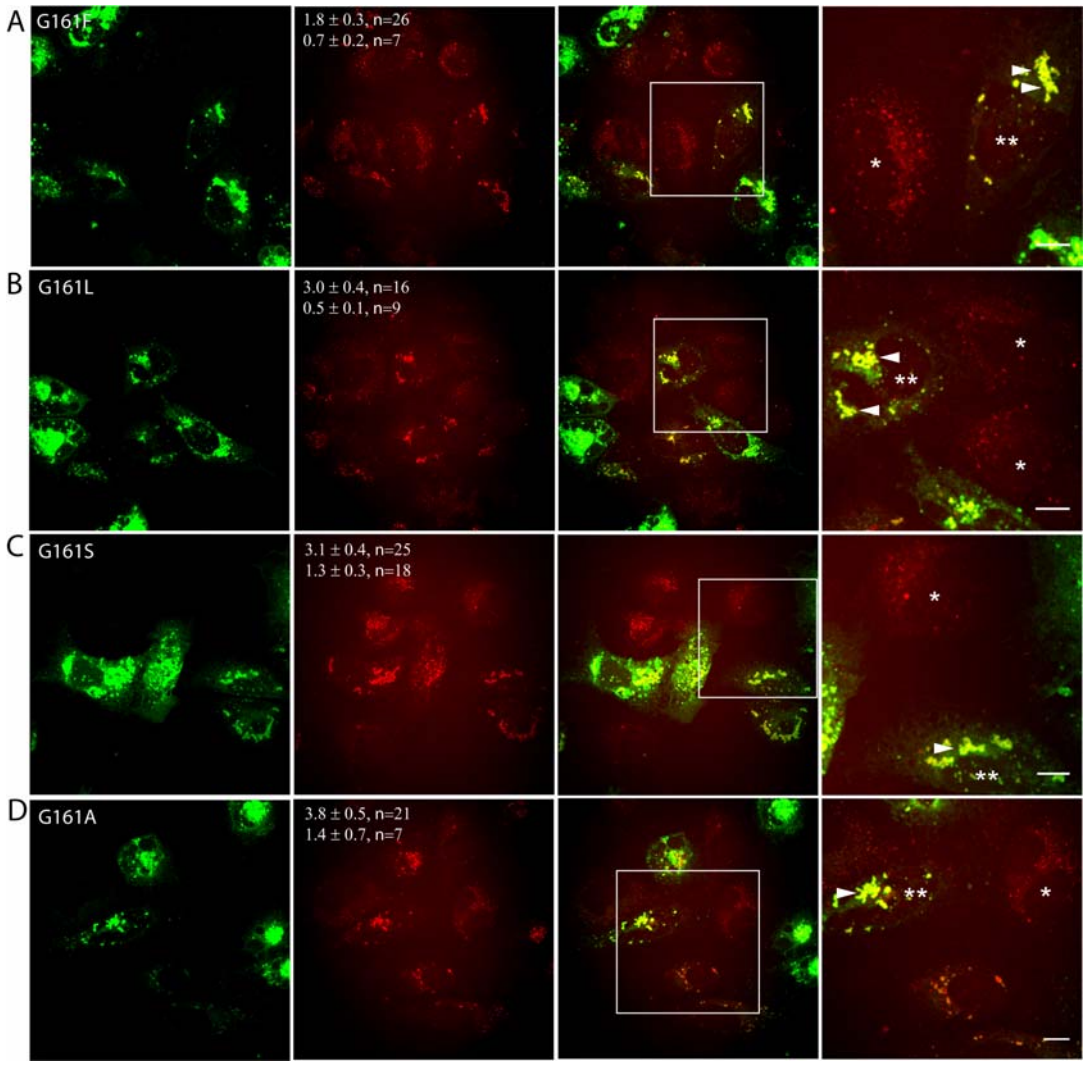

Figure 4.5: Simultaneous CARS and TPF microscopy captures LD changes induced by single amino acid mutations of position 161 in GFP-tagged DII-core^{161} expressing Huh-7 cells. All images were collected approximately 20 hours after Huh-7 cells were transfected with (A) DII-core^{G161F}, (B) DII-core^{G161L}, (C) DII-core^{G161S}, and (D) DII-core^{G161A}. CARS imaging captures DII-core^{161} induced LD biogenesis and redistribution towards the perinuclear region under the expression of all DII-core^{161} mutants (A-D, column 4, arrowheads). The two values in panel 2 represent the average LD volume for cells expressing DII-core^{161} (top value, double asterisks) and non-expressing DII-core^{161} cells (single asterisks) within the same field of view (bottom value) as measured by voxel analysis. The n represents the number of cells quantified for LD density. This experiment was conducted under two biological replicates. Column 4 represents magnified images that are selected by a region of interest from the merged image (column 3) to project a clearer view of colocalization between DII-core^{161} mutants and LDs. The scale bar represents 10µm.

ratio calculated to be 0.47 (Table 4.1). Furthermore, the DII-core^{G161L} mutant also induced a decrease in mean LD speed that was slower than what was observed for the DII-core^{wt}, with a ratio calculated to be 0.58. Conversely, for the hydrophilic mutant, DII-core^{G161S}, the mean LD speed was observed to be faster when compared to the above hydrophobic mutants, with a ratio calculated to be 0.77. The mutant with an alanine substitution, DII-core^{G161A}, induced similar effects to DII-core^{G161S}. From these observations it appears that the binding strength of DII-core^{161} protein on LDs inversely correlates to the mean LD speed as summarized in table 1 and figure 4.4.

Similar to what was observed for DII-core^{wt}, two LD populations also exist within DII-core^{161} mutant expressing Huh-7 cells. Therefore we can directly measure LD trajectories of differential travel distances for individual LDs within the same cell, depending on whether the LD is bound or not bound to DII-core^{161}. We used DII-core^{G161F} expressing Huh-7 cells as a representative image to evaluate both LD populations (Appendix 4.1 A-C). The trajectories from DII-core^{G161F} coated LDs ultimately traveled for shorter distances compared to non DII-core^{G161F} coated LDs within the same cell (Appendix 4.1 D, box 1 vs. box 2, inset 1 vs. inset 2). Correspondingly, LDs in non DII-core^{G161F} expressing cells also resulted in larger travel distances that were similar to the latter result (Appendix 4.1 D, box 3 & inset 3). These observations show that the LD mean speed and mean travel distances are affected only upon direct binding to DII-core^{G161F}. This was consistently observed through all of the DII-core^{161} mutants.

Lower frequency of high velocity travel runs and high frequency of pauses contribute to slower mean speeds for DII-core coated LDs

To investigate a cause for DII-core's induced suppression of the mean LD speed, we further explored whether there was a change to the frequency of low to high instantaneous velocities by

comparing DII-core^{wt} coated LDs to LDs in mock cells. As previously mentioned, dynein and kinesin motors are each responsible for cargo transport only for one direction. Given this, measuring the velocities can also provide us information about whether the mobility of DII-core^{wt} coated LDs travel more frequently for one direction, and thus, reveal differential activity between the two motors. To track the trajectories of individual LDs we used the center of the nucleus as a fixed point relative to the position of the LD. Correspondingly, LDs travel runs that were directed towards the MTOC (retrograde manner) was identified as negative displacement, while LDs that moved away from the MTOC (anterograde motion), was identified as positive displacement (Fig. 4.6 A-B). To better organize the differential velocity profiles for measured LDs, the data sets were segregated into low (15.7-50 nm/sec), medium (50.1-180 nm/sec), and high velocity (>180.1 nm/sec) travel runs (Fig. 4.6 C-D). By particle tracking LDs transported in both directions, we observed that, the frequency of high velocity travel runs for DII-core^{wt} coated LDs were lower when compared to LDs from the mock sample (Fig. 4.6 C, compare ratios). We presented this by calculating a ratio that divided the frequency for DII-core^{wt} coated LDs by LDs from the mock, at each range, to better identify their relationships. For example, at high velocity travel runs, the ratios were calculated to be 0.47 for the anterograde direction, and 0.48 for the retrograde direction (Fig. 4.6 C). Moreover, the frequency of medium velocity travel runs for DII-core^{wt} coated LDs by comparison to LDs from the mock cells were also lower (Fig. 4.6 C-D). The differential frequencies for the high and medium velocities was also consistent to what was observed for DII-core^{wt} coated LDs in Huh-7 cells expressing an HCV subgenomic replicon (Fig. 4.6 D). These observations could explain, in part, that a lower frequency of high velocity travel runs for DII-core^{wt} coated LDs, may result in shorter travel distances, and this was independent of the presence of non-structural proteins that are involved in HCV replication (Fig. 4.6).

Next, we postulated that the frequency of high velocity travel runs is expected to also be lower for DII-core^{161} mutant coated LDs, by comparison to their respective mocks. If the frequency

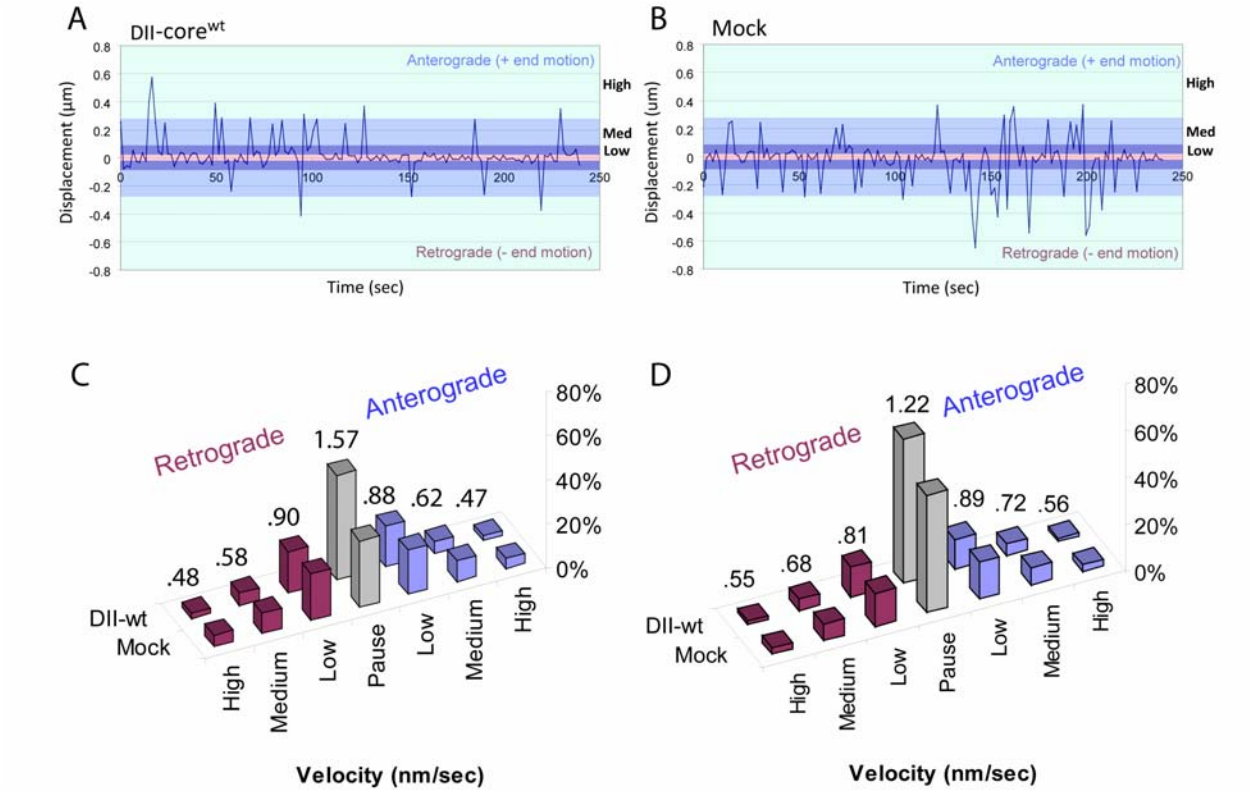

Figure 4.6: Velocities of DII-core^{wt} coated LDs are measured in naïve Huh-7 cells and Huh-7 cells stably expressing an HCV subgenomic replicon. (A-B) Representing an average measurement of a larger data set, LD velocities in retrograde or anterograde directed transport are measured in Huh-7 cells expressing (A) DII-core^{wt} and (B) without DII-core^{wt}. The velocity amplitudes at each time point are divided into parameters of, low (light blue shade), medium (blue shade), and high (purple shade) velocities for both directions. The pink parameter line is indicated by a paused event, which was determined by obtaining the average speed of LDs from nocadazole treated Huh-7 cells. (C-D) The frequency of low (15.7 nm/sec – 50 nm/sec), medium (50.1 nm/sec – 180 nm/sec), and high velocity (> 180.1 nm/sec) measurements, expressed as a percentage, in both directions, are plotted after particle tracking LDs in DII-core^{wt} expressing (C) Huh-7 cells, and (D) Huh-7 cells harbouring an HCV subgenomic replicon. (C-D) The velocities are measured for DII-core^{wt} coated LDs in DII-core^{wt} expressing cells, and LDs from mock cells not expressing DII-core^{wt}. The ratios above each set of columns are calculated by dividing the frequency for each velocity interval of DII-core^{wt} coated LDs by their respective mock LDs.

of high velocity travel runs are involved in modulating overall speeds for DII-core^{161} mutant coated LDs, we also expect that the binding strength trend for DII-core^{161} coated LDs would also produce a similar trend for the frequency of high velocity travel runs. To confirm this, after examining the relative velocities by particle tracking, we observed that a lower frequency of high velocity travel runs for DII-core^{161} mutant coated LDs was observed by comparison to their respective mock samples (Fig. 4.7 A-D). Also, the relative differences in these ratios between the mutants also corresponded to their expected LD binding strengths. For example, the lowest ratio for the frequency of high velocity travel runs by comparison to the mock, was observed to be the highest binding strength mutant, DII-core^{G1161F}, with a ratio of 0.32 and 0.31 for retrograde and anterograde (Fig. 4.7 A). By contrast, DII-core^{G161S} demonstrated the highest ratio with 0.95 and 0.83 (Fig. 4.7 B). For the mutants with binding strengths that fall in the mid range between DII-core^{G161F} and DII-core^{G161S}, they were observed to have ratios 0.57 and 0.52 for DII-core^{G161L} and 0.71 and 0.67 for DII-core^{G161A} (Fig. 4.7 C-D). These observations demonstrate that the relative overall distances traveled for DII-core^{161} coated LDs corresponds to the relative frequency of high velocity LD travel runs.

While observing LD transport, we noticed that, not only do LDs travel at various velocities, but they also appear to pause in a stalled state. We postulated that higher frequencies of LD pauses can also contribute to smaller mean distances traveled by DII-core coated LDs. To identify LD pauses, in chapter 3, we used a microtubule depolymerizing drug, nocadazole (as described in chapter 3), which would halt motor protein dependent active transport. The data obtained showed that these LDs, although subtle, were calculated to move at approximately 15.7nm/sec. Therefore, we chose this parameter as the minimal threshold that would identify LD movement by active transport; velocities below this threshold range were categorized as pauses (Fig. 4.6 & Fig. 4.7 A-D). On the other hand, LD speeds that are detected higher than this threshold would correspondingly be placed in a range of low, medium, or high velocity travel runs. In general we observed that the pauses were more frequent for all the DII-core^{161} mutants and DII-core^{wt} by comparison to their respective mocks (Fig. 4.7 A-D).

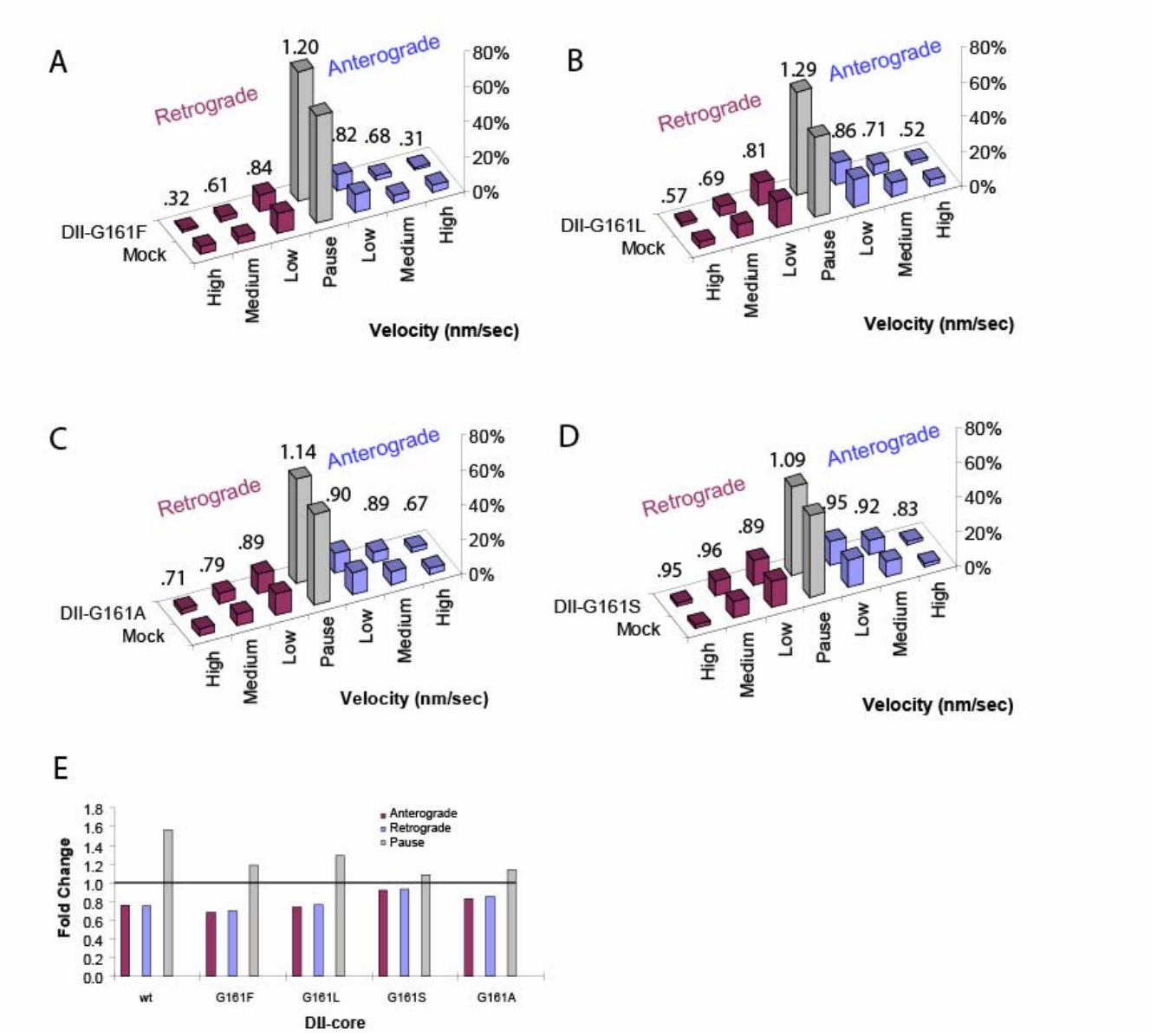

Figure 4.7: LD velocities are measured in Huh-7 cells expressing DII-core^{161} mutants. (A-D) The frequency of pauses (<15.7nm/sec), low (15.7 nm/sec – 50 nm/sec), medium (50.1 nm/sec – 180 nm/sec), and high velocity (> 180.1 nm/sec) measurements, expressed as a percentage, in both directions are plotted for LDs in cells expressing (A) DII-core^{G161F}, (B) DII-core^{G161L}, (C) DII-core^{G161A}, (D) DII-core^{G161S}. The ratios above each set of columns is calculated by dividing the frequency for each velocity interval of DII-core coated LDs by their respective mock LDs. (E) The total frequency of retrograde, anterograde, and pauses were also collected and presented as a fold-change measurement that compared LDs in all DII-core^{161} mutants with each of their respective mocks.

Because the mobility of LDs is often observed to move back and forth in opposite directions, we further calculated the frequency of directional switches. From the data, we failed to observe any trend that would correlate DII-core LD binding strengths to how often directional switching is observed (Appendix 4.2). Although we also did not observe a trend by comparing binding strengths to the frequency of LD pauses, in general, the observation for the higher frequency of LD pauses for DII-core coated LDs is likely to contribute to the shortening of mean LD travel distances and mean LD speed.

DII-core bound LDs spend equal amount of time traveling in both the retrograde and anterograde direction

In chapter 3, live-cell imaging by CARS and DIC microscopy visualized core protein's induced LD migration towards the perinuclear region at replication complexes and assembly. Based on this data, and previously work completed by Boulant *et al.*, it was suggested that when core is bound to LDs, it may directly or indirectly favour a molecular motor imbalance by exclusively activating one motor [5]. Because the expression of DII-core induced DII-core coated LD migration towards the perinuclear region, if a molecular motor imbalance plays a role in core-controlled LD transport, then we would observe a greater frequency of travel runs in the retrograde direction. To examine this, we counted the total frequency of travel runs for one direction that combined low, medium, and high velocity travel runs. It appears that the frequency of travel runs for DII-core coated LDs for the mutants and wt in both directions were similar, indicating that directionality is unaffected (Fig. 4.7 E). This prompted us to further assess whether equal travel runs for both directions are dependent on the cytoplasmic location, relative to the nucleus, since DII-core coated LDs was also observed to be scattered throughout the cell (Appendix 4.3). In order to study this, we have separated regions of the cell positioned either close to the perinuclear region, middle of the cytoplasm, and

further away in the peripheral regions (Fig. 4.8 C). We used DII-core^{G161A} expressing cells as a representative from a larger data set in figure 4.8 that illustrates the defined segregated locations (close, mid, far). After measuring DII-core coated LD velocities for the mutants and wild-type, it appears that for each segregated location, no obvious trends were observed, suggesting that movement of DII-core coated LDs travel equally in both directions and is unrelated to its location in the cell (Appendix 4.4).

LD aggregates at the extreme perinuclear region demonstrate limited mobility

Two distinct populations of DII-core coated LDs that are shown by CARS and DIC imaging appear in all the DII-core mutants and the wt. The first population is represented by DII-core coated LDs that remain scattered throughout the cell (Appendix 4.3, white arrowheads). The second population demonstrates large DII-core coated LDs that are tightly aggregated at the perinuclear region (Appendix 4.3, red arrowheads. Up until this point, we have applied particle tracking studies for DII-core coated LDs from the first population, in order to understand how dynamics of LDs that are controlled by DII-core binding, are affected during the early stages of assembly before the LDs are redistributed towards the perinuclear region. Therefore, using DII-core^{G161A} as a representative image, we measured the velocities of the second population of DII-core coated LDs in the perinuclear region (Fig. 4.8). We showed that these large LDs tightly localized together had limited mobility with minimal spikes in velocity that indicate active transport (Fig. 4.8 C&G). In contrast, DII-core coated LDs outside of these regions continued to experience bidirectional travel runs (Fig. 4.8 A-F). These observations suggest that, although DII-core coated LDs remain mobile at areas outside the perinuclear region, once they reach the perinuclear region, mobility is completely halted. This observation suggests that other factors may be involved in stabilizing DII-core coated LD localization, once it has reached the perinuclear region.

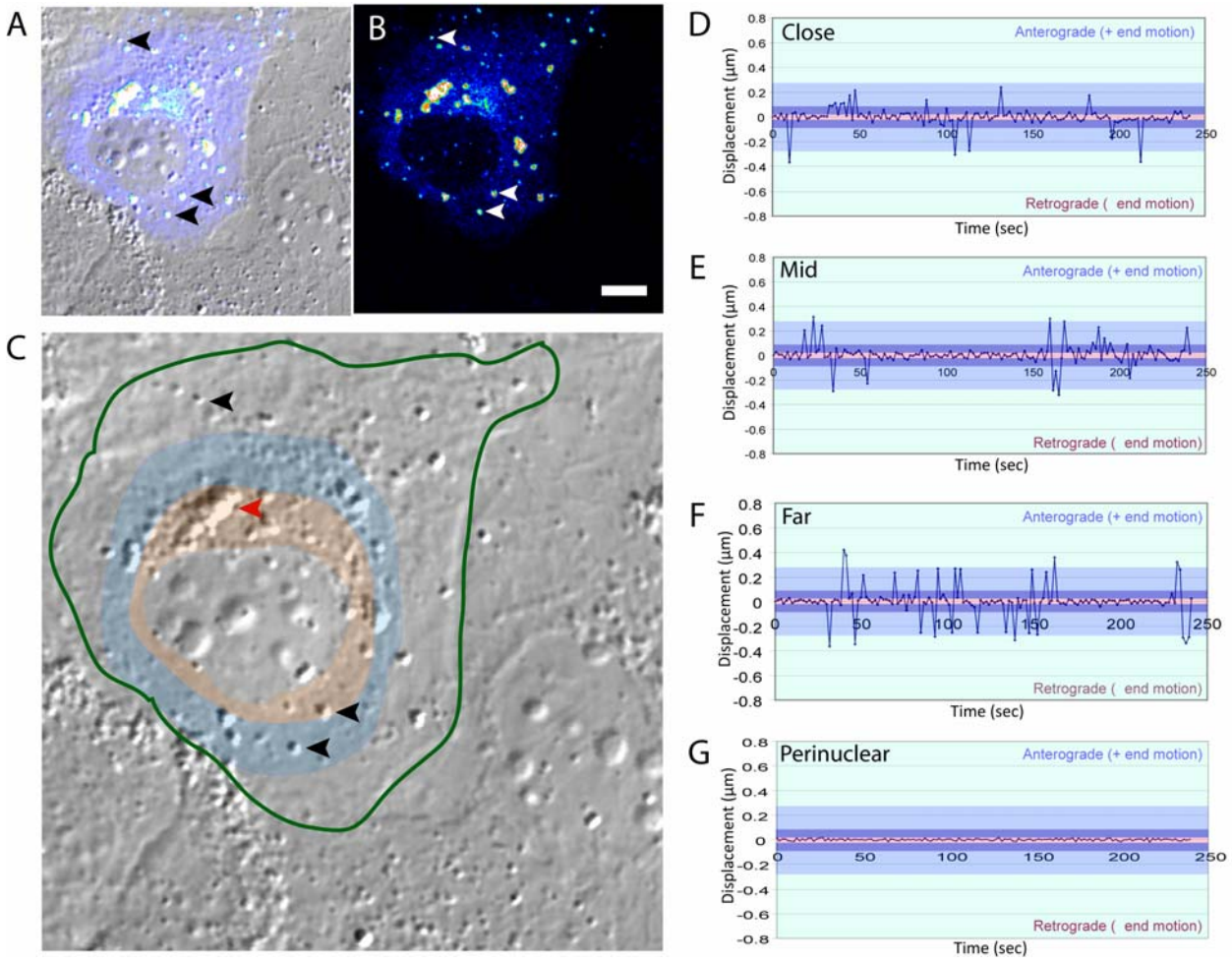

Figure 4.8: Tracking LD mobility at distinct locations of the cell. The frequency for retrograde and anterograde directed LD transport is equally observed at all locations of the cell other than in the perinuclear region where LDs are densely compacted with higher amounts of DII-core protein. While all of the mutants were tracked accordingly, Huh-7 cells expressing DII-core^{G161A} is a representative image acquired from a large data set. Huh-7 cells expressing DII-core^{G161A} is shown as (A) a merged image of DIC and TPF, and (B) TPF. DII-core^{G161A} coated LDs are selected, and indicated by the arrows, to demonstrate fluorescence overlap between TPF and DIC. (C) LDs localized in different areas within the transfected cell (green outline) were segregated into regions relative to the center of the nucleus, such as close (orange shading), mid (blue), and far (no shading). Each black arrow represents a DII-core^{G161A} coated LD for each of the segregated region, and the velocities (low: light blue shade; medium: blue shade; high: purple shade) were measured for each direction in the close (D), mid (E), far (F) regions. The red arrow selects for a region of dense LDs in the perinuclear region with higher levels of DII-core^{G161A}. (G) The velocity of the LD, identified by the red arrow was measured. All scale bars represent 10µm.

Discussion

Molecular motors, such as dynein and kinesin, function by a mechanoenzyme core containing ATPase activity where, upon ATP hydrolysis, facilitate active transport along the plus-end (towards cellular periphery) and minus-end (towards nucleus) of microtubules [1, 54]. Upon entry, viruses are capable of binding to molecular motor proteins that traffic on microtubules to achieve transport. This is common for the adenovirus, herpes simplex virus (HSV), and human immunodeficiency virus (HIV), which have capsid and tegument viral proteins on the surface of the viral particle that, upon immediate entry into the cell, bind and travel by motor induced transport to ensure that viral particles are properly delivered to specific cellular regions to establish infection [55-59]. While HCV is equally capable of hijacking the microtubule network for its own use, this occurs after viral RNA translation, whereby viral proteins are the likely viral components that mediate interactions with motor proteins [12]. For example, NS5A-containing replication complexes were shown to be mobile [60]. In this occurrence, NS5A-containing complexes were shown to travel by salutatory, long-range, rapid transport that were dependent on the microtubule network [60]. Indeed, functional binding of HCV core protein on LDs, play a critical role in core-induced LD transport towards the perinuclear region, and this processes is required at the early stages of viral assembly [5]. However, understanding the properties of core-induced modulation of dynamic LD trafficking is limited.

LD mobility in hepatocytes resembles bidirectional motions with random instantaneous LD accelerations. Although widely debated, it is likely that both motors are simultaneously bound, despite that net displacement for cargos would require preferential activity for one motor, and this is controlled by regulatory mechanisms that are not fully understood [1, 2, 49]. It is suggested that cargos may also be controlled by tug-of-war events, which is defined by both motors exerting equal force in opposite directions until the force is greater for one motor to induce net motion [4]. Many of these

proposed mechanisms that focus on LDs as cytoplasmic cargos, for example, are mostly studied in *Drosophila* and in *yeast*, with limited information found for liver cells [4, 44]. Our present study uses molecular imaging to particle track LD trajectories in live-hepatocytes once they are bound to DII-core protein. Included in this chapter was the evaluation of whether LD dynamics were affected when single amino acid mutations of DII-core that have been shown to affect its binding strength to LDs were introduced in Huh-7 cells. Our attempts to visualize core trafficking was successful by the use of a GFP fusion protein that is encoded into the N-terminus of DII-core protein. We showed that GFP-tagged DII-core expression for both the wt and mutants retained its ability to colocalize with LDs (Fig. 4.1 C & Fig. 4.5 A-D). We also demonstrate that DII-core-induced LD migration towards the perinuclear region was also retained (Fig. 4.1 C & Fig. 4.5 A-D). Because these preserved properties are similarly observed for functional full-length core protein, our observations indicate that this is a suitable method to study core-induced LD dynamics. Importantly, CARS microscopy detected an upregulation of *de novo* LD biosynthesis that was induced by DII-core expression. This is consistent with previous studies, in which DII-core^{wt} expression was identified to be capable of altering host metabolic energy pathways that are diverted for lipid biosynthesis (manuscript submitted). The increase in LDs can also be explained by DII-core's potential ability to decrease LD turnover, especially by a blockade of lipolytic enzymes while DII-core is bound to the LD surface, as this was a reported mechanism by Harris et al [61].

We have previously shown that LDs migrate towards regions known for replication and assembly as early as 20 hours, post-expression, of core protein [6]. Based on this, we aimed to capture the dynamics of LD motions just prior to this time point at a pertinent stage when LDs are seized by DII-core for viral induced trafficking. After examining the average speeds of DII-core coated LDs for both wt and mutants, remarkably, we observed slower mean speeds and a decrease in mean travel distances for DII-core coated LDs, by comparison to LDs in non-expressing DII-core cells (Table 4.1; Fig. 4.2; Appendix 4.1). These observations suggest that, in the absence of DI, DII expression

can cause a loss in speed. Correspondingly, while there are relative differences between each the DII-core mutants that affected the mean speed and mean travel distances, these differences also correlate with their degree of LD binding strengths (Table 4.1). Furthermore, a decrease in mean speeds that correlate with an increase in LD binding strength appear to align with calculated whole-residue free energies measured by peptide transfer from water to membrane bilayers [62]. While slower mean speeds and shorter mean travel distances are observed for DII-core wt and mutants, this can be explained by several reasons. First, we observed that the frequency of high velocity travel runs for DII-core coated LDs was lower by comparison to LDs in mock cells not expressing DII-core (Fig. 4.6 & Fig. 4.7). Secondly, the frequency of pauses was greater in DII-core coated LDs (Fig. 4.6 & Fig. 4.7). These observations suggest that, when DII-core protein is bound to the LD surface this may potentially modify the complex relationship between motor proteins and the LD, and may interfere with the number of engaged motors. While it has been suggested that, in vivo, the number of engaged motors can directly correlate to travel distances of cargo transport, it has also been reported that other mechanisms, such as cytoplasmic viscosity and cargo loads, are likely to mediate a greater role in controlling travel distances of cargo transport [47, 51]. In *Drosophila*, the termination of LD travel runs has been implicated by four proteins that control this mechanism, which include dynactin, Klar, Halo, and LSD2 [44-46, 48]. These accessory proteins have been shown to mediate changes in travel distances during embryo development while playing active roles outside of cargo mediated transport [45, 48]. It is possible that our observations for DII-core induced LD dynamics may be controlled by specific host liver proteins that are related to similar mechanisms as mentioned above. Nevertheless, our findings suggest that these transient interactions of DII-core and LDs may interfere with the number or activity of engaged motors than what is normally observed in naïve cells. Consistent with this, Counihan *et al.* also observed that core coated LDs decreased LD motility [19]. Important to note that, although the range observed for LD velocities was lower when compared to values reported by *Drosophila*, our observations were consistent with particle tracking velocities for adenovirus in HeLa cells [48, 63].

Current models hypothesize that, while only one may be active, both motors always remain associated with the cargo during transport [2, 47, 51]. Our data supports bidirectional travel runs for both naïve LDs and DII-core coated LDs, confirming that activity is engaged by both molecular motors (Fig. 4.6 & Fig. 4.7). Because this is observed for DII-core^{wt} and DII-core^{161} mutants, this suggests that differences in binding strength do not control directionality. Although we expect both motors to be active, we were surprised that, after measuring the frequency of retrograde and anterograde directed transport for DII-core coated LDs, the frequency for both directions was shown to be equally prevalent (Fig. 4.7 E). It was hypothesized that DII-core induced LD migration to the perinuclear region could be driven by an exclusively active dynein-mediated motor mechanism [5, 23]. Instead, however, our results indicate that both motors are actively engaged on the LD when bound to DII-core, which is consistent with particle tracking imaging studies that identified bidirectional transport for adenovirus particles [63, 64]. Supporting this, Suomalainen *et al.* suggested that bidirectional mobility may be the indirect result of a viral strategy to ensure that motor proteins always remain bound to the virus, and can be transported when required without limiting this step [64]. It is possible for DII-core expressing cells that, although we observed migration of LDs to the perinuclear region, along with equal bidirectional travel runs, our time-course measurements may imply that the four minute duration of imaging is too-short to quantitatively measure an imbalance between active motors. Considering this, it also takes approximately 20 hours to fully migrate towards the perinuclear region. Nevertheless, mechanisms that are reported in other viruses that utilize proteins that are also expressed in the liver, may help explain why bidirectional travels of equal frequency are observed, in addition to, LD-mediated perinuclear migration. For example, Suomalainen *et al.* demonstrated that minus-end directed mobility of newly entered adenovirus particles on microtubules was dependent on transient activation of protein kinase A (PKA) and p38/ mitogen-activated protein kinase (MAPK) pathway, despite that bidirectional motions remained to be observed [64]. They show that inhibitors of PKA and p38, resulted in peripheral cellular localization of the virus, rather than at the perinuclear region [64]. Accordingly, HCV core protein expression activates the p38/MAPK pathway, which is

involved in regulation of cell signalling and downstream phosphorylation events in the liver [65-67]. In HCV infection, PKA is involved in phosphorylating heat shock proteins (hsp) that directly bind to core, which is hypothesized to be required for proper folding of core [68].

One study investigated the involvement of cytosolic member of HSP70 family of chaperones, heat shock cognate-70 protein (hsc70), which was identified to be binding partners of HCV core protein and are strongly implicated in viral budding and egress [69]. Consistent with this idea, hsc70 was also shown to be involved in regulating kinesin function by relieving its interaction with membrane bound organelles [58, 69]. The appearance of hsc70 may be an accessory protein that is required to regulate motor transport with the release of kinesin motors, a plausible factor that allows dynein-exclusive minus-end directed transport. Moreover, Suomalainen *et al.* suggested that the activity of PKA may play a role in modifying adaptor proteins involved in bridging the interactions between the cargo and the motor [64]. These reported mechanisms suggest that core-induced directionality is likely mediated by other host factors other than a single motor dominant mechanism for core-induced LD localization.

A unique feature of several viruses is their ability to covertly piggy-back along the proteosomal degradation pathway during autophagy [70-72]. Interestingly, hsc70 that is a reported binding partner of core protein, as mentioned above, has also been implicated in autophagy in hepatocytes [69]. As part of an innate response, core protein aggregation on the LD surface may be recognized as misfolded proteins that, in turn, activate proteosomal-mediated degradation [71, 72]. Upon recognition of misfolded proteins as cargo, dynein motors can shuttle this cargo to the MTOC, which leads to an accumulation of sequestered proteins by forming aggresomes that are then degraded [73]. For HCV, however, the degradation of the entire LD bound to core may be beneficial in the viral assembly process. Lysosomal degradation of the LD may concentrate all the components required to facilitate efficient viral assembly and egress, which is a mechanism that belongs to the Dengue virus, a close relative to HCV [74, 75]. The lipid rich pool of fatty acids, mainly triglycerides, as remnants after

LD degradation may possibly serve as important intermediates to form intermediate-VLDL particles that co-secreted with HCV viral particle [76, 77]. Hijacking the autophagic pathway may potentially be a strategy for HCV propagation.

We have highlighted important dynamics of core-directed mobility for DII-core coated LDs, and demonstrated that bidirectional motion is observed for all other DII-core coated LDs that are located outside of the critical perinuclear region (Fig. 4.8). This prompted us to investigate the movement of LDs within these perinuclear regions where there appears to be higher levels of localized DII-core protein (Fig. 4.8 C&G). From this we noticed minimal movement that is indicative of exclusively paused or trapped LDs. These large static complexes are, similarly, observed for larger of the two populations of NS5A-containing replication complexes [60]. Based on this observation, two possible mechanisms may play a role in DII-core's effect on limiting LD mobility at these sites. First, it is plausible that once DII-core coated LDs reach a critical area of the cell, the motors will disengage allowing DII-core coated LDs to accumulate. Indeed, Miyanari *et al.* reported that LDs are required at the replication and assembly sites [26]. This accumulation may effectively link early and late viral assembly stages. Second, DII-core coated LDs may be stabilized at the perinuclear region by the recruitment of additional host proteins to prevent LDs from traveling away from the perinuclear region. This stability may potentially be mediated by the hijacking of the autophagic pathway that forms aggresomes within sites of replication and assembly, as indicated above [71, 72]. The accumulation of aggresomes sequestered around the MTOC may prevent motors from binding, and results in densely packed LDs that are stabilized without accessible motor proteins. This is consistent with our findings for these large static structures of aggregated LDs, along with higher concentrations of DII-core protein in these regions. Alternatively, host proteins that are recruited to LDs by core protein at the perinuclear regions may play a role in stabilizing LD at these sites. More recently, a subunit of host clathrin adaptor protein complex 2 (AP2M1) has been shown to bind to core by recognizing a highly conserved tyrosine-based sorting signal, YXXφ (φ being a bulky hydrophobic

residue) along the DII region [78]. These proteins sort intracellular cargo via a clathrin adaptor and can mediate endocytic functions. Importantly, disrupting AP2M1 from interacting with core eliminates viral assembly [78]. Notably, the same AP2M1 binding motif was also identified in the region of E1 proteins. Such a feature supports the idea that AP2M1 is recruited to LDs via DII of core protein, and likely mediates intracellular trafficking of core to sites of assembly where E1 and E2 proteins reside, prior to the envelopment of the viral particle. This engagement can possibly stabilize the LD from being bound to motor proteins once LDs reach this critical area at the perinuclear region.

From our particle tracking observations, we have provided a unique insight into core's dynamic control of LD-induced migration. We showed that DII, alone, can cause a decrease in LD speeds and does not control LD directionality. From our evaluation of bidirectional transport of DII-core coated LDs, it is likely that additional host proteins may play a role in aiding the disengagement of motor proteins from core coated LDs. Nevertheless, we showed that a GFP fusion tag to DII of core remains functional and can provide a unique capability to study binding strength relationships in a spatial and temporal manner.

Future Directions

Given the observations reported in this chapter, our next steps would include evaluating single amino acid mutations in other regions of DII. Our exciting observations was reported from evaluations of mutations at the second α-amphiphatic helices of DII, which exposes the potential for direct amino acid substitutions in other regions of DII, such as the first α-amphipathic helix or the hydrophobic loop. It would also be interesting to assess whether synergism is observed for more than one mutation or a combination of many. While many proteins, as mentioned in this chapter's discussion, which have been shown to play a pertinent role in regulating motor proteins, it would be plausible to study these proteins in the context of HCV, using our multimodal imaging set-up.

Because visualize label-free LDs, we can fine-tune a strategy to acquire multiple fluorescently labeled proteins that are of interest, which can be detected by multiple channels, and probe for any direct interactions with core and LDs. This may potentially provide a suitable method to acquire live interactions that bridge the gap between early stages and late stages of viral assembly, which is a mechanism that has yet to fully be understood.

Materials and Methods

Tissue culture

Human hepatoma cells (Huh-7) were grown in DMEM medium supplemented with 100 nM nonessential amino acids, 50 U/mL penicillin, 50 μg/mL streptomycin, and 10% FBS (CANSERA, Rexdale, ON). Huh-7 cells harboring the pFK-I389neo/NS3-3′/5.1 subgenomic replicon were maintained in the same culture medium supplemented with 250 μg/mL G418 Geneticin (GIBCO-BRL, Burlington, ON). The pFK-I389neo/NS3-3′/5.1 subgenomic replicon was kindly provided by Ralf Bartenschlager (Institute of Hygiene, University of Heidelberg, Germany).

Overexpression of DII-core protein

Huh7 cells were seeded at 8.0 x 10^4 cells/well in borosilicate Lab-Tek chambers (VWR, Mississauga, ON). After 24 h, at a confluency of 60–70%, cells were transfected with DII-core wild-type and DII-core mutants suspended in transfection media including lipofectamine 2000 (Invitrogen Canada Inc., Burlington, ON). DII-core plasmids for the wild-type and single amino acid mutations were kindly provided by John McLauchlan (Medical Research Council Unit – Center for Virus Research, University of Glasgow, Scotland). After 4 h, DMEM in 20% FBS was added in equal volume to the chambers.

Simultaneous coherent anti-Stokes Raman scattering and two-photon fluorescence microscopies

The CARS microscopy system uses a single femtosecond Ti:sapphire oscillator as the excitation source, as previously described [52, 79].

Laser scanning simultaneous two-photon excited fluorescence and differential interference contrast microscopies

An Olympus FV300 laser scanning microscopy system on an IX71 inverted microscope was used for imaging experiments. A 40x Uapo 1.15NA water immersion objective and a long working distance 0.55 NA condenser were used. The FV300 was adapted for two-photon fluorescence. Source was a Coherent Mira 900 Ti:sapphire laser producing pulses of approximately 100 fs at 800 nm wavelength with an 80 MHz repetition rate. Laser scanning microscopy can be readily adapted to DIC by taking advantage of the high inherent polarization in most laser sources. The DIC optics were adjusted as they would typically be for transmitted light use: with the prisms removed the condenser polarizer is adjusted to cross with the objective polarizer. For laser scanning, the analyzer, which is in a fluorescence cube in the IX71, is removed from the beam path. To optimally align the polarization of the laser with that of the microscope optics, a 700–1000 nm achromatic half wave plate (WPA1212 Casix) was placed in the laser path before entering the FV300 scan-box. The polarization of the laser was adjusted by rotating this wave plate to minimize the amount of light collected through the condenser polarizer. The DIC prisms are inserted and the path and the bias of the objective prism adjusted to the optimal image.

Particle tracking of LDs in Huh-7 cells

Particle tracking LD movements to assess both speed and distances traveled was captured using the spot tracker add-on with ImageJ, as previously described [6]. The spot tracker followed the light shaded halo contrast of LDs as a result of changes in refractive index captured by DIC imaging. Measuring directional displacements (plus and minus-end directed motion) was calculated by determining the position of the LD at each time point interval, relative to a fixed reference point in the center of the nucleus.

Quantitative voxel analysis

Calculating lipid volumes from CARS images was determined using a voxel counter in ImageJ as previously described [6, 80]. In each image, multiple cells within the same field of view were counted to determine an average percentage of lipid volume.

References

1. Welte, M., Bidirectional transport along microtubules. *Curr. Biol.* **2004,** 14, R525-537.

2. Gross, S.; Vershinin, M.; Shubeita, G., Cargo transport: two motors are sometimes better than one. *Curr. Biol.* **2007,** 17, R478-486.

3. Gross, S.; Welte, M.; Block, S., Wieschaus, E. F., Dynein-mediated cargo transport in vivo. A switch controls travel distance. *J. Cell Biol.* **2000**, 148, 945-956.

4. Müller, M. J. I.; Klumpp, S.; Lipowsky, R., Tug-of-war as a cooperative mechanism for bidirectional cargo transport by molecular motors. *Proc. Natl. Acad. Sci. U. S. A.* **2008,** 105, 4609-4614.

5. Boulant, S.; Douglas, M.; Moody, L.; Budkowska, A.; Targett-Adams, P.; McLauchlan, J., Hepatitis C virus core protein induces lipid droplet redistribution in a microtubule- and dynein-dependent manner. *Traffic* **2008,** 9, 1268-1350.

6. Lyn, R.K; Kennedy, D.C; Stolow, A.; Ridsdale, A.; Pezacki, J.P, Dynamics of lipid droplets induced by the hepatitis C virus core protein. *Biochem. Biophys. Res. Commun.* **2010,** 399, (4), 518-542.

7. Boulant, S.; Targett-Adams, P.; McLauchlan, J., Disrupting the association of hepatitis C virus core protein with lipid droplets correlates with a loss in production of infectious virus. *J. Gen. Virol.* **2007,** 88, 2204-2217.

8. McLauchlan, J., Properties of the hepatitis C virus core protein: a structural protein that modulates cellular processes. *J. Viral Hepat.* **2000,** 7, 2-14.

9. McLauchlan, J., Lipid droplets and hepatitis C virus infection. *Biochim. Biophys. Acta* **2009,** 1791, 552-561.

10. Okamoto, K.; Mori, Y.; Komoda, Y.; Okamoto, T.; Okochi, M.; Takeda, M.; Suzuki, T.; Moriishi, K.; Matsuura, Y., Intramembrane processing by signal peptide peptidase regulates the membrane localization of hepatitis C virus core protein and viral propagation. *J. Virol.* **2008,** 82, 8349-8410.

11. Ait-Goughoulte, M.; Hourioux, C.; Patient, R.; Trassard, S.; Brand, D.; Roingeard, P., Core protein cleavage by signal peptide peptidase is required for hepatitis C virus-like particle assembly. *J. Gen. Virol.* **2006,** 87, 855-915.

12. McLauchlan, J.; Lemberg, M.; Hope, G.; Martoglio, B., Intramembrane proteolysis promotes trafficking of hepatitis C virus core protein to lipid droplets. *EMBO J.* **2002**, 21, 3980-3988.

13. Pérez-Berná, A.; Veiga, A.; Castanho, M.; Villalaín, J., Hepatitis C virus core protein binding to lipid membranes: the role of domains 1 and 2. *J. Viral Hepat.* **2008,** 15, 346-402.

14. Boulant, S.; Montserret, R.; Hope, R.; Ratinier, M.; Targett-Adams, P.; Lavergne, J.-P.; Penin, F.; McLauchlan, J., Structural determinants that target the hepatitis C virus core protein to lipid droplets. *J. Biol. Chem.* **2006,** 281, 22236-22247.

15. Barba, G.; Harper, F.; Harada, T.; Kohara, M.; Goulinet, S.; Matsuura, Y.; Eder, G.; Schaff, Z.; Chapman, M. J.; Miyamura, T.; Brechot, C., Hepatitis C virus core protein shows a cytoplasmic localization and associates to cellular lipid storage droplets. *Proc. Natl. Acad. Sci. U. S. A.* **1997,** 94, 1200-1205.

16. Roohvand, F.; Maillard, P.; Lavergne, J.-P.; Boulant, S.; Walic, M.; Andréo, U.; Goueslain, L.; Helle, F.; Mallet, A.; McLauchlan, J.; Budkowska, A., Initiation of hepatitis C virus infection requires the dynamic microtubule network: role of the viral nucleocapsid protein. *J. Biol. Chem.* **2009,** 284, 13778-13869.

17. Shavinskaya, A.; Boulant, S.; Penin, F.; McLauchlan, J.; Bartenschlager, R., The lipid droplet binding domain of hepatitis C virus core protein is a major determinant for efficient virus assembly. *J. Biol. Chem.* **2007,** 282, 37158-37169.

18. Popescu, C.-I.; Rouillé, Y.; Dubuisson, J., Hepatitis C virus assembly imaging. *Viruses* **2011,** 3, 2238-2254.

19. Counihan, N.; Rawlinson, S.; Lindenbach, B., Trafficking of hepatitis C virus core protein during virus particle assembly. *PLoS Pathog.* **2011,** 7, e1002302.

20. Boulant, S.; Vanbelle, C.; Ebel, C.; Penin, F.; Lavergne, J.-P., Hepatitis C Virus Core Protein Is a Dimeric Alpha-Helical Protein Exhibiting Membrane Protein Features. *J. Virol.* **2005,** 79, 11353-11365.

21. Hope, R. G.; McLauchlan, J., Sequence motifs required for lipid droplet association and protein stability are unique to the hepatitis C virus core protein. *J. Gen. Virol.* **2000,** 81, 1913-1925.

22. Kopp, M.; Murray, C.; Jones, C.; Rice, C., Genetic analysis of the carboxy-terminal region of the hepatitis C virus core protein. *J. Virol.* **2010,** 84, 1666-1739.

23. Targett-Adams, P.; Hope, G.; Boulant, S.; McLauchlan, J., Maturation of hepatitis C virus core protein by signal peptide peptidase is required for virus production. *J. Biol. Chem.* **2008,** 283, 16850-16859.

24. Herker, E.; Harris, C.; Hernandez, C.L.; Carpentier, A.; Kaehlcke, K.; Rosenberg, A.; Farese, R.; Ott, M., Efficient hepatitis C virus particle formation requires diacylglycerol acyltransferase-1. *Nat. Med.* **2010,** 16, 1295-1303.

25. Hope, R. G.; Murphy, D. J.; McLauchlan, J., The Domains Required to Direct Core Proteins of Hepatitis C Virus and GB Virus-B to Lipid Droplets Share Common Features with Plant Oleosin Proteins. *J. Biol. Chem.* **2002,** 277, 4261-4270.

26. Miyanari, Y.; Atsuzawa, K.; Usuda, N.; Watashi, K.; Hishiki, T.; Zayas, M.; Bartenschlager, R.; Wakita, T.; Hijikata, M.; Shimotohno, K., The lipid droplet is an important organelle for hepatitis C virus production. *Nat. Cell Biol.* **2007,** 9, 1089-1186.

27. Alsaleh, K.; Delavalle, P.-Y.; Pillez, A.; Duverlie, G.; Descamps, V.; Rouillé, Y.; Dubuisson, J.; Wychowski, C., Identification of basic amino acids at the N-terminal end of the core protein that are crucial for hepatitis C virus infectivity. *J. Virol.* **2010,** 84, 12515-12543.

28. Kushima, Y.; Wakita, T.; Hijikata, M., A Disulfide-Bonded Dimer of the Core Protein of Hepatitis C Virus Is Important for Virus-Like Particle Production. *J. Virol.* **2010,** 84, 9118-9127.

29. Mousseau, G.; Kota, S.; Takahashi, V.; Frick, D. N.; Strosberg, A. D., Dimerization-driven interaction of hepatitis C virus core protein with NS3 helicase. *J. Gen. Virol.* **2011,** 92, 101-111.

30. Kota, S.; Scampavia, L.; Spicer, T.; Beeler, A.; Takahashi, V.; Snyder, J.; Porco, J.; Hodder, P.; Strosberg, A., A time-resolved fluorescence-resonance energy transfer assay for identifying inhibitors of hepatitis C virus core dimerization. *Assay Drug Dev. Technol.* **2010,** 8, 96-105.

31. Kota, S.; Takahashi, V.; Ni, F.; Snyder, J. K.; Strosberg, A. D., Direct Binding of a Hepatitis C Virus Inhibitor to the Viral Capsid Protein. *PLoS ONE* **2012,** 7, e32207.

32. Wei, W.; Cai, C.; Kota, S.; Takahashi, V.; Ni, F.; Strosberg, A. D.; Snyder, J. K., New small molecule inhibitors of hepatitis C virus. *Bioorg. Med. Chem. Lett.* **2009,** 19, 6926-6930.

33. Ni, F.; Kota, S.; Takahashi, V.; Strosberg, A. D.; Snyder, J. K., Potent inhibitors of hepatitis C core dimerization as new leads for anti-hepatitis C agents. *Bioorg. Med. Chem. Lett.* **2011,** 21, 2198-2202.

34. Arkin, M. R.; Wells, J. A., Small-molecule inhibitors of protein-protein interactions: progressing towards the dream. *Nat. Rev. Drug Discov.* **2004,** 3, 301-317.

35. Blair, W. S.; Pickford, C.; Irving, S. L.; Brown, D. G.; Anderson, M.; Bazin, R.; Cao, J.; Ciaramella, G.; Isaacson, J.; Jackson, L.; Hunt, R.; Kjerrstrom, A.; Nieman, J. A.; Patick, A. K.; Perros, M.; Scott, A. D.; Whitby, K.; Wu, H.; Butler, S. L., HIV Capsid is a Tractable Target for Small Molecule Therapeutic Intervention. *PLoS Pathog.* **2010,** 6, e1001220.

36. Liu, Z.-X.; Nishida, H.; He, J.-W.; Lai, M. M. C.; Feng, N.; Dennert, G., Hepatitis C Virus Genotype 1b Core Protein Does Not Exert Immunomodulatory Effects on Virus-Induced Cellular Immunity. *J. Virol.* **2002,** 76, 990-997.

37. Alvisi, G.; Madan, V.; Bartenschlager, R., Hepatitis c virus and host cell lipids: An intimate connection. *RNA Biol.* **2011,** 8, 258-269.

38. Chisari, F., Unscrambling hepatitis C virus-host interactions. *Nature* **2005,** 436, 930-932.

39. Su, A.; Pezacki, J.; Wodicka, L.; Brideau, A.; Supekova, L.; Thimme, R.; Wieland, S.; Bukh, J.; Purcell, R.; Schultz, P.; Chisari, F., Genomic analysis of the host response to hepatitis C virus infection. *Proc. Natl. Acad. Sci. U. S. A.* **2002,** 99, 15669-15743.

40. Lai, C.-K.; Jeng, K.-S.; Machida, K.; Lai, M., Hepatitis C virus egress and release depend on endosomal trafficking of core protein. *J. Virol.* **2010,** 84, 11590-11598.

41. Jones, D.; McLauchlan, J., Hepatitis C virus: assembly and release of virus particles. *J. Biol. Chem.* **2010,** 285, 22733-22742.

42. Perlemuter, G.; Sabile, A.; Letteron, P.; Vona, G.; Topilco, A.; Chrétien, Y.; Koike, K.; Pessayre, D.; Chapman, J.; Barba, G.; Bréchot, C., Hepatitis C virus core protein inhibits microsomal triglyceride transfer protein activity and very low density lipoprotein secretion: a model of viral-related steatosis. *FASEB J.* **2002,** 16, 185-279.

43. Syed, G.; Amako, Y.; Siddiqui, A., Hepatitis C virus hijacks host lipid metabolism. *Trends Endocrinol. Metab.* **2010,** 21, 33-73.

44. Welte, M.; Gross, S.; Postner, M.; Block, S.; Wieschaus, E. F., Developmental Regulation of Vesicle Transport in Drosophila Embryos: Forces and Kinetics. *Cell* **1998**, 92, 547-557.

45. Gross, S. P.; Guo, Y.; Martinez, J. E.; Welte, M. A., A Determinant for Directionality of Organelle Transport in Drosophila Embryos. *Curr. Biol.* **2003,** 13, 1660-1668.

46. Gross, S. P.; Welte, M. A.; Block, S. M.; Wieschaus, E. F., Coordination of opposite-polarity microtubule motors. *J. Cell Biol.* **2002,** 156, 715-724.

47. Shubeita, G. T.; Tran, S. L.; Xu, J.; Vershinin, M.; Cermelli, S.; Cotton, S. L.; Welte, M. A.; Gross, S. P., Consequences of Motor Copy Number on the Intracellular Transport of Kinesin-1-Driven Lipid Droplets. *Cell* **2008,** 135, 1098-1107.

48. Welte, M. A.; Cermelli, S.; Griner, J.; Viera, A.; Guo, Y.; Kim, D.-H.; Gindhart, J. G.; Gross, S. P., Regulation of Lipid-Droplet Transport by the Perilipin Homolog LSD2. *Curr. Biol.* **2005,** 15, 1266-1275.

49. Kunwar, A.; Tripathy, S.; Xu, J.; Mattson, M.; Anand, P.; Sigua, R.; Vershinin, M.; McKenney, R.; Yu, C.; Mogilner, A.; Gross, S., Mechanical stochastic tug-of-war models cannot explain bidirectional lipid-droplet transport. *Proc. Natl. Acad. Sci. U. S. A.* **2011,** 108, 18960-18965.

50. Kulic, I.; Brown, A.; Kim, H.; Kural, C.; Blehm, B.; Selvin, P.; Nelson, P.; Gelfand, V., The role of microtubule movement in bidirectional organelle transport. *Proc. Natl. Acad. Sci. U. S. A.* **2008,** 105, 10011-10017.

51. Kural, C.; Kim, H.; Syed, S.; Goshima, G.; Gelfand, V. I.; Selvin, P. R., Kinesin and Dynein Move a Peroxisome in Vivo: A Tug-of-War or Coordinated Movement? *Science* **2005,** 308, 1469-1472.

52. Pegoraro, A. F.; Ridsdale, A.; Moffatt, D. J.; Pezacki, J. P.; Thomas, B.; Fu, L.; Dong, L.; Fermann, M.; Stolow, A., All-fiber CARS microscopy of live cells. *Opt. Express* **2009,** 17, 20700-20706.

53. Pezacki, J. P.; Blake, J.; Danielson, D.; Kennedy, D. C.; Lyn, R. K.; Singaravelu, R., Chemical contrast for imaging living systems: molecular vibrations drive CARS microscopy. *Nat. Chem. Biol.* **2011,** 7, 137-182.

54. Burgess, S. A.; Walker, M. L.; Sakakibara, H.; Knight, P. J.; Oiwa, K., Dynein structure and power stroke. *Nature* **2003,** 421, 715-718.

55. Dodding, M.; Way, M., Coupling viruses to dynein and kinesin-1. *EMBO J* **2011,** 30, 3527-3566.

56. Suomalainen, M.; Nakano, M. Y.; Keller, S.; Boucke, K.; Stidwill, R. P.; Greber, U. F., Microtubule-dependent Plus- and Minus End-directed Motilities Are Competing Processes for Nuclear Targeting of Adenovirus. *J. Cell Biol.* **1999,** 144, 657-672.

57. Lyman, M. G.; Enquist, L. W., Herpesvirus Interactions with the Host Cytoskeleton. *J. Virol.* **2009,** 83, 2058-2066.

58. McDonald, D.; Vodicka, M. A.; Lucero, G.; Svitkina, T. M.; Borisy, G. G.; Emerman, M.; Hope, T. J., Visualization of the intracellular behavior of HIV in living cells. *J. Cell Biol.* **2002,** 159, 441-452.

59. Henry, T.; Gorvel, J.-P.; Méresse, S., Molecular motors hijacking by intracellular pathogens. *Cell. Microbiol.* **2006,** 8, 23-32.

60. Wölk, B.; Buchele, B.; Moradpour, D.; Rice, C. M., A Dynamic View of Hepatitis C Virus Replication Complexes. *J. Virol.* **2008,** 82, 10519-10531.

61. Harris, C.; Herker, E.; Farese, R. V.; Ott, M., Hepatitis C Virus Core Protein Decreases Lipid Droplet Turnover. *J. Biol. Chem.* **2011,** 286, 42615-42625.

62. White, S. H.; Wimley, W. C., Hydrophobic interactions of peptides with membrane interfaces. *Biochim. Biophys. Acta* **1998,** 1376, 339-352.

63. Engelke, M.; Burckhardt, C.; Morf, M.; Greber, U., The dynactin complex enhances the speed of microtubule-dependent motions of adenovirus both towards and away from the nucleus. *Viruses* **2011,** 3, 233-286.

64. Suomalainen, M.; Nakano, M. Y.; Boucke, K.; Keller, S.; Greber, U. F., Adenovirus-activated PKA and p38/MAPK pathways boost microtubule-mediated nuclear targeting of virus. *EMBO J* **2001,** 20, (6), 1310-1319.

65. Spaziani, A.; Alisi, A.; Sanna, D.; Balsano, C., Role of p38 MAPK and RNA-dependent Protein Kinase (PKR) in Hepatitis C Virus Core-dependent Nuclear Delocalization of Cyclin B1. *J. Biol. Chem.* **2006,** 281, 10983-10989.

66. Hayashi, J.; Aoki, H.; Kajino, K.; Moriyama, M.; Arakawa, Y.; Hino, O., Hepatitis C virus core protein activates the MAPK/ERK cascade synergistically with tumor promoter TPA, but not with epidermal growth factor or transforming growth factor α. *Hepatology* **2000,** 32, 958-961.

67. Erhardt, A.; Hassan, M.; Heintges, T.; Häussinger, D., Hepatitis C Virus Core Protein Induces Cell Proliferation and Activates ERK, JNK, and p38 MAP Kinases Together with the MAP Kinase Phosphatase MKP-1 in a HepG2 Tet-Off Cell Line. *Virology* **2002,** 292, 272-284.

68. Kang, S.-M.; Shin, M.-J.; Kim, J.-H.; Oh, J.-W., Proteomic profiling of cellular proteins interacting with the hepatitis C virus core protein. *Proteomics* **2005,** 5, 2227-2237.

69. Parent, R.; Qu, X.; Petit, M.-A.; Beretta, L., The heat shock cognate protein 70 is associated with hepatitis C virus particles and modulates virus infectivity. *Hepatology* **2009,** 49, 1798-1809.

70. Dreux, M.; Chisari, F. V., Impact of the Autophagy Machinery on Hepatitis C Virus Infection. *Viruses* **2011,** 3, 1342-1357.

71. Wileman, T., Aggresomes and Autophagy Generate Sites for Virus Replication. *Science* **2006,** 312, 875-878.

72. Wileman, T., Aggresomes and Pericentriolar Sites of Virus Assembly: Cellular Defense or Viral Design? *Ann. Rev. Microbiol.* **2007,** 61, 149-167.

73. Leopold, P. L.; Pfister, K. K., Viral Strategies for Intracellular Trafficking: Motors and Microtubules. *Traffic* **2006,** 7, 516-523.

74. Heaton, N. S.; Randall, G., Dengue Virus and Autophagy. *Viruses* **2011,** 3, 1332-1341.

75. Saka, H. A., Valdivia, Raphael H., Emerging Roles for Lipid Droplets in Immunity and Host-Pathogen Interactions. *Ann. Rev. Cell Dev. Biol.* **2012,** 28, 411-437.

76. Huang, H.; Sun, F.; Owen, D. M.; Li, W.; Chen, Y.; Gale, M.; Ye, J., Hepatitis C virus production by human hepatocytes dependent on assembly and secretion of very low-density lipoproteins. *Proc. Natl. Acad. Sci. U. S. A.* **2007,** 104, 5848-5853.

77. Shelness, G. S.; Sellers, J. A., Very-low-density lipoprotein assembly and secretion. *Curr. Opin. Lipidol.* **2001,** 12, 151-157.

78. Neveu, G.; Barouch-Bentov, R.; Ziv-Av, A.; Gerber, D.; Jacob, Y.; Einav, S., Identification and Targeting of an Interaction between a Tyrosine Motif within Hepatitis C Virus Core Protein and AP2M1 Essential for Viral Assembly. *PLoS Pathog.* **2012,** 8, e1002845.

79. Pegoraro, A. F.; Ridsdale, A.; Moffatt, D. J.; Jia, Y.; Pezacki, J. P.; Stolow, A., Optimally chirped multimodal CARS microscopy based on a single Ti:sapphire oscillator. *Opt. Express* **2009,** 17, 2984-3080.

80. Lyn, R. K.; Kennedy, D. C.; Sagan, S. M.; Blais, D. R.; Rouleau, Y.; Pegoraro, A. F.; Xie, X. S.; Stolow, A.; Pezacki, J. P., Direct imaging of the disruption of hepatitis C virus replication complexes by inhibitors of lipid metabolism. *Virology* **2009,** 394, 130-172.

5

Altered membranes at HCV replication complexes are disrupted by inhibiting stearoyl-CoA desaturase

Introduction

The current estimate for chronic HCV infections is greater than 2.35% of the global population [1]. This global health problem is conceivable more widespread because of undiagnosed infections, since acute infections are asymptomatic [2]. Chronic infection leads to liver damage, and is a leading cause of liver transplants world-wide [3, 4]. Due to its error-prone polymerase, HCV viral genomes are highly heterogeneous in sequence and this has made the development of broadly-effective vaccine quite difficult [5-8]. For these reasons, current regiments rely on direct-acting antivirals (DAAs) that must be co-administered with peg-IFN and RBV, both of which are designated as standard of care treatments [9]. The first generation of DAA HCV protease inhibitors represent potent therapeutics that have improved sustained virologic response rates from approximately 50 to 70-75% [10, 11]. However, it is only effective in one of six genotypes (genotype 1) and its harsh side effects are added to those that are already experienced from standard of care treatments [8, 10-12]. As a

result, many patients are unable to tolerate the treatment, promoting antiviral resistant genomes [8, 12]. An alternative strategy is to target viral-dependent host interactions critical for HCV pathogenesis [8, 12-14].

An expanding list of identified HCV host-virus interactions can be exploited by using known inhibitors that target host cell factors [8, 12, 13]. An example that is currently in clinical development is that of cyclophilin, a member of a family of cellular peptidyl-prolyl cis-trans isomerases that acts as an interacting partner with HCV non-structural proteins, NS5A and NS5B polymerase [15-19]. The advantage of identifying host targets allows broader effects across all HCV genotypes and increases the barrier to drug resistance [8]. Therapeutically, the goal has been to eliminate the dependency for peg-IFN and RBV and develop a strategy to minimize the development of drug resistant genomes [8, 13]. Along this strategy, metabolic pathways involved in supplementing lipid substrates required to develop viral compartments and viral associated interacting host partners for HCV, represent viable targets [20].

The liver is one of the main organs regulating human lipid homeostasis. Interestingly, every step of the HCV life cycle involves interactions with host lipids – partially attributing for the hepatic tropism exhibited by the virus [21-24]. HCV is capable of diverting host metabolic pathways for up-regulating lipogenesis [25-27]. For example, part of this increase in lipogenesis is to increase host protein lipidation required for competent viral replication in genotype 1, and are also direct substrates for lipid-rich LD organelles, giving rise to larger LDs [28-31].

The lipid signature of ER membranes is also altered by the virus to induce formation of membranous structures that support viral replication [32-34]. This is often observed for positive-stranded RNA viruses [34]. The altered membrane structures that topologically form platforms are initially generated by viral hijacking of host-ER membranes [35-38]. The result is a phenotypic modification of the ER, including interconnected membranous webs that contain multiple invaginated piths, each of which can house an individual replication complex [34, 39, 40]. These piths enable HCV RNA to hide from endogenous host defenses, as its opening is largely surrounded by a LD bound to HCV core

protein, which can block access [34, 41-43]. Furthermore, the high radii of curvature allows for the concentration of viral components and host lipids required for replication [34, 44, 45]. The mechanisms by which high radii of curvature is formed, however, remains unknown. On the molecular level, current models suggest that these complexes conceptually resemble inverted piths that protrude towards the ER lumen with a topology that is consistent with negatively curved membranes [46, 47]. Furthermore, these complexes that contain functional replicating viral RNA, are nuclease resistant and are formed in abundance and are tightly surrounded by large LDs, which provide that necessary LD-associated environment [41, 48, 49]. Electron microscopy has revealed that these aggregated complexes form a membranous web and that the altered membranes are classical signatures of HCV viral infection [34, 38].

The dynamic processes by which HCV is able to control the intracellular environment to build membrane-induced microenvironments is extremely unique. Membrane curvature in dynamic phospholipid bilayers can be altered through different fatty acids embedded in the membrane. Bending the membrane requires energy and fatty acids have been shown to affect the packing of phospholipid fatty-acyl chains, inducing either positive or negative curvature, depending on the structure of the lipid and fatty acid head group [50, 51]. It was reported that oleic acid is required to augment membrane fluidity in physiologically relevant phospholipid membrane bilayers, and also enable negative curvature [52]. As such, we examined the effects of oleic acid and its involvement in viral-induced negatively curved membranes.

Oleic acid, in the form of oleate, is obtained from dietary sources, but is also available through *de novo* biosynthesis. A key enzyme in this biosynthesis is stearoyl-CoA desaturase (SCD) [53]. In humans, SCD-1 is highly expressed in the liver, while the other isoform, SCD-5 is primarily expressed in the brain and pancreas [53, 54]. The biochemistry of SCD has been well characterized in mice and humans, which share significant similarity, particularly in SCD-1 [53]. SCD introduces a cis double bond in a highly specific manner at the Δ9 position, with greater selectivity for palmitoyl- and stearoyl-CoA, amongst long-chain acyl-CoAs [53]. The monounsaturated fatty acid (MUFA) products generated by SCD-1 enzymatic activity, are shuttled as substrates for the synthesis of membrane

phospholipid fatty-acyl chains, triglyceride biogenesis, and cholesterol esterification [46, 50, 55]. In support of this, SCD-1 activity is located at the vicinity of Diacyl glycerol acyltransferase (DGAT) and glycerol 3-phosphate acyltransferase (GPAT) enzymes, likely to concentrate available MUFAs [54]. The former enzyme is involved in triglyceride biosynthesis and the latter is involved cholesterol esters biosynthesis [54]. Furthermore, studies investigating triglyceride and very-low density lipoprotein content in SCD-1 knockout mice, were significantly lowered [56]. Also, esterification of cholesterol, which is a neutral lipid and component of LDs, is also upregulated upon transfecting SCD-1 gene in Chinese hamster ovary cells [57]. It is possible that because the depletion of monounsaturated fatty acids raises the ratio levels of saturated fatty acids (SFAs), this abundance can reduce levels of malonyl-CoA and can also disrupt phospholipid membrane properties [58]. Given the key role that SCD-1 plays in membranes that are altered by the virus, we wished to investigate its role in HCV pathogenesis.

In this study we examined SCD-1's role in HCV propagation and membrane alteration. We show that SCD-1 is pro-viral for HCV. SCD-1 also inhibits HCV replication. Inhibition of HCV is not due to limiting hepatic LDs required for HCV replication, but because it disrupts the HCV-induced alterations in membranes, which disrupt nuclease-resistant HCV replication complexes.

Hypothesis

Efficient HCV replication requires the presence of unsaturated fatty acid, such as oleic acid, in the ER phospholipid membranes that enable curvature for dynamic remodeling to induce HCV-altered membranes required for the HCV replication complex.

Results

SCD-1 inhibition disrupts HCV replication

The processes involved in HCV replication and assembly are highly dependant on host lipids. For this reason, targeting enzymes involved in lipid biogenesis is a therapeutic target for inhibiting HCV. A variety of small molecule inhibitors have been used to show that inhibiting lipogenesis negatively affects HCV replication [27]. We sought to inhibit the SCD-1 enzyme, since it has been shown to be upregulated in HCV and has a crucial role in MUFA synthesis [59]. Unsaturated fatty acids (UFAs) are embedded within the ER lumen membranes, and are incorporated as fatty-acyl chains for phospholipid and triglyceride biogenesis [46, 53]. To determine whether HCV replication is dependent on SCD-1 activity, we treated human hepatoma cells (Huh-7) stably expressing an HCV replicon with different concentrations of compound L-001783231-000N that has previously been shown to inhibit SCD-1 (Fig. 5.1 A&B) [60]. We measured the HCV RNA levels by qRTPCR after 96 hr treatments with the SCD-1 inhibitor and found a dramatic reduction in viral RNA levels in a dose-dependent manner (Fig. 5.1C). The EC_{50} level of inhibition was determined to be 62nM, and toxicity was absent at all concentrations tested (Appendix 5.1). These results suggest that SCD-1 is required for HCV replication.

SCD-1 inhibitor mediated repression of HCV replication is independent of changes in hepatic LD phenotype

Neutral lipids that combine triglycerides along with cholesterol esters of the mevalonate pathway are the major components of LD storage organelles [61]. Because MUFAs such as oleic acid are highly incorporated into triglycerides, it is conceivable that there will be a reduction in

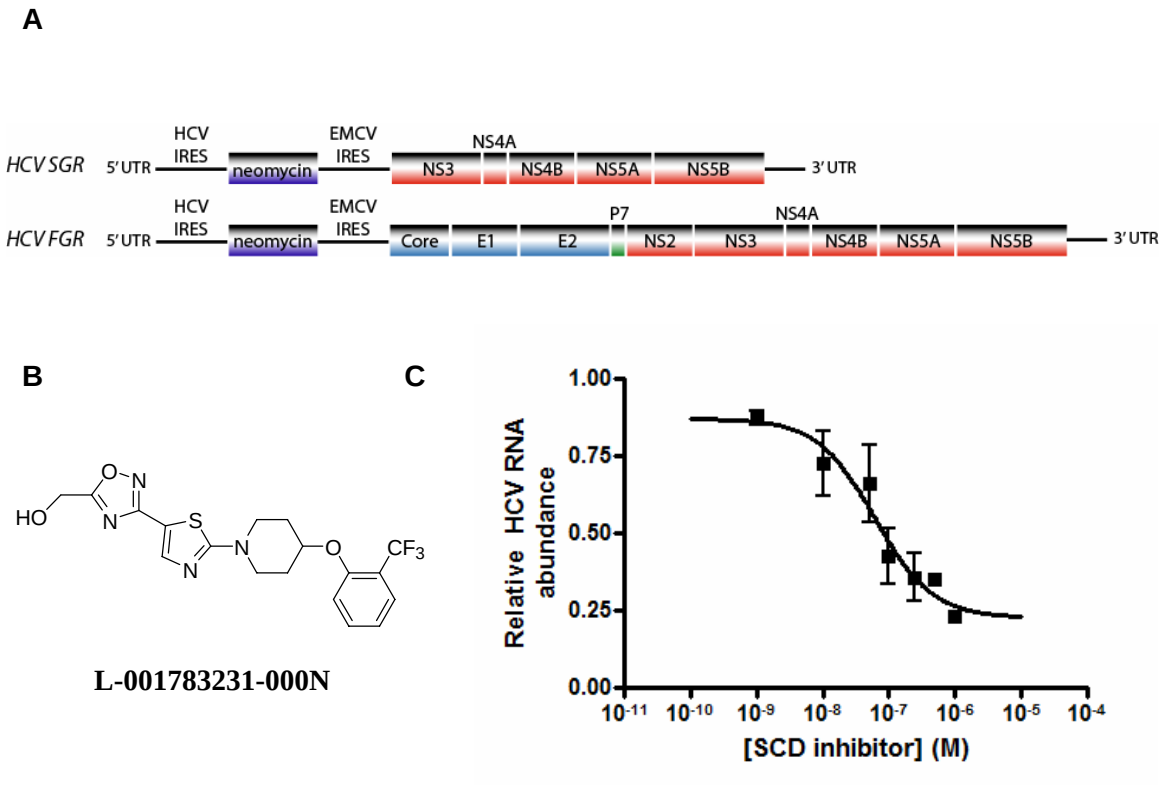

Figure 5.1: SCD-1 enzymatic activity is important for HCV replication. (A) Huh-7 cells stably expressing an HCV subgenomic replicon (SGR, genotype 1a) or Huh-7.5 cells stably expressing a full-length genomic replicon (FGR, genotype 1b) contain two internal ribosomal entry sites (IRES) that encode for HCV non-structural proteins, NS3-NS5B, along with a geneticin gene for stable replication were treated with various concentrations of an (B) SCD-1 thiazole analogue inhibitor. (C) Quantitative real-time PCR (qRTPCR) demonstrates a decrease in HCV RNA levels induced by inhibiting SCD-1 in a dose-dependent manner. All treatments including the mock contained an equal amount of DMSO. The error bars represent the standard error of the mean for three independent trials (n>3).

storage of these neutral lipids in LDs upon SCD-1 inhibition [53]. To investigate how inhibiting SCD-1 may affect the LD phenotype, we treated human hepatoma cells stably expressing an HCV subgenomic replicon with the SCD-1 inhibitor at concentrations ranging from 1 nM to 1 μM. Analogous treatments were performed in human hepatoma cells not expressing HCV, a cell line whose hepatic lipid content is highly responsive to modulation of lipid metabolic pathways [62, 63]. We then performed cellular imaging using coherent anti-Stokes Raman scattering (CARS) microscopy, a label-free method for LD detection that provides a method to monitor changes in LDs without perturbing the sample with chemical staining [64, 65]. The vibrational signal is resonantly enhanced when CARS tunes into inherent natural vibrations of C-H stretches abundantly compacted in LDs [64, 66]. Using CARS we detected a small change in LD density when Huh-7 cells stably expressing an HCV subgenomic replicon was treated with concentrations above 100nM with the SCD-1 inhibitor. We measured this by voxel analysis, which quantifies lipid volumes from the threshold CARS signal specific for LDs [62, 63]. By contrast, the LD phenotype and density, in comparison to the mock treatment, were observed to be at same level in SCD-1 inhibitor treated cells below the concentration of 100nM. Interestingly, at the concentration required for the EC_{50} level of HCV inhibition, we noticed no differences in LD phenotype and LD densities. As expected, the LD phenotype for Huh-7 cells not expressing HCV showed the same pattern. This indicates that there is no appreciable reduction in LD size or density, at concentrations of SCD-1 inhibitor required for significant HCV inhibition. We did observe a measurable decrease in the abundance of LDs at higher SCD-1 inhibitor concentrations (Fig. 5.2 A-D).

To determine if the effects observed by CARS was specific to SCD-1 inhibition, we further evaluated the changes in LDs in the presence of an HCV protease inhibitor, MK-4519, that targets NS3 protease without any known effects on cellular lipid metabolism (Fig. 5.3) [67]. We tested this hypothesis by using Huh-7.5 cells stably expressing a full-length HCV replicon and treated them for 96 hours with NS3 protease inhibitor, MK-4519 (Fig. 5.3 A). Besides the dose in drug concentrations used, the treatment procedure and length of time are similar to those of cells treated with the SCD-1

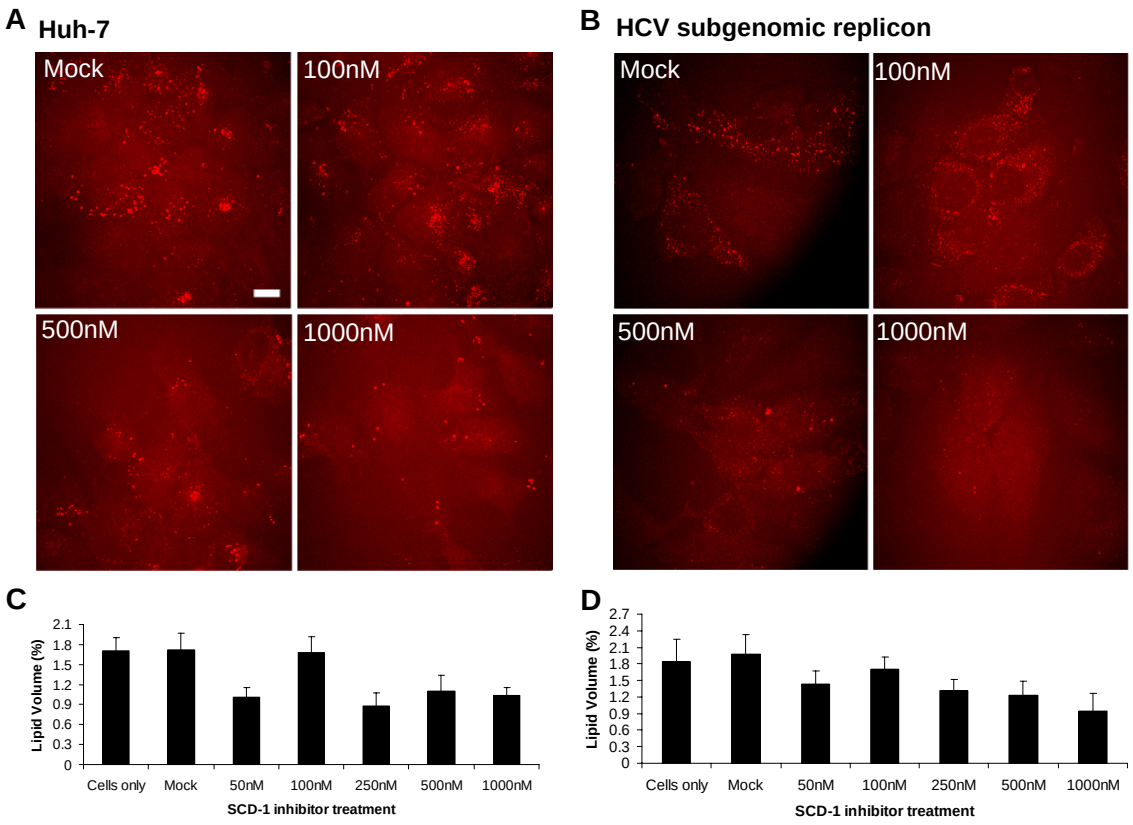

Figure 5.2: Characterizing the LD phenotype with SCD-1 inhibitor treatment. (A) Huh-7 cells only and (B) Huh-7 cells stably expressing an HCV replicon were treated with concentrations: 100nM, 500nM, and 1000nM and non-treated (mock) of the SCD-1 inhibitor and imaged by CARS microscopy. These are representative images for each of the concentrations used and the experiment was repeated twice (n=2). The LD density was measured by voxel analysis for multiple cells (n, represents the number of cells measured for LD density) under different field of views for each concentration when (C) Huh-7 cells (n>25 for all concentrations) and (D) Huh-7 cells stably expressing an HCV subgenomic replicon (n>25 for all concentrations) were treated with the various concentrations of the SCD-1 inhibitor. The bar graphs illustrate the average of the number of cells measured by voxel analysis with error bars representing the standard error of the mean. Scale bar = 10μm.

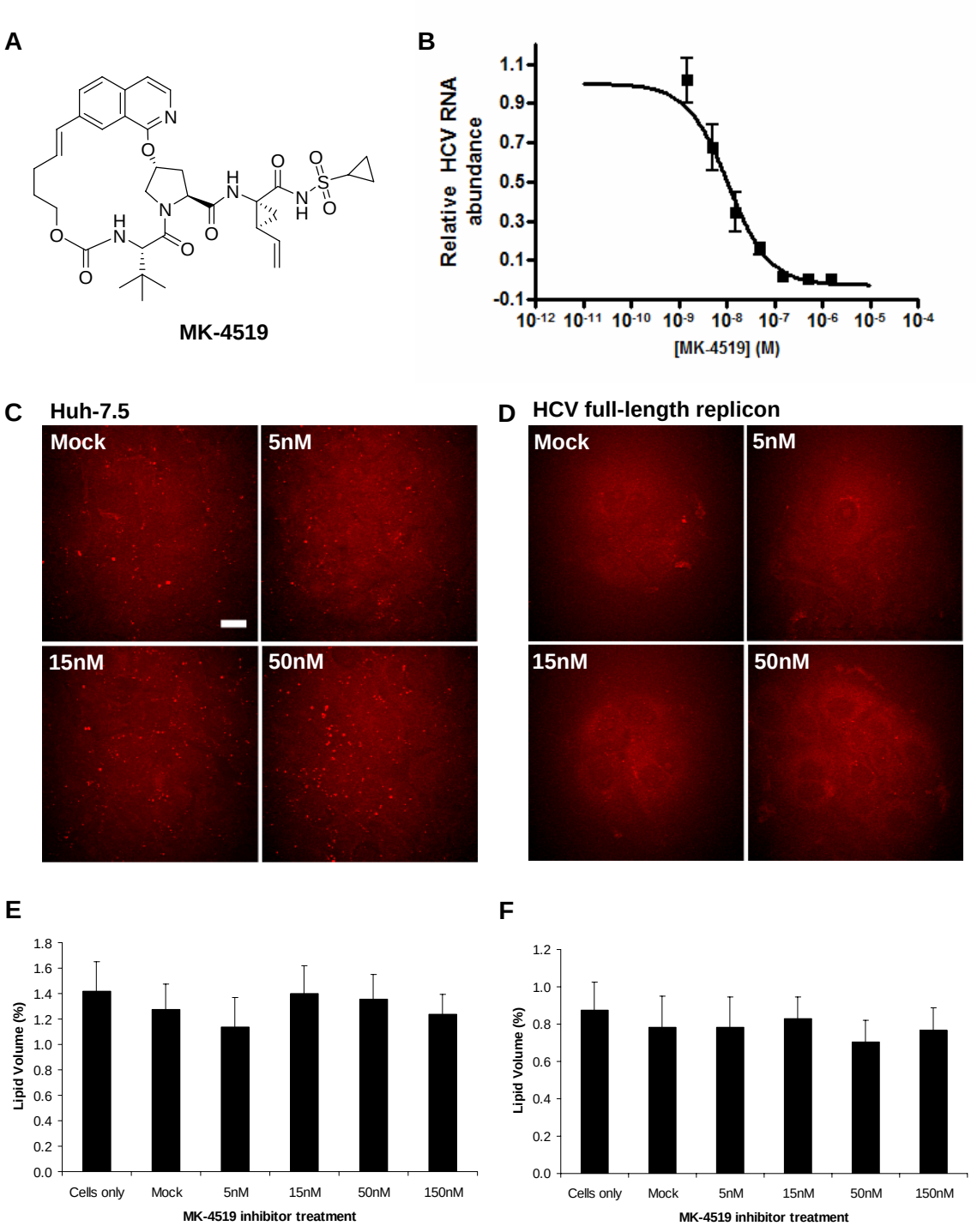

Figure 5.3: Characterizing the effects of HCV inhibition and LD phenotype with MK-4519, NS3 inhibitor treatment. (A) Chemical structure of MK-4519 (B) Inhibition of HCV RNA was assessed by qRTPCR of Huh-7.5 cells stably expressing full-length HCV genomic replicon cells treated with

various concentrations of MK-4519 (C) Huh-7.5 cells only and (D) Huh-7.5 cells stably expressing full-length HCV replicon were treated with concentrations: 50nM, 15nM, and 5nM and non-treated (mock) of the MK-4519 and imaged by CARS microscopy. These are representative images for each of the concentrations used and the experiment was repeated twice (n=2). The LD density was measured by voxel analysis for multiple cells (n, represents the number of cells measured for LD density) under different field of views for each concentration when (E) Huh-7.5 cells (n>25 for all concentrations) and (F) Huh-7.5 cells stably expressing full-length HCV replicon (n>25 for all concentrations) were treated with the various concentrations of MK-4519. The bar graphs illustrate the average of the number of cells measured by voxel analysis with error bars representing the standard error of the mean. Scale bar = 10μm.

inhibitor. As expected, treatment with MK-4519 showed a dose-dependent effect in viral replication. The EC_{50} with MK-4519 was found to be 8.26 nM, respectively (Fig. 5.3 B) [73]. Although this value was higher than 1.8 nM, reported by Brown *et al.*, these in vitro studies can observe a slight offset that is dependent on the cell lines used. Upon MK-4519 treatment, CARS demonstrated that no changes in LD phenotype were observed across all concentrations, and quantitative voxel analysis indicated that the density of LDs was similar across all concentrations (Fig. 5.3 C-F).

Dispersion of ds-HCV RNA is observed upon inhibiting HCV

Our CARS imaging data suggest that SCD-1 inhibitor-mediated repression of HCV occurs prior to any effect on LDs. This indicates that a different mechanism may be at play for SCD-1 inhibitor mediated repression of HCV. We postulated that the pharmacological blockade of SCD-1 would result in a change to membrane fluidity or the curvature required for functional HCV replication complexes. To determine whether the antiviral effects of inhibiting SCD-1 is affecting replication complexes, we assessed the cellular localization of ds-HCV RNA intermediates [62]. Because RNA replication is mediated by transcribing a negative strand that acts as a template, ds-HCV RNA intermediates are formed on active replication complexes. We visualized these intermediates using an antibody specific for dsRNA, as previously described in chapter 2.

We began by treating Huh-7 cells stably expressing an HCV subgenomic replicon with SCD-1 inhibitor at varying concentrations between 100nM and 1000nM (Fig. 5.4 C&D). Molecular imaging by confocal microscopy revealed that in untreated cells, ds-HCV RNA exhibits a punctate staining pattern within the cytoplasmic space of the cell (Fig. 5.4 A). Under mock treatment, a similar punctate pattern was also observed, as expected (Fig. 5.4 B). However, by adding 100nM and 1000nM of SCD-1 inhibitor, we detected the dispersion pattern of ds-RNA intermediates that are

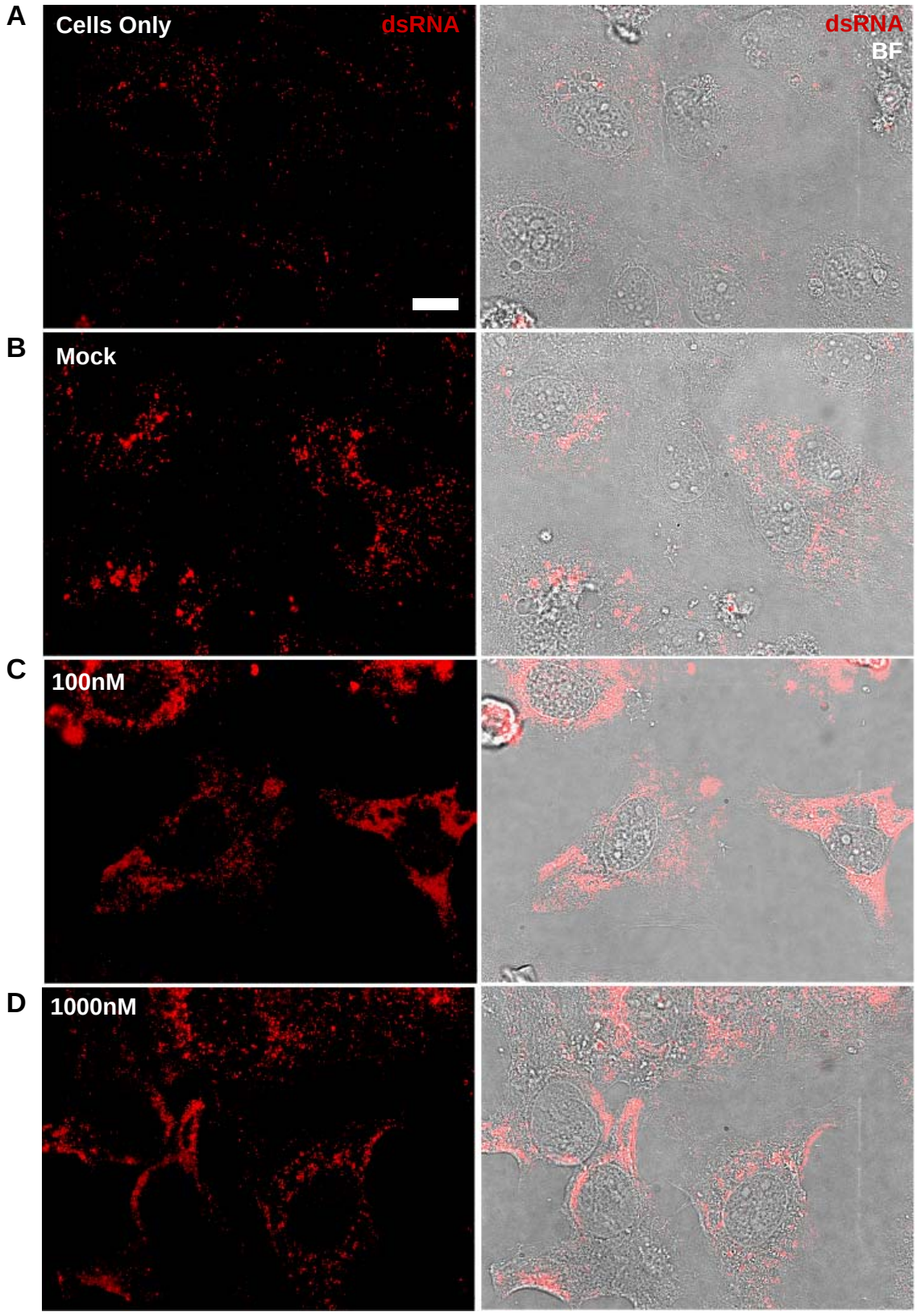
A
Cells Only
dsRNA
dsRNA
BF
B
Mock
C
100nM
D
1000nM

Figure 5.4: Imaging changes in ds-HCV RNA localization when treated with the SCD-1 inhibitor. Ds-HCV RNA intermediates using J2 antibody were detected by immunofluorescence in cells stably expressing an HCV subgenomic replicon. Bright field images are also included to show distinct nuclei regions of the cells. Control samples, (A) cells only and (B) mock, which contains the same volume of DMSO added at the highest concentration of the SCD-1 inhibitor inhibitor treatment, showed high levels of punctate staining throughout the cell but with higher concentrations in the perinuclear region. The SCD-1 inhibitor treatments at (C) 100nM and at (D) 1000nM showed a more diffuse pattern suggesting that these dsRNA-intermediates are not localized in the functional replication complexes as a result of dispersion away from these complexes. Scale bar = 10μm.

consistent with its escape from the viral replication complexes. We reasoned that the exclusion of ds-HCV RNA from these replication complexes has caused the down-regulation of HCV replication as they are no longer associated with host and viral proteins that mediate replication, as previously reported [62]. Notably, the dispersion was evident at the 100nM concentration (Fig. 5.4 C) where we did not observe a change in the LDs. This further supports that the observed antiviral activity of the SCD-1 inhibitor is independent of the drug's effects in modulating LD storage. Overall, our data suggests that inhibiting SCD-1 may decrease HCV replication by potentially disrupting the replicase complex ultimately inhibiting HCV replication.

RNA protection assay shows that inhibiting SCD-1 exposes viral replication complexes to nucleases

Given that our results suggest that the antiviral effect of the SCD-1 inhibitor correlated with a dispersion of HCV replication complexes, we sought to identify the molecular mechanism by which SCD-1 inhibition induces this ds-HCV RNA dispersion. We hypothesized that this dispersion is mediated by the opening of replication complexes due to a depletion of intracellular MUFAs. Previous studies had demonstrated that the HCV RNA in replication complexes are nuclease resistant [48]. On the molecular level, the membranes reflect high curvature radii that enable vesicle-like formation. We hypothesize that the replication complexes require high curvature radii induced by oleic acid derived of phospholipids that give rise to the detergent and nuclease resistant properties, as previously reported [41, 48, 49]. Therefore inhibiting SCD-1 may modulate the topology of these replication complexes by decreasing the amount of oleic acid available to incorporation into the membranes. This would prevent curvature, rendering HCV RNA susceptible to endogenous nucleases that are employed by the cell as a cellular defense mechanism (Fig. 5.5 A).

To examine this possibility, we performed a previously described *in situ* RNase protection assay (RPA) to analyze the susceptibility of HCV RNA to degradation by exogenous nucleases [41, 48].

Miyanari *et al.* had previously shown in the presence of a detergent which permeabilizes the cell membrane (digitonin) and exogenous nucleases, HCV RNA in replication complexes remains intact [41, 48]. However, upon disruption of the ER membrane integrity using an additional non-ionic detergent (NP-40), HCV RNA became susceptible to nuclease-mediated degradation. We hypothesized that SCD-1 inhibition would act in a similar fashion as NP-40, disrupting the structural integrity of HCV replication complexes. To assess this, we performed semi-quantitative PCR for HCV RNA levels followed by densitometry to quantify the magnitudes of HCV RNA degradation after probing for nuclease accessibility to HCV RNA. The RPA was performed during mock (Fig. 5.5 B, lanes 1-6) and SCD-1 inhibitor (Fig. 5.5 B, lanes 7-11) treatments to examine the influence of SCD-1 on the nuclease and detergent resistant properties of viral RNA at replication complexes (Fig. 5.5). Cells were treated with 500nM of the SCD-1 inhibitor (Fig. 5.1 C & Fig. 5.5 B) to ensure that we see an approximate 50% decrease in HCV RNA levels for comparability purposes.

An integrity gel probing for 28S and 18S rRNA was also conducted as a control. These ribosomal RNAs are susceptible to degradation by cytoplasmic nucleases, and their degradation is a positive control for both cell membrane permeabilization and nuclease activity (Fig. 5.5 B). As expected, in treatments containing both nuclease and digitonin, 28S and 18S rRNA are readily degraded (Fig. 5.5 B, Lanes 3 & 9). In the absence of digitonin, the nuclease fails to enter the cytoplasm, and as expected, no degradation is observed (Fig. 5.5 B, lane 6). Additionally, when Np-40 was added in the absence of nuclease and digitonin, ribosomal RNAs remained intact (Fig. 5.5 B, lanes 4 & 10). SCD-1 inhibition alone has no effect on the integrity of ribosomal RNA bands (Fig. 5.5 B, lane 7).

Looking at HCV RNA levels, as expected, SCD-1 treatment results in an overall decrease in HCV levels that are independent of detergent and nuclease treatment (compare Fig. 5.5 B, lanes 1-6 to 7-11). Interestingly, we observed that the treatment of digitonin plus nuclease for SCD-1 inhibitor treated cells (Fig. 5.5 B, lane 9) produced HCV RNA levels that are similar to those observed by the

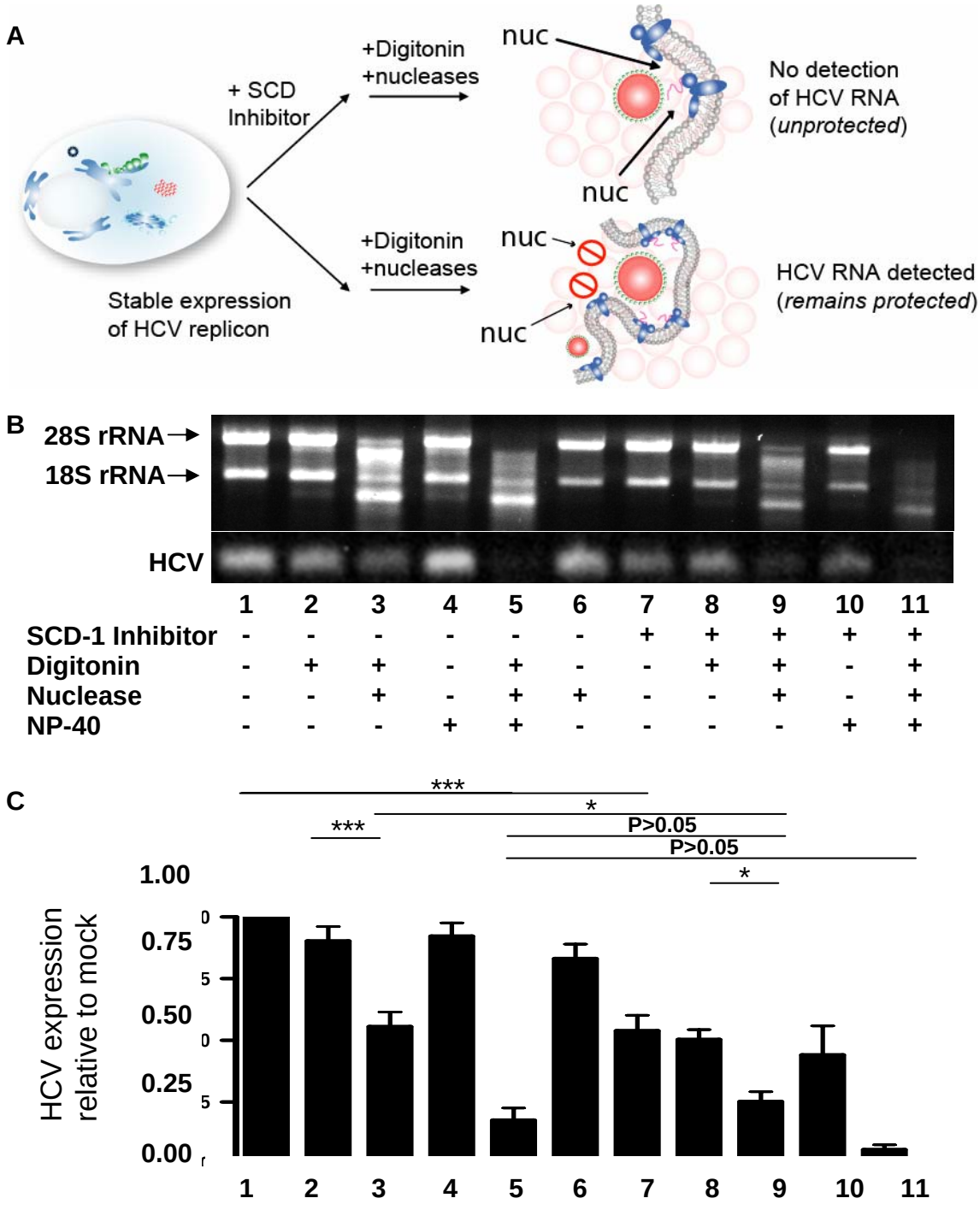

Figure 5.5: Measuring HCV RNA susceptibility to exogenously added nuclease after inhibiting SCD-1. (A) Schematic demonstrating hypothesized mechanistic membrane disruptions by inhibiting SCD-1, which may alter HCV RNA's susceptibility to nucleases as visualized for mock and SCD-1 inhibitor treated cells. (B) Huh-7 cells stably expressing an HCV subgenomic replicon are treated with mock (Lanes 1-6) and SCD-1 inhibitor (Lanes 7-11) at 500 nM for 96 hours. A representative

integrity gel for one trial illustrates detectable 18S and 28S ribosomal RNA after RPA treatments. Degradation to 18S and 28S is observed only upon permeabilizing the plasma membrane with digitonin, and treated by nuclease with or without np-40 (Lanes 3,5,9,11). The HCV RNA protection assay included the addition of digitonin (Lanes 2,3,5,8,9,11), nuclease (Lanes 3,5,6,9,11), NP-40 (Lanes 4,5,10,11). A representative amplification of HCV RNA by semi-quantitative PCR illustrates the relative levels that were affected by inhibiting SCD-1 (C) 5 trials of the semi-quantitative PCR detecting HCV RNA was averaged using densitometry by the signal band intensity using HCV without any treatment as the baseline (Lane 1).

addition of all three RPA treatments for the mock (Fig. 5.5 B, lane 5). This suggests that the SCD-1 inhibitor disrupts the structural integrity of HCV replication complexes quite similarly to NP-40, which allows exogenous nucleases access to HCV RNA. While nuclease treatment does decrease HCV RNA levels in mock plus digitonin treated cells, consistent with previous reports, this decrease is greater in SCD-1 inhibitor treated cells (Fig. 5.5 B, lane 9 & 8 vs. lane 3 & 2). For SCD-1 inhibitor treated cells, the HCV RNA levels for digitonin plus nucleases showed an approximate 50.7% reduction in HCV RNA (Fig. 5.5 B, lane 8 vs lane 9; Appendix 5.2 C). By contrast, for mock treated cells, we see a smaller change corresponding to a 39% decrease in HCV RNA levels, respectively (Fig. 5.5 B, lane 2 vs 3; Appendix 5.2 C). This further supports the notion that SCD-1 inhibitor treated HCV replicon containing cells are more susceptible to nucleases where SCD-1 inhibitor treatment allows nuclease access into the replication complexes to degrade HCV RNA to a greater extent than mock treated cells. After repeating the nuclease protection assay (N=5), we observed that HCV RNA levels in digitonin plus nuclease treatments for SCD-1 inhibitor treated HCV replicon containing cells showed no statistically significant difference in comparison to digitonin, nuclease, and NP-40 treatment in mock treated cells, which further confirms the hypothesis that the inhibitory effects of SCD-1 mimic NP-40 treatment in disrupting the protective environment of the membranous webs (Fig. 5.5 C & Appendix 5.2). As expected, no significant degradation of HCV RNA was observed in cells treated with digitonin only (Fig. 5.5 B, lane 1), NP-40 only (Fig. 5.5 B, lane 4), and nuclease only (Fig. 5.5 B, lane 6), in both mock and SCD-1 inhibitor (Fig. 5.5 B, lanes 8 & 10) treated groups. Ultimately, the RPA demonstrates that SCD-1 inhibition induces a change in the nuclease resistant replication complexes, which then become accessible to endogenous or exogenous nucleases added.

Discussion

Viral induced membrane rearrangements that became sites of viral replication are common for positive-strand RNA viruses and typically occur at the rough ER in surrounding perinuclear regions [34, 38, 42, 47]. Within the *Flaviviridae* family, double membrane vesicles with a size of approximately 50-400nm are induced by Kunjin and Dengue virus, with the former capable of additionally inducing convoluted and paracrystalline arrayed structures [35, 68]. On the other hand, HCV's induced membrane alterations are represented by multi-vesicular bodies tightly confined in a web-like structure, described as the membranous web [37, 38]. To support these membrane alterations there are a number of induced changes in the membrane composition [47, 69]. For membranes to adopt a curved geometry, a common mechanism involves asymmetric organization of phospholipids [46, 69, 70]. The topology of curved membranes are determined, in part, by the natural geometry of phospholipids and factors that affect membrane fluidity due to the composition of unsaturated fatty-acyl chains incorporated into these phospholipids. For example, when considering the size of the phospholipid, the relative cross-section between the hydrophilic head group and hydrophobic tail can dictate spontaneous curvature [70, 71]. Smaller head groups and larger hydrophobic tails render a conical shape, such as phosphatidylethanolamine (PtdEtn), and increases the potential for negative curvature when tightly packed with phosphatidylcholine (PtdCho), which exhibits a more cylindrical geometric shape that has a tendency to form a planar bilayer [46, 47, 70, 71]. Also, integral membrane proteins and amphipathic proteins that can wedge themselves between the phospholipids, and with a high degree of penetration, can add structural curvature in the membrane [47, 72]. Moreover, highly structured membrane proteins can interact with one facial side of the membrane that covers a large surface area and can facilitate membrane curvature [73]. A combination of these mechanisms likely accommodates viral-induced membrane alterations that are used by HCV as sites for viral replication. These sites contain highly curved membranes that require additional factors for inducing curvature.

It was reported that fatty acids, specifically MUFAs and SFAs are required for HCV replication [27]. Modulation in the abundance of intracellular lipids is observed under HCV infection by upregulated multiple enzymatic metabolic processes involved in lipid biosynthesis [25, 26]. Such host factors in lipogenesis include FAS, SREBP, and SCD-1 [59, 74, 75]. In this study, we used a highly specific inhibitor of SCD-1, compound L-001783231-000N, that would limit the production of oleic acid in Huh-7 cells stably expressing an HCV subgenomic replicon (Fig. 5.1 B). Our study demonstrates that inhibiting SCD-1 displays potent nanomolar inhibition of HCV replication. This identifies a crucial role for SCD-1 enzymatic activity in HCV replication.

We wished to delineate the mechanism by which SCD-1 inhibition negatively modulated HCV RNA levels. Given SCD-1's crucial role in lipogenesis, one possibility was that SCD-1 inhibition decreased cellular lipid content, in this case unsaturated lipids, which has previously been shown to be an effective strategy in combating HCV [25, 27, 30]. We used CARS microscopy to monitor lipid content and localization, and the effects of the SCD-1 inhibitor on *de novo* LD biosynthesis, and homeostasis in human hepatocytes [65, 66]. Furthermore, CARS can measure and quantitatively assess the number and density of cytoplasmic LDs [62, 63, 65]. We showed that HCV replication is inhibited upon treatment with an inhibitor of SCD-1 (Fig. 5.1 B-C). By using CARS microscopy, we sought to correlate the inhibition of HCV RNA replication with SCD-1 inhibitor treated cells directly with changes in LD phenotype (Fig. 5.2). We expected to observe significant changes in hepatic LD content at inhibitory concentrations of the SCD-1 inhibitor, as observed in SCD knockout mice [76]. However, only high concentrations of the SCD-1 inhibitor resulted in a change in LD phenotype (Fig. 5.2). SCD-1 inhibition modulated hepatic lipid content only at high concentration, and this observation was shown to be specific for the SCD-1 inhibitor, by using an NS3 viral protease inhibitor, MK-4519, which did not induce changes in LD phenotype, but did inhibit the virus (Fig. 5.3). Because oleoyl-CoA is incorporated in fatty acyl chains that are ultimately stored in LDs, the antiviral activity by inhibiting SCD-1 may, in part, be due to global altered regulation of triglyceride levels found in LDs. However, we show that this is not the dominant mechanism. Rather, the CARS

microscopy data suggests that, in SCD-1 inhibitor treated cells, LDs are not changing at the concentration that inhibit HCV, suggesting that it is possible that an alternative mechanism exists that consequently disrupts viral replication through membrane alterations by SCD-1 inhibition.

We considered the possibility that HCV induced SCD-1 activity augments membrane fluidity and/or induces the synthesis of lipids required to form modified membranes. SCD-1 inhibition might ultimately disrupt these membrane alterations, thus exposing HCV RNA to cellular defenses. This idea is consistent with our observations that showed the dispersion of ds-HCV RNA intermediates (Fig. 5.4). Our results further suggest that replication complexes may require desaturase activity for the formation of oleoyl-CoA in order to maintain negative membrane curvature. Oleic acid has been shown to spontaneously induce negative curvature in PtdEth, which comprise a major phospholipid at the ER membrane in mammalian cells [52]. The cis bond at Δ9 position of C:18:1 oleic acid was shown to be highly important for negative membrane curvature while congeners of other C:18 fatty acids such as elaidic (trans C:18:1) and stearic acid (C18:0) did not induce the same effects [52]. The involvement of oleic acid in facilitating highly curved ER membranes in HCV replication was assessed by an *in situ* RNase protection assay which probed the susceptibility of HCV RNA to exogenous mediated nuclease degradation (Fig. 5.5). If HCV RNA replication complexes had no structural dependency for oleic acid, then exogenously added nucleases would remain impermeable to sites of replicating HCV RNA, consistent with intact naïve nuclease resistant replication complexes in HCV infection, as shown by Miyanari *et al* [48]. Alternatively, if depletion of oleic acid by SCD-1 inhibition modifies the membrane environment and disrupts negative curvature, exogenously added nucleases would be capable of degrading HCV RNA. In our findings, the HCV RNA that is normally resistant to nuclease treatment becomes susceptible to nuclease degradation upon treatment with the SCD-1 inhibitor (Fig. 5.5 C, lane 9). We observed that exogenous nucleases in permeabilized cells showed slight degradation of HCV without SCD-1 inhibitor treatments and this is consistent with a study by Miyanari *et al.* (Fig. 5.5 C, lane 3) [41]. This is expected considering that replicating HCV RNA is not exclusively located at replication complexes tightly linked at LD-

associated membranes. However, in the presence of the SCD-1 inhibitor, exogenous nucleases were able to penetrate and degrade HCV RNA, consistent with a viral dependence on oleic acid that is likely incorporated in phospholipids at the replication complexes (Fig. 5.5 C).

The requirement of oleic acid for viral replication was similarly demonstrated for the Brome mosaic virus and Poliovirus [44, 77]. Brome mosaic virus required five times more supplementation of UFAs for normal growth in SCD mutant deficient yeast, suggesting that UFA levels are required at the site of replication to form stabilized replicase complexes [44]. Furthermore, SCD $^{-/-}$ mice expressing the brome mosaic virus showed that replication was significantly hampered at the early stages of replication [44]. The authors were unable to observe negative-strand RNA, which is required as a template for viral RNA synthesis, suggesting that membranes required to properly shape the curvature of viral replication complexes were disrupted by the absence of UFAs [44, 45, 78]. These findings support SCD's role in maintaining membranes at viral replication complexes.

The requirement for oleic acid during HCV infection at altered membranes and membranous webs is further supported by expression of metabolic genes induced by the viral protein, NS4B, whose expression is sufficient to induce membranous webs [38]. Interestingly, NS4B expression in Huh-7 cells has been shown to enhance the expression of sterol regulatory element binding proteins (master regulator of lipid metabolism, SREBP) that induce lipogenesis by up-regulating fatty-acid synthase and SCD-1 expression [75]. We have showed that SCD-1 activity is required for the structural modulation of curved membranes that support HCV RNA replication. Other lipids are likely involved in aiding the formation of the proper membrane environment for competent viral replication, however. For example, membrane lipids, phosphatidylinositol-4-phosphate (PI4P), which requires the activity of PI4KIIIα kinase, has been shown to be up-regulated and localized in HCV replication compartments [33, 79]. The current model suggests that NS5A is required to activate PI4PIIIα to increase PI4P levels, for physical incorporation amongst the phospholipids at the replication complexes [33]. Furthermore, sphingolipids have been shown to play an important role for maintaining the integrity of

the replication complexes [32, 80]. Here we show that SCD-1 products such as oleic acid are also required.

While cis-double bonds in membranes are required for membrane fluidity, it is possible that a depletion of MUFAs will increase available SFAs at the membranes and may disrupt viral or host protein-protein interactions involved in replication [81-83]. Increasing membrane fluidity may enable the propensity for membranes to curve, however, polyunsaturated fatty acids exhibit an opposite effect by interfering with membrane fluidity which has shown to disrupt HCV replication [27, 50, 84]. Because we show that SCD-1 activity is required for HCV replication, inhibiting SCD-1 will deplete MUFAS, and may increase the availability of SFAs or polyunsaturated fatty acids that disrupt HCV.

In this study, we have shown that inhibiting SCD-1 decreases HCV RNA replication. This is most likely caused by altering the membrane environment at replication complexes. We demonstrate that SCD-1 inhibition increases the susceptibility of HCV RNA to exogenous nucleases in permeabilized cells suggesting that SCD-1 inhibition may be disrupting oleic acid-induced negative membrane curvature. Inhibition of SCD-1 represents a novel strategy for the development of antivirals that target host-virus interactions at the membranes. We have shown that HCV induces altered membranes and that these membranes are structurally dependent on SCD-1 expression. Inhibiting SCD-1 is potential therapeutic strategy that can be applied to HCV and other positive-stranded RNA viruses.

Future Directions

Given the exciting observations reported in this chapter, next steps should involve the use of electron microscopy to directly visualize whether inhibiting SCD-1 in Huh-7 cells expressing HCV disrupts the curvature of altered membranes [38]. Electron microscopy gives the highest possible resolution images of subcellular environments and thus is expected to give greater insight into the role of SCD-1 and the mechanism of SCD-1 inhibition by the inhibitor L-001783231-000N. If

differences in membrane alterations between SCD-1 treated and non-treated HCV expressing Huh-7 cells are observed this would confirm that SCD-1 activity is required to maintain negative membrane curvature for HCV replication and plays a role in membranous web formation. It would be interesting to correlate the cellular localizations between active SCD-1 enzymes and HCV replication complexes. In theory, activity based probes may be useful in targeting the desaturase class of enzymes, such as SCD-1 [85]. This technique involves conjugating an alkyne moiety tag to the SCD-1 inhibitor [85]. Once this probe binds to the intended SCD-1 active enzymatic pocket, the alkyne moiety can then be covalently attached, by click-chemistry, to a fluorescent tag containing an azide substituent [85]. This can serve as a useful tool for imaging differentially active SCD-1 enzymatic activity between Huh-7 cells expressing and non-expressing HCV. Now that SCD-1 has been shown to be a potential therapeutic target in HCV expressing cell culture models, it would be interesting to evaluate its efficacy in an *in vivo* mice model with chimeric human livers [86]. With this model we can potentially test whether inhibiting SCD-1 is effective against multiple HCV genotypes [86]. This serves as a clinical relevant model to confirm the SCD-1 inhibitor compound L-001783231-000N as an antiviral therapeutic.

Materials and Methods

Cell culture treatments with SCD-1 inhibitor and MK-4519

Human hepatoma cells (Huh-7.5) were grown in DMEM medium supplemented with 100 nM nonessential amino acids, 50 U/mL penicillin, 50 μg/mL streptomycin, and 10% FBS (CANSERA, Rexdale, ON). The Huh7.5 cell line stably expressing the full-length HCV genotype 1b replicon with a S2204I adaptive mutation in NS5A (Huh7.5-FGR) was a kind gift from Dr. Charles M. Rice (Rockefeller University, New York, USA) and Apath LLC (St. Louis, MO, USA). Huh-7 cells harboring the pFK-I389neo/NS3-3′/5.1 subgenomic replicon were maintained in the same culture medium supplemented with 250 μg/mL G418 Geneticin (GIBCO-BRL, Burlington, ON). The pFK-

I389neo/NS3-3′/5.1 subgenomic replicon was kindly provided by Ralf Bartenschlager (Institute of Hygiene, University of Heidelberg, Germany). At a confluency between 20-30%, the cells were treated with various concentrations for both the L-001783231-000N inhibitor and MK-4519 for 96 hours. A total volume of 2 mL per Lab-Tek chamber for CARS imaging and 1 mL for six-well plates were used for total treatment.

Simultaneous coherent anti-Stokes Raman scattering and two-photon fluorescence microscopies

The CARS microscopy system uses a single femtosecond Ti:sapphire oscillator as the excitation source, as previously described [62, 64, 66].

Quantitative voxel analysis

Quantitative data from the CARS images was determined using a voxel counting routine in ImageJ as previously described [62, 63]. In each image, multiple cells within the same field of view were counted for a % lipid volume average.

Detecting ds-HCV RNA with confocal microscopy

Huh-7 cells harboring the HCV subgenomic replicon were seeded at $8.0x10^4$ cells/well in DMEM on coverslips in a 12-well plate. After 24 h, at a confluency of 25%–30%, cells were treated with L-001783231-000N inhibitor for 96 h. After L-001783231-000N inhibitor treatments, cells were washed once with PBS pH 7.4 and fixed with precooled 100% methanol for 10 min at−20 °C. Cells were washed three times with 1× PBS and incubated for 1 h at room temperature with a mouse monoclonal antibody specific for dsRNA (J2, 1:300 dilution in PBS, Scicons, Hungary). After three more washes with PBS, cells were incubated with Cy2-labeled donkey antimouse IgG secondary antibody (1:1000 dilution in PBS, Jackson ImmunoResearch Laboratories, Inc., Westgrove, PA) for 1 h at room temperature. Following three more washes with 1× PBS, cells were rinsed in H2O before

being mounted onto slides with 50% glycerol in PBS. Cells images were captured using an Olympus IX81 inverted microscope (Olympus America Inc.) and fluorescence was detected through a 100× NA 1.40 oil objective. The images were analyzed using ImagePro software (MediaCybernatics) and ImageJ.

HCV RNA levels were quantified using two methods:

1. RNA extraction and quantitative RT-PCR

RNA isolation from hepatocytes was performed using TriZol (Invitrogen) as per the manufacturer's protocol. RNA integrity was confirmed by electrophoresis on 0.8% agarose gel in 1X TBE (Ambion, Austin, TX). Quantitative PCR (qPCR) of HCV levels was performed on an iCycler (Bio-Rad, Hercules, CA) using iQ SYBR Green Supermix (Bio-Rad, Hercules, CA), as per manufacturer's protocol. The primer sequences are described in the table below. A 20 μL reaction was assembled according to the manufacturer's protocol. For data analysis, the $2^{-\Delta\Delta Ct}$ method was used and mean fold changes in expression are shown relative to mock or control transfected samples [87].

Primer Name	**Nucleotide Sequence**
18S rRNA FWD	GCGATGCGGCGGCGTTATTC
18S rRNA REV	CAATCTGTCAATCCTGTCCGTGTCC
HCV IRES FWD	GTCTGCGGAACCGGTGAGTA
HCV IRES REV	GCCCAAATCTCCAGGCATT

2. RNA extraction, RNA integrity, and semi-quantitative PCR:

Total RNA was extracted using the RNeasy Mini Kits (Qiagen, Germantown, MD). The RNA integrity was assessed by electrophoresis on a 0.8% agarose, 1X TBE gel (Ambion, Austin, TX). 250ng of total RNA was reverse transcribed into cDNA using the Superscript II Reverse

Transcriptase kit (Invitrogen, Carlsbad CA). Hexamers and dNTPs were purchased from Applied Biosystems (Applied Biosystems, Foster City, CA). Using equal amounts of cDNA, 18S rRNA and HCV were amplified on an iCycler (Bio-Rad, Hercules, CA) using iQ SYBR Green Supermix (Bio-Rad, Hercules, CA), as per the manufacturer's protocol. The primer sequences for 18S rRNA are described in the table above. Various cycle numbers were assessed to determine the cycling conditions for sub-saturating levels of the amplicon to ensure exponential amplification. The resulting amplified genes were visualized by electrophoresis on a 2% agarose 1X TAE gel. Densitometry was calculated using Image J 1.45S [88].

HCV expression was expressed as a fold change relative to mock-digitonin treated Huh-7-SGR cells, by dividing the densitometry of each treatment by the densitometry of the mock-digitonin treated sample isolated on the same day.

Statistical Analysis:

Statistical differences in HCV expression levels, determined by semi-qPCR, were assessed using the paired student t-test in GraphPad Prism v4.01 (GraphPad Software Inc., La Jolla, CA).

RNAase Protection Assay

The RNAase protection assay was adapted from Miyanari *et al* [48]. After 96 hours of mock or SCD-1 inhibitor treatment, the cells were washed once with cold buffer B ((20 mM HEPES-KOH (pH 7.7), 110 mM potassium acetate, 2mM magnesium acetate, 1mM EGTA, and 2mM dithiothreitol)). For selected samples undergoing digitonin (Sigma-Aldrich, Oakville, ON) treatment, buffer B containing 50 μg/ml of digitonin was added to cells for 5 mins at 27°C. The reaction was stopped by washing twice with cold buffer B. For samples treated with micrococcal nuclease (MJS Biolynx, Brockville, ON) and/or nonidet P-40 (Bioshop Canada Inc., Burlington, ON), the cells were washed twice with buffer D ((20 mM HEPES-KOH (pH 7.7), 110 mM potassium acetate, 2 mM magnesium acetate, 2mM dithiothreitol, and 1mM $CaCl_2$)) and was added 0.1 unit/mL micrococcal nuclease, with or

without, 0.45% Nonidet P-40 for 15 mins at 37°C. Samples treated with 0.45% Nonidet P-40 only was incubated for 10 mins at 37°C.

References

1. Lavanchy, D., Evolving epidemiology of hepatitis C virus. *Clin. Microbiol. Infect.* **2011,** 17, 107-115.

2. Chisari, F., Unscrambling hepatitis C virus-host interactions. *Nature* **2005,** 436, 930-932.

3. Vilarinho, S.; Lifton, R., Liver transplantation: from inception to clinical practice. *Cell* **2012,** 150, 1096-1099.

4. Wise, M.; Bialek, S.; Finelli, L.; Bell, B.; Sorvillo, F., Changing trends in hepatitis C-related mortality in the United States, 1995-2004. *Hepatology* **2008,** 47, 1128-1135.

5. Moradpour, D.; Penin, F.; Rice, C. M., Replication of hepatitis C virus. *Nat. Rev. Microbiol.* **2007,** 5, 453-463.

6. Lindenbach, B.; Rice, C., Unravelling hepatitis C virus replication from genome to function. *Nature* **2005,** 436, 933-938.

7. Simmonds, P.; Bukh, J.; Combet, C.; Deléage, G.; Enomoto, N.; Feinstone, S.; Halfon, P.; Inchauspé, G.; Kuiken, C.; Maertens, G.; Mizokami, M.; Murphy, D. G.; Okamoto, H.; Pawlotsky, J.-M.; Penin, F.; Sablon, E.; Shin-I, T.; Stuyver, L.; Thiel, H.-J.; Viazov, S.; Weiner, A.; Widell, A., Consensus proposals for a unified system of nomenclature of hepatitis C virus genotypes. *Hepatology* **2005,** 42, (4), 962-973.

8. Salloum, S.; Tai, A., Treating hepatitis C infection by targeting the host. *Transl. Res.* **2012,** 159, 421-429.

9. Assis, D.; Lim, J., New pharmacotherapy for hepatitis C. *Clin. Pharmacol. Ther.* **2012,** 92, 294-305.

10. Poordad, F.; McCone, J.; Bacon, B.; Bruno, S.; Manns, M. P.; Sulkowski, M. S.; Jacobson, I. M.; Reddy, K. R.; Goodman, Z. D.; Boparai, N.; DiNubile, M. J.; Sniukiene, V.; Brass, C. A.; Albrecht, J. K.; Bronowicki, J.-P.; Investigators, S.-. Boceprevir for untreated chronic HCV genotype 1 infection. *N. Engl. J. Med.* **2011,** 364, 1195-1206.

11. Jacobson, I. M.; McHutchison, J. G.; Dusheiko, G.; Di Bisceglie, A. M.; Reddy, K. R.; Bzowej, N. H.; Marcellin, P.; Muir, A. J.; Ferenci, P.; Flisiak, R.; George, J.; Rizzetto, M.; Shouval, D.; Sola, R.; Terg, R. A.; Yoshida, E. M.; Adda, N.; Bengtsson, L.; Sankoh, A. J.; Kieffer, T. L.; George, S.; Kauffman, R. S.; Zeuzem, S.; Team, A. S., Telaprevir for previously untreated chronic hepatitis C virus infection. *N. Engl. J. Med.* **2011,** 364, 2405-2416.

12. Sheridan, D.; Neely, R.; Bassendine, M., Hepatitis C virus and lipids in the era of direct acting antivirals (DAAs). *Clin. Res. Hepatol. Gastroenterol.* **2012**, 37, 10-16.

13. Bassendine, M.; Sheridan, D.; Felmlee, D.; Bridge, S.; Toms, G.; Neely, R., HCV and the hepatic lipid pathway as a potential treatment target. *J. Hepatol.* **2011,** 55, 1428-1440.

14. Thompson, A.; McHutchison, J., Antiviral resistance and specifically targeted therapy for HCV (STAT-C). *J. Viral Hepat.* **2009,** 16, 377-387.

15. Paeshuyse, J.; Kaul, A.; De Clercq, E.; Rosenwirth, B.; Dumont, J.-M.; Scalfaro, P.; Bartenschlager, R.; Neyts, J., The non-immunosuppressive cyclosporin DEBIO-025 is a potent inhibitor of hepatitis C virus replication in vitro. *Hepatology* **2006,** 43, 761-770.

16. Inoue, K.; Umehara, T.; Ruegg, U.; Yasui, F.; Watanabe, T.; Yasuda, H.; Dumont, J.-M.; Scalfaro, P.; Yoshiba, M.; Kohara, M., Evaluation of a cyclophilin inhibitor in hepatitis C virus-infected chimeric mice in vivo. *Hepatology* **2007,** 45, 921-928.

17. Coelmont, L.; Hanoulle, X.; Chatterji, U.; Berger, C.; Snoeck, J.; Bobardt, M.; Lim, P.; Vliegen, I.; Paeshuyse, J.; Vuagniaux, G.; Vandamme, A.-M.; Bartenschlager, R.; Gallay, P.; Lippens, G.; Neyts, J., DEB025 (Alisporivir) inhibits hepatitis C virus replication by preventing a cyclophilin A induced cis-trans isomerisation in domain II of NS5A. *PloS ONE* **2010,** 5, e13687 .

18. Flisiak, R.; Feinman, S. V.; Jablkowski, M.; Horban, A.; Kryczka, W.; Pawlowska, M.; Heathcote, J. E.; Mazzella, G.; Vandelli, C.; Nicolas-Métral, V.; Grosgurin, P.; Liz, J. S.; Scalfaro, P.; Porchet, H.; Crabbé, R., The cyclophilin inhibitor Debio 025 combined with PEG IFNα2a significantly reduces viral load in treatment-naïve hepatitis C patients. *Hepatology* **2009,** 49, (5), 1460-1468.

19. Flisiak, R.; Jaroszewicz, J.; Flisiak, I.; Łapiński, T., Update on alisporivir in treatment of viral hepatitis C. *Expert Opin. Investig. Drugs* **2012,** 21, 375-382.

20. Ikeda, M.; Kato, N., Modulation of host metabolism as a target of new antivirals. *Adv. Drug Deliv. Rev.* **2007,** 59, 1277-1289.

21. Pezacki, J.; Singaravelu, R.; Lyn, R., Host-virus interactions during hepatitis C virus infection: a complex and dynamic molecular biosystem. *Mol. Biosyst.* **2010,** 6, 1131-1142.

22. Herker, E.; Ott, M., Unique ties between hepatitis C virus replication and intracellular lipids. *Trends Endocrinol. Metab.* **2011,** 22, 241-248.

23. Targett-Adams, P.; Boulant, S.; Douglas, M.; McLauchlan, J., Lipid metabolism and HCV infection. *Viruses* **2010,** 2, 1195-1217.

24. Syed, G.; Amako, Y.; Siddiqui, A., Hepatitis C virus hijacks host lipid metabolism. *Trends Endocrinol. Metab.* **2010,** 21, 33-40.

25. Su, A.; Pezacki, J.; Wodicka, L.; Brideau, A.; Supekova, L.; Thimme, R.; Wieland, S.; Bukh, J.; Purcell, R.; Schultz, P.; Chisari, F., Genomic analysis of the host response to hepatitis C virus infection. *Proc. Natl. Acad. Sci. U. S. A.* **2002,** 99, 15669-15674.

26. Diamond, D.; Syder, A.; Jacobs, J.; Sorensen, C.; Walters, K.-A.; Proll, S.; McDermott, J.; Gritsenko, M.; Zhang, Q.; Zhao, R.; Metz, T.; Camp, D.; Waters, K.; Smith, R.; Rice, C.; Katze, M., Temporal proteome and lipidome profiles reveal hepatitis C virus-associated reprogramming of hepatocellular metabolism and bioenergetics. *PLoS Pathog.* **2010,** 6, e1000719.

27. Kapadia, S.; Chisari, F., Hepatitis C virus RNA replication is regulated by host geranylgeranylation and fatty acids. *Proc. Natl. Acad. Sci. U. S. A.* **2005,** 102, 2561-2566.

28. Lee, W.-M.; Ahlquist, P., Membrane synthesis, specific lipid requirements, and localized lipid composition changes associated with a positive-strand RNA virus RNA replication protein. *J. Virol.* **2003,** 77, 12819-12828.

29. Walther, T.; Farese, R., Lipid droplets and cellular lipid metabolism. *Annu. Rev. Biochem.* **2012,** 81, 687-714.

30. Ye, J.; Wang, C.; Sumpter, R.; Brown, M.; Goldstein, J.; Gale, M., Disruption of hepatitis C virus RNA replication through inhibition of host protein geranylgeranylation. *Proc. Natl. Acad. Sci. U. S. A.* **2003,** 100, 15865-15870.

31. Wang, C.; Gale, M.; Keller, B.; Huang, H.; Brown, M.; Goldstein, J.; Ye, J., Identification of FBL2 as a geranylgeranylated cellular protein required for hepatitis C virus RNA replication. *Mole. Cell* **2005,** 18, 425-434.

32. Sakamoto, H.; Okamoto, K.; Aoki, M.; Kato, H.; Katsume, A.; Ohta, A.; Tsukuda, T.; Shimma, N.; Aoki, Y.; Arisawa, M.; Kohara, M.; Sudoh, M., Host sphingolipid biosynthesis as a target for hepatitis C virus therapy. *Nat. Chem. Biol.* **2005,** 1, 333-337.

33. Reiss, S.; Rebhan, I.; Backes, P.; Romero-Brey, I.; Erfle, H.; Matula, P.; Kaderali, L.; Poenisch, M.; Blankenburg, H.; Hiet, M.-S.; Longerich, T.; Diehl, S.; Ramirez, F.; Balla, T.; Rohr, K.; Kaul, A.; Bühler, S.; Pepperkok, R.; Lengauer, T.; Albrecht, M.; Eils, R.; Schirmacher, P.; Lohmann, V.; Bartenschlager, R., Recruitment and activation of a lipid kinase by hepatitis C virus NS5A is essential for integrity of the membranous replication compartment. *Cell Host Microbe* **2011,** 9, 32-45.

34. Miller, S.; Krijnse-Locker, J., Modification of intracellular membrane structures for virus replication. *Nat. Rev. Microbiol.* **2008,** 6, 363-374.

35. Miller, S.; Kastner, S.; Krijnse-Locker, J.; Bühler, S.; Bartenschlager, R., The non-structural protein 4A of dengue virus is an integral membrane protein inducing membrane alterations in a 2K-regulated manner. *J. Biol. Chem.* **2007,** 282, 8873-8882.

36. Bienz, K.; Egger, D.; Rasser, Y.; Bossart, W., Intracellular distribution of poliovirus proteins and the induction of virus-specific cytoplasmic structures. *Virology* **1983,** 131, 39-48.

37. Gosert, R.; Egger, D.; Lohmann, V.; Bartenschlager, R.; Blum, H. E.; Bienz, K.; Moradpour, D., Identification of the hepatitis C virus RNA replication complex in Huh-7 cells harboring subgenomic replicons. *J. Virol.* **2003**, 77, 5487-5492.

38. Egger, D.; Wölk, B.; Gosert, R.; Bianchi, L.; Blum, H. E.; Moradpour, D; Bienz, K., Expression of hepatitis C virus proteins induces distinct membrane alterations including a candidate viral replication complex. *J. Virol.* **2002**, 76, 5974-5984.

39. Tolonen, N.; Doglio, L.; Schleich, S.; Krijnse Locker, J., Vaccinia virus DNA replication occurs in endoplasmic reticulum-enclosed cytoplasmic mini-nuclei. *Mol. Biol. Cell* **2001,** 12, 2031-2046.

40. Wolk, B.; Büchele, B.; Moradpour, D.; Rice, C., A dynamic view of hepatitis C virus replication complexes. *J. Virol.* **2008,** 82, 10519-10531.

41. Miyanari, Y.; Atsuzawa, K.; Usuda, N.; Watashi, K.; Hishiki, T.; Zayas, M.; Bartenschlager, R.; Wakita, T.; Hijikata, M.; Shimotohno, K., The lipid droplet is an important organelle for hepatitis C virus production. *Nat. Cell Biol.* **2007,** 9, 1089-1097.

42. Mackenzie, J., Wrapping things up about virus RNA replication. *Traffic* **2005,** 6, 967-977.

43. Novoa, R.; Calderita, G.; Arranz, R.; Fontana, J.; Granzow, H.; Risco, C., Virus factories: associations of cell organelles for viral replication and morphogenesis. *Biol. Cell* **2005,** 97, 147-172.

44. Lee, W.; Ishikawa, M.; Ahlquist, P., Mutation of host delta9 fatty acid desaturase inhibits brome mosaic virus RNA replication between template recognition and RNA synthesis. *J. Virol.* **2001,** 75, 2097-2106.

45. Diaz, A.; Wang, X.; Ahlquist, P., Membrane-shaping host reticulon proteins play crucial roles in viral RNA replication compartment formation and function. *Proc. Natl. Acad. Sci. U. S. A.* **2010,** 107, 16291-16296.

46. Van Meer, G.; Voelker, D.; Feigenson, G., Membrane lipids: where they are and how they behave. *Nat. Rev. Mol. Cell Biol.* **2008,** 9, 112-124.

47. Zimmerberg, J.; Kozlov, M., How proteins produce cellular membrane curvature. *Nat. Rev. Mol. Cell Biol.* **2006,** 7, 9-19.

48. Miyanari, Y.; Hijikata, M.; Yamaji, M.; Hosaka, M.; Takahashi, H.; Shimotohno, K., Hepatitis C virus non-structural proteins in the probable membranous compartment function in viral genome replication. *J. Biol. Chem.* **2003,** 278, 50301-50308.

49. Shi, S.; Lee, K.; Aizaki, H.; Hwang, S.B.; Lai, M. M., Hepatitis C virus RNA replication occurs on a detergent-resistant membrane that cofractionates with caveolin-2. *J. Virol.* **2003**, 77, 4160-4168.

50. Stubbs, C.; Smith, A., The modification of mammalian membrane polyunsaturated fatty acid composition in relation to membrane fluidity and function. *Biochim. Biophys. Acta* **1984,** 779, 89-137.

51. Hac-Wydro, K.; Wydro, P., The influence of fatty acids on model cholesterol/phospholipid membranes. *Chem. Phys. Lipids* **2007,** 150, 66-81.

52. Funari, S. S.; Barceló, F.; Escribá, P. V., Effects of oleic acid and its congeners, elaidic and stearic acids, on the structural properties of phosphatidylethanolamine membranes. *J. Lipid Res.* **2003,** 44, 567-575.

53. Ntambi, J., Regulation of stearoyl-CoA desaturase by polyunsaturated fatty acids and cholesterol. *J. Lipid Res.* **1999**, 40, 1549-1558.

54. Paton, C.; Ntambi, J., Biochemical and physiological function of stearoyl-CoA desaturase. *Am. J. Physiol. Endocrinol. Metab.* **2009,** 297, 28-37.

55. Nohturfft, A.; Zhang, S., Coordination of lipid metabolism in membrane biogenesis. *Annu. Rev. Cell Dev. Biol.* **2009,** 25, 539-566.

56. Chu, K.; Miyazaki, M.; Man, W.; Ntambi, J., Stearoyl-coenzyme A desaturase 1 deficiency protects against hypertriglyceridemia and increases plasma high-density lipoprotein cholesterol induced by liver X receptor activation. *Mol. Cell. Biol.* **2006,** 26, 6786-6798.

57. Miyazaki, M.; Kim, Y.; Gray-Keller, M.; Attie, A.; Ntambi, J., The biosynthesis of hepatic cholesterol esters and triglycerides is impaired in mice with a disruption of the gene for stearoyl-CoA desaturase 1. *J. Biol. Chem.* **2000,** 275, 30132-30138.

58. Stukey, J.; McDonough, V.; Martin, C., The OLE1 gene of Saccharomyces cerevisiae encodes the delta 9 fatty acid desaturase and can be functionally replaced by the rat stearoyl-CoA desaturase gene. *J. Biol. Chem.* **1990,** 265, 20144-20149.

59. Park, C.-Y.; Jun, H.-J.; Wakita, T.; Cheong, J.; Hwang, S., Hepatitis C virus nonstructural 4B protein modulates sterol regulatory element-binding protein signaling via the AKT pathway. *J. Biol. Chem.* **2009,** 284, 9237-9246.

60. Ramtohul, Y. K.; Black, C.; Chan, C.-C.; Crane, S.; Guay, J.; Guiral, S. b.; Huang, Z.; Oballa, R.; Xu, L.-J.; Zhang, L.; Li, C. S., SAR and optimization of thiazole analogs as potent stearoyl-CoA desaturase inhibitors. *Bioorg. Med. Chem. Lett.* **2010,** 20, 1593-1597.

61. Martin, S.; Parton, R., Lipid droplets: a unified view of a dynamic organelle. *Nat. Rev. Mol. Cell Biol.* **2006,** 7, 373-378.

62. Lyn, R. K.; Kennedy, D. C.; Sagan, S. M.; Blais, D. R.; Rouleau, Y.; Pegoraro, A. F.; Xie, X. S.; Stolow, A.; Pezacki, J. P., Direct imaging of the disruption of hepatitis C virus replication complexes by inhibitors of lipid metabolism. *Virology* **2009,** 394, 130-142.

63. Lyn, R. K.; Kennedy, D. C.; Stolow, A.; Ridsdale, A.; Pezacki, J. P., Dynamics of lipid droplets induced by the hepatitis C virus core protein. *Biochem. Biophys. Res. Commun* **2010,** 399, 518-524.

64. Pegoraro, A. F.; Ridsdale, A.; Moffatt, D. J.; Pezacki, J. P.; Thomas, B. K.; Fu, L.; Dong, L.; Fermann, M. E.; Stolow, A., All-fiber CARS microscopy of live cells. *Opt. Express* **2009,** 17, 20700-20706.

65. Pezacki, J. P.; Blake, J. A.; Danielson, D. C.; Kennedy, D. C.; Lyn, R. K.; Singaravelu, R., Chemical contrast for imaging living systems: molecular vibrations drive CARS microscopy. *Nat. Chem. Biol.* **2011,** 7, 137-145.

66. Pegoraro, A. F.; Ridsdale, A.; Moffatt, D. J.; Jia, Y.; Pezacki, J. P.; Stolow, A., Optimally chirped multimodal CARS microscopy based on a single Ti:sapphire oscillator. *Opt. Express* **2009,** 17, 2984-2996.

67. Brown, A. N.; McSharry, J. J.; Adams, J. R.; Kulawy, R.; Barnard, R. J. O.; Newhard, W.; Corbin, A.; Hazuda, D. J.; Louie, A.; Drusano, G. L., Pharmacodynamic Analysis of a Serine Protease Inhibitor, MK-4519, against Hepatitis C Virus Using a Novel In Vitro Pharmacodynamic System. *Antimicrob. Agents Chemother.* **2012,** 56, 1170-1181.

68. Westaway, E.; Mackenzie, J.; Khromykh, A., Kunjin RNA replication and applications of Kunjin replicons. *Adv. Virus Res.* **2003,** 59, 99-140.

69. Reynwar, B.; Illya, G.; Harmandaris, V. A.; Müller, M.; Kremer, K.; Deserno, M., Aggregation and vesiculation of membrane proteins by curvature-mediated interactions. *Nature* **2007,** 447, 461-464.

70. Chan, R.; Tanner, L.; Wenk, M., Implications for lipids during replication of enveloped viruses. *Chem. Phys. Lipids* **2010,** 163, 449-459.

71. Scales, S.; Scheller, R., Lipid membranes shape up. *Nature* **1999,** 401, 123-124.

72. Voeltz, G.; Prinz, W.; Shibata, Y.; Rist, J.; Rapoport, T., A class of membrane proteins shaping the tubular endoplasmic reticulum. *Cell* **2006,** 124, 573-586.

73. Peter, B.; Kent, H.; Mills, I.; Vallis, Y.; Butler, P.; Evans, P.; McMahon, H., BAR domains as sensors of membrane curvature: the amphiphysin BAR structure. *Science* **2004,** 303, 495-499.

74. Jackel-Cram, C.; Babiuk, L.; Liu, Q., Up-regulation of fatty acid synthase promoter by hepatitis C virus core protein: genotype-3a core has a stronger effect than genotype-1b core. *J, Hepatol.* **2007,** 46, 999-1008.

75. Waris, G.; Felmlee, D.; Negro, F.; Siddiqui, A., Hepatitis C virus induces proteolytic cleavage of sterol regulatory element binding proteins and stimulates their phosphorylation via oxidative stress. *J. Virol.* **2007,** 81, 8122-8130.

76. Ntambi, J. M.; Miyazaki, M.; Stoehr, J. P.; Lan, H.; Kendziorski, C. M.; Yandell, B. S.; Song, Y.; Cohen, P.; Friedman, J. M.; Attie, A. D., Loss of stearoyl-CoA desaturase-1 function protects mice against adiposity. *Proc. Natl. Acad. Sci. U. S. A.* **2002,** 99, 11482-11486.

77. Guinea, R.; Carrasco, L., Effects of fatty acids on lipid synthesis and viral RNA replication in poliovirus-infected cells. *Virology* **1991,** 185, 473-476.

78. Schneiter, R.; Kohlwein, S., Organelle structure, function, and inheritance in yeast: a role for fatty acid synthesis? *Cell* **1997,** 88, 431-434.

79. Berger, K.; Cooper, J.; Heaton, N.; Yoon, R.; Oakland, T.; Jordan, T.; Mateu, G.; Grakoui, A.; Randall, G., Roles for endocytic trafficking and phosphatidylinositol 4-kinase III alpha in hepatitis C virus replication. *Proc. Natl. Acad. Sci. U. S. A.* **2009,** 106, 7577-7582.

80. Aizaki, H.; Morikawa, K.; Fukasawa, M.; Hara, H.; Inoue, Y.; Tani, H.; Saito, K.; Nishijima, M.; Hanada, K.; Matsuura, Y.; Lai, M.; Miyamura, T.; Wakita, T.; Suzuki, T., Critical role of virion-associated cholesterol and sphingolipid in hepatitis C virus infection. *J. Virol.* **2008,** 82, 5715-5724.

81. Phillips, R.; Ursell, T.; Wiggins, P.; Sens, P., Emerging roles for lipids in shaping membrane-protein function. *Nature* **2009,** 459, 379-385.

82. Kinnunen, P. K. J., On the molecular-level mechanisms of peripheral protein-membrane interactions induced by lipids forming inverted non-lamellar phases. *Chem. Phys. Lipids* **1996,** 81, 151-166.

83. Kinnunen, P. K. J.; Kõiv, A.; Lehtonen, J. Y.; Rytömaa, M.; Mustonen, P., Lipid dynamics and peripheral interactions of proteins with membrane surfaces. *Chem. Phys. Lipids* **1994,** 73, 181-207.

84. Stulnig, T., Immunomodulation by polyunsaturated fatty acids: mechanisms and effects. *Int. Arch. Allergy Immunol.* **2003,** 132, 310-321.

85. Cravatt, B. F.; Wright, A. T.; Kozarich, J. W., Activity-Based Protein Profiling: From Enzyme Chemistry to Proteomic Chemistry. *Annu. Rev. Biochem.* **2008,** 77, 383-414.

86. Mercer, D. F.; Schiller, D. E.; Elliott, J. F.; Douglas, D. N.; Hao, C.; Rinfret, A.; Addison, W. R.; Fischer, K. P.; Churchill, T. A.; Lakey, J. R. T.; Tyrrell, D. L. J.; Kneteman, N. M., Hepatitis C virus replication in mice with chimeric human livers. *Nat. Med.* **2001,** 7, 927-933.

87. Livak, K.; Schmittgen, T., Analysis of relative gene expression data using real-time quantitative PCR and the 2(-Delta Delta C(T)) Method. *Methods* **2001,** 25, 402-408.

88. Schneider, C.; Rasband, W.; Eliceiri, K., NIH Image to ImageJ: 25 years of image analysis. *Nat. Methods* **2012,** 9, 671-675.

6

Summary and Conclusions

HCV relies on multiple host factors that support viral propagation. It is becoming increasingly clear that identifying small molecule inhibitors that target host factors exploited by the virus will expand available HCV treatment options. There are several advantages of host-targeted antivirals by comparison to direct-acting antivirals. These include increasing the barrier of viral resistance and broadly targeting all HCV genotypes. As such, a thorough understanding of critical host-virus interactions is crucial to the development of additional therapeutic strategies. This outlook has directly influenced the overall goals of the projects presented in this thesis.

Many steps in HCV's lifecycle are directly linked to host lipid metabolism. HCV is capable of hijacking hepatic LD organelles and modulating differential expression of genes that control LD biosynthesis. Hepatic LDs are dynamic organelles that are highly mobile in the cell; hence, the interactions between viral proteins and the LD are highly dynamic. Probing real-time interactions can be accomplished using molecular imaging tools, such as CARS microscopy. CARS imaging detects label-free hepatic LDs with high contrast. When used in combination with two-photon fluorescence and DIC imaging, this multimodal imaging system can simultaneously probe dynamic interactions between viral proteins and LDs under video rate imaging. Furthermore, multimodal imaging was also applied to identify antiviral properties of small molecule inhibitors that target host lipid metabolic processes.

While numerous host factors have been reported to support viral replication, I focused my efforts on those involved in lipid metabolism. Lipid homeostasis is tightly regulated by the PPAR family of transcription factors. These nuclear hormone receptors activate the expression of genes regulated by peroxisome response elements. It is not surprising that PPARs represent viable targets that repress HCV replication. In chapter 2, I reported that a PPARα antagonist, BA, had induced a rapid increase in cytoplasmic levels of LDs. An increase in LD size and abundance was likely the result of blocking PPAR-induced transcription of genes that control for fatty acid catabolism. Moreover, a fusion of independent LDs was also observed in the presence of BA, suggesting that the PPAR pathway contributes to larger LDs.

It was previously reported that BA treatments rapidly inhibited HCV replication. Given that the kinetics of HCV inhibition correlated to the same kinetics of a rapid increase in LD abundance, I further investigated whether viral RNA was affected upon BA treatments. To visualize viral RNA, I incorporated a fluorophore probe labeled at the 5' end of HCV subgenomic replicon RNA to track its localization during BA treatment while simultaneously imaging LDs. From these experiments, I observed a progressive dispersion of labeled viral RNA from an initial punctate phenotype, indicative of functional replication complexes. The data correlates dispersion of viral RNA with decreased replication, suggesting that BA disrupts active replication complexes. From these observations, it is plausible that BA treatment limits available lipid intermediates responsible for prenylating host proteins, such as FBL-2, which is required to bind NS5A for efficient replication. Furthermore, a rapid induction of larger LDs may also disrupt the replication complex environment since these sites are adjacent to LDs.

In parallel to the BA experiments, an inhibitor of the rate-limiting step of cholesterol biosynthesis was also examined. While a decrease in LD abundance was expected from blocking cholesterol biosynthesis, an opposite effect occurred. After carefully examining the biosynthetic pathway of triglycerides and cholesterol, a homeostatic mechanism likely instigated an upregulation

in g TG levels to compensate for a decrease in intracellular cholesterol levels (via shuttling acetyl-CoA along towards the malonyl-CoA pathway).

In this study, the labeled RNA proved to be a valuable tool employed to visualize the disruption of HCV replication complexes upon PPARα antagonism. This strategy using simultaneous CARS and two-photon fluorescence microscopy may be employed to identify plausible mechanisms for other inhibitors that target host lipid metabolism.

Viral assembly requires the binding of HCV core protein to LDs during infection. Core protein progressively loads onto the surface of LDs, which then enables core-induced LD migration towards specialized regions for viral particle assembly. There are numerous studies that have observed core protein and LD interactions at various time points, but they lack a visualization of the dynamics of this process. In efforts to capture this, I turned to the use of CARS and DIC microscopy. Applying these imaging tools may also provide new insights by which core induces changes in LD localization. Using CARS microscopy, I captured an approximate 7-fold increase of LD abundance under HCV genotype 3a core protein expression. Furthermore, video-rate imaging captured a progressive migration of LDs towards the perinuclear region in core protein expressing cells, and full migration of LDs occurred approximately 27 hours post-core transfection. This revealed that core-induced biogenesis of LDs occurred before LDs fully migrated towards the perinuclear region.

Given the sudden directional mobility of LDs by DIC microscopy, this prompted tracking of LD trajectories in order to quantify both LD speeds and overall travel distances. From this, I discovered that LDs in core protein expressing cells moved slower, on average, by comparison to LDs in non-core expressing cells. An initial hypothesis suggested that core protein may exclusively limit the activity of only one molecular motor, which may cause a slow down LD speeds and control directionality; however, further studies in chapter 4 may suggest alternative mechanisms of core-controlled LD mobility.

Taken together, the methods used for particle tracking showed remarkable capability to track LD trajectories, and provided a further understanding core-induced LD mobility. Equipped with live-

cell capabilities, I demonstrated that quantifying LD levels by CARS microscopy may also be a useful tool to characterize and study the severity of core-induced steatosis.

Followed by the discovery that LD dynamics are modulated upon core protein expression, I expanded this study with use of a fusion protein comprised of GFP fused to domain II of core protein. By comparison to the bicistronic plasmid expressing GFP and core employed in chapter 3, this construct offered several advantages. Since domain II of core protein functions as the LD binding domain, the trajectories of GFP-DII-core and LDs were simultaneously tracked. The GFP-DII-core fusion protein offered an excellent model to study core-induced dynamics of LDs.

My results showed that expression of GFP-DII-core led to slower mean speeds, similarly seen for LDs in cells expressing full-length core protein in chapter 3. Furthermore, single amino acid mutations of varying hydrophobicity that replaced a glycine residue (position 161) located in the second amphipathic helix of DII-core, resulted in differential modulation of LD speeds by comparison to the wild-type residue. Notably, for small amino acid mutations, such as alanine and serine, an increase in speed was observed by comparison to the wildtype. By contrast, substitutions with large hydrophobic amino acids, such as phenylalanine and leucine, resulted in a shift to slower mean speeds. The data collected suggests that slower mean speeds may correlate to an increasing degree of hydrophobicity, according to the White and Wimley hydrophobicity scale for membrane interfaces. Correspondingly, an increase in hydrophobicity may be favoured considering that the amino acid residue at this position was modeled to sit-in plane towards the hydrophobic core of the LD. In a parallel study, the binding strength measurements of core protein to LDs also supported that substitutions with greater hydrophobicity bound stronger to the LD. These results do not rule out, however, that differential modulation of LDs speeds may result from a conformational change that alters the proper folding of the protein due single amino acid mutations. It is possible that core protein may limit the number of active motors on the LD surface or potentially disrupt its interaction with naïve LD-binding proteins. Upon investigating LD velocities, I showed that, by comparison to the mock, DII-core coated LDs experienced a lower frequency of high velocity travel runs, along

with an increase in the frequency of pauses. These measurements likely explain why an average of shorter distances traveled and lower average speeds were observed in comparison to the mock.

Furthermore, bidirectional mobility was observed for DII-core coated LDs, suggesting that DII-core may not exclusively limit activity to one motor. However, when LDs amassed in the perinuclear region, it appeared that LDs remained stabilized, suggesting that additional host proteins may play an active role in its stability. Identifying additional mechanisms by which core induces LD mobility towards the perinuclear region remains a topic of interest to the HCV research community. Overall, I have demonstrated that D2 is sufficient to induce relocalization of LDs, and the rate of relocalization appears linked to the hydrophobicity of specific amino acids. The multimodal imaging tools used herein could also provide the capacity to assess host proteins of interest to identify mechanisms of core-induced LD mobility.

Unsaturated fatty acids are largely incorporated as fatty-acyl chains for triglycerides, membranes phospholipids, and esterifying cholesterol. For membranes, unsaturated fatty acids increase membrane fluidity and curvature. Stearoyl-CoA desaturase is responsible for converting saturated fatty acids, such as palmitoyl- and stearoyl-CoA, to their unsaturated forms, palmitoleoyl- and oleoyl-CoA. In collaboration with Merck, I showed that an inhibitor of SCD disrupted HCV replication. At the early stages of this investigation, it was unclear, however, how the products of SCD were beneficial to viral replication.

While studying the antiviral properties of an SCD inhibitor, CARS microscopy imaging revealed that only high concentrations of the SCD inhibitor had impacted a decrease in LD abundance, but had no effect on LDs near the EC_{50} level of HCV inhibition. This suggested that there was minimal correlation between HCV inhibition and the abundance of LDs upon SCD inhibition. Alternatively, blocking the synthesis of oleoyl-CoA may potentially disrupt the membranes required for viral replication. In accordance with this, like many other viruses in the *Flaviviridae* family, HCV induces highly curved altered membranes to protect viral replication complexes from host-defense nucleases. In support of this, my results demonstrate that HCV RNA remained protected against

exogenously added nucleases to HCV replicon expressing cells. However, upon SCD inhibitor treatment, HCV RNA was rendered susceptible to exogenous nucleases, suggesting that the products of SCD activity supported a functional role of maintaining the integrity of curved membranes. This was further confirmed when dsRNA (viral RNA replicating intermediates) was observed to be dispersed throughout the cell upon SCD inhibitor treatment, demonstrating a disruption to the replication complexes. In the absence of SCD inhibitor treatment, dsRNA remained punctate and localized at the replication complexes. These results strongly suggest that SCD inhibition disrupts the integrity of altered membranes that form active HCV replication complexes.

In parallel to this study, Merck had investigated structure activity relationships for inhibitors of SCD that focused on modifying its chemical selectivity towards organic anionic transport proteins in the liver, in efforts to reduce off-targeted effects that may increase side-effects. This is a positive step towards moving inhibitors of SCD into the clinic. Taken together, the combination of molecular imaging tools and biochemical techniques led to better understanding of the antiviral properties upon inhibiting SCD activity in HCV replicon cells.

Conclusions

The study of host-virus interactions is fundamental. I have demonstrated, in this thesis, that host-targeted inhibitors of lipid metabolism offer exciting new avenues for potential antiviral therapies. The projects in this thesis have identified several plausible antiviral mechanisms for small molecule inhibitors that target lipid metabolism in HCV expressing cells. Several therapeutics that target the host are currently in clinical trials, which demonstrates their applicability as an alternative therapeutic strategy to DAAs. Furthermore, I have uncovered dynamic properties of LD mobility when bound to viral core protein. The use of multimodal imaging techniques represents an impressive

tool to identify and understand additional host-virus interactions that can be targets for future drug development.

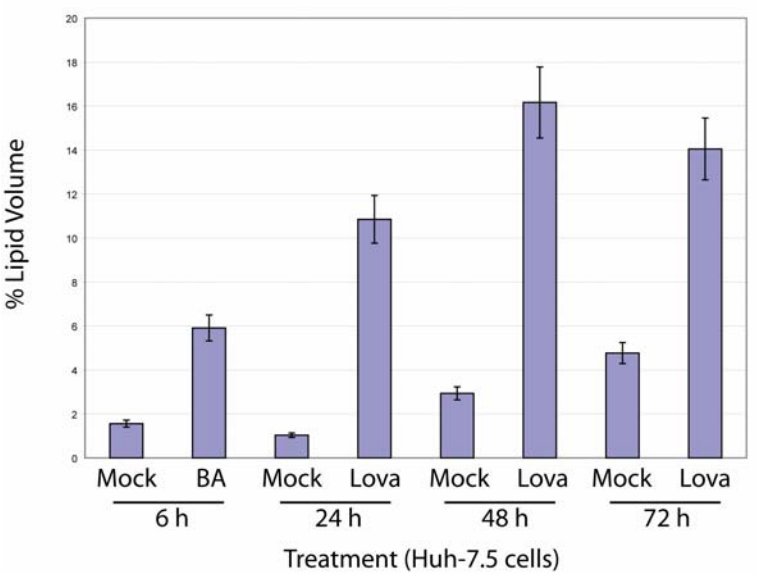

Appendix 2.1: Percent lipid volume per cell as determined by CARS microscopy using voxel counting in ImageJ for BA and lovastatin treated Huh-7.5 cells fixed at 6, 24, 48, and 72 h.

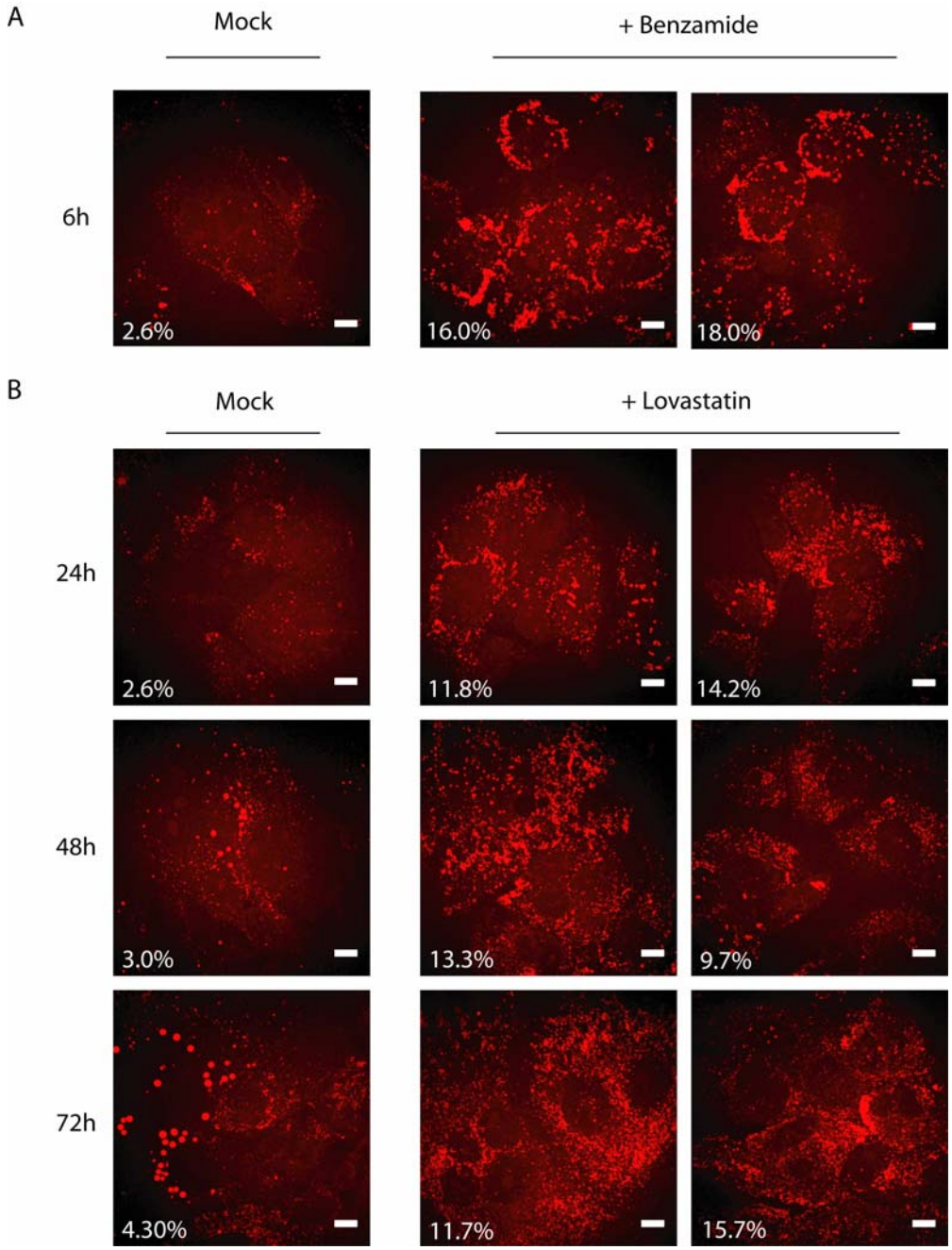

Appendix 2.2: Changes in LD phenotype observed in Huh-7.5 cells treated with (a) BA and (b) lovastatin that were fixed at various indicated time points prior to CARS imaging. To limit uptake of lipids from the culture media, serum levels were lowered to 2%. Values on the bottom left corner of the CARS images represent voxel analysis indicating the lipid droplet volume per cell (average of 5 cells per sample). Scale bars: 10 μm.

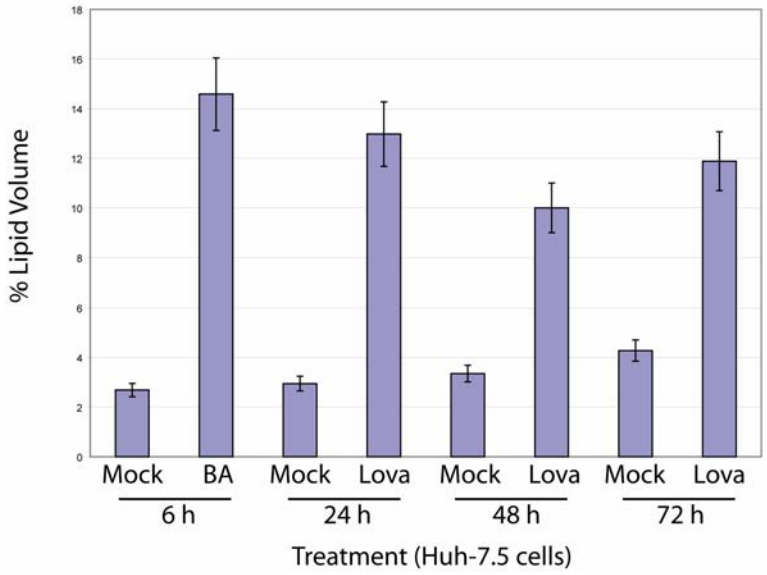

Appendix 2.3: Percent lipid volume per cell as determined by CARS microscopy using voxel counting in ImageJ for BA and lovastatin treated Huh-7.5 cells fixed at 6, 24, 48, and 72 h cultured under low serum conditions (2% serum).

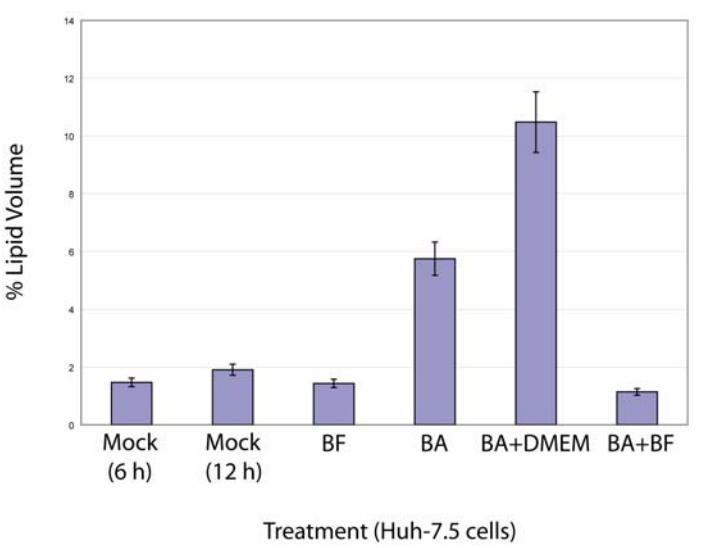

Appendix 2.4: Percent lipid volume per cell as determined by CARS microscopy using voxel counting in ImageJ for BF treated Huh-7.5 cells for 6 h, following a BA treatment for 6 h.

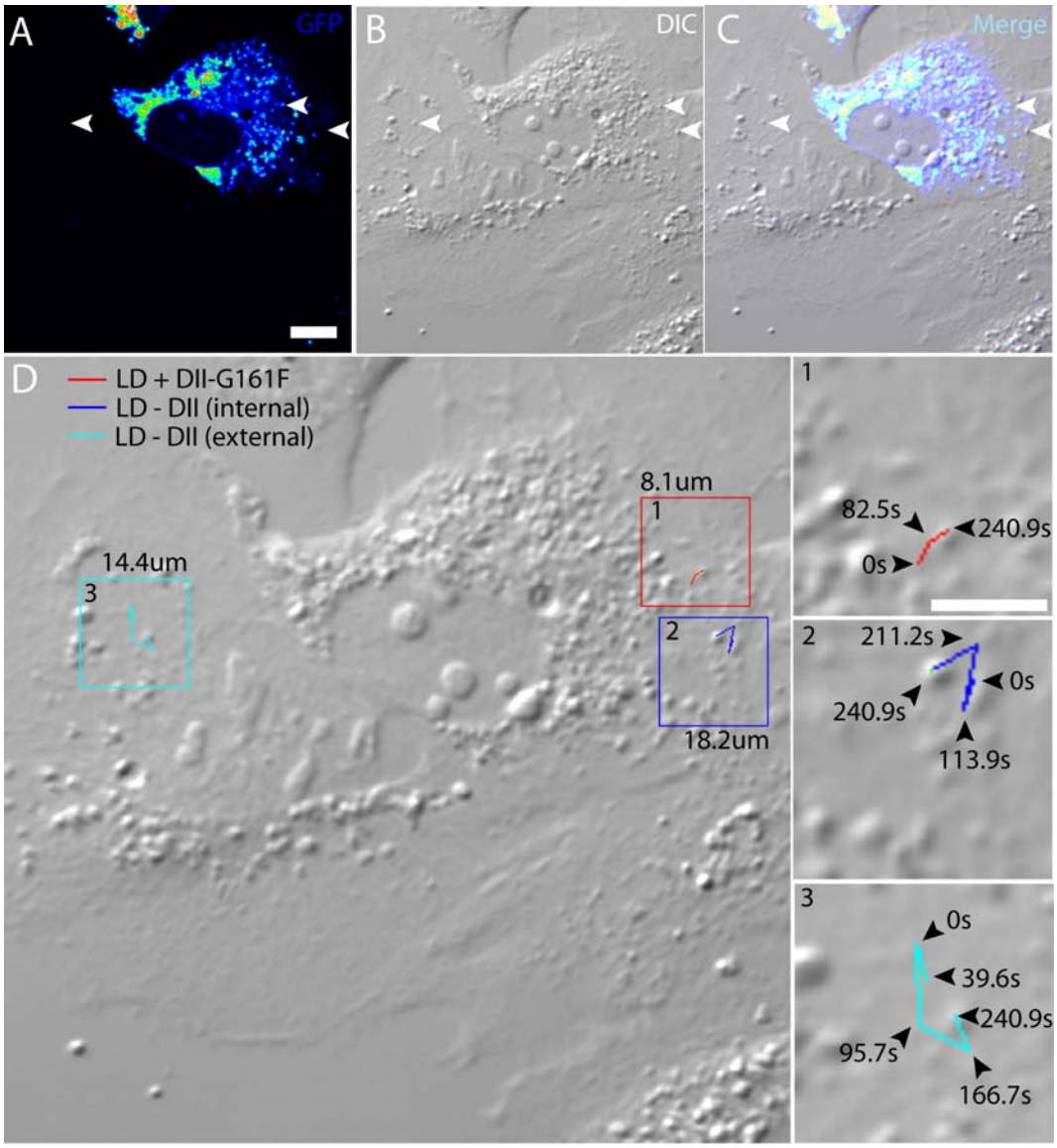

Appendix 4.1: DII-core^{G161F} coated LDs are particle tracked using simultaneous TPF and DIC microscopy. This is a representative image of DII-core^{G161F} expressed in Huh-7 cells. Three individual LDs with dissimilar environments were selected (A-C, white arrows), and their trajectories were measured to calculate the overall distances traveled. (D) A larger DIC image of (B) includes boxes to identify each LD trajectory (inset 1-3). The value above each box (D) indicates their overall travel distances for (1) DII-core^{G161F} coated LD, (2) non DII-core^{G161F} coated LD within the same cell, (3) and a LD in an adjacent cell not expressing DII-core^{G161F}**.** Each LD trajectory is magnified to demonstrate the LD track with selective freeze frame time-intervals representing the LD position at their indicated times. All of the LDs are tracked according to the same start and end time. All scale bars represent 10µm.

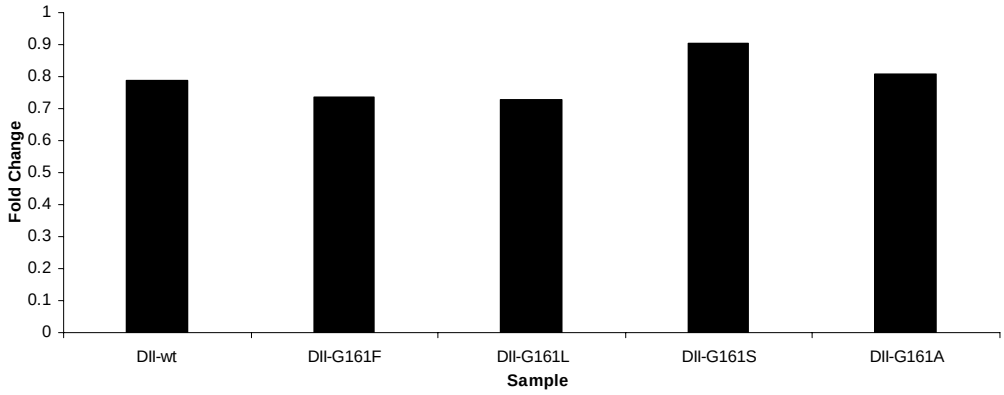

Appendix 4.2: Fold change differences in the number of directional switches for DII-core coated LDs. The fold change difference was calculated by dividing the average number of directional switches for each DII-core^{mut} coated LD by their respective mock LDs in cells not expressing any of the DII-core^{mut}. A directional switch was determined by the amount of times DII-core^{mut} coated LDs had changed between the retrograde and anterograde transport. The frequency of pauses was not included as a directional change.

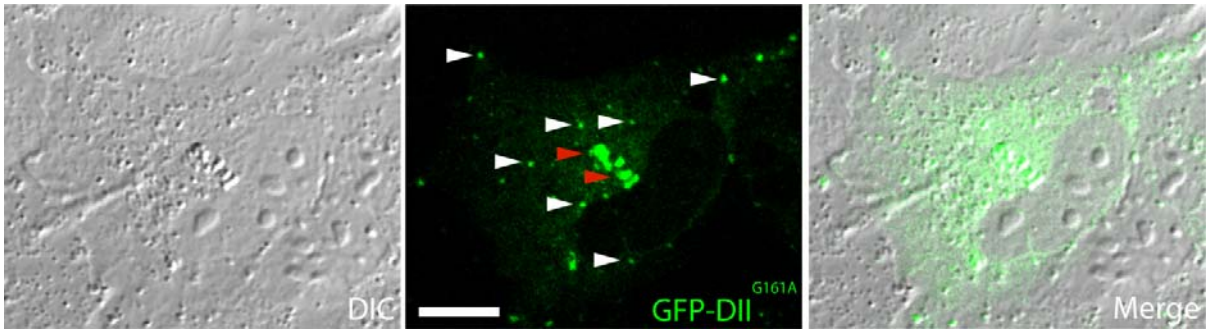

Appendix 4.3: Two populations of DII-core^{G161A} coated LDs. This is a representative image with a pattern that is typically observed in all other DII-core constructs. The white arrow represents a LD population of individual LDs that are bound to DII-core^{G161A}. The red arrow corresponds to tightly packed LDs with a high abundance of DII-core^{G161A} colocalized at the same region. Individual LDs are indistinguishable at this region. All scale bars represent 10µm.

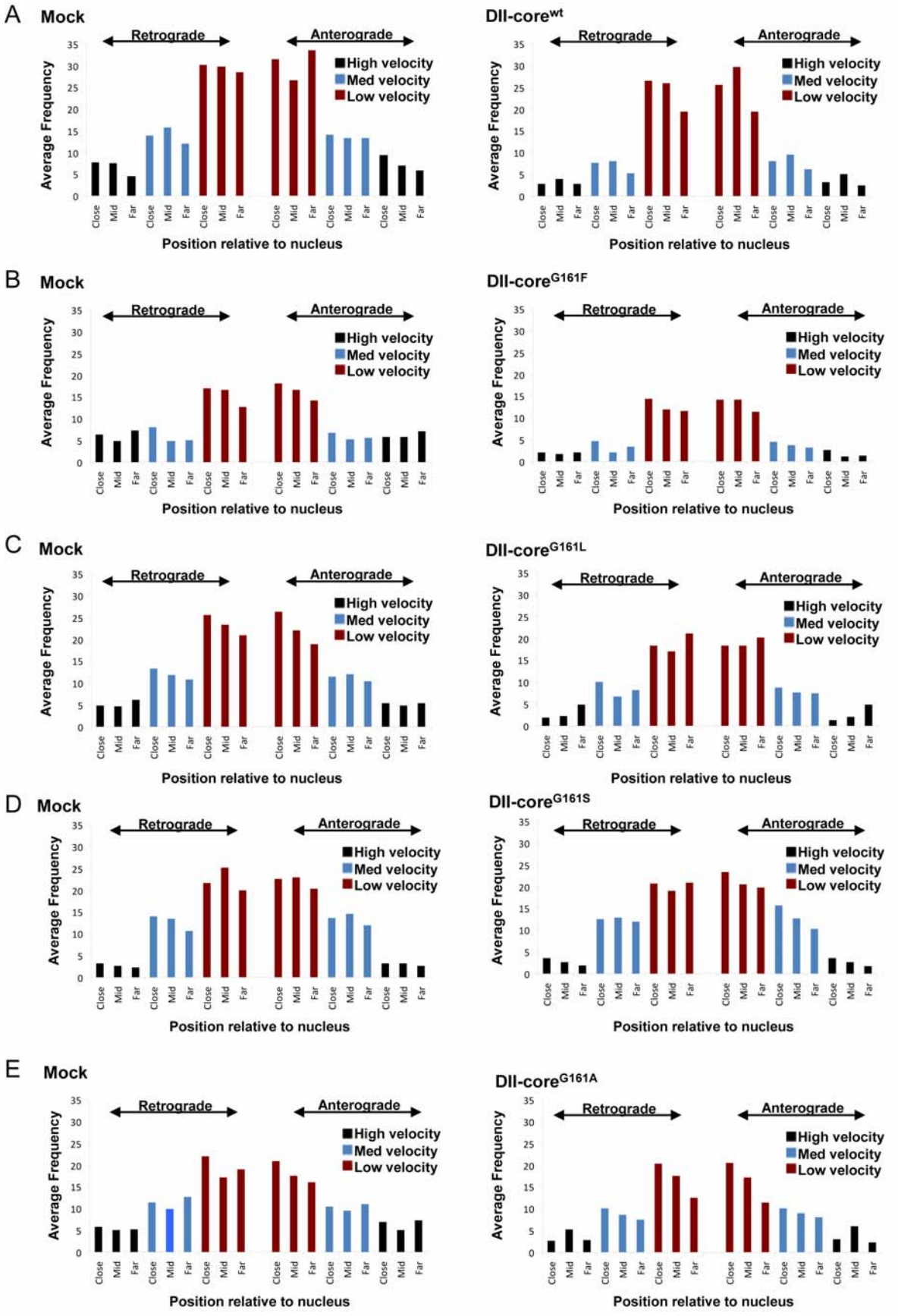
A
Mock
Dll-core^wt
B
Mock
Dll-core^G161F
C
Mock
Dll-core^G161L
D
Mock
Dll-core^G161S
E
Mock
Dll-core^G161A
Retrograde
Anterograde
High velocity
Med velocity
Low velocity
Average Frequency
Close
Mid
Far
Position relative to nucleus

Appendix 4.4: Frequency of LD velocities at three different regions in Huh-7 cells expressing DII-core^{mut} and in the mock. The average frequency of low, medium, and high velocity runs for each direction was calculated for LDs bound to (A) DII-core^{wt}, (B) DII-core^{G161F}, (B) DII-core^{G161L}, (C) DII-core^{G161A}, (D) DII-core^{G161S}. The data was separated according to where the LD was located at a position that was relative to the nucleus, either at a close, medium, or far location.

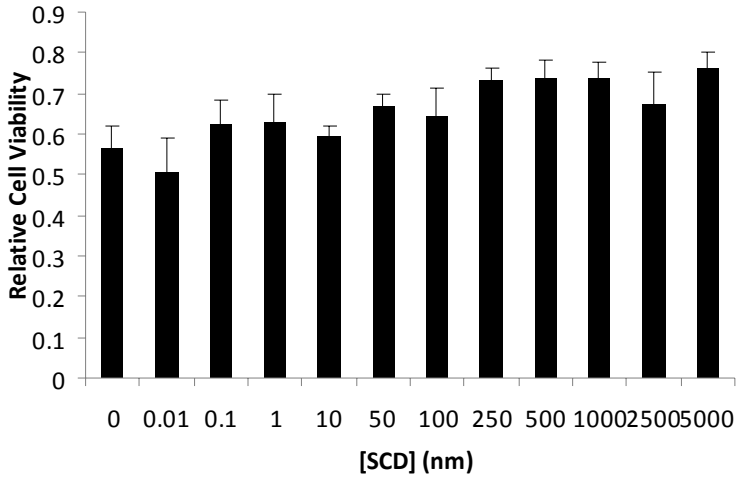

Appendix 5.1: Measuring the toxicity of the SCD-1 inhibitor. An MTT assay confirms toxicity was absent when Huh-7 cells stably expressing an HCV subgenomic replicon was treated with an SCD-1 inhibitor for 96 hours by the following concentrations.

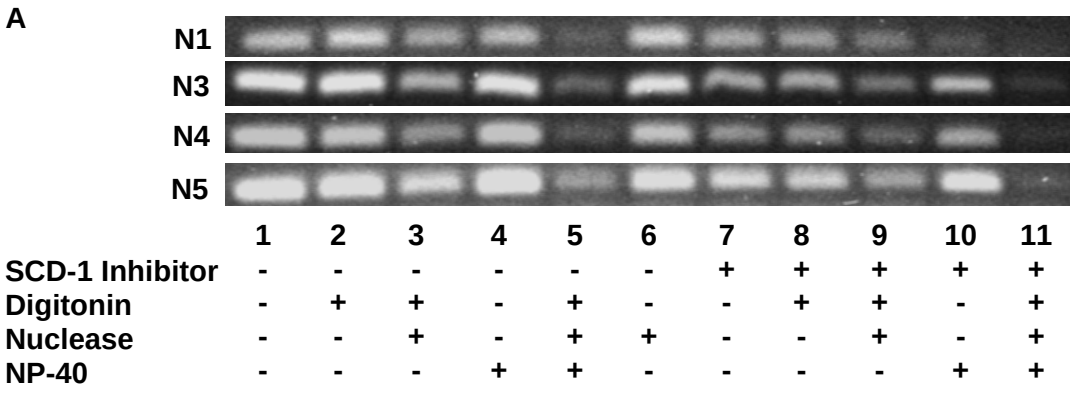

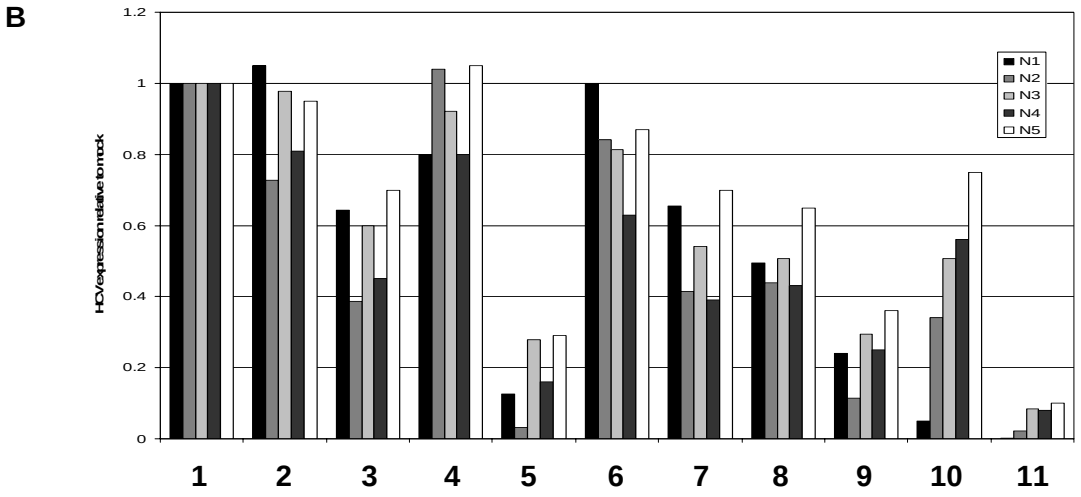

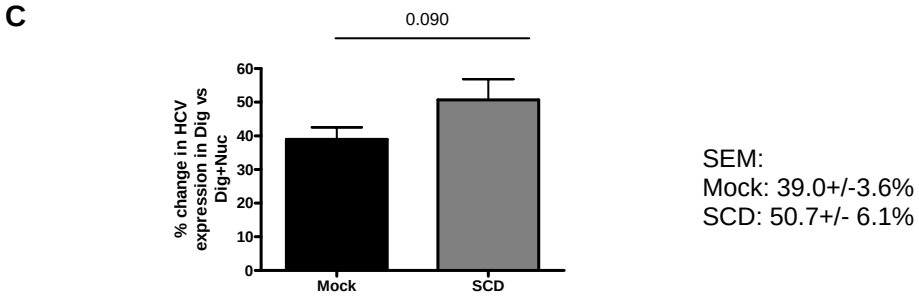

Appendix 5.2: Measuring HCV RNA susceptibility to exogenously added nuclease after inhibiting SCD-1. (A) Huh-7 cells stably expressing an HCV subgenomic replicon are treated with mock (Lanes 1-6) and SCD-1 inhibitor (Lanes 7-11) at 500nM for 96 hours. Four representative amplifications of HCV RNA by semi-quantitative PCR illustrates the relative levels that were affected by inhibiting SCD-1. The second trial (N2) was shown as a representative in Figure 5. (B) The densitometry for

each trial in (A) is quantified and individually shown. (C) The change in magnitude between digitonin and digitonin + nuclease treatments for both mock and SCD-1 inhibitor treated cells is assessed. This graph demonstrates the average qualitative assessment from densitometry that calculates the difference between lane 2 vs lane 3, in comparison to the difference in lane 8 vs lane 9 in (B).

Claims to Original Research

1. Demonstrated that a dispersion of HCV RNA away from replication complexes correlated to the abolishment of HCV replication upon antagonizing PPARα with a small molecule inhibitor.
2. Discovered that HCV core-3a protein suppresses lipid droplet speeds and travel distances.
3. Investigated how differential binding strengths of GFP-tagged domain II of core protein controls bidirectional velocities of LDs.
4. Studied the antiviral properties of a stearoyl-CoA desaturase inhibitor and showed that oleoyl-CoA may be required to maintain the membrane integrity of HCV replication complexes.

Publications from this work

- Singaravelu, R., Chen, R., **Lyn, R.K.**, Jones, D.M., O'Hara, S., Rouleau, Y., Cheng, J., Srinivasan, P., Nasheri, N., Russell, R.S., Tyrrell, D.L., Pezacki, J.P. Hepatology. Accepted 2013
- Mazumder, N., **Lyn, R.K.**, Singaravelu, R., Ridsdale, A., Moffat, D.J., Hu, C-W., Tsai, H-R., McLauchlan, J., Stolow, A., Kao, F-J., Pezacki, J.P. Fluorescence lifetime imaging of alterations to cellular metabolism by domain 2 of the hepatitis C virus core protein. PLOS One 2013. 8(6): e66738
- Pezacki, J.P., Blake, J.A., Danielson, D.C., Kennedy, D.C., **Lyn, R.K.**, Singaravelu, R. Chemical contrast for imaging living systems: molecular vibrations drive CARS microscopy. Nat. Chem. Bio. 2011. 7(3): 137-45
- Nasheri, N., Singaravelu, R., Goodmurphy, M., **Lyn, R.K.**, Pezacki, J.P. Competing roles of microRNA-122 recognition elements in hepatitis C virus RNA. Virology 2011. 410(2): 336-44
- **Lyn, R.K.**, Kennedy, D.C., Stolow, A., Ridsdale, A., Pezacki, J.P. Dynamics of lipid droplets induced by the hepatitis C virus core protein. Biochem. Biophys. Res. Commun. 2010. 399(4): 518-24
- Blais, D.R., **Lyn, R.K.**, Joyce, M., Rouleau, Y., Pegoraro, A.F., Stolow, A., Tyrrell, D.L., Pezacki, J.P. Activity-based protein profiling identifies a host protein carboxylesterase 1 that is differentially active during hepatitis c replication. J. Biol. Chem. 2010. 285(33): 25602-12
- Pezacki, J.P., Singaravelu, R., **Lyn, R.K.** Host-virus interactions during hepatitis c virus infection: A complex and dynamic molecular biosystem. Mol. Biosyst. 2010. 6(7): 1131-42

- **Lyn, R.K.**, Kennedy, D.C., Sagan, S.M., Blais, D.R., Rouleau, Y., Pegoraro, A.F., Xie, X.S., Stolow, A., Pezacki, J.P. Direct imaging of the disruption of hepatitis c virus replication complexes by inhibitors of lipid metabolism. Virology 2009. 394(1): 130-42

- Kennedy, D.C., Tay, L.L., **Lyn, R.K.**, Rouleau Y., Hulse J., Pezacki, J.P., Nanoscale aggregation of cellular beta2-adrenergic receptors measured by plasmonic interactions of functionalized nanoparticles. ACS Nano. 2009. 3(8): 2329-39

- Van Der Wiel, I.M., Cheng, J., Koukiekolo, R., **Lyn R.K.**, Stevens, N., O'Connor, N., Turro, N.J., Pezacki, J.P. FLEth RNA intercalating probe is a convenient reporter for small interfering RNAs. J. Am. Chem. Soc. 2009. 131(29):9872-3

- Kennedy, D.C., **Lyn, R.K.**, Pezacki, J.P. Cellular lipid metabolism is influenced by the coordination environment of copper. J. Am. Chem. Soc. 2009. 131(7):2444-5